Bulletin
of
The Geological Society of America

VOLUME 67 April 1956 NUMBER 4

CONTENTS

Pages

Direct radiometric measurement by gamma-ray scintillation spectrometer. By Patrick M. Hurley
Part I: Uranium and thorium series in equilibrium 395–404
Part II: Uranium, thorium, and potassium in common rocks 405–412

Origin of the Chuska sandstone, Arizona-New Mexico: A structural and petrographic study of a Tertiary eolian sediment. By H. E. Wright, Jr. 413–434

Geology and structure of the Franklin-Sterling area, New Jersey. By J. M. Hague, J. L. Baum, L. A. Herrmann, and R. J. Pickering 435–474

Seismic-refraction measurements in the Atlantic Ocean. Part VII: Atlantic Ocean Basin, west of Bermuda. By Samuel Katz and Maurice Ewing 475–510

Gravity reconnaissance survey of Puerto Rico. By G. Lynn Shurbet and Maurice Ewing 511–534

Short Note

Size and roundness in sediments: A discussion. By William F. Tanner 535–536

Subscription $15.00 per year.

Printing Office: Mt. Royal & Guilford Aves., Baltimore 2, Md.

Communications for publications should be addressed to The Geological Society of America, Dr. H. R. Aldrich, Secretary, 419 West 117 Street, New York, N. Y.

Please give notice of change of address 4 weeks in advance. Claims for nonreceipt of the Bulletin of a given month must be sent to the Secretary of the Society before the end of the second succeeding month.

Entered as second-class matter at the Post Office at Baltimore, Md., under the Act of Congress of July 16, 1894.
Accepted for mailing at special rate of postage provided for in Section 1103 Act of October 3, 1917, authorized on July 8, 1918.

PAPERS IN PRESS FOR FORTHCOMING ISSUES

Geology and Petrology of Enchanted Rock Batholith, Llano and Gillespie Counties, Texas. By Robert M. Hutchinson

Evolution of Drainage Systems and Slopes in Badlands at Perth Amboy, New Jersey. By S. A. Schumm

Quantitative Slope Analysis. By A. N. Strahler

Physical Limnology and Sedimentation in a Glacial Lake. By W. H. Mathews

Geomorphology and Glacial History of Southernmost Baffin Island. By J. H. Mercer

Structures of Porphyritic Granite and Associated Metamorphic Rocks of East Manbhum, Bihar, India. By S. Sen

Coarse Conglomerates of the Middle Ordovician in the Southern Appalachian Valley. By John M. Kellberg and Leland F. Grant

Hemphillian Mammalian Assemblage from Northeastern Oregon. By J. Arnold Shotwell

Three-dimensional Applied Potential Studies at Austinville, Virginia. By H. V. McMurry and A. D. Hoagland

BULLETIN OF THE GEOLOGICAL SOCIETY OF AMERICA
VOL. 67, 395-404, 8 FIGS. APRIL 1956

DIRECT RADIOMETRIC MEASUREMENT BY GAMMA-RAY SCINTILLATION SPECTROMETER

PART I: URANIUM AND THORIUM SERIES IN EQUILIBRIUM

BY PATRICK M. HURLEY

ABSTRACT

Where uranium and thorium are in secular equilibrium with their decay products, these elements may be determined by this direct radiometric method if the materials show more than 0.01 per cent equivalent uranium. This method is based on the measurement in a scintillation spectrometer of the relative amplitude of the response from the 238 kev gamma ray from Pb^{212}. Tests on known samples containing different relative proportions of uranium and thorium have verified the predicted precision of better than 4 per cent standard deviation per single comparison with a standard when the element measured is a major contributor to the activity.

CONTENTS

TEXT

	Page
Introduction	395
Acknowledgments	397
Instrumentation	397
Relative spectra of the uranium and thorium series	399
Method of analysis and tests	400
Source geometry	403
References cited	404

ILLUSTRATIONS

Figure	Page
1. Detail of photomultiplier, crystal source holder, and shield	398
2. Gamma scintillation spectrum for uranium series in equilibrium	398
3. Gamma scintillation spectrum for thorium series in equilibrium	399
4. Comparison of U and Th series spectra below 0.4 Mev showing bands used for Th/U analysis	399
5. Factors in selection of optimum channel width for thorium discrimination	400
6. Uranium, thorium, and U/Th as functions of R_r, Q_r	401
7. Estimated precision for different proportions of uranium and thorium, for single comparison against standard	402
8. Deviation from normal value of count per unit sample weight, as function of total sample weight, showing absorber end effect	403

TABLES

Table	Page
1. Principal gamma rays in the uranium and thorium series	396
2. Results of the method on a number of test samples	403

INTRODUCTION

The scintillation spectrometer may be used for radio-chemical analysis (Kahn and Lyon, 1953) if the material is not too complicated by unknown proportions of different gamma-ray emitters. Where different gamma-ray emitters are present, the analysis generally requires a separation of photoelectric absorption and counting efficiency from other absorption processes, and the calibration in absolute terms becomes difficult. Where the uranium or thorium series is in equilibrium this difficulty is eliminated because the proportion of gamma emitters remains constant, and an analysis for either uranium or thorium may be made on the basis of total counts in any part of the spectum as long as source geometry and absorption are constant or corrections for variations are made. This allows discrimination of the thorium and the uranium series by counting two bands in the spectrum, selected to give

TABLE 1.—PRINCIPAL GAMMA RAYS IN URANIUM AND THORIUM SERIES*

Z	Isotope	A	Energy in Mev of gamma rays
			URANIUM 238 SERIES
92	Uranium	238	~0.05 Coincident with 22 per cent of alpha rays
90	Thorium	234	0.093 20 per cent of disintegrations
91	Protactinium	234	0.82 Weak
92	Uranium	234	γ_1 0.053, γ_2 0.093, γ_3 0.118 $\gamma_1/\gamma_2/\gamma_3 = 1/\sim 0.2/0.4$
90	Thorium	230	0.068, (0.14, 0.24) $e/\gamma \sim 46$ with 25 per cent of alpha rays
88	Radium	226	0.188 $e/\gamma = 0.5$ to 0.9 with 5.7 per cent of alpha rays
86	Emanation	222	
84	Polonium	218	
82	Lead	214	γ_1 0.053, γ_2 0.242, γ_3 0.257, γ_4 0.295, γ_5 0.352 $\gamma_2/\gamma_4/\gamma_5 = 0.2/0.55/1.0$
83	Bismuth	214	γ_1 0.609, γ_2 0.766, γ_3 0.933, γ_4 1.120, γ_5 1.238, γ_6 1.379, γ_7 1.520, γ_8 1.761, γ_9 1.820, γ_{10} 2.200. γ_{11} 2.420 in ratio 9/1.3/1.1/2.6/1.0/0.9/0.7/3.2/0.2/1.0/0.5 with β
84	Polonium	214	
82	Lead	210	0.0467 (3 per cent) ($e/\gamma \sim 20$)
83	Bismuth	210	No γ
84	Polonium	210	0.80 $\sim 10^{-3}$ per cent
			THORIUM 232 SERIES
90	Thorium	232	~0.055 (0.075) Coincident with 24 per cent of alpha rays
88	Radium	228	~0.03
89	Actinium	228	0.058, 0.129, 0.184, 0.338, 0.462, 0.914, 0.969
90	Thorium	228	0.0843 2 per cent $e/\gamma \sim 12$ with 28 per cent of alpha rays
88	Radium	224	0.241 e_k/γ 0.1 with 4.6 per cent of alpha rays
86	Emanation	220	
84	Polonium	216	
82	Lead	212	γ_1 0.115, γ_2 0.176, γ_3 0.238, γ_4 0.249, γ_5 0.299 $\gamma_3 \sim 40$ per cent of disintegrations; $\gamma_5 \sim 4$ per cent of disintegrations
83	Bismuth	212	With α: 0.040 (~4 per cent), 0.144, 0.164, 0.288, 0.328, 0.432, 0.452, 0.472 With β^-: 2.20, 1.81 (~7 per cent), 1.61 (~7 per cent), 1.34 (~5 per cent), 1.03 (~6 per cent), 0.83 (~19 per cent), 0.72 (~19 per cent)
84	Polonium	212	
81	Thallium	208	(Equilibrium disintegrations of Tl 208 only 35 per cent of other elements in series owing to branching of Bi 212) 2.62 (~100 per cent, $e/\gamma \sim 0.002$); 0.859 (~15 per cent, $e/\gamma \sim 0.02$); 0.582 (~80 per cent, $e/\gamma \sim 0.02$); 0.510 (~25 per cent, $e/\gamma \sim 0.08$); 0.277 (~10 per cent, $e/\gamma \sim 0.3$)

* From Hollander, Perlman, and Seaborg (1953). Unless otherwise stated, abundance is given as the number of unconverted gamma rays emitted per 100 disintegrations. The ratio e/γ is the number of conversion electrons emitted relative to the number of unconverted gamma rays emitted.

a ratio that varies for different proportions of the two series.

There is a considerable need for a rapid radiometric measurement of uranium in thorium-bearing minerals and of thorium in uranium-bearing minerals. The requirement that the two series must be in secular equilibrium reduces the general usefulness of this method. However, most radioactive mineral occurrences are in equilibrium or essentially so. In the uranium series, 95 per cent of equilibrium is established in 3.5×10^5 years; in the thorium series only 30 years is required. Emanation leakage may keep the mineral out of equilibrium and cause an error in determination of the abundance of the parent and of the

ratio of the uranium to thorium, because thoron will not diffuse as far as radon. Generally this error is not significant, and its importance can be estimated from knowledge of the physical nature and history of the mineral aggregate. Chemical leaching of the daughter elements is more difficult to estimate.

This investigation was limited to materials in which the uranium content and its products, or its thorium equivalent in activity, exceeded 0.01 per cent. A similar technique can be used for samples containing as little as a few parts per million equivalent uranium with the use of a modified source. This modified technique is applicable to common rocks but requires source-absorption correction and discrimination of potassium. It is described in Part II of this report.

The method of measurement here described has several advantages. Source absorption can be made negligible for materials of ore grade, which is one of the biggest problems in methods using the discrimination of alpha particles (Pierson, 1951). The method proposed by Eichholz *et al.* (1953), using combined beta-gamma count, eliminates the problem of equilibrium and looks very good. Information on the precision of their method for mixtures of uranium and thorium does not permit comparison with the method proposed here. Larger samples can be used than in the beta-gamma methods. This has an important advantage in the assay of granites, for example, in which much of the activity occurs in accessory minerals and where it is difficult to obtain a small representative sample. This method is quite rapid for routine work.

Development of scintillation spectrometry has been described adequately by Hofstadter and McIntyre (1950). Scintillation counters are in common use in the exploration for uranium. Gamma rays acting on the scintillation crystal may give up all or some of their energy in the crystal. When the gamma ray gives up its entire energy, a pulse of light proportional to the energy of the gamma may result. This occurs for the most part when photoelectrons are produced which do not emerge from the crystal. An imperfect line spectrum of light pulses is then superimposed on a continuous spectrum of pulses resulting from gamma rays which have lost only part of their energy by Compton scattering or from photoelectrons that have emerged from the crystal. Discrete spectra may also result from higher-energy gamma rays producing electron pairs. These pulses are reduced in magnitude by an amount equivalent to at least 1.02 Mev, which is the energy required to form the electron pair.

Abundance of gamma rays of different energy resulting from the breakdown of the uranium and thorium series is indicated by the partial list in Table 1. Only prominent ones emerge as peaks above the base spectrum.

Light pulses in the crystal are transformed linearly into voltage pulses by a photomultiplier tube and amplifier. These pulses are fed into an analyzer in which an adjustable base-level threshold eliminates all pulses below a certain amplitude. Riding above this base-line threshold is another adjustable voltage level above which all pulses are eliminated. The instrument therefore provides a channel, or gate, of adjustable width which can be set at any voltage and which can be used to scan the spectrum of pulses. Pulses passing through the gate are recorded on a scaler or rate meter. More than one analyzer channel may be fed the same signal of pulses, thereby counting different parts of the spectrum at the same time. Channel width and the voltage level at which it operates may be calibrated in terms of gamma-ray energy. In the work described here, two channels are used as the analyses depend on the measurement of ratios.

Acknowledgments

This research was conducted by the U. S. Geological Survey on behalf of the Division of Research of the U. S. Atomic Energy Commission. The New Brunswick Laboratory of the Commission supplied analyzed samples of thorium-free uraninite and thorium-rich monazite for standards. Instruments were made available by the Office of Naval Research, U. S. Department of Defense.

Instrumentation

An initial survey of the spectra of the uranium and thorium series showed that the

peak caused by lead 212 in the thorium series occurred in a region of fairly constant response in the uranium series and might best fulfill the needs for discrimination of the two series. Furthermore, higher counting rates at the low-energy part of the spectrum make it desirable to work in this part of the spectrum.

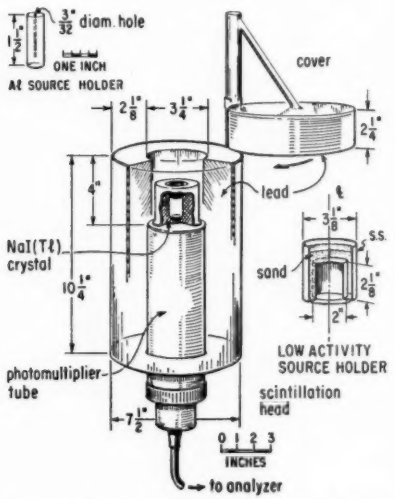

FIGURE 1.—DETAIL OF PHOTOMULTIPLIER, CRYSTAL SOURCE HOLDER, AND SHIELD

In a radioassay with gamma rays of this low energy, the thickness of the source must be small or a correction must be made for source absorption if a container of fixed dimensions is used. The sample holders for a source in a well-type crystal and for a source surrounding a crystal are illustrated in Figure 1, together with the arrangement of the scintillation head and shield. The source holder for the well-type crystal is an aluminum cylinder 15 mm in diameter with a 3-mm hole drilled in the center to carry the sample; it is used exclusively for the range of sample activity considered here. A wall thickness of 6 mm excludes the most energetic beta rays and provides a centered support for the thin column of sample powder. The crystal is thallium-activated sodium iodide, 1¾ inches in diameter by 2 inches high, in a light-tight aluminum container. The crystal faces a 5819 photomultiplier tube and is housed in a cylindrical lead shield which has a wall 2 inches thick (Irvine, 1954). This has a lead cap which is mounted on a vertical rod and which swings sideways to permit changing of samples. The pulse signal is amplified linearly,

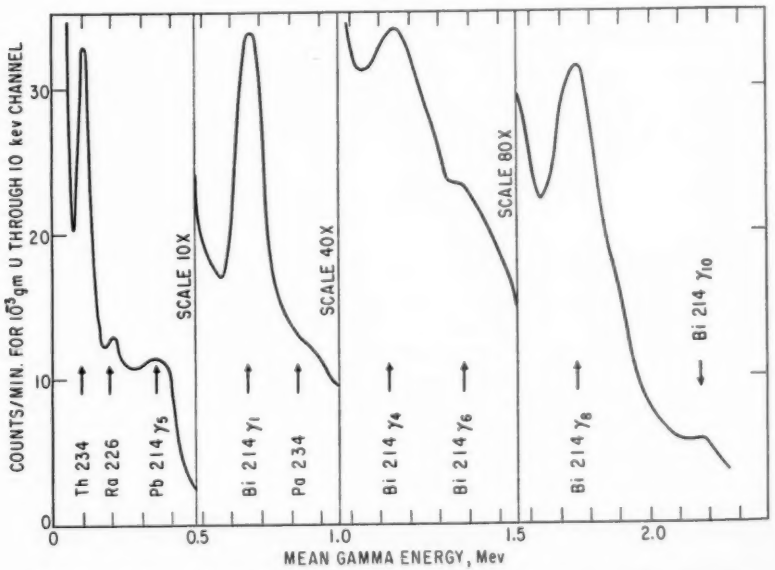

FIGURE 2.—GAMMA SCINTILLATION SPECTRUM FOR URANIUM SERIES IN EQUILIBRIUM

and appropriate bands from the spectrum are admitted by the analyzers and recorded on the scalers. The supply to all electronic components is regulated for voltage, and large variations in temperature are avoided by air conditioning and an open array of the components.

These spectra were obtained by using a channel width of from 15 to 60 kev and taking counts at intervals of 5–25 kev over the entire range. Individual points are not shown in the plots because they are so numerous at the

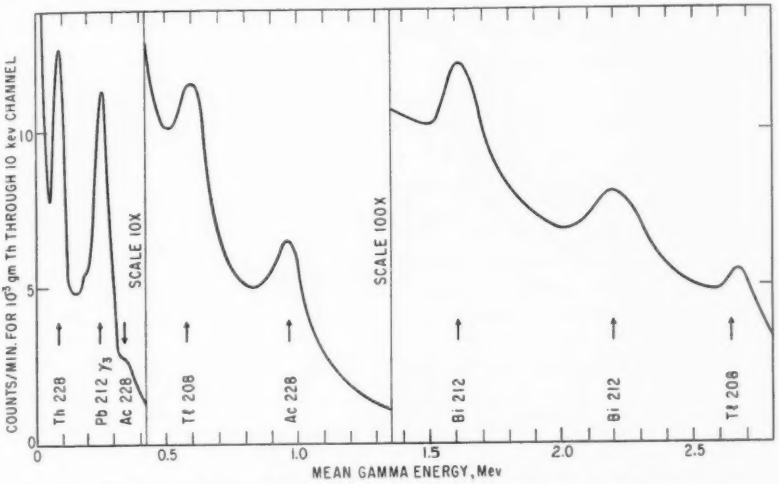

FIGURE 3.—GAMMA SCINTILLATION SPECTRUM FOR THORIUM SERIES IN EQUILIBRIUM

RELATIVE SPECTRA OF THE URANIUM AND THORIUM SERIES

Relative scintillation spectra of gamma radiation from the uranium and thorium series in secular equilibrium were obtained from analyzed mineral sources containing these elements (Figs. 2, 3). The New Brunswick Laboratory of the U. S. Atomic Energy Commission supplied analyzed samples of thorium-free uraninite and thorium-rich monazite that were used as standards. The contribution caused by the small amount of uranium in the monazite had to be deducted from all analyses in order to get the effect of an essentially pure thorium standard. The spectrum for the uranium series is shown in Figure 2, and that for the thorium series in Figure 3. In the range up to 400 kev, the photopeak caused by lead 212 in the thorium spectrum contrasts with the uranium spectrum in this interval (Fig. 4).

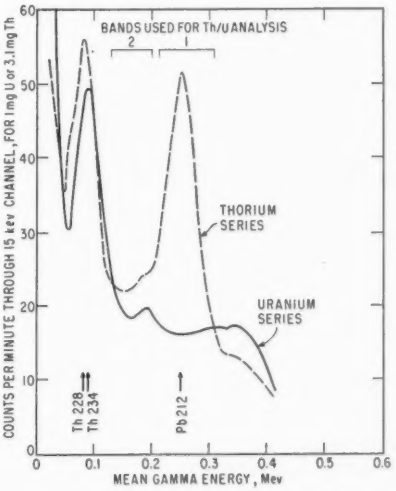

FIGURE 4.—COMPARISON OF U AND TH SERIES SPECTRA BELOW 0.4 MEV SHOWING BANDS USED FOR TH/U ANALYSIS

Plotted on basis of equal parent disintegrations in each source.

low-energy end that they obscure the character of the plot, and also because the number of counts in each run was not constant. Over much of the low-energy parts of the spectra, the standard deviation is less than two line widths. Resolution was diminished by use of the 6-mm aluminum beta absorber over the whole range, although it was not required except in the low-energy region.

Method of Analysis and Tests

Determination of the ratio of thorium to uranium (Fig. 4) depends on the comparison of a count from a band centered at 238 kev with a band centered at 180 kev. The width of the channels used for this ratio measurement is chosen on the basis of highest overall precision per unit of time required for the entire analysis (Fig. 5). Each analysis includes one or more calibrations with a standard. The drift error depends on the time interval between the calibrations. The counting error is the square root of the total count. The total count per unit time is proportional to channel width, which is inversely proportional to the resolution of the lead 212 peak. Optimum channel width depends on the drift rate of the instrument.

A determination of the plateau width for the lead 212 photopeak versus channel width is also shown in Figure 5. This plateau was defined as the width at the time of the peak included in a 3 per cent drop from the peak value, the width being given in terms of per cent of change of the base-line discriminator. The slope of this plot indicates that the sharpness of the peak decreases and that base-line drift causes reduced error as channel width is increased. This compensates to some extent the effect due to the square-root variations of the counting error and creates an optimum for the channel width which is still dominantly dependent on drift rate.

Knowledge of the drift rate of each channel is maintained by plotting the calibration values in each channel for a standard source and noting whether the points make a fairly smooth plot. In the present instrument the total amplitude of the drift variation may be as much as 5 per cent over a period of several days. An operational procedure may be established in which the channel width is left constant and analyses that show large drift variations are discarded.

Operating procedure is as follows: A standard uranium source (3000 counts per minute is

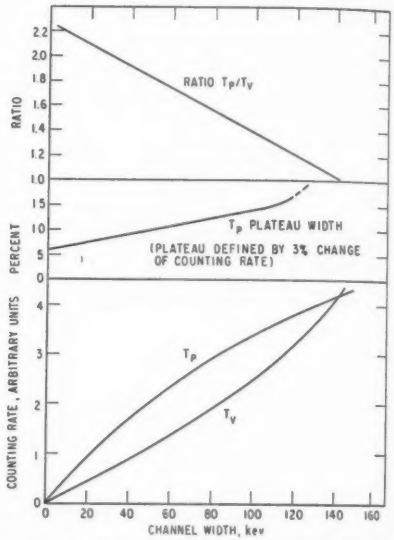

Figure 5.—Factors in Selection of Optimum Channel Width for Thorium Discrimination

satisfactory) is used to correct for variations in the counting response. After several measurements of this standard, a mean value for each channel is found, and some arbitrary value close to the mean value is chosen to represent a datum for the channel. Henceforth, all readings are corrected with reference to this datum. Thus, if the standard source is run before and after an unknown and shows that channel 1 is counting 5 per cent below the datum level, the reading for the unknown is corrected upward by 5 per cent to make it homogeneous with the fixed calibration constants, which are also based on the datum values.

At the start of a batch of samples the two channels are centered on the valley and the peak respectively by using a thorium-rich source and varying the base-line discriminator a small amount each way. A standard thorium source is then run, preceded and followed by the standard uranium source, which is always used to correct the measured values for in-

strument drift. After this, the unknowns are run alternately with the uranium standard. Calibrations with the standard thorium source are made only when needed; usually the thorium calibration holds well for several runs. As only ratios are involved, all variations in the background level and in the scintillation head and amplifier cancel out because they are common to both channels.

Calculation of the quantities of uranium and thorium in an unknown is as follows. Counting rate means net counting rate after background has been removed and corrected for drift by calibration with the uranium standard.

U = weight of uranium standard in micrograms.
U_v = mean valley channel counting rate for the uranium standard, *i.e.*, the datum value, in counts/minute.
U_p = mean peak channel counting rate for the uranium standard, in counts/minute.
T = weight of thorium in thorium standard in micrograms.
T_v = valley channel counting rate for the thorium standard corrected for drift and also corrected for the small amount of uranium in this standard in counts/minute.
T_p = peak channel counting rate for the thorium standard corrected for drift and also corrected for the small amount of uranium in this standard in counts/minute.
R_v = valley channel counting rate for unknown sample in counts/minute.
R_p = peak channel counting rate for unknown sample in counts/minute.
X = counting rate in R_v due to uranium only in counts/minute.

$X\frac{U_p}{U_v}$ = counting rate in R_p due to uranium

$(R_v - X)\frac{T_p}{T_v}$ = counting rate in R_p due to thorium

$$X = R_v\left\{\frac{\frac{T_p}{T_v} - \frac{R_p}{R_v}}{\frac{T_p}{T_v} - \frac{U_p}{U_v}}\right\}$$

If

$$\frac{T_p}{T_v} = Q_t;\ \frac{R_p}{R_v} = Q_r;\ \frac{U_p}{U_v} = Q_u,$$

$$\text{uranium in unknown} = R_v\frac{U}{U_v}\left\{\frac{Q_t - Q_r}{Q_t - Q_u}\right\} \text{ micrograms.}$$

If

$$\frac{Q_t - Q_r}{Q_t - Q_u} = F;\ \frac{U}{U_v} = C_u;\ \frac{T}{T_v} = C_t,$$

then:

Uranium in unknown = R_vC_uF micrograms, and thorium in unknown = $R_vC_t(1 - F)$ micrograms.

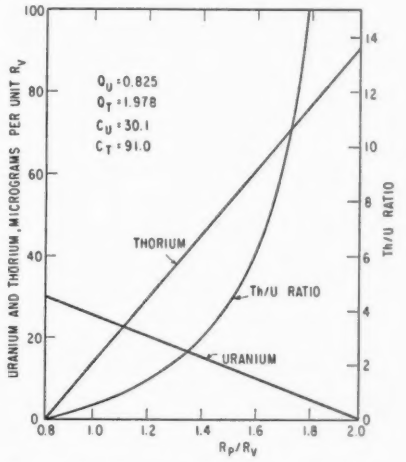

FIGURE 6.—URANIUM, THORIUM, AND U/TH AS FUNCTIONS OF R_v, Q_r

The uranium, thorium, and Th/U ratio are shown as functions of R_v and Q_r in Figure 6. With 6 mm of aluminum used for the absorption of beta particles, and 24-kev channel widths, the calibration constants for the instrument and particular source geometry were as follows:

C_u = 30.5 micrograms of uranium per count per minute
Q_u = 0.825
C_t = 91 micrograms of thorium per count per minute
Q_t = 1.978

Average background in both channels is about 9 counts per minute. This channel width is used for materials of ore grade; twice this channel width may be used for materials lower in activity to reduce the overall time per analysis as less time is spent for calibration and correction for instrument drift. Samples weighing as much as 0.5 gm may be used in the ore-grade source holder in the crystal well.

A factor of 10 in sample size is gained if the source absorption is taken into account either by correction or by making standards of approximately the same material as the unknown and still using the well-type crystal.

As R_v and R_p are usually about equal, their errors are similarly almost the same, so that

$$E_5 \cong \sqrt{2}\left(\frac{E_1}{R_v}\right).$$

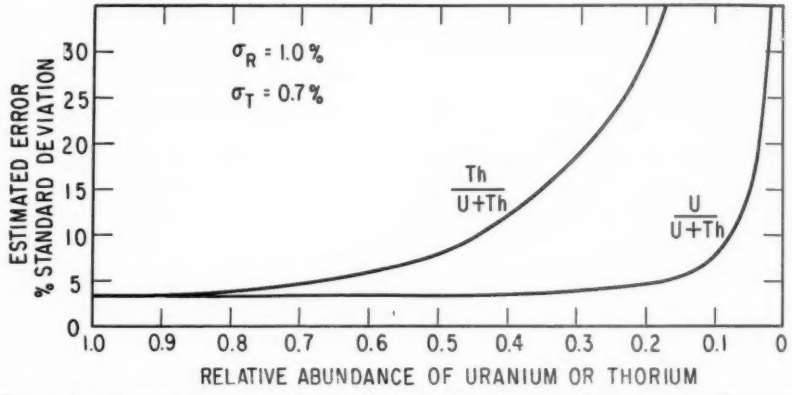

FIGURE 7.—ESTIMATED PRECISION FOR DIFFERENT PROPORTIONS OF URANIUM AND THORIUM, FOR SINGLE COMPARISON AGAINST STANDARD

Another large factor is gained by using samples of 150 gm surrounding the crystal.

Precision of the method depends on the relative abundance of uranium and thorium in the sample. The smaller the amount of thorium relative to uranium, the greater is the precision of the uranium analysis and the less the precision of the thorium analysis, and vice versa. Thoroughness of the drift correction is more important than added counts after a certain number is reached.

Let E_1 and E_2 be the errors as standard deviations in R_v and R_p, which include both counting-statistical-error and error in drift correction. Errors E_3 and E_4 are similar in T_v and T_p. The error E_5 associated with Q_r is

$$E_5 = Q_r \sqrt{\left(\frac{E_1}{R_v}\right)^2 + \left(\frac{E_2}{R_p}\right)^2}$$

and the error E_6 associated with Q_t is

$$E_6 = Q_t \sqrt{\left(\frac{E_3}{T_v}\right)^2 + \left(\frac{E_4}{T_p}\right)^2}.$$

The error in the uranium measurement is obtained from

$$(R_v \pm E_1) = \left\{\frac{Q_t \pm E_6 - Q_r \pm E_5}{Q_t \pm E_6 - Q_u \pm 0}\right\}.$$

Quantity Q_t is always about 2, and $\frac{E_3}{T_v}$ is about equal to $\frac{E_4}{T_p}$ because the drift-correction error is largest and common to both. Therefore

$$E_6 \cong 2\sqrt{2}\left(\frac{E_3}{T_v}\right).$$

Except in unusually bad periods of drift the errors in R_v and R_p are estimated to be about 1 per cent standard deviation, and the errors in T_v and T_p about 0.7 per cent standard deviation. This gives

$$\text{Uranium} = C_u(R_v \pm 0.01R_v) \cdot \left\{\frac{2 \pm 2\sqrt{2}(.007) - Q_r \pm \sqrt{2}(.007)}{2 \pm 2\sqrt{2}(.007) - 0.8 \pm 0}\right\}.$$

Quantity Q_r ranges from 1 to 2 so that F ranges between 0 and 1, and the estimated error in the uranium determination ranges from 3.3 per cent to infinity depending on whether the activity caused by uranium is 100 per cent or 0. A plot of estimated errors on the bases outlined above is given in Figure 7. The curves for uranium and thorium differ because uranium has approximately three times the activity of thorium.

The method and the estimate of precision were tested on several samples covering a range of the ratio of uranium to thorium. These test samples were made up of amounts of uranium and thorium standards mixed together in different proportions, so that, except for possible inhomogeneity in the standard material, the test samples were of known composition. The results of test analyses are given in Table 2. Total time for the analysis refers to actual time, which for most samples exceeded the time needed if the procedure were made routine and only the necessary and optimum number of counts were made. Errors of most of the analyses are well within the estimated precision given in Figure 7. The larger errors occurred when the running plot of instrument drift showed unusually large fluctuation. These fluctuations could have been eliminated on the basis of a specified maximum permissible drift rate.

TABLE 2.—RESULTS OF RADIOACTIVE MEASUREMENTS OF TEST SAMPLES

Test sample	Uranium (mg)	Thorium (mg)	Measured uranium (mg)	Per cent error	Measured thorium (mg)	Per cent error	Total analysis time (min)*
1	56.3	<0.05	56.0	0.5	0	..	30
2	58.2	31.1	56.8	2.4	29.8	4.0	22
			56.8	2.4	31.3	0.6	50
			56.7	2.4	32.5	4.8	45
Mean			56.8	2.4	31.2	0.6	
3	32.7	31.1	33.5	2.6	29.1	6.5	39
			33.3	1.8	30.2	2.9	55
Mean			33.4	2.2	29.7	4.7	
4	24.7	31.3	26.2	6.1	27.6	11.7	45
			25.1	1.6	30.1	3.8	34
			25.1	1.6	30.1	3.8	24
Mean			25.4	3.1	29.3	6.4	
5	15.4	31.5	14.4	6.4	34.0	8.0	42
			15.5	0.6	30.8	2.1	25
Mean			14.9	2.9	32.4	2.9	
6	1.22	32.1	1.22	0.1	31.2	3.0	100

* Includes calibrations, weighing, and calculations

SOURCE GEOMETRY

In reference to the cross section of the source in Figure 8,

A_u = gamma events in unit length of source per unit time, at energy u

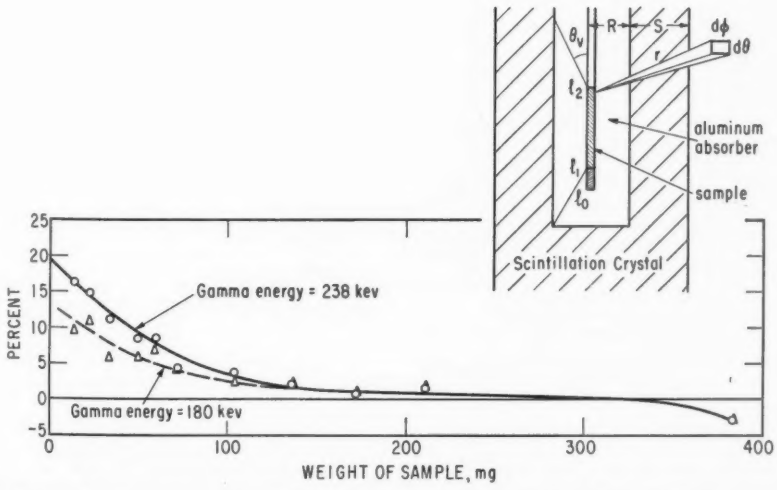

FIGURE 8.—DEVIATION FROM NORMAL VALUE OF COUNT PER UNIT SAMPLE WEIGHT, AS FUNCTION OF TOTAL SAMPLE WEIGHT, SHOWING ABSORBER END EFFECT

μ_a = absorption coefficient of absorber at energy u

μ_s = photoelectric absorption coefficient of $NaI(Tl)$ at energy u

θ_u = an angle of incidence above which most of the unabsorbed gamma rays from the region $l_1 - l_2$ emerge, and below which the proportion of gamma rays is small enough so that the end effects of the absorber cause an error that is either not significant or else may be corrected simply in the flat part of the accompanying curve

K = constant of proportionality which involves the proportion of pulses equivalent to energy u that result from Compton scattering, efficiency, and other factors.

Any unit of source length in the interval l_1 to l_2 in which there is no significant end effect will give rise to a count of gamma rays at energy v as follows:

$$C = \frac{A_v K}{4\pi r^2} \int_0^{\pi} \int_0^{2\pi} r^2 \sin\theta \cdot \exp[-(R\mu_a/\sin\theta + S\mu_a/\sin\theta)] \cdot d\theta \cdot d\phi$$

$$= A_v k \int_0^{\pi/2} \exp[-csc\,\theta(R\mu_a + S\mu_s)] \cdot \sin\theta \cdot d\theta$$

Source length in the interval l_0 to l_1 contributes a count greater than any equal length in the interval l_1 to l_2. The total count in the interval l_0 to l_1 is

$$C_0 = \frac{A_0 K l_1}{2} \int_0^{\pi/2} \exp[-csc\,\theta(R\mu_a + S\mu_s)] \cdot \sin\theta \cdot d\theta + \frac{C_0}{B(\mu)}$$

where B is some value between 1 and 2 depending on the geometry of the bottom of the hole with respect to the end of the absorber. For any fixed source cylinder B is also a function of μ, which varies with the gamma energy being measured.

When the length of the sample in the holder exceeds l_2, the upper end of the crystal affects the count. The two end effects cause a slight decrease of count with increase of sample volume in the region l_1 to l_2 (Fig. 8). The integrals together with the factor K are evaluated only by direct calibration using increasing amounts of sample, but they explain the shape of the curves and the reason why the effect at the higher energy p is less than the effect at the lower energy v.

In practice it may be sufficient to keep the sample weight within the limits of the flat part of the curve without correction as was done with the test samples (Table 2), or to fill the length l_0 to l_1 with inactive material of about the same composition as the sample, before adding the sample, to remove the lower end effect. For precise work it might be necessary to use such curves as given in Figure 8 and to correct values of R_v, and R_p and Q accordingly.

References Cited

Eichholz, G. G., Hilborn, J. W., and McMahon, C., 1953, The determination of uranium and thorium in ores: Canadian Jour. Physics, v. 31, p. 613–628.

Hofstadter, R., and McIntyre, J. A., 1950, Gamma-ray spectroscopy with crystals of NaI(Tl): Nucleonics, v. 7, no. 3, p. 32–37.

Hollander, J. M., Perlman, I., and Seaborg, G. T., 1953, Tables of isotopes: Rev. Modern Physics, v. 25, p. 469–651.

Irvine, J. W., 1954, Simple efficient shield for well-type scintillation crystals: Nucleonics, v. 12, no. 10, p. 62–63.

Kahn, B., and Lyon, W. S., 1953, Scintillation spectrometer in radiochemical analysis: Nucleonics, v. 11, no. 11, p. 61–63.

Pierson, D. H., 1951, Alpha-particle assay and the measurement of the thorium-uranium ratio in radioactive ores: Phys. Soc. Proc., Sect. B, v. 64, p. 876–888.

U. S. Geological Survey, Washington 25, D. C., and Massachusetts Institute of Technology, Cambridge 39, Mass.

Manuscript Received by the Secretary of the Society, April 12, 1955

Publication Authorized by the Director, U. S. Geological Survey

BULLETIN OF THE GEOLOGICAL SOCIETY OF AMERICA
VOL. 67, PP. 405–412, 3 FIGS. APRIL 1956

DIRECT RADIOMETRIC MEASUREMENT BY GAMMA-RAY SCINTILLATION SPECTROMETER

PART II: URANIUM, THORIUM, AND POTASSIUM IN COMMON ROCKS

BY PATRICK M. HURLEY

ABSTRACT

The method described in Part I of this report has been extended to the measurement of the uranium and thorium series and potassium in common rocks, or materials of comparable activity, in which the series are in secular equilibrium. The counting rate in an additional band centered on the photopeak from the 1.46 Mev gamma ray of K^{40} permits the measurement of potassium and the removal of the counts due to the potassium in the other channels.

CONTENTS

TEXT

	Page
Introduction	405
Acknowledgments	406
Method of analysis	406
Calculation of results	408
Test results	409
Operating procedure and error	409
Small samples of intermediate grade	410
Other geological applications	411
References cited	411

ILLUSTRATIONS

Figure	Page
1. Scintillation spectrum for 200-gm sample containing 0.6124 gm Th and 0.0245 gm U	406
2. Gamma-scintillation spectrum for 150-gm sample of K_2CO_3	407
3. Effect of source absorption in thick sources of heavy minerals in well-type crystal	410

TABLES

Table	Page
1. Test measurements for uranium and thorium	409
2. Potassium test analyses	409

INTRODUCTION

This part of the report covers an investigation of possible methods of direct radiometric assay of uranium and thorium in common rocks. As the radiation from K^{40} is important at this level of activity, it must be assayed separately and taken into account. This requires either a three-channel instrument or a two-channel instrument and a separate measurement for the potassium.

The method requires that the scintillation crystal be surrounded by the powdered sample in order to obtain sufficient counts for analysis, but the thickness of the sample layer must not be so great that the photopeaks are swamped by Compton-scattered radiation from within the source. A sample weight of approximately 200 gm with a layer about a half an inch thick surrounding the scintillation crystal was found to be satisfactory. The method is capable of analyzing, to a few parts per million, rocks or other solid materials in powdered form or liquids containing the radioactive series in equilibrium. Similarly potassium can be analyzed to a fraction of a per cent.

The uranium and thorium series must be in equilibrium in order to determine these parent elements. Actually the method measures the quantities of the elements in the series below radium 226 and radium 224. In the uranium series elements above radium do not have gamma rays of sufficient energy to give counts in the range that is measured, except for a possible slight contribution from protactinium 234. The radium-226 gamma at 188 kev lies in the band accepted by the lowest energy channel.

The crucial question is whether the radioactive series are in equilibrium in common rocks, and therefore whether the sample should be analyzed by this method. It may be possible to judge fairly well if geological information on the sample is available. Usefulness of the method may be largely restricted to fresh samples of common rocks or minerals in which the uranium and thorium are fairly uniformly distributed and syngenetic. Epigenetic enrichments of uranium by hypogene or supergene processes may be so leached that they are out of equilibrium at times, although probably less than suspected.

Tendency to overestimate the lack of equilibrium may be due to the fact that equilibrium is re-established faster than the whole surface zone is lowered by chemical weathering and erosion. For example, a leached zone and an underlying zone of enrichment will have existed a long time compared to the half-lives of Ra^{226} (1622 years), Ra^{228} (6.7 years), or Th^{230} (80,000 years), which control the rate at which equilibrium is maintained. Spotty concentrations of uranium in limonitic material may give spurious counts due to excess thorium 230; similarly, recent efflorescences or depositions of uranium may give low results because of lack of the equilibrium amount of thorium 230. Control assays for uranium by standard methods should be made to establish the validity of the assumption of equilibrium in any area being sampled.

The escape of radon from the sample after it is pulverized must also be considered. The principal contributions to the counts below radium are from Pb^{214} and Bi^{214}. A reduction in the amount of these will be controlled by the 27-minute half-life of Pb^{214} if radon is removed. The highest ratio of emanating radon to total radon expectable in a pulverized sample of a common rock is about 25 per cent, if the radium in the rock is 50 per cent in surface films and half of its radon recoils inward rather than outward. Usually granitic rocks show only a small per cent emanation; volcanic, sedimentary, and metamorphic rocks show none. At most the radon loss may be a few per cent. This can be eliminated by storing the rock sample in a plastic sample holder with cover and running it in the spectrometer without uncovering.

ACKNOWLEDGMENTS

This research was conducted by the U. S. Geological Survey on behalf of the Division of Research of the U. S. Atomic Energy Commission. The instruments used in the investigation were made available by the Office of Naval Research, U. S. Department of Defense.

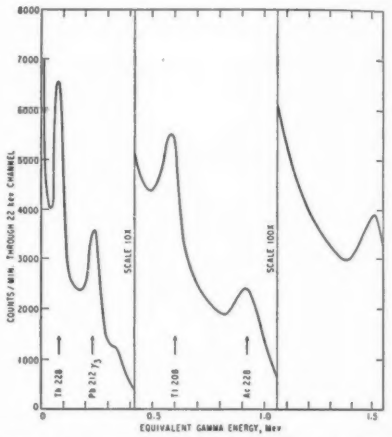

FIGURE 1.—SCINTILLATION SPECTRUM FOR 200-GM SAMPLE CONTAINING 0.6124 GM TH AND 0.0245 GM U

METHOD OF ANALYSIS

Except for the correction for potassium the method of analysis for uranium and thorium is similar to that described in Part I. A 200-gm sample of rock or mineral powder is placed in the low-activity source holder, and counts are made with the base level of the first two channels set at 168 and 226 kev, respectively. A channel width of 25 kev is commonly used in each of these.

A spectrum was plotted for a sample in the low-activity sample holder surrounding the crystal to see if the peaks are reduced in height by absorbtion in the source. Figure 1 illustrates this spectrum from a synthetic mixture containing 200 gm of quartz and olivine, 0.612 gm of thorium, and 0.0245 gm of uranium. The ratio of channel 2 over channel 1 is 1.370 in a pure thorium standard and 0.718 for a pure uranium standard. The ratio of these two figures is 1.91, which is actually no less than that of a sample located in the

center well for equal channel widths. The effect of the source absorption does not decrease the sensitivity of the method when the sample is about half an inch thick.

Tests made on the effect of source absorption using different types of rocks enriched by known amounts of uraninite and monazite showed no difference between the most felsic and most mafic rocks tested. This permits indiscriminate analysis of quartz- and silicate-bearing rocks without the necessity of a source-absorption correction, so long as the weight is kept constant and the sample occupies approximately the same volume. Leaving the heavier rock samples in open packing and shaking the sample holder so that lighter rock samples are closer packed permits maintenance of a fairly constant volume.

The third channel is centered on the photopeak of K^{40}, and pulses are admitted through a channel width equivalent to 134 kev. These three channels provide three equations for the three unknowns which can be solved simply for the three constituents.

The discrimination of thorium from uranium is provided by the ratio of counts from channel 2 over channel 1. This ratio for pure thorium series is 1.91 times greater than for pure uranium series. The discrimination of potassium from uranium and thorium is given by the ratio of channel 3 over channel 1. For a sample containing only potassium this ratio is 13.4 times greater than for a sample containing only uranium series and 16.5 times greater than a sample containing only thorium series. This is because the potassium scintillation spectrum is different in shape from that of the uranium or thorium series. The spectrum is sharply terminated above 1.46 Mev which is the energy of the K^{40} gamma, and, as shown in Figure 2, the scattered gammas of lower energy increase in abundance little in the range down to 0.5 Mev.

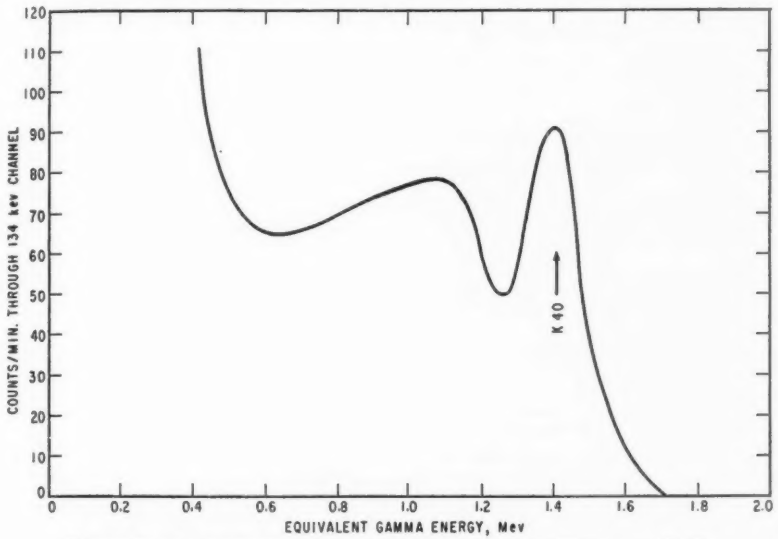

FIGURE 2.—GAMMA-SCINTILLATION SPECTRUM FOR 150-GM SAMPLE OF K_2CO_3

About the same conditions mentioned in Part I of the report hold for the drift of the instrument. Standards were made by adding a known amount of uraninite or monazite to 200 gm of an intermediate igneous rock. In using the thorium standard a correction is made for the amount of uranium in the monazite. The uraninite and the monazite must be carefully analyzed for both uranium and thorium. Potassium carbonate is usually used to make up potassium standards. The uraninite and monazite used for all standards were supplied by the New Brunswick Laboratory of the

Atomic Energy Commission through the kindness of C. J. Rodden, Director. All analyses are thus based on these A.E.C. chemical analyses for uranium and thorium.

Calculation of Results

Channels 1, 2, and 3 are those with base-level settings at 0.168, 0.226, and 1.39 Mev, respectively. All references to counting rate mean net counting rate after background has been removed and corrected for drift. Unless otherwise specified, the counting rate also refers to that obtained from a 200-gm sample in the standard sample holder.

U = uranium content of uranium standard, ppm.

U_1, U_2, U_3 = counting rate from uranium standard in channels 1, 2, and 3, counts per minute.

T = thorium content of thorium standard, ppm.

T_1, T_2, T_3 = counting rate from thorium standard in channels 1, 2, and 3, thorium only (uranium contribution subtracted)

K = potassium content of potassium standard, per cent.

K_1, K_2, K_3 = counting rate from potassium standard in channels 1, 2, and 3

R_1, R_2, R_3 = counting rate from unknown sample in channels 1, 2, and 3

In the value found for R_1 if X, Y, Z are the counts per minute due to U, Th, and K, respectively, the solution of the following equations will give the required results.

$$X + Y + Z = R_1$$
$$(U_2/U_1)X + (T_2/T_1)Y + (K_2/K_1)Z = R_2$$
$$(U_3/U_1)X + (T_3/T_1)Y + (K_3/K_1)Z = R_3$$

$$\text{Or} \quad X = \frac{\begin{vmatrix} R_1 & 1 & 1 \\ R_2 & T_2/T_1 & K_2/K_1 \\ R_3 & T_3/T_1 & K_3/K_1 \end{vmatrix}}{\begin{vmatrix} 1 & 1 & 1 \\ U_2/U_1 & T_2/T_1 & K_2/K_1 \\ U_3/U_1 & T_3/T_1 & K_3/K_1 \end{vmatrix}}$$

$$= \frac{A_1R_1 + A_2R_2 + A_3R_3}{A_4}$$

where
$$A_1 = \frac{T_2}{T_1} \cdot \frac{K_3}{K_1} - \frac{K_2}{K_1} \cdot \frac{T_3}{T_1}$$

$$A_2 = \frac{T_3}{T_1} - \frac{K_3}{K_1}$$

$$A_3 = \frac{K_2}{K_1} - \frac{T_2}{T_1}$$

$$A_4 = \frac{U_3}{U_1}A_3 + \frac{U_2}{U_1}A_2 + A_1$$

Similarly:

$$Y = \frac{B_1R_1 + B_2R_2 + B_3R_3}{A_4}$$

where
$$B_1 = \frac{K_2}{K_1} \cdot \frac{U_3}{U_1} - \frac{U_2}{U_1} \cdot \frac{K_3}{K_1}$$

$$B_2 = \frac{K_3}{K_1} - \frac{U_3}{U_1}$$

$$B_3 = \frac{U_2}{U_1} - \frac{K_2}{K_1}$$

$$\text{Uranium} = X \cdot U/U_1 \text{ ppm}$$

$$\text{Thorium} = Y \cdot T/T_1 \text{ ppm}$$

$$\text{Potassium} = \frac{K}{K_3}\left(R_3 - X \cdot \frac{U_3}{U_1} - Y \cdot \frac{T_3}{T_1}\right) \text{ per cent}$$

Because the calibration constants are determined on the basis of standard sample weight (*e.g.*, 200 gm), the unknown must also be this weight.

In the spectrometer used in this investigation, the following values were found for the various constants:

$U_2/U_1 = 0.718$
$U_3/U_1 = 0.133$
$T_2/T_1 = 1.370$
$T_3/T_1 = 0.107$
$K_2/K_1 = 0.800$
$K_3/K_1 = 1.770$
$U/U_1 = 0.470$ ppm U per c/m
$T/T_1 = 1.265$ ppm Th per c/m
$K/K_3 = 0.451$ per cent K per c/m

Average backgrounds are 14.1, 12.5, and 8.0 c/m for channels 1, 2, and 3, respectively.

From these values:

$A_1 = 2.34$ $A_2 = -1.66$ $A_3 = -0.57$ $A_4 = 1.069$
$B_1 = -1.164$ $B_2 = 1.637$ $B_3 = -0.082$

Test Results

Tables 1 and 2 show test analyses on synthetic samples and on rock samples that have been analyzed by different methods. The synthetic materials were made up from mixtures of quartz and dunite or diabase, to which were added known amounts of standard uraninite or monazite similar to the standards used for calibration.

Table 1.—Test Measurements for Uranium and Thorium

Sample	Uranium (ppm)		Thorium (ppm)	
	By scintillation count	By other methods	By scintillation count	By other methods
Synthetic mixture				
Quartz and dunite	134	122	3010	3062
Palisade diabase	203	204	0	<1
Palisade diabase	0.7	0.6	1.6	2.1
NBS Milford granite	0.8	0.7	9.0	Unknown
NBS Deccan trap	0.7	0.6	2.8	Do.
Conway granite				
54-S-137	10.3	7.6	32	Do.
54-S-121	9.1	10.7	46.4	Do.
54-S-128	12.7	12.1	67	Do.
54-S-109	13.8	17.8	61	Do.

Table 2.—Potassium Test Analyses

Sample	K_2O by other methods (per cent)	K_2O measured (per cent)
NBS Gabbro-diorite	1.56	1.56
NBS Deccan trap	0.78	0.75
NBS Chelmsford granite	5.5	5.0
NBS Columbia River basalt	0.98	0.80
NBS Kimberlite	1.2	1.1
Conway granite		
54-S-137	4.6	4.5
54-S-121	4.7	4.6
54-S-128	4.3	4.7
54-S-109	4.2	4.5

The standard rock samples from the National Bureau of Standards (NBS) were analyzed for radium by the Bureau and by other laboratories. Analyses were also provided for potassium but not for thorium. The author analyzed the Palisade diabase for radium and thorium by radon and thoron alpha counting (Hurley and Goodman, 1941). The samples of Conway granite were supplied and analyzed for uranium and potassium by members of the U. S. Geological Survey. No thorium analyses were available on these. The results show agreement within the expectable error.

Since thorium analyses of common rocks by other methods are difficult to make, reliably analyzed samples were not available for this test. However, there is no reason to expect that the accuracy of a thorium analysis by this method will be less than the accuracy of a uranium analysis if the calibration standards are correct and if the thorium activity in the rock is similar to the uranium activity. Fortunately this last condition is true in most common rocks.

Operating Procedure and Error

The gain controls and voltage on the photomultiplier tube are adjusted experimentally to give optimum response and to cover the range of the spectrum that is of interest within the maximum spread of the base-level discriminators. This is done to spread the low-energy part of the spectrum. Pulses are shaped with minimum rise time available. Zero points for each high-level discriminator are determined by a plot of count versus channel width in a flat part of a spectrum. The correlation of base-level discriminator voltage with gamma energy is established by use of gamma sources of known energy, although this is not necessary if the uranium and thorium series spectra are plotted in terms of base-level voltage because settings for the different channels are adjusted to lie on the tops of the peaks of K^{40} and Pb^{212} and the bottom of the valley immediately below Pb^{212}. For this work over-all gain is adjusted so that 1 per cent of the base-discriminator range is equivalent to about 25-kev gamma energy. A lower ratio could be used if potassium were not being measured.

Instrument drift is critical in attempts to stay close to the top of a peak, so it is neces-

sary to run standards at frequent intervals. Rather than change all calibration constants slightly for each run, it is more convenient to find an average value for each constant and use these as arbitrary constants for each channel. All readings on samples are corrected according to the amount the standard source is above or below this arbitrary value at that time. This process removes the effect of long-period drifting above or below the arbitrary value. Short-period drifting can be offset only by voltage regulation and repeated analyses.

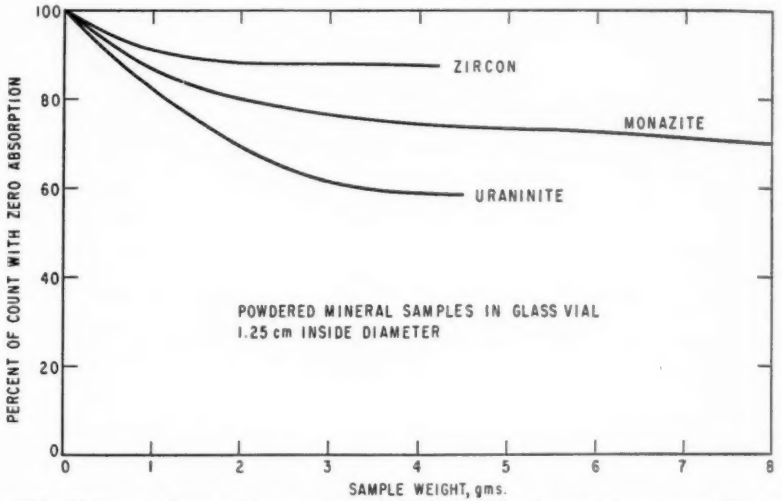

FIGURE 3.—EFFECT OF SOURCE ABSORPTION IN THICK SOURCES OF HEAVY MINERALS IN WELL-TYPE CRYSTAL

The equivalent uranium, or uranium plus thorium equivalent in activity, can be obtained more precisely than the separate values for uranium and thorium. A small error in the channel-1 or -2 counts will cause a relatively larger error in the ratio of thorium to uranium. As other methods of thorium analysis are so tedious, it would be worth while to combine this method with a separate uranium analysis on the sample in order to gain the great improvement in precision, if the thorium analysis is the principal objective.

Estimated expectable error of analysis as a function of the proportion of uranium or thorium in the sample, illustrated in Figure 7 of Part I of this report, applies to determinations in common rocks, except that an error in potassium determination will contribute errors of the same sign in the channel-1 and channel-2 readings. Effect on the ratio will be slight. Also the lower count-to-background ratio in these low-activity samples substantially increases the standard deviations of the net counts. As the last factor can be partly compensated for by longer runs, errors in a single measurement on a sample containing a few ppm of uranium and thorium should be less than twice those given in Figure 7 of Part I and should be the same function of the Th/U ratio.

A normal granite will run 20 to 60 counts per minute above a background of 14 counts per minute in channels 1 and 2 and about 10 counts per minute above a background of 8 in channel 3. The standards are made to have high counting rates, and a 10-minute run is sufficient. The total time for the measurement of uranium, thorium, and potassium in a granite sample is commonly about 2 hours for a single-crystal counter, and total time required of the analyst is about 15 minutes.

SMALL SAMPLES OF INTERMEDIATE GRADE

Samples containing more than 100 ppm of uranium or thorium and their series in equilibrium may be assayed for these constituents

in quantities of only 1–10 gm. The sample is carried in a glass bottle (1½-cm outside diameter) that fits into a well-type scintillation crystal. The potassium contribution is negligible at this level of activity. A method of analyzing ore-grade samples of uranium- and thorium-bearing materials described in Part I eliminates source absorption by use of a small-bore sample holder and a sample of about 200 mg. When 1 or more gm is assayed, it is necessary to correct for source absorption.

The curves in Figure 3 indicate for samples of different materials the variation in counting rate per gram as the sample size is increased. A set of such curves covering the range of materials to be analyzed provides corrections for source absorption. For any weight of unknown the increase in counting rate with no source absorption is obtained from the appropriate curve.

Other Geological Applications

Instrument drift that causes a single channel to shift off a peak can be eliminated largely by covering a width greater than the peak by more than 1 channel. Instruments are now being made that have as many as 50 channels. With such an instrument the entire spectrum can be plotted in detail and compared with a similarly plotted spectrum for the standard. Recording counting-rate meters will give a continuous plot of the activity in any channel, and the ratios of channels can also be recorded. Counting rates can be increased by larger crystals or several crystal sources feeding into the single spectrometer. Larger crystals will will also increase the amplitude of the photopeaks relative to scattered background.

With these possibilities it is feasible to make devices that will continuously record the grade of ore in a mill or serve as quality-control or monitoring devices for a variety of materials that contain any or all these constituents. Uranium ores, monazite sands, and potassium salts in brine are obvious examples. In continuous recording it is essential that the thickness of the stream of material is thin enough so that photopeaks are not obliterated by Compton-scattered radiation. This can be done by surrounding the crystal through which the material passes with an annular source volume. The spectrometer can be used in stratigraphic correlation or mapping in which chemical variations involving these constituents form the basis of the lithologic units. The U/Th ratios in many shales are known to be related to distance offshore of depositional site. An investigation is being conducted on the measurement of Th^{230} in ocean core material utilizing the 68-kev peak of Th^{230} that appears in the spectrum and eliminating the contribution from interfering photons of nearly the same energy by a separate determination of Th^{232}.

References Cited

Hurley, P. M., 1956, Direct radiometric measurement by gamma-ray scintillation spectrometer Part I: Uranium and thorium series in equilibrium: Geol. Soc. America Bull., v. 67, p. 395–404

Hurley, P. M., and Goodman, C., 1941, Helium retention in common rock minerals: Geol. Soc. America Bull., v. 52, p. 545–559

U. S. Geological Survey, Washington 25, D. C., and Massachusetts Institute of Technology, Cambridge 39, Mass.

Manuscript Received by the Secretary of the Society, September 22, 1955

Publication Authorized by the Director, U. S. Geological Survey

BULLETIN OF THE GEOLOGICAL SOCIETY OF AMERICA
VOL. 67, PP. 413-434, 6 FIGS., 3 PLS. APRIL 1956

ORIGIN OF THE CHUSKA SANDSTONE, ARIZONA–NEW MEXICO: A STRUCTURAL AND PETROGRAPHIC STUDY OF A TERTIARY EOLIAN SEDIMENT

By H. E. Wright, Jr.

Abstract

The Chuska sandstone as here restricted forms the cap rock of the Chuska Mountains, which extend 60 miles along the Arizona-New Mexico State line north of Gallup, New Mexico. Its maximum preserved thickness is about 1750 feet. It is unfossiliferous, cross-bedded throughout, and contains no shale or conglomerate interbeds; there are several thin ash beds. The cross-bedding dips consistently in the northern quadrants at angles around 25°. Alternating strong to weak chalcedonic and opaline cement in thick layers throughout the formation provides a topography of alternating resistant ledges and gentle slopes.

Rosiwal analyses of four samples averaged 74 per cent quartz and 23 per cent feldspar. Sixteen samples have an average median diameter of 0.21 mm and are well sorted and slightly skewed. These values are compared with those of eolian sands described in the literature, and an evaluation is made of the use of particle-size parameters as criteria for postulating depositional environment.

The average intercept sphericity for 8 samples is 0.78; the average roundness for 15 samples is 0.51. Nine samples showed that an average of 29 per cent of the grains had frosted or pitted surfaces. Shape, roundness, and frosting are probably inherited from source sediments.

The nature of the cross-bedding and the uniformity of texture imply accumulation of dune sand by winds from the south-southwest. Available median diameters, sphericities, roundness, and frosting were plotted against distance in the presumed direction of transport. No firm trends are evident in the 38 miles between outside samples.

The restricted Chuska sandstone and the underlying fluvial Deza formation, together forming Gregory's Chuska sandstone, truncate the Mesaverde group (Upper Cretaceous) and are unconformably overlain by middle or upper Pliocene volcanics. The suggested Miocene (?) age is based on physiographic data.

CONTENTS

TEXT

	Page
Introduction	414
Acknowledgments	414
General description	414
Outline of study	416
Cross-bedding	416
General description	416
Field measurement and graphical analysis	416
Interpretation	417
Conclusions	418
Mineralogy of the clastic grains	419
Particle size	419
General	419
Methods and results	419
Significance of results	423
General	423
Sorting and median grain size	423
Skewness	425
Relation of particle size to direction of transport	427
Sphericity, roundness, and frosting	427
Age and correlation of the Chuska sandstone	427
Introduction	427
Correlation with San José formation	428
Correlation with Pliocene sediments	428
Introduction	428
Lithologic comparisons	428
Relation to volcanics	429
Underlying erosion surfaces and drainage development	429
Conclusions	431
References cited	432

ILLUSTRATIONS

Figure — Page
1. Geologic map of Chuska Mountains showing locations of samples ... 415
2. Analysis of cross-bedding of Chuska sandstone ... 418
3. Histograms of clastic grain size for Chuska sandstone ... 421
4. Cumulative curves of clastic grain size for Chuska sandstone ... 422
5. Graph of particle size, shape, roundness, and frosting plotted against distance in direction of transport ... 425
6. Geologic cross sections from Black Mesa, Arizona, to San Juan Basin, New Mexico ... 426

Plate — Facing Page
1. Tertiary sediments unconformable on Mesozoic rocks ... 416
2. Chuska Mountains and Chuska sandstone ... 417
3. Map of parts of northeastern Arizona and northwestern New Mexico showing distribution of Cenozoic rocks ... 426

TABLES

Table — Page
1. Mechanical composition and the size and shape parameters of Chuska sandstone ... 420
2. Summary of particle-size analyses of eolian sands from different areas and certain water-laid sands ... 423

Introduction

The Chuska Mountains are a narrow highland about 60 miles long on the Navajo Indian Reservation extending N-NW across the Arizona-New Mexico State line (Fig. 1). The range is capped by resistant ledges of Chuska sandstone, which rests unconformably on the east-dipping Mesozoic formations of the Defiance monocline and adjacent structures. This isolated area of Tertiary sediments is one of few on the Colorado Plateau, and knowledge of its characteristics and origin aids in reconstructing the Cenozoic physiographic and structural history of the Plateau Province.

Gregory's report (1917) on the geology of the Navajo Country served as the starting point of the present investigation, although the Chuska Mountains had been mentioned in the earlier geographical surveys of the Southwest. Recent work in the area has concerned primarily Mesozoic stratigraphy and Tertiary volcanic rocks.

Acknowledgments

The writer first visited the Chuska Mountains with Kirk Bryan in 1940. Field work was done in 1946, 1949, and 1950 with the aid of grants from The Geological Society of America and the Graduate School of the University of Minnesota. Field assistants were H. T. Ames and J. H. Birman in 1946, R. M. Becker and R. H. Cress in 1949, and C. R. Appledorn, E. H. Hughes, K. F. Johnson, and A. V. Martini in 1950. J. H. Birman made the sieve analyses of the Chuska sandstone at Brown University. Aerial photographs for use in the field were kindly loaned by the Navajo Indian Service, Window Rock, Arizona. To all these individuals and organizations the writer is grateful. He is obliged also to J. E. Allen, New Mexico Bureau of Mines and Mineral Resources, for supplying unpublished information on his recent mapping in the Tohatchi area (Allen and Balk, 1954).

General Description

The Chuska Mountains have a fairly flat crest 8500–9500 feet above sea level and stand about 4000 feet above the San Juan Basin on the east and 2000 feet above the Defiance Plateau on the west. They are covered with a heavy stand of Western Yellow Pine above about 7000 feet. The crest is dotted with small lakes and swamps possibly connected with Pleistocene periglacial frost action. The scarps on both sides of the range are indented by short canyons, but along the east flank south of Toadlena landsliding of Chuska sandstone over Cretaceous shale has prevented development of important stream canyons (Pl. 2, fig. 1).

The Chuska sandstone is underlain conformably at the southern end of the range by about 250 feet of horizontally bedded fluvial sand constituting the Deza formation (Wright, 1954). This rests unconformably on various Mesozoic formations, including the Tohatchi formation, described by Gregory as the basal Tertiary sediment in this area but by Allen (1953) as a conformable formation in the Mesaverde group (Upper Cretaceous).

Other formations underlying the Deza and Chuska formations include the Triassic Chinle shale; the Jurassic Wingate, Carmel, Entrada,

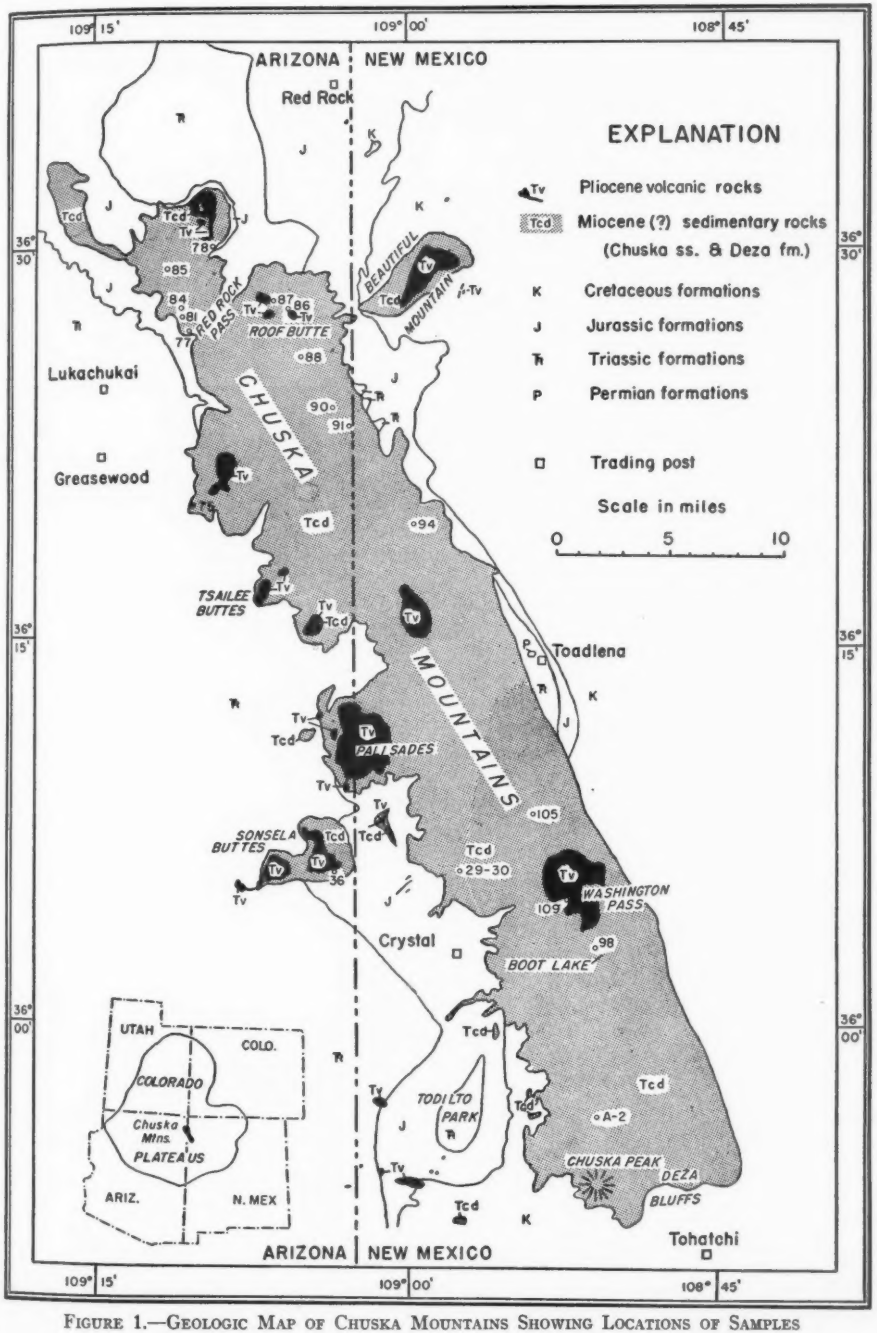

FIGURE 1.—GEOLOGIC MAP OF CHUSKA MOUNTAINS SHOWING LOCATIONS OF SAMPLES

Todilto, Summerville, and Morrison formations; and the Cretaceous Dakota (?) sandstone and Mancos shale (Wright and Becker, 1951). The erosion surface on which the Tertiary sediments rest is about 7650–7900 feet above sea level. Local relief of 50 feet on this unconformity can be seen on the buried hogbacks of Cretaceous sandstone east of Todilto Park (Pl. 1).

The Chuska sandstone over most of the mountains is 500–1200 feet thick. Greater thicknesses are preserved where it is capped by younger volcanic rocks, but even there the sandstone had been eroded before burial or intrusion. At Roof Butte, east of Lukachukai, about 1750 feet of Chuska sandstone is preserved, plus about 150 feet of Deza formation. Almost as much is preserved a few miles north where a dike has protected the upper sandstone from erosion.

The Chuska sandstone is buff to white, fine- to medium-grained, and cross-bedded. No shale or conglomerate was found in the sandstone, but horizontal layers of white unlaminated volcanic ash a few feet thick were found at five localities. Successive layers of sandstone averaging 30–50 feet thick are alternately well cemented and poorly cemented and form alternating cliffs and slopes on the flanks of the Chuska Mountains.

Outline of Study

This paper is concerned primarily with an analysis of the cross-bedding, the petrography of the clastic grains, and the age and correlation of the Chuska sandstone. The cement, which consists of bands of chalcedony and opal with minor amounts of microcrystalline quartz, normal quartz, and heulandite (Wright, 1951), will be considered in a subsequent article. Full treatment of the genesis of this cement involves the background offered in this paper on the origin of the sediment.

Cross-Bedding

General Description

The Chuska sandstone is cross-bedded throughout most of its vertical and lateral extent in both the well-cemented and poorly cemented zones. In only a few exposures noted are the sands horizontally bedded.

The cross-bedded units range from 5 to 15 feet thick. Individual laminae visible on most outcrops because of differential weathering or iron staining probably reflect differential wind-packing, grain size, and cementation (Pl. 2, fig. 2). Laminae range from a millimeter to a few inches thick and can be traced as far as 50 feet across some outcrops. The laminae are concave upward, and their changing dip makes them tangent at the base of the unit and truncated at the top. Some cross-bedded units can be followed 150 feet across the breadth of outcrops; and the dip direction of laminae in some places changes as much as 55°.

Finer lamination is visible in some hand specimens, especially under fluorescent light, which reveals the variable content of opaline cement. In some thin sections laminae several grains thick are visible because of slight differences in grain size. No textural gradation was noted.

No ripple marks, rain imprints, footprints, or similar primary structures were found on planes of laminae.

Field Measurement and Graphical Analysis

Several hundred measurements of cross-bedding were made in the Chuska sandstone. One special group of 157 readings was taken in an area, 1.3 by 0.6 miles, around Boot Lake, 2 miles south of Washington Pass. This area is about 8750 feet above sea level, and the beds exposed are about 1000 feet above the base of the formation. About 100 of the readings represent two observations each from 50 outcrops

---

Plate 1.—TERTIARY SEDIMENTS UNCONFORMABLE ON MESOZOIC ROCKS

Todilto Park near southwest end of Chuska Mountains. Todilto Park dome is a small structure along the Defiance monocline. Unconformable contact is shown by inked line. (Photos 5014–16, Navajo Reservation, by Soil Conservation Service, U. S. Dept. Agric.)

TERTIARY SEDIMENTS UNCONFORMABLE ON MESOZOIC ROCKS

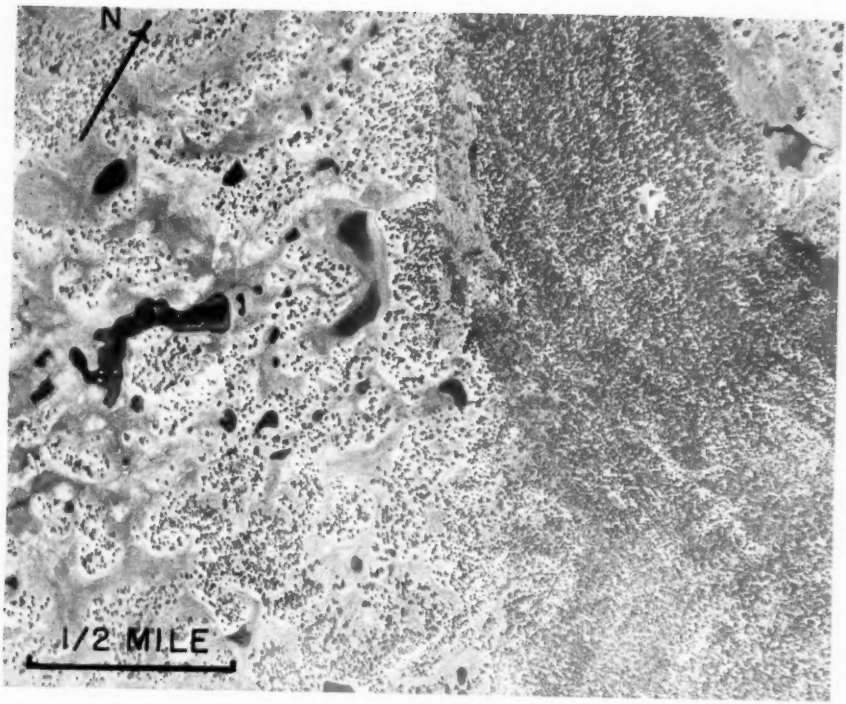

FIGURE 1

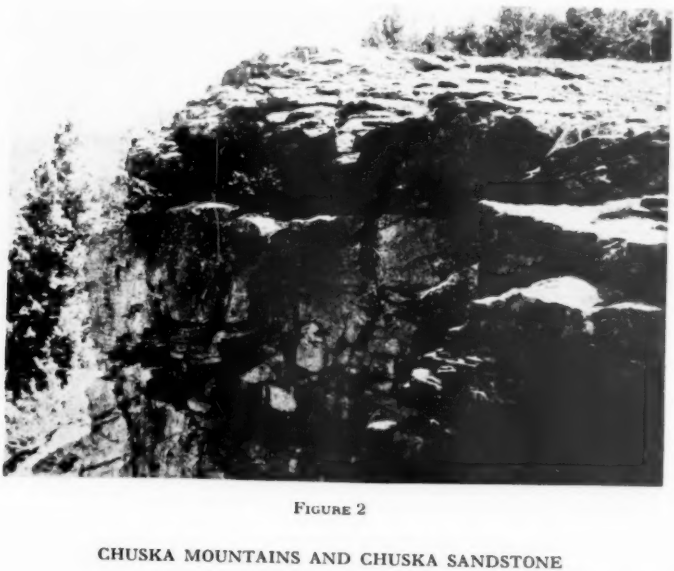

FIGURE 2

CHUSKA MOUNTAINS AND CHUSKA SANDSTONE

in which the dip attitude in a single unit changes across the outcrop by 5°–55°. Dip directions were read to the nearest 5° and plotted on a rose-type diagram in 10-degree sectors (Fig. 2). Dip angles were read to the nearest 2°; on the rose diagram the average dip angle for each 10-degree sector of dip direction is shown by figures around the circumference. The curve below the rose diagram shows the frequency of dip amount (without regard to direction) plotted in 5-degree intervals.

An additional 176 readings of cross-bedding were selected to represent the entire formation and plotted separately (Fig. 2, left). At those localities where the dip angle changes across the outcrop the maximum angle was measured. About two-thirds of the readings were taken on the crest of the southern half of the range, which has better and more accessible exposures, and represents beds 500–1000 feet above the base of the formation. Few readings could be made on weakly cemented layers because of inadequate exposures, particularly in the lower few hundred feet of the formation. However, the similarity of the two sets of diagrams suggests that the cross-bedding of the entire formation has the same characteristics as that in the area of detailed sampling at Boot Lake.

The rose diagrams show that practically all dip directions are in the northern hemicircle. Each diagram is roughly symmetrical about a line oriented about N. 20° E.

The histograms and frequency curves of dip angles show that the maximum percentage of dips lies in the 23- to 27-degree range. The mode thus is about 25°. Average dip is 22° for the entire Chuska sandstone and 23° for the Boot Lake area. Cumulative curves show that 50 per cent of the dip angles are in the range 15°–25° for the entire formation and 17°–25° for Boot Lake and that the median dips are 20° and 21° respectively. These figures and the shape of the frequency curves show a greater spread of low dips than of dips near the maximum angle of repose of dry sand (34°).

Notations of average dip amount for each 10-degree sector of dip direction on the diagrams show that there is no consistent relation between dip amount and dip direction.

Interpretation

Uniformity of dip direction and dominance of dip angles in the range of 15°–25° indicate that the Chuska sandstone was deposited by wind rather than water. The high dip angles also suggest that the laminae were formed on the lee slopes rather than the windward slopes of dunes. A secondary maximum of relatively low dips in the direction opposite the maximum (*i.e.*, on the windward side), identified by Shotton (1937) for the Lower Bunter sandstone in England, could not be recognized in the Chuska sandstone. The dunes must have migrated at a moderate rate so that windward-slope laminae were eroded by the progression of the dune. Deposition would have been on the lee (north) side of the crest by accretion at moderate angles, with some development of a slip face in the area of maximum deposition to produce dips reaching the angle of repose (34°) (Bagnold, 1941, p. 241). No explanation is offered for the 5 per cent of dips exceeding 34°. There is no perceptible regional dip to the formation that could produce a general steepening of all cross-laminations.

If the dunes had been longitudinal, they would have two maxima in opposite directions representing the two flanks. They are interpreted instead as crescentic, the two wings being represented in the rose diagrams by the two lateral maxima. These lateral maxima

PLATE 2.—CHUSKA MOUNTAINS AND CHUSKA SANDSTONE

FIGURE 1.—Crest and east scarp of Chuska Mountains 2 miles south of Washington Pass. Boot Lake near west edge. Origin of lakes is unknown but may be related to Pleistocene frost action (nivation). Heavily wooded east scarp is about 1000 feet high; faint parallel stripes show ridges and troughs believed to result from slumping of strips of Chuska sandstone over Cretaceous shale. (Photos 5268–69, Navajo Reservation, by Soil Conservation Service, U. S. Dept. Agric.)

FIGURE 2.—Ledge of cross-bedded Chuska sandstone capping Chuska Mountains south of Washington Pass.

suggest that the wings enclosed an arc of about 120°, although the maximum measured curvature on single outcrops was only 55°. The

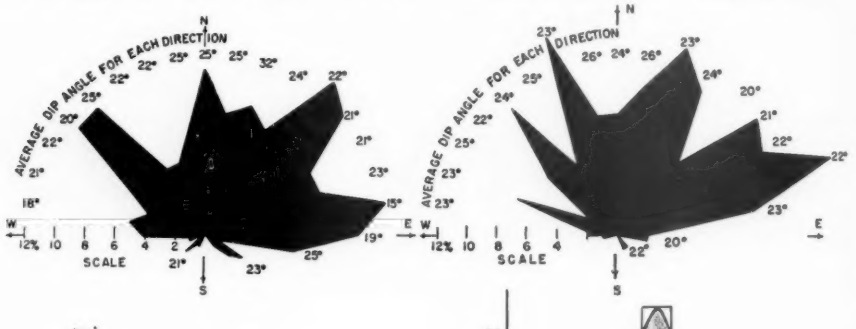

FIGURE 2.—ANALYSIS OF CROSS-BEDDING OF CHUSKA SANDSTONE

Rose diagram for dip direction; frequency curve for dip amount. *Left*, 176 measurements over entire Chuska Mountains. *Right*, 157 measurements in Boot Lake area, 2 miles south of Washington Pass.

direction of curvature on such outcrops indicates that the crescents were concave to the north (leeward). The dunes therefore were transverse rather than parabolic (Hack, 1941) and may be considered barchans with only moderate development of the slip face.

The cross-bedding of the Chuska sandstone resembles that of the Lower Bunter sandstone of England (Shotton, 1937) and that of the Coconino sandstone of Arizona (Reiche, 1938), the subjects of the only two statistical studies of eolian cross-bedding known to the writer. The Lower Bunter sandstone (Triassic), where studied by Shotton in outcrop and in a boring, consists of 850 feet of cross-bedded red sandstone without shale beds or pebble beds. The particle-size characteristics suggested eolian deposition to Shotton, and rose diagrams of dip direction were used to show the orientation of inferred barchans. The maximum of the frequency curve for lee-slope dips determined by Shotton is 26°, and the curve resembles the two Chuska sandstone curves.

The Coconino sandstone (Permian), 1000 feet thick in places, is massively cross-bedded. The eolian origin shown by McKee (1934) was confirmed by the statistical study of the cross-bedding by Reiche (1938). Reiche measured the cross-bedding at 23 localities across northern Arizona and showed that at each locality 90 per cent of the dip directions lay within an arc of 80°–232°. The wind directions indicated were from the north in some areas, and northwest and northeast in others. An angle of about 140° between limbs of the barchans was inferred, and actual angles of 45°–96° were measured on outcrops.

Conclusions

The area of deposition of the Chuska sandstone is visualized as a desert basin, at least 60 miles from north to south, with sand rapidly accumulating as a complex of slowly migrating transverse dunes. Modern dunes of this type in north-central Arizona are formed best under conditions of abundant sand supply, moderate winds, and deficient vegetation (Hack, 1941, p. 260). At least 1750 feet of eolian sand piled up in the basin after the interval of fluvial deposition marked by the Deza formation, and

little change in conditions occurred during the eolian activity.

Mineralogy of the Clastic Grains

The Chuska sandstone consists primarily of grains of quartz and feldspar with minor amounts of chert, quartzite, and sparse heavy minerals. Rosiwal analyses of four well-indurated samples showed:

Sample Number	78	84	86	98	Average
Quartz	82%	74%	69%	74%	74%
Feldspar	14	21	30	26	23
Other	4	5	1	—	3

No firm explanation for the high feldspar content is offered. The analysis of cross-bedding indicates that the sands were blown from the south-southwest, where at present there are broad outcrops of Mesozoic and Permian rocks, areas of Tertiary fluvial sediments west of the Zuni Mountains, and the volcanics of the Datil-Mogollon field. Mineralogical analyses of 42 samples of Permian and Mesozoic rocks from measured stratigraphic sections in Todilto Park, near the southwest end of the Chuska Mountains, by Willard (Allen and Balk, 1954, p. 139–149) show that some sandstones and siltstones of the De Chelly sandstone (Permian), the Jurassic formations, and the Mesaverde group have 7–20 per cent feldspar, whereas those of the Triassic formations, the Dakota (?) sandstone, and other units of the Mesaverde group have little feldspar.

The Tertiary sediments west of the Zuni Mountains are an extension of the Pliocene Bidahochi formation of the Hopi Country (Repenning and Irwin, 1954). They were derived in part from the granite core of the Zuni Mountains and probably have a high feldspar content. However, they are younger than the Chuska sandstone as here correlated and are not a possible source. During the Miocene (?), at an earlier stage of physiographic development, a comparable set of sands might have been washed into this area, blown north-northeastward, and deposited as the Chuska sands. It is unlikely, however, that the Chuska sands had any such source, because a single cycle of fluvial and eolian transport is probably insufficient to account for the high degree of sphericity and rounding in the Chuska sands. Twenhofel (1946a) observed that Oregon coastal beach sands and dune sands are still subangular after hundreds of miles of transport from crystalline source rocks in the Columbia River headwaters.

A third possible feldspar-rich source of the Chuska sands is the early-middle Tertiary intermediate volcanic rocks of the Datil-Mogollon area more than 125 miles south of the Chuska Mountains. The same objection applies here as to the Zuni granite sands: the insufficiency of single-cycle transport to produce rounded subspherical shapes, although the distance involved is greater. Furthermore, one might expect a higher content of heavy minerals in single-cycle transport from volcanic terrane.

Although no mechanism for the apparent enrichment of feldspar can be proposed, the most likely source for the Chuska sands is the Jurassic and some Cretaceous sandstones which were widely exposed during the Miocene (?) in the area south of the Defiance uplift. Willard's analyses (Allen and Balk, 1954, Pl. 14) show that the Jurassic sands, many of which are eolian, have the least angularity and a moderately high feldspar content. The high degree of roundness and sphericity of the Chuska sands probably is largely inherited from source sands. Until further analyses are available these Jurassic formations appear to be the most likely sources for the Chuska sands.

Particle Size

General

The Chuska sandstone is texturally uniform. No beds of clay, silt, coarse sand, grit, or conglomerate were found. This uniformity and the analysis of the cross-bedding strongly indicate eolian origin. The particle-size analysis was made to examine more exactly the size parameters of such a large body of eolian sand and to determine possible progressive changes in direction of transport.

Methods and Results

Particle-size analyses were made on 16 representative spot samples of Chuska sand-

TABLE 1.—MECHANICAL COMPOSITION AND THE SIZE AND SHAPE PARAMETERS OF CHUSKA SANDSTONE

Sample No.	A-2	29	30	36	75	77	81	84	85	87	88	90	91	94	105	109	Range	Ave.
Distance from S. end of mtns. (miles)	5	16	16	16	32	40	41	41	43	41	39	36	35	31	17	15		
Elevation	8700	8460	8590	8360	7820	7680	8620	8750	8590	8720	8790	8170	8360	8770	8700	8300		
Size grades (mm)																		
.991–.701	.2	.9		.2	.2											.3		
.701–.495	3.8	19.7		.9	3.6	.2	.1				.1	.5	.3	.4		11.6		
.495–.350	22.0	52.9	.3	5.5	18.5	.3	2.9	.5	3.0	1.0	1.6	9.5	11.0	1.1		31.3		
.350–.250	34.1	22.9	9.3	17.7	13.9	1.2	18.9	8.7	15.7	26.6	62.4	29.0	41.6	11.5	1.5	17.6		
.250–.177	14.4	1.3	47.5	23.5	13.4	35.9	20.4	33.6	23.1	29.8	19.5	15.9	28.4	48.7	18.1	12.8		
.177–.125	13.4	.4	35.5	24.0	23.6	42.4	25.8	40.9	26.0	18.4	5.4	19.2	12.9	30.4	50.7	12.7		
.125–.088	7.7	.5	6.5	19.4	17.4	13.5	19.1	9.7	18.6	15.2	4.0	17.0	4.4	5.7	23.0	7.6		
.088–.062	3.4	.6	.8	7.0	8.0	4.2	9.8	4.4	7.9	7.1	3.7	7.5	1.3	1.9	4.9	4.4		
.062–.038	1.0	.8	.1	1.8	1.4	2.3	3.0	2.2	5.7	1.9	3.3	1.4	.1	.3	1.8	1.7		
Total	100.0	100.0	100.0	100.0	100.0	100.0	100.0	100.0	100.0	100.0	100.0	100.0	100.0	100.0	100.0	100.0		
< .038 mm	1.4	3.3	2.3	6.2	1.4	4.8	5.0	2.7	11.5	1.4	6.8	2.4	0.0	0.1	4.3	4.0		
Consolidation	Fri.*	Fri.	Fri.	Firm	Loose	Firm	Fri.	Firm	Firm	Loose	Firm	Loose	Loose	Loose	Firm	Firm		
Q_1	.354	.490	.220	.246	.330	.197	.235	.210	.227	.255	.309	.295	.310	.230	.168	.427		
M	.280	.410	.185	.170	.175	.160	.158	.165	.156	.190	.235	.195	.258	.188	.144	.301	.14–.41	.21
Q_3	.175	.346	.148	.118	.121	.131	.110	.135	.108	.126	.211	.123	.180	.150	.108	.169		
So	1.45	1.19	1.18	1.44	1.65	1.23	1.46	1.25	1.45	1.42	1.21	1.55	1.32	1.24	1.25	1.19	1.18–1.65	1.34
Sk	−.79	+1.01	−.95	1.00	+1.31	+1.01	+1.03	+1.04	+1.01	−.89	+1.18	−.95	−.85	−.98	−.87	−.80	.79–1.31	.98
Sphericity†	.78	.79			.78	.77	.78		.81			.78				.73	.73–.81	.78
Roundness†	.54	.53	.52	.55	.49	.44	.52	.52	.50	.50	.51	.50	.52			.51	.44–.55	.51
Frosting %†	32	26			18	31	17	41	38			24				46	18–46	29

* Friable.

† On size grade .350–.495 mm.

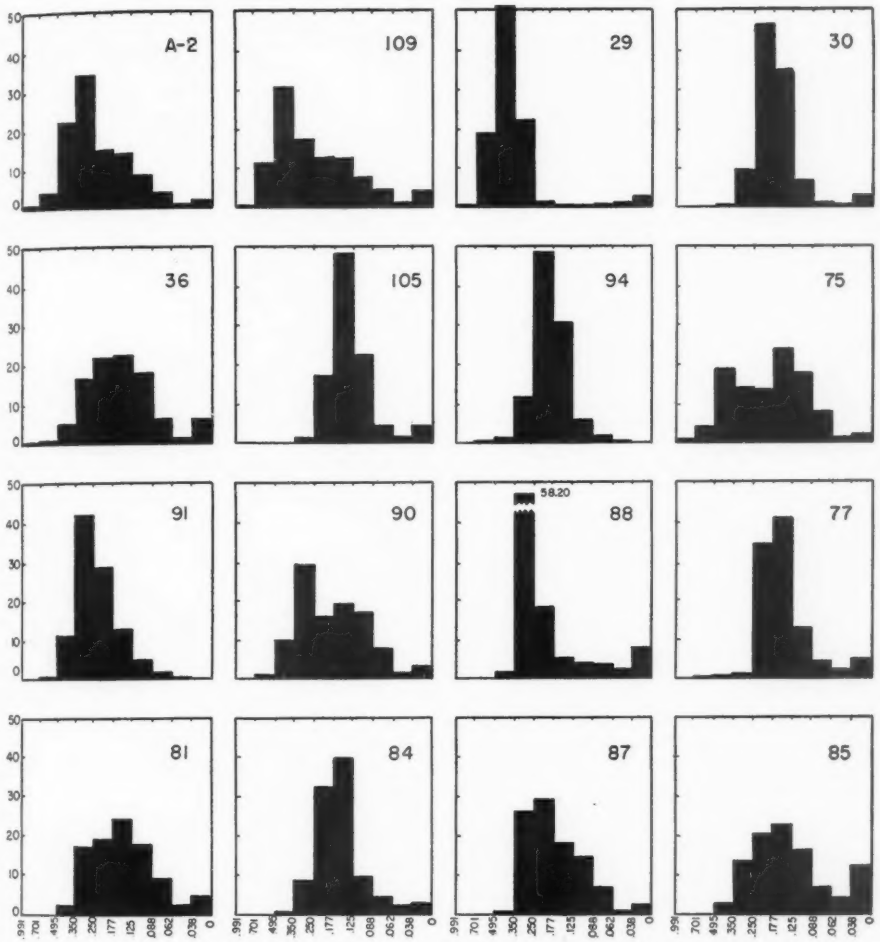

FIGURE 3.—HISTOGRAMS OF CLASTIC GRAIN SIZE FOR CHUSKA SANDSTONE

Samples are arranged in increasing distance from south end of mountains. For locations of samples, see Figure 1.

stone, each sample weighing about 500 grams. Six samples were loose sand which could be sieved without special preparation. Three samples were moderately consolidated and were prepared for analysis by prolonged soaking followed by rubbing between wooden blocks. The remaining seven samples, more firmly cemented with silica, were given an initial 2-day soaking in concentrated sodium hyposulfite and dried to allow the force of crystallization of the "hypo" to disaggregate the grains.

Samples prepared were quartered to about 50 grams and sieved through Tyler screens with a Ro-Tap shaker. Fractions were examined under a microscope for aggregate clastic grains.

The percentage weights of each fraction are shown in Table 1 and on histograms (Fig. 3). The relatively high weight percentages in the <.038-mm fraction result from the high content of fragmented cement. The quantity is greater in the more strongly cemented samples, as is shown by the Consolidation line in Table 1. Each analysis was recalculated without the cement-rich <.038-mm fraction, and it appears

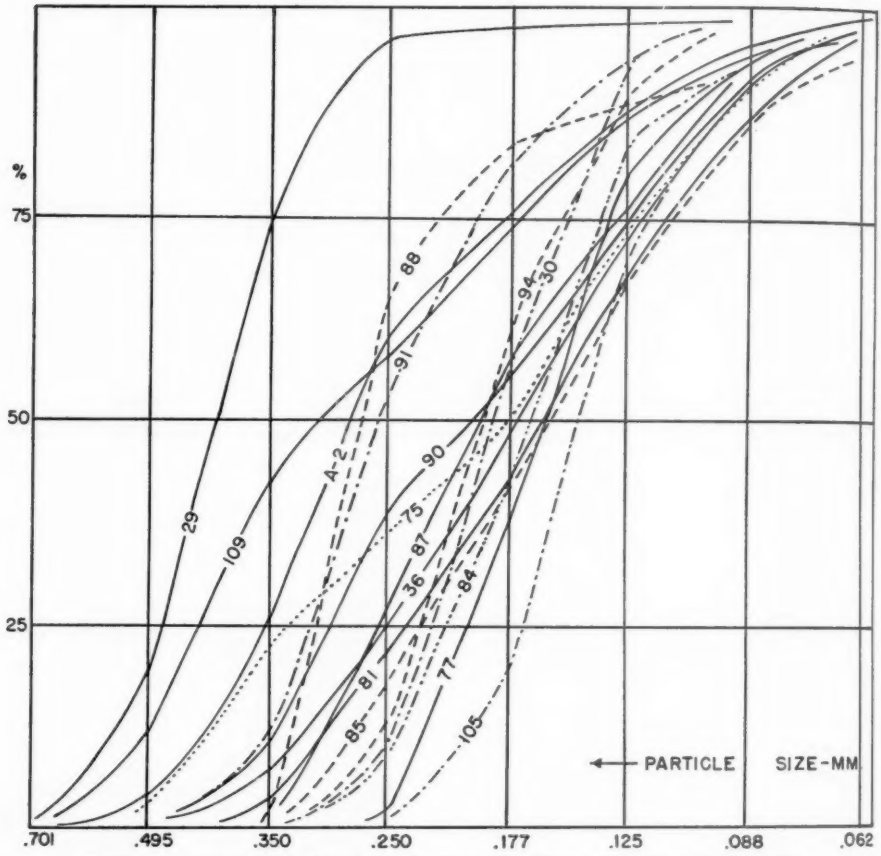

FIGURE 4.—CUMULATIVE CURVES OF CLASTIC GRAIN SIZE FOR CHUSKA SANDSTONE

in this form in Table 1 and in the cumulative grain-size curves (Fig. 4). Although the .038- to .062-mm fraction also contains some fragmented cement, it was not eliminated in the recalculation, and the curves may hold a slight error.

The median grain size for the 16 samples of Chuska sandstone averages 0.21 mm. The median ranges between 0.14 and 0.30 mm, except for 1 at 0.40 mm.

The histograms of 2 samples (75, 90) show double maxima. These are a result of textural lamination, which is visible in some thin sections. Lamination also appears in some hand specimens under ultraviolet light because of the fluorescence of opal-chalcedony cement, which is more prominent in the coarser laminae.

Sorting was determined by computation of Trask's coefficient ($So = Q_1/Q_3$), where So is unity for perfect sorting. In the 16 samples of Chuska sandstone So ranged from 1.18 to 1.65 with an average value of 1.34 (Table 1).

Skewness was computed by Trask's coefficient, $Sk = Q_1Q_3/M^2$, in which $Sk > 1$ denotes samples skewed on the coarse side of the median, and $Sk < 1$ indicates sand rich in fines. Skewness in the 16 samples of Chuska sandstone ranged from 0.79 to 1.31 (Table 1) and averaged 0.98. Skewness values of 0.95 to 1.05 are within the limits of error of mechanical analysis and construction of the cumulative curves. If these values are eliminated, 5 remaining samples are skewed on the fine side, and 2 on the coarse side.

TABLE 2.—SUMMARY OF PARTICLE-SIZE ANALYSES OF EOLIAN SANDS FROM DIFFERENT AREAS AND CERTAIN WATER-LAID SANDS

	No. of samples	Median M		Sorting SO		Skewness Sk		Strongly skewed*	F:C Ratio†
		Range	Avg.	Range	Avg.	Range	Avg.		
Eolian Sands									
1. Eolian sands of Syria, etc. (Dapples, 1941)	13	.15–.31	.23	1.17–1.74	1.39	.81–1.28	1.01	4+ 5–	
2. Inland dunes** (Udden, 1914)	37	.16–.32	.20	1.20–1.57	1.34	.87–1.48	1.04	8+ 2–	7:30
3. Coastal dunes, Oregon (Twenhofel, 1946a)	19	.16–.31	.22	1.17–1.44	1.30	.93–1.09	.99	2+ 3–	11:8
4. Coastal dune, England (Barrett, 1930)	7	.25–.28	.26	1.11–1.18	1.14	.96–1.06	1.05	4+ 0–	1:6
5. Inland and coastal dunes (Keller, 1945)	446								351:95
6. Lower Bunter ss. England (Shotton, 1937)	27	.13–.41	.20	1.18–1.61	1.41	.73–1.13	.96	4+ 9–	
7. Chuska ss.	16	.14–.41	.21	1.18–1.65	1.34	.79–1.31	.98	2+ 5–	8:8
Water-laid Sands									
8. Marine sands, Cape Cod Bay with M = .15–.30 (Hough, 1941)	22	.15–.30	.21	1.17–1.90	1.41	.72–1.50	1.02	5+ 3–	
9. Marine sands, many localities, with M = .15–.30 (Trask, 1932)	14	.15–.30	.17	1.26–4.14	1.98	.39–1.89	.89	2+ 9–	
10. Mississippi R. bed sediment near New Orleans (Inman, 1949)	?		.19		1.21		.99		

* Number of samples skewed on coarse side (+) or fine side (−) of median, excluding Sk = .95–1.05.

† F or C stands for samples in which the size grade with the second highest percentage is on the fine or coarse side respectively of the maximum percentage.

** Sample 221 omitted because percentages in mechanical analysis totaled 109 per cent.

Significance of Results

General.—In Table 2 the average value and range of values for median grain size, sorting coefficient, and skewness coefficient were copied directly or calculated from published data on other eolian sandstones. The values are closely comparable, and those of the Chuska sandstone are typical of the group. The median grain sizes fall in the boundary range between fine sand (.125–.250 mm) and medium sand (.250–.500 mm), and the values of the sorting coefficient are not far from unity.

Sorting and median grain size.—According to Trask's (1932, p. 72) measure of the degree of sorting (*So* < 2.5 for well sorted, *So* = 2.5–4.5 for normally sorted, *So* > 4.5 for poorly sorted), the eolian sandstone samples listed in Table 2 are well sorted. This measure is not, however, particularly relevant to a comparison of eolian, fluvial, and marine sand for it is based on 170 samples showing a wide but unevenly distributed range of median diameters from coarse sand to fine clay. Several studies have shown that fine- and medium-grained sand has better sorting than coarser or finer water-laid sediment. Hough (1942, p. 19) found that in more than 150 samples of sand, gravel, and mud from Cape Cod Bay the best sorting occurred in sand with median diameters of 0.1–0.2 mm. To compare these Cape Cod Bay marine sands with the groups of eolian

sand in Table 2, the writer recalculated from Hough's data the sorting coefficients of 22 sand samples which had median diameters in the range of 0.15–0.30 mm and found an average *So* value of 1.41 with a range of 1.17–1.90. These values are similar to those for the eolian sand samples. Extraction from Trask's list of 170 marine sediments did not yield such similarity: 14 samples with median diameters of 0.15–0.30 mm had an average *So* of 1.98 with a range of 1.26–4.14. This relation illustrates the danger of generalizing from analyses of unrelated samples.

The same relation of sorting to median diameter can be found for fluvial sediment. Inman (1949, p. 66) found in a review of analyses of Mississippi River sediment that sorting values approached unity as the median diameter decreased downstream until fine sand was reached, and then became markedly poorer.

Approx. miles below Cairo, Ill.	Median diam. (mm)	*So*	*Sk*
a. 140	.98	1.93	1.60
b. 710	.42	1.41	1.18
c. 920	.19	1.21	.99
d. 1050	.09	5.25	.11

A high degree of sorting, then, may be expected in selected fine and medium sand whether it is marine, fluvial, or eolian, if the basin of deposition is sufficiently large and uniform to permit extended washing or reworking of the sand. Simple averages of median grain size and sorting coefficient are not diagnostic of a particular environment, and this analysis is not critical in evaluation of the genesis of Chuska sandstone.

Of greater importance than either average median or the sorting coefficient in the comparison of fluvial and eolian sand is the range of medians for a volume of sediment as large as that of the Chuska sandstone. In the analyses of Mississippi River sediment used by Inman, the lateral variation of sediment texture was large, because some samples came from the channel bottom, some from bars, and others were influenced by tributary loads. These lateral variations do not show up in Inman's tabulation, which expresses only the general downstream changes in size parameters. A study of the bed sediment of the Missouri River downstream from Kansas City (U. S. Army Corps of Engineers, 1935, p. 1098–1101), where 800 out of 1300 samples had median grain diameters in the fine- and medium-grained sand ranges, showed great variations both longitudinally and transversely over short distances. Coarse gravel and fine silt occurred within 1000 feet, because of bars, chutes, crossings, pools, channel constrictions, and other irregularities which permit a wide range of water velocities. Such abrupt lateral variations in grain size are normal in fluvial sediment and would be recorded as vertical variations as the deposit accumulates. The variations could ordinarily be detected without mechanical analyses, but under conditions of uniform fluvial deposition the variations might be perceived only by the range of median diameters and sorting coefficients in a group of samples from which no field selection had been made.

In eolian sand the range of diameters would be limited by the narrow range of available velocities capable of transporting sand grains. Bagnold (1941, p. 92) showed that the pickup of grains smaller than about 0.1 mm is difficult because of cohesion, but once picked up the small grains remain in suspension and are blown away. Fines are thus readily removed from eolian sand and may accumulate elsewhere as loess. The maximum size of eolian sand is controlled by maximum wind velocities common in the area. Minor variations in wind velocity in dune areas are shown by Bagnold's studies of sand movement and by Shotton's (1937) description of eolian textural lamination in the Lower Bunter sandstone. Analyses of two samples of Chuska sandstone show double peaks in the size distribution; one peak is in fine sand and one in medium sand.

Uniformity of particle size throughout the Chuska sandstone is therefore of particular importance in regard to its origin. Although 16 samples might be insufficient to represent a volume of sand 60 by 10 miles with a thickness of at least 1750 feet, field observation of many other exposures revealed no coarse sand or gravel beds or silt and clay layers. The laboratory analyses support and specify the impression of uniformity established in the field.

Skewness.—The narrow range of skewness for the eolian sands (Table 2), as expressed by Trask's coefficient $Sk = Q_1Q_3/M^2$, indicates a high degree of sorting. The direction of skewness shows in the values for the average; some are skewed coarse, and some fine. If the slightly skewed (Sk = .95–1.05) samples are excepted, the more strongly skewed samples of the Lower Bunter sandstone and of the Chuska sandstone are skewed mostly on the fine side, and the samples of Barrett's coastal dune in England and Udden's inland dunes are skewed dominantly on the coarse side. Of the strongly skewed samples from other studies there is no preference in the sense of skewness.

Keller (1945) expressed skewness by attaching the symbol *F* or *C* to each particle-size analysis to indicate that the second-largest grade size was finer or coarser than the grade size of maximum percentage. He then determined an *F*:*C* ratio for a group of samples from a particular area or sediment. The *F*:*C* ratio for 446 dune sands from 8 inland and coastal localities in western United States ranged from 11:1 to 2.5:1, with an overall ratio of 351:95 or 3.7:1. This ratio was compared to a ratio of 1.1:1 for 63 beach sands along the coast of California and Oregon and suggested a simple index for differentiating eolian from beach sands. He applied the index to 4 Paleozoic sandstones and found *F*:*C* ratios of 0.2:1 for the Wyopo sandstone, 0.4:1 for the Tensleep, 0.9:1 for the St. Peter, and 1.1:1 for the Navajo; he concluded from the low ratios that all were marine.

Keller admitted that this measure of frequency-curve symmetry depended in part on the arbitrary spacing of the size grades for mechanical analysis but felt that, for the dune and beach sands studied, the consistent contrast of ratios suggested that the index might be diagnostic.

The writer applied Keller's *F*:*C* ratio to other groups of eolian sands for which mechanical analyses were available and found the ratio high in some and low in others (Table 2). In the Chuska sandstone the ratio is 8:8. In the 37 analyses of eolian sands listed by Udden, who was one of the first to explore the relations of particle-size distribution to environment of deposition, the *F*:*C* ratio is as much below unity as Keller's is above unity.

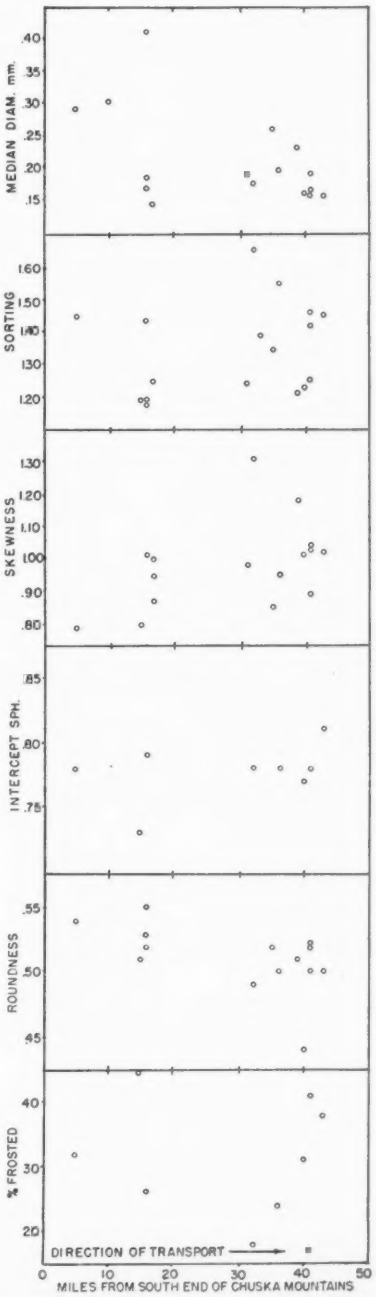

FIGURE 5.—GRAPH OF PARTICLE SIZE, SHAPE, ROUNDNESS, AND FROSTING PLOTTED AGAINST DISTANCE IN DIRECTION OF TRANSPORT

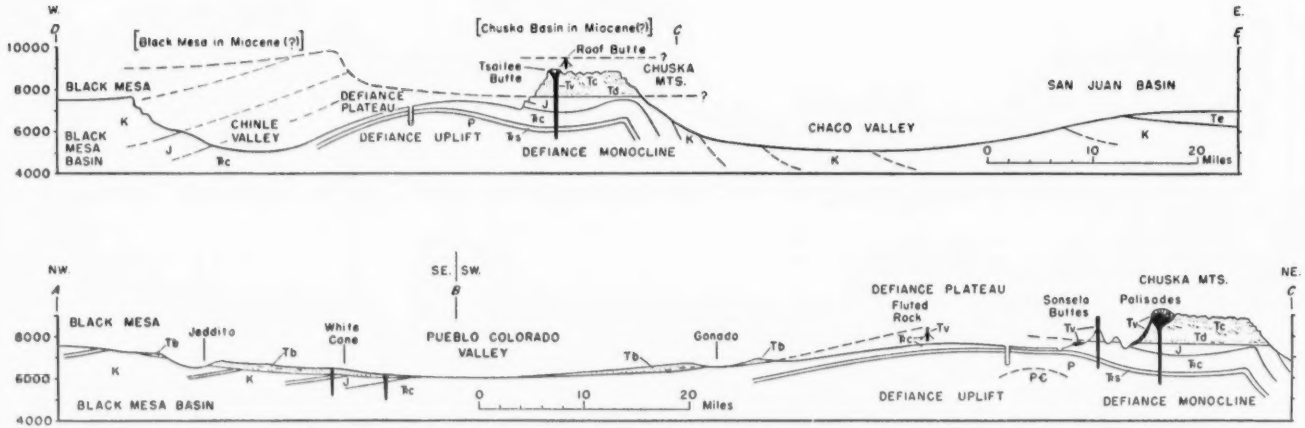

FIGURE 6.—GEOLOGIC CROSS SECTIONS FROM BLACK MESA, ARIZONA, TO SAN JUAN BASIN, NEW MEXICO

Along lines ABC and ECD of Plate 3, showing possible reconstruction of topography for Miocene (?), at end of deposition of Chuska sandstone. Fluted Rock and Roof Butte are projected into the planes of section. Vertical exaggeration 10.5×. Topographic control from U. S. Geological Survey maps of De Chelly and Fort Defiance quadrangles (1892). PE = Precambrian, P = Permian, ks = Shinarump conglomerate, kc = Chinle formation, J = Jurassic, K = Cretaceous, Te = early Tertiary sediments, Tc – Td = Chuska and Deza formations (Miocene?), Tb = Bidahochi formation (Pliocene), Tv = Navajo-Hopi volcanics (Pliocene).

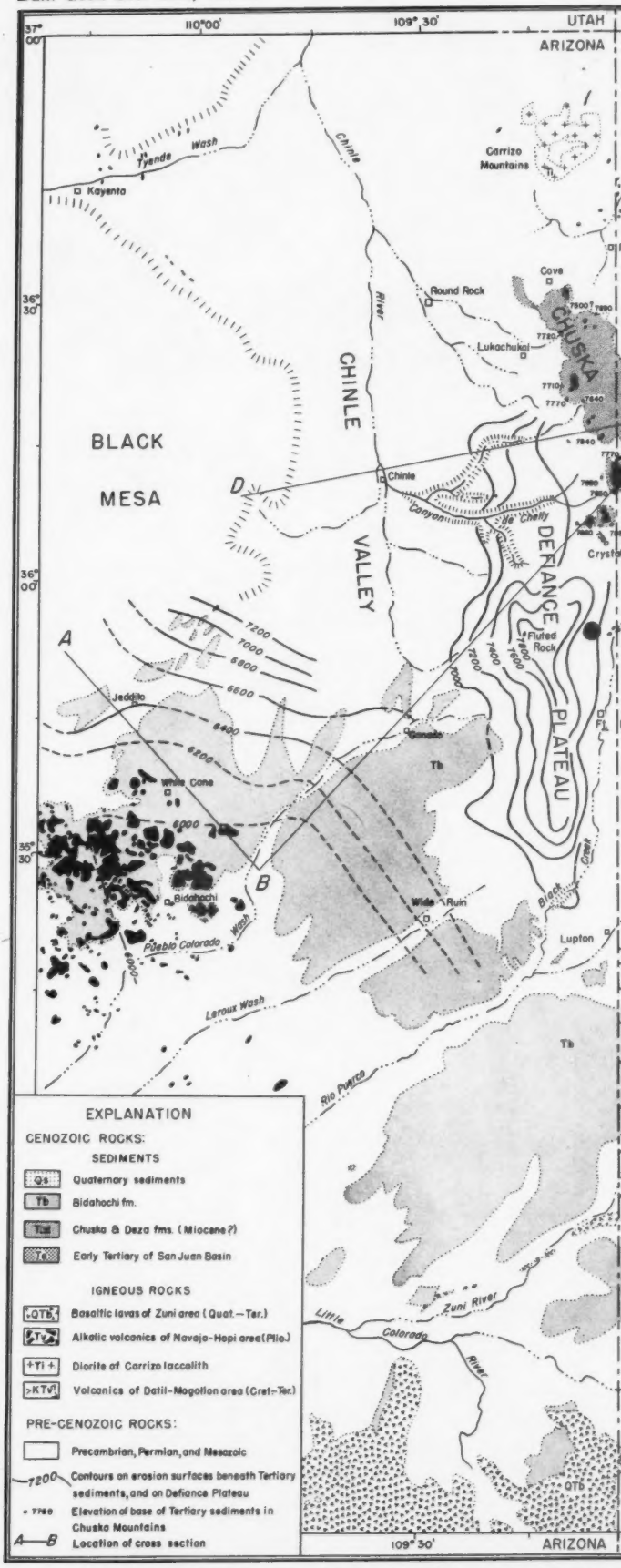

MAP OF PARTS OF NORTHEASTERN ARIZONA

Showing distribution of Cenozoic rocks. Geology and genera
of Black Mesa are taken from Hack (1942), those west of Zuni Mo
Plateau are taken from De Chelly and Ft. Defiance topographic
except for Chuska Mountains and near-by volcanics, is taken
New Mexico (1928), slightly modified from Harrell and Eckel (19

UMI

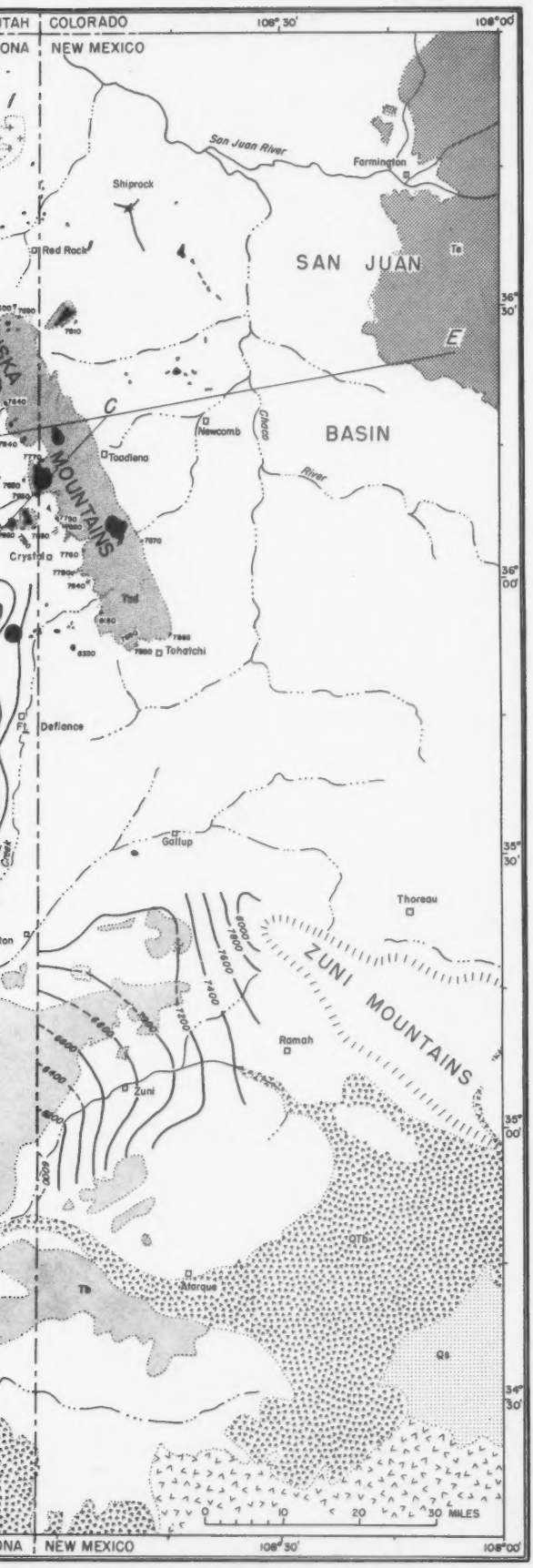

NA AND NORTHWESTERN NEW MEXICO

neralized contours on sub-Tertiary erosion surface south
i Mountains from McCann (1938). Contours in Defiance
phic sheets of U. S. Geol. Survey (1892). Rest of map,
ken from state geologic maps of Arizona (1923) and
(1939).

In fact Udden (1914, p. 681) generalized that in analyses of eolian sands a larger percentage of the sample was on the coarse side of the grade of the maximum percentage than on the fine side.

There appears to be no consistent direction of skewness in eolian sands, at least in the several groups of analyses surveyed. A more elaborate statistical study, with the use of the complete mechanical analysis of Keller's 446 dune sands, might yield a clearer relation.

Relation of particle-size to direction of transport.—To discover any possible trends in size parameters for the Chuska sandstone in relation to length of transport, a plot was made of median diameter, sorting coefficient, and skewness coefficient against distance in the direction of transport (Fig. 5). The direction of transport had been inferred from the cross-bedding. No significant trends were perceptible in the 38 miles between outside samples. Distance of transport is insufficient to reveal improved sorting or other changes in particle-size distribution.

To discern possible trends in size characteristics during accumulation of the sands, the size parameters were plotted against elevation. The samples represented different levels through 1100 feet of the 1750 feet maximum preserved thickness of the formation. No trends were evident.

Sphericity, Roundness, and Frosting

The intercept sphericity (Krumbein, 1941) of the .350- to .495-mm size grade was determined for eight samples of Chuska sandstone by the wedge method of Rittenhouse (1943). Test measurements on other size grades showed that sphericity decreases with particle size. The range of intercept sphericity for the samples is 0.73 to 0.81, with the average 0.78 (Table 1). Most of the grains measured were quartz, but values were similar for feldspar.

The roundness of 100–200 grains in the .350- to .495-mm size grade was determined by use of Krumbein's (1941) chart of roundness groups on 14 samples of Chuska sandstone. All measurements were made on the same day to reduce personal error, which is high in this method. The roundness values range from 0.44 to 0.55 but are greater than 0.50 in all but two samples (Table 1). These values compare with values obtained at the same time on other sands: 0.54 for St. Peter sandstone from Illinois and 0.21 for a glacio-fluvial sand from Rhode Island. In the classification of roundness by Russell and Taylor (1937, p. 248), the average for the Chuska sandstone (0.51) would fall in the category "round".

The relatively high values of sphericity and roundness in the Chuska sandstone suggest eolian abrasion, if wind wear is more effective than water wear in increasing sphericity and roundness (Twenhofel, 1946b). This factor is difficult to evaluate here because the sand grains probably inherited their shapes in part from Mesozoic sandstones, some of which contain rounded, subspherical sand grains.

Progressive decrease in rounding and sphericity in the direction of transport has been detected in beach sands and river sands and is presumably caused by selective transport in suspension in water (Pettijohn, 1949, p. 431–434). For eolian transport, MacCarthy and Huddle (1938) ascribed increase in sphericity to selective transport by saltation in air. For the Chuska sandstone, evidence of progressive changes was sought by a plot of these values against distance in the direction of transport (Fig. 5). For sphericity the points are scattered. For roundness there is a suggestion of decrease in the direction of transport, but the points are widely scattered. Sphericity and roundness were also plotted against elevation; no significant relations were evident.

The frosted or pitted surface on quartz grains suggests eolian abrasion (Cailleux, 1942). In 9 samples of Chuska sandstone the percentage of grains with surfaces at least half frosted ranges from 18 to 46, with an average of 29 per cent (Table 1). There is no relation between percentage of frosted grains and distance in the direction of transport (Fig. 5).

Age and Correlation of the Chuska Sandstone

Introduction

The Chuska sandstone and underlying Deza formation form one of the few areas of Tertiary sediments on the Colorado Plateaus. In the nearby San Juan Basin early Tertiary rocks lie generally conformably on Upper Cretaceous rocks (Fig. 6; Pl. 3). Southwest of the Chuska

Mountains are the calcareous alluvial and lacustrine sand and clay and interbedded alkalic volcanics of the Bidahochi formation, which contains middle or upper Pliocene fossils (Hack, 1942). These sediments can be traced discontinuously southeastward to the west base of the Zuni Mountains, less than 30 miles south of the Chuska Mountains.

Correlation with San José Formation

Gregory (1917, p. 81) suggested correlating the Chuska sandstone with the Wasatch formation (now called San José formation) on the basis of lithology and position. The Chuska sandstone in Gregory's terminology is interpreted by the writer to include the Deza formation and the overlying Chuska sandstone (Wright, 1954). The Deza formation is fluvial like the San José formation, but the Chuska sandstone has no Tertiary lithologic counterpart on the Colorado Plateaus. The San José formation lies in the center of the San Juan Basin as the youngest unit of a series of terrestrial sediments and on the east edge of the basin it is sharply turned up against a thrust zone. The Chuska sediments, on the other hand, postdate the west-bounding structure of the San Juan Basin, and are not deformed except at one locality at the south end of the range, where there occurs a series of faults that may be interpreted as landslide faults (Wright, 1954). Unless the east and west structural borders of the San Juan Basin were formed at different times, the Chuska sandstone must be younger than the San José formation.

Correlation with Pliocene Sediments

Introduction.—The lower (fluvial) portion of the Chuska sandstone of Gregory, since named Deza formation (Wright, 1954), was correlated by Reiche (1941, p. 54–55) with the sediments west of the Zuni Mountains which McCann (1938, p. 276) had in turn correlated with the Pliocene Bidahochi formation of the Hopi Country. Hack (1942, p. 350) correlated the erosion surfaces beneath the Tertiary sediments of all three areas—Chuska, west Zuni, and Hopi. Allen and Balk (1954, p. 99) reported lithologic similarity between the Chuska sandstone and the west Zuni sediments and assigned a probable Pliocene age to the Chuska. In a restudy of the Bidahochi formation, Repenning and Irwin (1954) identified a lower lacustrine member, an intermediate volcanic member, and an upper fluvial member. They confirmed Williams' (1936) correlation of the volcanic member with the volcanics of the Chuska Mountains and correlated the Chuska sandstone with the lower Bidahochi formation on the basis of lithologic similarity and the nature of the erosion surface beneath the Tertiary sediments of the Chuska, west Zuni, and Hopi areas.

Lithologic comparisons.—The Chuska sandstone consists of highly cross-bedded fine- to medium-grained eolian sandstone with siliceous cement. The Bidahochi formation, where examined west of Lupton, Arizona, near localities cited by Allen and Balk (1954, p. 99), consists of medium-grained to gritty calcareous fluvial sandstone similar to the Santa Fe formation of the Rio Grande depression. The comparison is more pertinent between the Bidahochi formation and parts of the Deza formation, which consists of fluvial and lacustrine sand and shale and some white ash (Wright, 1954); this similarity was noted by Reiche (1941). Repenning and Irwin (1954) traced these sediments from the Lupton area southeast to the west base of the Zuni Mountains, where they consist of soft white sandstone, reddish sand and clay, limestone, marl, tuff, and gravel, all alluvial and lacustrine in origin (McCann, 1938, p. 265). They can also be traced westward to the Hopi Country, where they consist "predominantly of white to very pale brown, cross-bedded, poorly cemented medium- to fine-grained argillaceous sandstone and a few beds of white rhyolitic ash" (Repenning and Irwin, 1954). Here, however, they are the upper member of the Bidahochi formation and overlie volcanics whose counterparts in the Chuska Mountains unconformably overlie the Chuska sandstone. Furthermore, the upper Bidahochi contains volcanic sands presumably eroded from the Chuska Mountains volcanics (Repenning and Irwin, 1954). The statement of these authors that "the lithologic character of the Chuska

sandstone is identical in many features of bedding and composition with the fluvial facies of the Bidahochi formation" is not only unacceptable on a lithologic basis (unless the relatively minor Deza formation is inferred) but is irrelevant, because the fluvial facies of the Bidahochi is the upper member and clearly younger than the Chuska sandstone.

The lower member of the Bidahochi formation is confined to the Hopi Country; it consists of "banded gray, brown, and pink flat-bedded mudstone and argillaceous fine-grained sandstone and a few beds of white rhyolitic ash", and is interpreted as lacustrine in origin (Repenning and Irwin, 1954). These beds are not sufficiently like the cross-bedded eolian Chuska sandstone to justify correlation although both formations contain white ash beds. The lower member of the Bidahochi formation resembles the Deza formation in several lithologic features, including the presence of white ash and a basal conglomerate.

Relation to volcanics.—The Navajo-Hopi volcanics consist of pyroclastics, flows, and intrusions of petrologically distinctive alkalic basalt (Williams, 1936). In the Hopi Country the volcanics form the middle member of the Bidahochi formation (Repenning and Irwin, 1954) and are characterized by diatremes (Hack, 1942). Near White Cone they bear vertebrate fossils which indicate a middle or late Pliocene age (Williams, 1936, p. 130). In and near the Chuska Mountains there are about 8 local areas of pyroclastics and flows, each with its own source, plus about 36 other necks and dikes (Appledorn and Wright, manuscript). Most of the major volcanic centers are complexes of extrusive breccias and flows resting at various levels on the eroded Chuska sandstone with both the extrusives and the sandstone intruded by plugs, dikes, and sills. Some show the structure of collapse calderas. At Palisades a breccia and flow were deposited on a 30-degree slope cut through 800 feet of Chuska sandstone and 200 feet into the underlying Jurassic rocks (Fig. 6). The volcanics were deposited after the deposition, cementation, and erosion of at least 2000 feet of Chuska sandstone and underlying rocks and are therefore considerably younger than the Chuska sandstone. The writer does not accept Repenning and Irwin's correlation of this 2000-foot disconformity with a slight unconformity between the lower and intermediate volcanic members of the Bidahochi formation.

Underlying erosion surfaces and drainage development.—The erosion surfaces beneath the Bidahochi and Deza-Chuska formations on first examination are similar in position and have been correlated by Hack (1942) and by Repenning and Irwin (1954). The surface underneath the Deza formation is about 7650–7900 feet above sea level. Elevations spotted on the map (Pl. 3) are corrected altimeter readings. No contouring is attempted because of the small number and variability of the readings. The variability is in part a result of errors in the readings (possibly as great as 50 feet) and in part reflects the true local relief along the buried hogbacks of the Defiance monocline. The high points on the surface at the southern end of the mountains are on hogbacks of Mesaverde sandstone, the most important ridge-former in the area.

Repenning and Irwin note that springs and perennial streams are confined to the west and southwest flanks of the mountains. They infer a westward slope to the surface beneath the Tertiary sediments and project this surface westward to the Bidahochi region at an appropriate angle. The writer, however, ascribes the lack of springs and canyons on the eastern flank south of Toadlena to the heavy blanket of landslide debris, localized to this area by the presence of Cretaceous clay under the Tertiary sediments.

Although the spot elevations on the sub-Deza surface show no consistent regional slope, analysis of the pebbles of the basal conglomerate of the Deza formation gives some indication of the slope direction. The conglomerate in the Crystal area bears angular pebbles and cobbles of cherty limestone which could have been carried only by east-flowing streams from outcrops of Chinle shale (Triassic) located several miles west of the Crystal area at that time.

The Defiance Plateau between the Chuska Mountains and the Hopi area has a gentle domal form reflecting the structure. The surface of the Plateau slightly truncates the

De Chelly sandstone (Permian), Shinarump conglomerate (Triassic), and Chinle shale (Triassic). It has an elevation ranging from 7800 feet in the center to 7000 feet on the southwest flank, where it is overlapped by the Pliocene Bidahochi formation; it thus appears to be an extension of the sub-Bidahochi surface. On the other hand, the highest portion of the Plateau is about the same elevation as the sub-Deza surface of the Chuska Mountains. At Fluted Rock, a small plug near the crest of the Plateau, remnants of Chinle sandstone occur at an elevation of about 8300 feet, or about 500 feet above the general Plateau surface. Inasmuch as Fluted Rock is a representative of the Pliocene alkalic volcanics, the Pliocene (sub-Bidahochi) land surface below which the plug was intruded must have been at least 8300 feet high, and the older sub-Deza surface must have existed at still higher elevations (Fig. 6).

The surface of the Defiance Plateau is therefore in part the exhumed sub-Bidahochi surface, but much of it is lower and younger. The relations are complicated by the fact that the sub-Bidahochi surface has been deformed; the lacustrine and fluvial sediments of the Bidahochi formation and its equivalents have been tilted by uplift of Black Mesa and Zuni Mountains (Hack, 1942; McCann, 1938). This uplift must have represented the late Pliocene regional uplift of the Colorado Plateaus rather than an accentuation of particular pre-existing structures, because although Black Mesa is a structural basin the movement in question was upward.

The Defiance Plateau may also have been uplifted at this time. Such an uplift across an established drainage pattern could have permitted the formation of the Canyon de Chelly, which has a maximum depth of 1000 feet where it transects the highest portion of the structural uplift. The Canyon de Chelly system would then be interpreted as the work of an antecedent stream in post-Bidahochi time—*i.e.*, late Pliocene or Pleistocene. The same is true for the canyon segment of Black Creek (Pl. 3), which crosses the plunging southern end of the Defiance Uplift in a canyon cut 500 feet through Permian sandstone.

Such an antecedent origin for these transverse canyons would demand formation of the major domal structure at this time, because the maximum depth of each canyon is along the axis of the uplift. Such a late date for important folding in this area is not supported by any other evidence.

A more satisfactory explanation for these transverse canyons is superposition. There are two unconformable covers from which these canyon streams could have been superposed—the Chuska sediments and the Bidahochi formation. The mouth of Black Creek Canyon is only a mile east of the preserved limit of Bidahochi formation, and possibly these sediments formerly extended farther over the south end of the plateau, up to at least 7200 feet, and covered the site of the future canyon. If a regional southwest tilt were introduced, a new consequent segment of Black Creek could develop in this area and be superposed onto the resistant Permian sandstones to form the canyon.

The origin of Canyon de Chelly might also be explained by superposition from the Bidahochi sediments. Although there is no evidence that the cover extended that far north, there was a continuous gradient from the Chuska Mountains to the Hopi area, for the upper Bidahochi contains volcanic sands presumably brought by streams from these mountains.

An alternative explanation is superposition from a more extended cover of Chuska sediments. A reconstruction is suggested in a cross section DCE from Black Mesa to the San Juan Basin (Fig. 6). The original western limit of the Deza-Chuska sediments is indeterminable, but, with as much as 1900 feet preserved at Roof Butte, these sediments probably extended some distance to the west. It is proposed that the basin or piedmont on which these sediments were deposited was bordered on the west by a subdued scarp leading to Black Mesa, which at that time might have been located far east of its present position and high enough to overlook the dune basin. After deposition and cementation of the Chuska sandstone, the Chinle River began to develop east of Black Mesa. It eventually cut through the Chuska sediments into weak Triassic shale and migrated westward down the west flank of the Defiance Uplift. Its

eastern tributaries from the retreating Chuska Mountains scarp became superposed across the plateau structure to form the Canyon de Chelly system. An area of low relief developed in Triassic lowlands southwest of the Defiance Plateau and extended onto the flanks of Black Mesa, Defiance Plateau, and Zuni Mountains. In this flanking area were deposited, in the middle or late Pliocene, the fluvial and lacustrine sediments of the Bidahochi formation and volcanics in the Hopi and Chuska areas. The Chuska Mountains, Zuni Mountains, and Black Mesa were all source areas for these sediments.

In the areas beyond the deposition of the Bidahochi formation, the Pliocene (sub-Bidahochi) land surface can be reconstructed from the maximum elevations of alkalic volcanics. The relations at Fluted Rock indicate that the Pliocene surface was at least 500 feet above the Defiance Plateau. Zilditloi, a large lava remnant 14 miles east of Fluted Rock, stands 1400 feet above Black Creek. The Chuska Mountains formed the principal highland area, just as today, with summits exceeding 9500 feet in elevation, an overall relief of at least 2000 feet, and valleys at least 1000 feet deep receiving the volcanics. Northeast of the mountains Shiprock neck rises 1800 feet above the San Juan Basin. All these volcanics were formed when the land level was at least the stated height above the present land surface.

With regional uplift near the end of the Pliocene much of the Bidahochi formation was stripped from the upland flanks, and the adjacent areas were lowered 500 to 1800 feet. Black Creek canyon may have formed at this time by superposition from Bidahochi sediments, and the rest of Black Creek valley was etched into soft Triassic shale. The Chuska Mountains have remained a highland but have retreated by stream erosion on both flanks and by landslide activity on the east flank south of Toadlena.

Conclusions

Correlation of the Chuska sandstone with the San José formation of the San Juan Basin is not accepted because of differences in lithology and structural position. Correlation with the upper fluvial member of the Bidahochi formation (Pliocene) is not accepted because of differences in lithology and because this unit is underlain by volcanic rocks which in the Chuska Mountains overlie the Chuska sandstone. Correlation with the lower lacustrine member of the Bidahochi formation is unlikely because of differences in lithology, because of the magnitude of the disconformity between the Chuska sandstone and the overlying volcanics, and because the underlying erosion surfaces do not require correlation. Some lithologic resemblance of the Deza formation and the lower Bidahochi is admitted, although the basal conglomerate in the two formations may be coincidental. The white ash which is common to the Deza, Chuska, and both lower and upper Bidahochi came from an unknown source of unknown age; rhyolitic volcanoes were active in Arizona and New Mexico at various times from the mid-Tertiary to the Pleistocene.

A Miocene(?) age for the Deza and Chuska formations and the erosion surface beneath them fits the reconstruction of the history of the Colorado Plateaus recently outlined by Gregory (1947). Other Miocene(?) formations of the Colorado Plateaus, the Muddy Creek formation of the Lake Mead region and the Brian Head formation of the High Plateaus of Utah, record an arid climate and volcanism. Miocene volcanism is also recorded in the Datil-Mogollon Mountains to the south and in the San Juan Mountains and Rio Grande depression to the east. The eolian nature of the Chuska sandstone reflects an arid climate, and the silica cementation may reflect volcanism nearby.

With this tentative correlation, the sequence of major Cenozoic geologic events in northwestern New Mexico and northeastern Arizona, revealed in the exposed rocks and the land forms, is as follows:

(1) Permian through Eocene(?). Deposition of terrestrial and marine sediments.

(2) Late Cretaceous and early Tertiary. Formation of major structures in Laramide Revolution—Black Mesa Basin, Defiance Uplift, and San Juan Basin.

(3) Miocene(?). Erosion of tilted rocks to form shallow basin in position of present

Chuska Mountains. Deposition of fluvial Deza formation by east-flowing streams, followed by prolonged deposition of sand dunes by southerly winds until at least 1900 feet of sediment had accumulated in the two formations. Cementation of the Chuska sandstone occurred during or shortly after accumulation.

(4) Miocene(?) and early Pliocene. Deep erosion into and through the Tertiary sediments; opening of broad lowlands in Triassic shale. Possible formation of Canyon de Chelly by superposition.

(5) Middle or late Pliocene. Deposition of fluvial and lacustrine sediments of Bidahochi formation around low southern flanks of Black Mesa and Defiance Plateau and west of Zuni Mountains. Volcanic activity in Navajo-Hopi field; in Chuska Mountains the volcanics were intruded into and extruded upon deeply eroded Chuska sandstone.

(6) Late Pliocene and Pleistocene. Regional uplift of Colorado Plateaus. Partial stripping of Pliocene sediments from Defiance Plateau; erosion of at least 500 feet from crest of plateau surface, 1400 feet in Black Creek valley, and 1800 feet in an area east of Chuska Mountains. Possible superposition of segment of Black Creek across southern end of Defiance Plateau. Continued dissection of Chuska Mountains; formation of lakes on the crest and landslides on the east flank.

References Cited

Allen, J. E., 1953, Tohatchi formation of Mesaverde group, western San Juan Basin, New Mexico: Am. Assoc. Petroleum Geologists Bull., v. 37, p. 2569–2571.

Allen, J. E., and Balk, Robert, 1954, Mineral resources of Fort Defiance and Tohatchi quadrangles, Arizona and New Mexico: N. Mex. Bur. Mines and Min. Res. Bull. 36, 192 p.

Bagnold, R. A., 1941, Physics of blown sand and desert dunes: London, Methuen and Co., 265 p.

Barrett, W. H., 1940, Grading of dune sand by wind: Geol. Mag., v. 67, p. 159–162

Calilleux, André, 1942, Les actions éoliennes périglaciares en Europe: Soc. Geol. France Mem. 47, 176 p.

Dapples, E. C., 1941, Surficial deposits of the deserts of Syria, Transjordan, Iraq, and western Iran: Jour. Sed. Petrology, v. 11, p. 124–141

Gregory, H. E., 1917, Geology of the Navajo country: U. S. Geol. Survey Prof. Paper 93, 161 p.

—— 1947, Colorado drainage basin: Am. Jour. Sci., v. 245, p. 694–705

Hack, J. T., 1941, Dunes of the western Navajo country: Geog. Rev., v. 31, p. 240–263

—— 1942, Sedimentation and volcanism in the Hopi Buttes: Geol. Soc. America Bull, v. 53, p. 335–372

Harrell, M. A., and Eckel, E. B., 1939, Groundwater resources of the Holbrook region, Arizona: U. S. Geol. Survey Water-Supply Paper 836-B, p. 19–105

Hough, J. L., 1942, Sediments of Cape Cod Bay, Mass.: Jour. Sed. Petrology, v. 12, p. 10–30

Inman, D. D., 1949, Sorting of sediments in the light of fluid mechanics: Jour. Sed. Petrology, v. 19, p. 51–70

Keller, W. D., 1945, Size distribution of sand in some dunes, beaches, and sandstones: Am. Assoc. Petroleum Geologists Bull., v. 29, p. 215–221

Krumbein, W. C., 1941, Measurement and geological significance of sedimentary particles: Jour. Sed. Petrology, v. 11, p. 64–72

McCann, F. T., 1938, Ancient erosion surface in the Gallup-Zuni area, New Mexico: Am. Jour. Sci., v. 236, p. 260–278

MacCarthy, G. R., and Huddle, J. W., 1938, Shape-sorting of sand grains by wind action: Am. Jour. Sci., v. 236, p. 64–73

McKee, E. D., 1934, The Coconino sandstone—its history and origin: Carnegie Inst. Wash. Pub. 440, p. 77–115

Pettijohn, F. J., 1949, Sedimentary rocks: N. Y., Harpers, 526 p.

Reiche, Parry, 1938, An analysis of cross-lamination: the Coconino sandstone: Jour. Geology, v. 46, p. 905–932

—— 1941, Erosion stages on the Arizona Plateau as reflected in a headwater drainage area: Plateau, v. 13, p. 54–64

Repenning, C. A., and Irwin, J. W., 1954, Bidahochi formation of Arizona and New Mexico; Am. Assoc. Petroleum Geologists Bull., v. 38, p. 1821–1827

Rittenhouse, Gordon, 1943, Measuring intercept sphericity of sand grains: Am. Jour. Sci., v. 271, p. 109–116

Russell, R. D., and Taylor, R. E., 1937, Roundness and shape of Mississippi River sands: Jour. Geology, v. 45, p. 225–267

Shotton, F. W., 1937, Lower Bunter sandstones of Worcestershire and Shropshire: Geol. Mag., v. 34, p. 534–553

Trask, P. D., 1932, Origin and environment of source sediments of petroleum: Houston, Gulf Pub. Co., 323 p.

Twenhofel, W. H., 1946a, Mineralogical and physical composition of the sands of the Oregon coast from Coos Bay to the mouth of the Columbia River: Oreg. Dept. Geology and Min. Res. Bull. 30, 64 p.

—— 1946b, Rounding of sand grains: Jour. Sed. Petrology, v. 15, p. 59–71

Udden, J. A., 1914, Mechanical composition of clastic sediments: Geol. Soc. America Bull., v. 25, p. 655–844

U. S. Army Corps of Engineers, 1935, Missouri River: 73d Congress, 2d Sess., House Doc. 238, 1245 p.

Williams, Howel, 1936, Pliocene volcanoes of the

Navajo-Hopi country: Geol. Soc. America Bull., v. 47, p. 111–172

Wright, H. E., Jr., 1951, Opal cement in thick Tertiary eolian sandstone, Chuska Mountains, Arizona-New Mexico (Abstract): Geol. Soc. America Bull., v. 62, p. 1492

—— 1954, The problem of the Tohatchi formation, Chuska Mountains, Arizona-New Mexico: Am. Assoc. Petroleum Geologists Bull., v. 38, p. 1827–1836

Wright, H. E., Jr., and Becker, R. M., 1951, Correlation of Jurassic formations along the Defiance monocline, Arizona-New Mexico: Am. Assoc. Petroleum Geologists Bull., v. 35, p. 607–614

University of Minnesota, Minneapolis 14, Minnesota

Manuscript Received by the Secretary of the Society May 25, 1954

BULLETIN OF THE GEOLOGICAL SOCIETY OF AMERICA
VOL. 67, PP. 435-474, 18 FIGS., 3 PLS. APRIL 1956

GEOLOGY AND STRUCTURE OF THE FRANKLIN-STERLING AREA, NEW JERSEY

By J. M. Hague, J. L. Baum, L. A. Herrmann, and R. J. Pickering

ABSTRACT

The Franklin-Sterling area is located in Sussex County, New Jersey, and Orange County, New York, along the western border of the New Jersey Highlands. A geologic study of the Precambrian rocks of the area which include metasedimentary, igneous, and probable metavolcanic types was undertaken by geologists of The New Jersey Zinc Company. The marble and paragneisses have been divided into stratigraphic units which are, from oldest to youngest, the Hamburgh Mountain gneisses, the Franklin marble band, the Cork Hill gneiss zone, the Wildcat marble band, and the Pochuck Mountain gneiss series. Some of the Precambrian igneous rocks were probably intruded during deformation as sills and phacoliths, whereas the granites and pegmatites were intruded as discordant bodies during or after the last stages of deformation. The Precambrian rocks have been metamorphosed to a high grade but show signs of subsequent hydrothermal metamorphism.

The major structures in the area are isoclinal, overturned synclines and anticlines formed during Precambrian time. Two sets of minor cross-folds were superimposed on the major folds. Paleozoic folding is apparent only in the Paleozoic rocks. The most recent fault movements were post-Ordovician but may have been controlled by Precambrian faulting. Two sets of cross-faults are associated with the major faults.

CONTENTS

TEXT

	Page
Introduction	436
Location and physiography of the area	436
Purpose	436
Previous work	437
Present study	437
Acknowledgments	437
Precambrian rocks	437
Marble	437
Introductory statement	437
Franklin band	438
Wildcat band	440
Other bands	440
Metasedimentary and metavolcanic gneisses	441
Introductory statement	441
Microcline gneiss	441
Hornblende gneiss	443
Biotite gneiss	446
Pyroxene gneiss and related rocks	446
Garnet gneiss	447
Graphitic gneiss	447
Igneous gneisses and rocks	448
Introductory statement	448
Losee gneiss	448
Oligoclase gneiss	449
Granodiorite gneiss	450
Byram gneiss	451
Granites and related rocks	453
Pegmatites	455
Cambrian and later rocks	455
Petrogenesis	456
Introductory statement	456
Origin of the microcline gneiss	456
Origin of the hornblende gneiss	457
Origin of the biotite gneiss and related rocks	457
Origin of the pyroxene gneiss and related rocks	457
Origin of the Losee gneiss	457
Origin of the oligoclase gneiss	458
Origin of the granodiorite gneiss	458
Origin of the Byram gneiss	458
Structural geology	459
Banding and foliation	459
Lineation	461
Minor folds	462
Cross-folds	462
Major folds	462
Mounts Adam and Eve area	462
Glenwood syncline	463
Pochuck Mountain syncline	463
Pimple Hills syncline	464
North Sparta folds	464
Lake Lenape syncline	464
Stag Pond folds	464
Losee anticlines	465
Post-Ordovician folds	465
Joints	465
Faults	465

	Page
Mechanics of deformation	465
Precambrian stratigraphy	467
Development of the stratigraphic approach	467
Method of construction	467
Proposed stratigraphic sequence	467
Introductory statement	467
Hamburgh Mountain gneiss series	468
Franklin marble	468
Cork Hill gneiss zone	469
Wildcat marble	469
Pochuck Mountain gneiss series	469
Metamorphism	469
Economic geology	469
Introductory statement	469
Zinc deposits	470
Iron deposits	471
Nonmetallic deposits	471
Geologic history and conclusions	472
References cited	473

ILLUSTRATIONS

Figure		Page
1.	Index map showing the location of the Franklin-Sterling area, New Jersey	437
2.	Block diagram showing the structure of a portion of the Pine Island quarry	438
3.	Hornblende gneiss containing irregular masses of marble	441
4.	Sketch of grain of microcline in a thin section of microcline gneiss	443
5.	Locally discordant contact between the Losee gneiss and included hornblende gneiss block	448
6.	Blocky inclusion of hornblende gneiss in the Stag Pond type of Losee geniss	448
7.	Sketch of a portion of a thin section of the Losee gneiss	449
8.	Gradation of hornblende gneiss into oligoclase gneiss	449
9.	Locally discordant contact between the Byram gneiss and type II hornblende gneiss	451
10.	Gradational contact between the Byram gneiss and type II hornblende gneiss	451
11.	Pegmatite intrusive into the granodiorite gneiss	455
12.	Concordant folded pegmatite vein in the microcline gneiss	455
13.	Variation diagram showing the mineralogical relationships among the Byram, granodiorite, and Losee gneisses	458
14.	Disconformable relationship between the banding and contact of biotite and hornblende gneisses	460
15.	Outcrop map showing relationship of contacts to banding on the east side of the Glenwood syncline	460
16.	Two interpretations of the pre-intrusion and pre-faulting structure of the Mounts Adam and Eve area	463
17.	Stereogram illustrating pre-faulting structural interpretation of the Wildcat marble horizon	466
18.	Generalized columnar section of the metasedimentary and metavolcanic rocks of the area	468

Plate		Facing page
1.	Geological and structural map of the Franklin-Sterling area, New Jersey	435
2.	Photomicrographs of feldspar in the Byram and microcline gneisses	452
3.	Structures in the Franklin marble, and in the pyroxene gneiss and hornblende gneiss	453

TABLES

Table		Page
1.	Modal analyses of microcline gneiss	444
2.	Modal analyses of hornblende gneiss and pyroxene-rich rocks	445
3.	Modal analyses of Losee and oligoclase gneisses	450
4.	Modal analyses of granodiorite gneiss	451
5.	Modal analyses of Byram gneiss	454

Introduction

Location and Physiography of the Area

The area described in this report is a rectangle 30 miles long and 5 miles wide which trends northeasterly and includes parts of Sussex County, New Jersey and Orange County, New York (Fig. 1). It is 50 miles northwest of the city of New York and is approached from the east on New Jersey State Highway 23. The area lies mainly in the New Jersey Highlands and its outliers and has a relief of several hundred feet. It is bounded on the southwest by Andover, New Jersey, on the northeast by Big Island, New York, on the northwest by Pochuck Mountain and the Pimple Hills, and on the southeast by Hamburgh and Sparta mountains. In the south the valley of the Wallkill and in the north Vernon valley extend through the central part of the area.

Purpose

The geology of the Franklin-Sterling area was studied by The New Jersey Zinc Company to aid in prospecting by: (1) subdividing the Pochuck gneiss and possibly some other gneisses into lithologic units to determine their detailed structure and so predict the structures in the Franklin band of marble, (2) delineating, with the aid of bands of gneiss, the zone in the Franklin band of marble which contains the Franklin and Sterling ore bodies, (3) determining the stratigraphic sequence of the metamorphic rocks, if possible. The main problem was the differentiation and mapping of the gneisses, but the bands of marble were also studied in some detail.

Previous Work

Nason (1889), Kemp (1893), Ries (1897), and Wolff and Brooks (1898) mapped in the Franklin-Sterling area. In 1908 Spencer *et al.* published the Franklin Furnace folio. This was followed in 1914 by the Raritan folio by Bayley *et al.* These remain the most detailed publications on the area to date. In 1914, Lewis and Kummel published a description of the geology of New Jersey, which Kummel (1940) later revised and rewrote. Bayley (1910) did detailed work on the iron mines, and Sims and Leonard (1952) and Neumann (1952) reported on the Andover mining district. Hotz (1953) and Sims (1953) have worked in adjacent lithologically similar areas. Other articles and papers describe the Franklin band of marble and the Franklin and Sterling ore bodies.

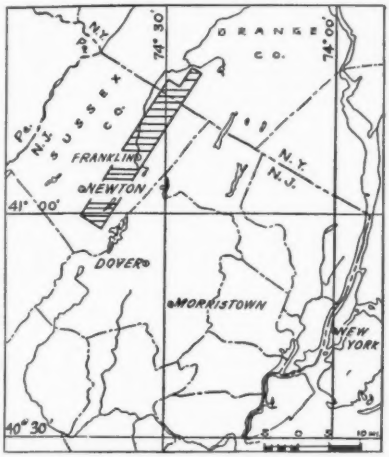

FIGURE 1.—INDEX MAP SHOWING THE LOCATION OF THE FRANKLIN-STERLING AREA, NEW JERSEY

Present Study

The present study by The New Jersey Zinc Company began in the summer of 1946 at the suggestion of A. W. Pinger, J. L. Baum, and J. M. Hague. Previously, limited reconnaissance work had been done on the gneisses by A. W. Pinger, O. N. Rove, and R. S. Cannon. A two-man field party has worked on the project each field season from 1946 to 1954, with the exception of 1952. E. L. Newcomb, W. H. Westphal, W. P. Williams, and E. J. Swapp made substantial contributions. C. H. Stockwell, in addition to doing detailed mapping of metamorphic rocks, made an extensive study of the regional lineations.

Hague and Baum did most of the field mapping of the gneisses in the northern three-fourths of the map area. The gneisses in the southern fourth of the area were mapped by Herrmann and Pickering, who also did further detailed mapping in the vicinity of the Glenwood syncline and in the area east of McAfee and Hamburgh Mountain. Herrmann and Pickering correlated and reclassified some of the gneisses to conform with recently obtained information and prepared the maps and figures for the report. Petrographic examinations were made by Herrmann.

Acknowledgments

The authors wish to express their appreciation to The New Jersey Zinc Company and its officers for permission to publish this paper, and to the members of the Research Department of The New Jersey Zinc Company for their services in preparing the numerous thin sections and spectrographic analyses used for this report. The authors also wish to thank Prof. M. P. Billings and Prof. A. F. Buddington for critical reading of the manuscript.

PRECAMBRIAN ROCKS

Marble

Introductory statement.—The several bands of Precambrian marble in the Franklin-Sterling area have been described in the Franklin Furnace folio by Spencer under the names Franklin limestone and white limestone. The rock is locally called white limestone as opposed to the Paleozoic Kittatinny limestone, known as blue limestone. In one place in the Franklin Furnace folio Spencer limits the term "Franklin limestone" to the band of marble which contains the Franklin and Sterling mines, but he maps all the marble bands as "Franklin limestone". Bayley (1914, p. 47) described the Franklin limestone as consisting of crystalline white limestone and dolomite, in places siliceous, with local belts of black gneiss, pegmatite, and

certain siliceous and slaty rocks. Since the marble is essentially the same in the various bands, it is referred to in this paper merely as marble, and the different marble bands are named.

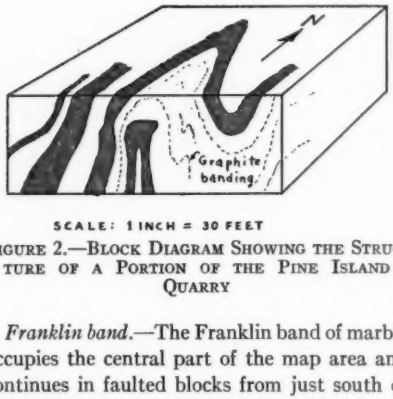

FIGURE 2.—BLOCK DIAGRAM SHOWING THE STRUCTURE OF A PORTION OF THE PINE ISLAND QUARRY

Franklin band.—The Franklin band of marble occupies the central part of the map area and continues in faulted blocks from just south of the Sterling mine northward through Franklin, Hamburg, and McAfee, to Big Island, New York. It also probably occurs 2½ miles northwest of Sparta in the vicinity of the Limecrest quarry. It is stratigraphically overlain by the Cork Hill zone of gneisses and underlain by the gneisses contained in the Byram gneiss on Hamburgh and Sparta mountains. The rock is a white to gray, coarse to locally fine-grained crystalline marble, which varies in magnesium content from very low to an almost pure dolomite. Bands or zones of low magnesium rock commonly alternate with bands or zones of dolomite or dolomitic marble, as at the Pine Island quarry (Fig. 2) 2½ miles north of Glenwood, and at the Farber quarry in the central part of the map area. Conformable dolomite bands are also present in a quarry 6000 feet S. 55°E. of Hamburg (Pl. 3, fig. 1). This alternation may represent original bedding in the carbonate rock. However, drill-hole data and the irregularity of dolomite distribution in quarry and mine exposures strongly suggest hydrothermal dolomitization. Sandy beds within the marble were observed in several quarries between Franklin and McAfee and apparently represent sedimentary bedding. Surface observations and information from drill holes disclose the presence in many places of thin alternating bands of impure marble and limy gneiss between the main bands of gneiss and marble. This indicates that the contact of the marble with the gneisses on either side is gradational and therefore a normal sedimentary contact.

Insoluble-residue studies of drill cores from the vicinity of the Sterling mine have indicated the presence of about 25 sulfides, silicates, and oxides which are minor disseminated constituents in the Franklin band of marble. The most abundant of these are graphite, tremolite, mica, pyrite, pyrrhotite, quartz, and talc, in order of decreasing abundance. Attempts to correlate drill cores from the Sterling mine by means of zones containing particular insoluble silicates were unsuccessful, which indicates the inconsistent distribution of such minerals. Attempts at correlation based on alternating beds of calcitic and magnesian marble were also unsuccessful.

Mineral orientations in the Franklin band of marble are of three types: (1) discontinuous bands of graphite and disseminated silicate minerals such as chondrodite and/or norbergite, diopside, etc., within the marble, (2) foliation formed by the sub-parallel orientation of graphite and phlogopite flakes, (3) parallel orientation of calcite rhombs. Foliation is common within the mineral banding—type (1)—, and in such cases the plane of foliation parallels the banding. In the third type of orientation the *c* crystallographic axis of the calcite is, in certain localities, roughly perpendicular to the plane of foliation and to the mineral banding where the three types of orientation occur together. In general, the mineral banding and foliation of the marble are parallel to persistent bands of gneiss and sandy beds within the marble, and to the contact with the gneisses on either side of the Franklin band. This has led many geologists to believe that the banding and foliation of the marble reflect its original bedding. However, the fact that the banding and foliation in some cases are parallel to all sides of blocks of gneiss and masses of pegmatite suggests that flowage has caused the banding and foliation to parallel competent beds whatever their attitude. Mineral bands have not been useful in stratigraphic mapping because they are discontinuous.

A characteristic feature of the Franklin band

of marble is the presence of blocks and discontinuous bands of silicic rock known locally as "black rock", which are wholly enclosed by the marble, and whose banding in general parallels the banding and foliation of the marble. The term "black rock" is misleading because the rocks are commonly light in color. They include hornblende, pyroxene, microcline, and biotite gneisses, Precambrian quartzite, and sphene-bearing pyroxene-scapolite rock. The gneisses occur in small blocks, commonly in rough alignment as if they were once thin gneiss bands which had been broken and displaced by the deformation of the marble. Also, the banding "flows" around pod-shaped pegmatites (Pl. 3, fig. 2) which may once have been continuous sills now stretched into boudins. Matching of blocks is difficult because of their wide separation and, in the case of the dark gneisses, the presence in many places of coarse, recrystallized borders of dark minerals and sphene-bearing pyroxene-scapolite rock. However, in a few locations there is definite evidence that once-continuous bands of gneiss have been broken and moved to form boudins, with the banding in the marble having "flowed" between them (Pl. 3, fig. 3). The writers believe these blocks and bands represent thin beds of clastic sediments which were formed by changes in deposition, or thin conformable volcanic flows or sills. The bands of dark biotite, pyroxene, and hornblende gneisses occurring in such manner are characterized by an abundance of disseminated and vein sulfides. Rocks of this latter type are particularly common in the core of the fold at the Sterling mine and in certain quarries northeast of Franklin. At one locality southwest of McAfee, thin discontinuous bands of type IV hornblende gneiss occur within the marble.

Coarse-grained sphene-bearing pyroxene-scapolite rock is common at the contact of the fragments of dark gneiss with the marble. In other locations only the sphene-bearing pyroxene-scapolite rock is present, constituting a second type of silicic rock found within the marble. This same type of rock is also found at the borders of calcite lenses in hornblende and pyroxene gneisses, forming an apparent gradation between the calcite and the enclosing gneiss.

What appear to be lenses or pods of Precambrian quartzite form a third type of silicic rock within the marble. The silicic rocks within the marble probably indicate local impurities in the original carbonate sediment.

A thin, fairly continuous zone of gneiss within the Franklin band of marble near the Franklin and Sterling mines has been locally called the Median gneiss because of its similarity in lithologic position to the gneiss of that name in the Balmat-Edwards district, New York. The Median gneiss is poorly exposed, but, from two areas of outcrop and a number of intercepts in diamond-drill holes, the band can be traced sporadically from the Sterling mine to McAfee. Its distance from the contact of the Franklin band of marble with the Cork Hill gneiss zone ranges from 1100 feet at the Sterling mine to 1800 feet at the north end of the Franklin orebody. Thus the Median gneiss is not precisely parallel to the Cork Hill-Franklin band contact but rather diverges from it northward along strike from the Sterling mine to Franklin. Near Hamburg its distance from the Cork Hill-Franklin band contact has not been determined because of faulting.

The Median gneiss ranges widely in thickness, from a minimum of 100 feet or less at Franklin to a maximum of 800 feet in the area 5000 feet southwest of McAfee. Under these conditions, the zone may locally be absent. In at least two drill holes the zone was repeated with 300–400 feet between the two gneissic layers.

The Median gneiss is variable in composition also. In general, it is composed of feldspathic quartzite, biotite gneiss, microcline gneiss, and local hornblende gneiss. Almandite garnet is found in some bands throughout the zone, and spectrographic analysis of a garnet specimen revealed appreciable amounts of ytterbium and lesser amounts of yttrium and erbium.

So far as can be observed, the Median gneiss band shows no more contortion than the Cork Hill-Franklin band contact. The internal structure of the marble between the two gneiss zones, however, is considerably more complicated. The folds in the Franklin and Sterling ore bodies testify to the distortion undergone by the marble. In at least one place cross-bedding was suspected in the gneiss, and this feature may be more common than supposed

because of the difficulty of recognizing it in deformed metamorphic rocks. Evidence of the general regularity and continuity of the Median gneiss is that where it was predicted by C. H. Stockwell, who studied the zone, it was subsequently penetrated by the drill.

Two outcrops of gneiss along the west side of the East fault, one of them half a mile south of McAfee and the other 4000 feet northeast of Franklin, are composed of similar rock types and may represent the eastern contact of the Franklin band of marble with the older gneisses to the east. They resemble the gneiss just east of the Franklin band of marble as exhibited in outcrops east of the East fault and 2 miles south of McAfee, and by drill-hole data 1 mile southeast of Franklin. If this is actually the contact, it is the only locality at which both contacts of the Franklin band are visible without a major fault between. However, the outcrops may merely represent one or two small bands of gneiss within the marble.

The Franklin band of marble contains numerous masses of pegmatite, granite, and other intrusive rocks.

Wildcat band.—The Wildcat band of marble, named for the small creek which flows through its outcrop southwest of Franklin, lies west of the main exposure of the Franklin band. It is separated from the Franklin band by the Cork Hill gneiss zone. It is also found west and southwest of Sparta. Throughout most of its outcrop length, the Wildcat horizon is represented by a single band of marble, but traced northward from Lake Mohawk into the area 2½ miles north of Sparta it gradually changes into a series of tightly folded bands of impure marble and calcareous hornblende and pyroxene gneisses (Pl. 3, fig. 4). As the horizon bends around the nose of a small anticline and continues southward, the calcareous bands die out. However, the sillimanite-bearing microcline gneiss, stratigraphically immediately below it, can be followed to the south, then around a pair of tight folds, and finally to the southwest toward the east limb of the Lake Lenape syncline. On the east limb of this syncline the calcareous horizon reappears as calcareous hornblende and pyroxene gneisses with the same sillimanite-bearing microcline gneiss immediately below it stratigraphically. As the southern end of the east limb is approached, the horizon becomes a distinct band of marble with associated limy pyroxene gneiss. The Wildcat band of marble reappears on the west limb of the Lake Lenape syncline and continues along that limb to the northeast, again into the area 2½ miles northeast of Sparta where it is represented by calcareous pyroxene gneiss. Here a constriction in the fold and faulting bring the Wildcat zones in the two limbs nearly into contact. The zone in the west limb can be traced to the north for a short distance and then is no longer seen in outcrop. It is presumably displaced by the Losee gneiss to the north.

Although no detailed work has been done on the mineralogy of the marble bands within the Wildcat horizon, the rock is in general indistinguishable from that of the Franklin band. Like the Franklin band, the Wildcat band of marble commonly contains blocks and discontinuous bands of gneiss and pegmatite.

Other bands.—A band of marble, exposed for only a short distance near Paleozoic cover, crops out in the area 1½ miles southwest of Andover, just southwest of the map area. Magnetite and associated pyroxene and garnet are exposed in a pit in the marble near its contact with the sillimanite-bearing microcline gneiss to the southeast. This pit is listed as the Glendon mine by Bayley (1910). The marble is doubtless a southward extension of the Wildcat marble band found in the east limb of the Lake Lenape syncline to the northeast.

The marble in the Stag Pond folds may be a separate band from the Wildcat or Franklin bands. It lies within a thin zone of rocks which are presumed to be partly metasedimentary and are bounded by Byram gneiss on one side and Losee gneiss on the other. The marble in the northeast limb of the northeast fold is characterized by an abundance of pyroxene, chondrodite or norbergite, and mica. The limb common to the two folds has magnetite smears and serpentinized forsterite as well as the three silicates previously mentioned. The southwest limb of the southwest fold contains pyroxene, mica, and very local graphite. Correlation of the Stag Pond band of marble with the Wildcat band is made difficult by the abundance of Byram and Losee gneisses which obscure its metasedimentary environment.

At the Roseville mine, three-fourths of a mile south of Stag Pond, thin bands of magnetite-bearing marble within dark hornblende and pyroxene gneisses grade laterally into gneiss through zones containing irregular masses of

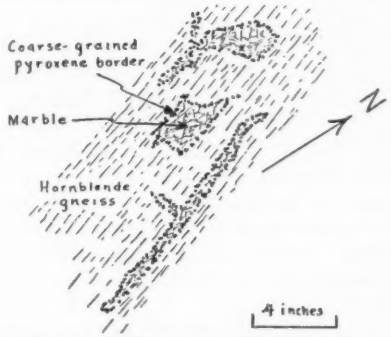

FIGURE 3.—HORNBLENDE GNEISS CONTAINING IRREGULAR MASSES OF MARBLE

marble (Fig. 3). Just west of the dark gneiss there is a band of light pyroxene gneiss, and farther west there is a great thickness of type II Byram gneiss characterized by feldspar augen. A short distance to the south, the marble horizon is assumed to be cut off by a postulated northeast-striking fault which displaces it about 1500 feet to the southwest.

Metasedimentary and Metavolcanic Gneisses

Introductory statement.—The gneisses described here as metasediments or metavolcanics include those previously described as the Pochuck gneiss and the light phase of the Byram gneiss by Spencer *et al.* (1908, p. 4–6), the Pochuck and Pickering gneisses by Bayley *et al.* (1914, p. 58–63) and Bayley (1941, p. 9, 10, 12–19), and the Pochuck gneiss and parts of the Byram and Losee gneisses by Kummel (1940, p. 58–60). Because none of the varieties of these gneisses is limited to any particular formation, the terms Pochuck gneiss and Pickering gneiss are not used in this paper, and the term Byram gneiss is limited as described later. The metasedimentary and metavolcanic rocks are named after their characteristic mineral or minerals. The microcline gneiss in the Franklin-Sterling area probably corresponds to the garnetiferous quartz-biotite gneiss of the Ringwood area (Hotz, 1953, p. 173–174).

Several of the varieties of gneiss are subdivided into two or more types because, although there may be only a slight compositional or structural difference between two types, a particular feature may characterize a particular type and can be used in field mapping. For example, although type I hornblende gneiss commonly contains disseminated pyroxene and local biotite, in type II hornblende gneiss pyroxene is concentrated in bands which alternate with hornblende and biotite-rich bands. However, there are locations where one type of gneiss grades along strike within a single band into another type. Only a few of the types within a particular variety of gneiss have been differentiated on the map.

Microcline gneiss.—Microcline gneiss occurs throughout the area and is particularly abundant west of Lake Mohawk, east and west of McAfee, and in the Lake Lenape, Pimple Hills, and Glenwood synclines. It is a light, fine- to medium-grained gneiss which contains quartz and microcline and locally sillimanite, garnet, and microperthite. The sillimanite occurs in lath- or rod-shaped aggregates of sillimanite needles and fine-grained quartz. The sillimanite-quartz aggregates range from tiny rods a few millimeters in diameter to large plates up to 6 inches long, 3 inches wide, and half an inch thick. The sillimanite favors certain bands within the microcline gneiss, and, although it is commonly very discontinuous, many sillimanite-bearing bands were traced to delineate structure. In many places where the sillimanite dies out within a favored band, small augen composed of white feldspar rims and green chloritic centers are found along strike. These apparently have a genetic relationship to the sillimanite plates, since they locally contain sillimanite, and during field mapping were used to indicate the proximity of sillimanite. Known distribution of sillimanite is indicated on the geologic map (Pl. 1), but, since the mineral was not recognized until field mapping had been under way for some time, it probably has a somewhat wider distribution than is shown. Garnet, in disseminated porphyroblasts, is a common accessory mineral in microcline gneiss. In many places it is associated with sillimanite but in general it has a much wider distribution. Although it favors certain bands, its occurrence,

like that of the sillimanite, is sporadic in those bands.

Biotite and chlorite are by far the most abundant dark minerals in the microcline gneiss, but magnetite is a common accessory mineral, and pyroxene and hornblende are found locally. In the band of microcline gneiss within the Byram gneiss 1 mile east of Wright Pond, and also in most bands of microcline gneiss southeast of Sparta, the most abundant dark mineral is magnetite, with only a small amount of biotite or chlorite. These bands also contain local sillimanite and garnet. This same type of rock in the area half a mile east and half a mile southeast of McAfee contains, in addition to the magnetite, a considerable proportion of pyroxene and associated serpentine and epidote. Locally, pyroxene is the dominant dark mineral. In the Mount Eve area the microcline gneiss consists of thin bands of quartz and pink microcline alternating with bands rich in hornblende. Local sillimanite and garnet are common. In spite of the variation in dark minerals, the microcline gneiss is distinctive in field mapping.

The band of microcline gneiss 1½ miles west of Lake Mohawk is unique in two respects: it contains neither sillimanite nor garnet, and the potassic feldspar is microperthite instead of microcline as in most areas of microcline gneiss. This latter characteristic will be discussed later under Petrogenesis. This band contains thin, conformable bands or lenses of hornblende gneiss, particularly near its contacts with the adjacent rocks.

The potash feldspar of the microcline gneiss is commonly pink, giving a distinctive pink, or pink and white, banded appearance to both the weathered outcrop and the fresh rock. The pink and white bands, commonly less than half an inch wide, consist of white, plagioclase-rich layers alternating with pink, microcline-rich layers. The rock appears migmatitic in places where the pink bands coarsen into pegmatite. The dark minerals are distributed fairly evenly through the rock. A second type of banding is formed by an alternation of bands very rich in quartz with bands poorer in quartz. These bands range in width from a quarter of an inch to several inches, but in general are ½–2 inches wide. Differential erosion produces a ribbed weathered surface on which the quartz-rich bands stand out in relief. On the fresh surface, the quartz-rich bands are dark gray in contrast to the buff to white of the bands richer in feldspar.

Wherever biotite or chlorite is the predominant dark mineral, the microcline gneiss exhibits a distinct foliation produced by the rough alignment of mica flakes. This foliation commonly occurs in conjunction with banding.

Where sillimanite occurs in the microcline gneiss it produces a strong lineation. Most large sillimanite aggregates are flattened in a plane parallel to the banding to form a coarse foliation. Garnet clusters are commonly associated with the sillimanite, and many are flattened in the same plane, accentuating the coarse foliation.

Where pink feldspar is absent the weathered surface of the microcline gneiss is buff and slightly iron-stained. The surface is commonly rounded and generally granular or saccharoidal. Where bands extremely rich in quartz are present, differential erosion has produced a strongly ribbed, but still generally rounded, surface.

In the area 1½ miles northeast of Perona Lake, quartz-rich microcline gneiss is interlayered with quartz-rich biotite gneiss. This zone can be traced for about 1 mile southwestward to where the microcline gneiss pinches out, leaving only the quartz-rich biotite gneiss. The two varieties of rock are similar in appearance, and both contain garnet and sillimanite locally.

The microscopic texture of the microcline gneiss ranges from granoblastic to granitic with irregular to interlocking grain boundaries. The grain size ranges from 0.03 mm to 2.0 mm, but most grains range between 0.3 to 1.0 mm. Many of the altered plagioclase grains have fresh myrmekitic borders (secondary albite?) next to microcline grains but not next to other grains (Pl. 2, fig. 6). Round poikilitic inclusions of quartz are commonly contained in larger grains of microcline and plagioclase.

Replacement textures are not common, but in some sections muscovite has replaced microcline, plagioclase, and biotite. Microcline may have partially replaced plagioclase which remains as irregular altered zones in unaltered microcline.

Microcline is microperthitic in some thin sections, but the ratio of albite blebs to microcline is low. Although its albite content typically does not exceed 5 per cent, the microcline contains up to 20 per cent of albite blebs in the microcline gneiss of the Pimple Hills, up to 80 per cent (microantiperthite) in the microcline gneiss west of Lake Mohawk, and up to 40 per cent in the microcline gneiss within Byram gneiss east of Stag Pond. Albite blebs make up 0–5 per cent of the microperthite in the area southwest of the Pimple Hills, less than 1 per cent in the region northeast of the Pimple Hills, and up to 5 per cent on the northwest side of Hamburgh Mountain. Portions of the microcline gneiss west of Lake Mohawk contain microantiperthite in which a plagioclase host contains blebs of microcline. The albite in microperthite usually forms veinlets or stringers originating at the grain boundaries and penetrating inward (Fig. 4). In the areas where albite constitutes 5 per cent or more of the microperthite, the intergrowth is much the same as in the Byram gneiss, especially in the area east of Stag Pond.

Microscopic structures in the microcline gneiss include subparallel orientation of biotite or chlorite flakes, occasional platy quartz grains with their shortest dimension parallel to the biotite foliation, sillimanite needles concentrated in quartz veinlets or quartz-rich zones, and occasional banding formed by microcline-rich layers alternating with quartz-plagioclase layers.

Table 1 gives the range in mineralogical composition of the microcline gneiss. Biotite is pleochroic from straw yellow to dark brown but is commonly altered to chlorite which contains numerous opaque specks of magnetite or other iron oxide formed perhaps by release of iron in the transformation from biotite to chlorite. Locally the microcline gneiss contains epidote, pyroxene, and hornblende.

Hornblende gneiss.—Type I hornblende gneiss is abundant in the areas 2 miles east of Stag Pond, three-fourths of a mile west of Franklin, 1 mile west of McAfee, and in the Lake Lenape and Glenwood synclines. It also occurs in less extensive bands in the Pimple Hills syncline and within the Byram, Losee, and metasedimentary or metavolcanic gneisses throughout the map area. It is a dark, fine- to medium-grained gneiss with local thin bands or lenses of biotite gneiss. Although the rock is generally black, it is greenish where pyroxene is abundant.

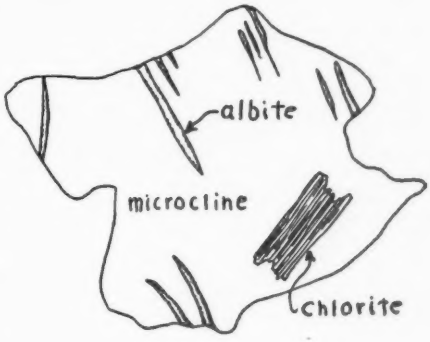

FIGURE 4.—SKETCH OF GRAIN OF MICROCLINE IN A THIN SECTION OF MICROCLINE GNEISS

The plagioclase feldspar is commonly green, particularly in fresh rock. Both hornblende and pyroxene occur throughout the rock, but biotite is only local. Accessory sphene is common in this rock as in most of the hornblende gneiss types. The banding in type I hornblende gneiss consists of alternating light and dark bands which range in thickness from an eighth of an inch to 1 inch but are generally less than half an inch thick. The dark bands consist of hornblende and pyroxene with minor feldspar and occasional biotite; the light bands are mostly feldspar with minor quartz and dark minerals. In the Glenwood syncline, small white feldspar augen with greenish centers occur locally in the hornblende gneiss. In one place they are present in possible pillows in the hornblende gneiss (Pl. 3, fig. 5). These "pillow" structures have been observed in several outcrops of type I hornblende gneiss in that area and suggest that at least part of the type I hornblende gneiss there may represent a volcanic flow. The "pillows" consist of type I hornblende gneiss, locally with feldspar augen, and are separated from each other by veinlike masses of fine- to coarse-grained pyroxene-scapolite rock. Locally,

TABLE 1.—MODAL ANALYSES OF MICROCLINE GNEISS

	Sample No.										Average composition
	V36-1	X24-2	V428-D	P80-D	V361-B	K37	K65	V312-B	K280	K287-W	
Microcline	....	35.0	....	....	....	....	21.3	45.6	....	42.0	41.3
Microperthite											
Microcline	52.8	....	51.6	47.4	30.8	46.2	....	....	40.4	....	
Albite	2.5	....	2.0	4.1	7.2	2.4	....	....	tr.	....	1.8
Quartz	33.3	41.7	40.3	37.6	37.7	43.7	35.4	27.1	38.8	39.0	37.5
Plagioclase	6.7 (An_6)	16.7 (An_6)	0.7	8.5 (An_{10})	22.8 (An_{16})	4.6 (An_6)	36.1 (An_{15})	17.6 (An_{12})	12.0 (An_{10})	14.7 (An_9)	14.0
Biotite and Chlorite	1.2	6.2	5.3	....	1.4	1.6	5.7	9.6	5.9	2.5	3.9
Sillimanite	....	....	tr.	....	....	....	....	tr.	....	....	tr.
Garnet	3.2	....	....	....	....	....	....	....	....	....	0.3
Apatite	....	....	tr.	....	....	....	....	....	....	....	tr.
Magnetite	....	....	....	1.8	tr.	1.5	1.6	....	....	0.2	0.5
Muscovite	....	....	tr.	....	....	....	tr.	tr.	2.8	1.4	0.4
Zircon	....	....	....	....	tr.	tr.	tr.	tr.	....	0.2	tr.
Alteration	0.2	0.4	tr.	0.6	....	....	....	....	....	....	0.1
Epidote	....	....	....	....	....	tr.	tr.	....	....	....	tr.
Totals	99.9	100.0	99.9	100.0	99.9	100.0	100.0	99.9	99.9	100.0	99.8

V36-1—5300 feet S. 60°E. of Howell's Pond, northwest of Lake Mohawk

X24-2—4200 feet N. 85°E. of Howell's Pond

V428-D—About one mile N. 15°W. of the northwest tip of Lake Mohawk

P80-D—From band within Byram gneiss, about 6000 feet southeast of the southeast tip of Stag Pond

V361-B—Microcline gneiss near contact with Byram gneiss, about 8500 feet S. 85°W. of southernmost tip of Lake Mohawk

K 37—About 10,000 feet S. 85°W. of Ogdensburg, in the Pimple Hills

K 65—Within the Cork Hill band of gneisses about 3500 feet southwest of the south end of the Franklin ore body

V312-B—About 5500 feet N. 20°W. of McAfee, on Pochuck Mountain

K280—2500 feet east of Lake Pochuck

K287-W—1500 feet southeast of Glenwood Lake, in the south end of the Glenwood syncline

coarse-grained hornblende occurs at the contact of the pyroxene-scapolite rock and the hornblende gneiss of the "pillows". Masses of pyroxene-scapolite rock also occur within the "pillows", and locally calcite is present and weathers out to form irregular cavities in the center of the "pillows". If the structures are pillows, they have been contorted and greatly elongated parallel to the mineral lineation. Top and bottom data are indistinct and locally contradictory within a single outcrop.

Parallel orientation of hornblende laths commonly produces a strong lineation in type I hornblende gneiss. In the central band of the Lake Lenape syncline, conformable pegmatite veinlets, less than 1 inch wide, of pink feldspar and quartz occur within the gneiss. This feature characterizes that particular band throughout the major portion of its length but has not been observed elsewhere. Weathered outcrops of type I hornblende gneiss are relatively dark and usually form ridges.

In many places, particularly west of Sparta, type I hornblende gneiss grades into dark biotite gneiss. Small bands of one variety of gneiss are abundant within the large band of the other variety on either side of the gradational contact. Such contacts are represented on the map by serrate dashed lines.

Type II hornblende gneiss occurs in bands half a mile west of Stag Pond, half a mile north of Sparta, in the Lake Lenape and Glenwood synclines, and in small bands within many of the other gneisses. It is a medium-dark to dark, fine- to medium-grained gneiss characterized by the distribution of its mafic minerals. The

hornblende, pyroxene, and biotite occur with feldspar in separate, discontinuous bands or lenses which give the rock an irregularly striped appearance. The weathered surface of type II hornblende gneiss is slightly rounded. Since type II hornblende gneiss was not recognized until much of the field mapping had been completed, it undoubtedly occurs in places other than those described.

The microscopic texture of types I and II hornblende gneiss is granoblastic, and grain boundaries are polyhedral to interpenetrating. Pyroxene, where present, forms small interstitial grains and masses between hornblende and plagioclase.

The mineralogical compositions of types I and II hornblende gneiss are given in Table 2. The composition of the plagioclase is radically different in the two types, but the hornblendes are very similar in optical properties. Hornblende properties from sample V35 are: α = 1.672 ± .002, β = 1.687 ± .002, γ = 1.697 ± .002; 2V = (−)58°; Z ∧ C = 14°. Hornblende properties from sample V491 are: α = 1.672 ± .002, β = 1.685 ± .002, γ = 1.695 ± .002; 2V = (−) 55°; Z ∧ C = 15°. The pleochroism of both samples is α = light yellowish green, β = dark brownish green, γ = dark green. Pyroxene from sample V502, located 1000 feet north of Stag Pond, has an index, β, of 1.705 ± .005. Its 2V and Z ∧ C are (+)60° and 45°, respectively. It is either augite or a member of the diopside-hedenbergite series. The pleochroism of biotite is straw yellow to very dark brown. Hypersthene occurs in hornblende gneiss from the area 9000 feet north-northwest of Sparta and locally from hornblende gneiss bands in the Stag Pond type of Losee gneiss. Hypersthene is brown in hand specimens and pleochroic from light green to pink in thin sections.

Type III hornblende gneiss occurs locally in bands within the Lake Lenape and Glenwood synclines, in bands in the Wildcat and Cork Hill horizons 2¼ miles northwest of Sparta and 3 miles north of Sparta, in the area 1 mile west of McAfee, and near the contact of the Cork Hill gneiss zone and the Wildcat marble band from south of the Sterling mine northward to Hamburg. It is indicated on the geologic map (Pl. 1) by marble lenses within hornblende gneiss. It is actually type I hornblende gneiss with occasional lenses of calcite and bands or lenses of pyroxene gneiss. The pyroxene gneiss is generally associated with the calcite lenses which vary considerably in abundance. The lenses of coarse-grained calcite, or marble, which are the characteristic feature of this type of hornblende gneiss, are conformable to the banding and are commonly surrounded by dark pyroxene gneiss or sphene-bearing pyroxene-scapolite rock. Sphene is common in the gneiss, and in one thin section it was concentrated at the contact of hornblende gneiss with a calcitic lens. The lenses range from a few inches in length and a fraction of an inch in width to several feet in length and 6 inches to 1 foot in width. The calcite is normally impure and typically contains pyroxene, mica and other

TABLE 2.—MODAL ANALYSES OF HORNBLENDE GNEISS AND PYROXENE-RICH ROCKS

	Sample no.			
	V 35	V 491	X 180	X 142
Plagioclase	29.9 (Ab_{75})	50.3 (An_{32})	....	....
Hornblende	58.7	21.1	....	tr.
Pyroxene	....	1.9	38.0	25.9
Biotite	0.6	4.0	....	....
Epidote	....	....	2.0	....
Quartz	8.5	5.7	....	tr.
Magnetite	1.9		....	....
Apatite	0.5			
Orthoclase	tr.	16.9	....	....
Microperthite	....	....	....	32.8
Sericite	....	....	....	tr.
Scapolite	....	....	59.0	40.0
Sphene	....	....	1.0	1.3
Alteration	tr.	tr.	....	....
Totals	100.1	99.9	100.0	100.0

* Plagioclase highly altered to sericite plus other unidentified material

V 35—Type I hornblende gneiss 4900 feet S. 60°E. of Howell's Pond, northwest of Lake Mohawk

V491—Type II hornblende gneiss, 2500 feet due west of the southwest tip of Stag Pond

X180—Pyroxene-scapolite gneiss from the southwest side of Mount Eve

X142—Pyroxene-scapolite rock inclusion within Mount Eve granite from the northeast side of Mount Adam

disseminated silicates. The banding in this rock is very tightly and irregularly contorted in many places. The weathered surface of the rock is distinctive because the calcite has been leached out to form lens-shaped cavities with very irregular outlines, which give the rock a pock-marked appearance (Pl. 3, fig. 6).

The microscopic texture of type III hornblende gneiss is the same as that of types I and II except that pyroxene, epidote, scapolite, sphene, serpentine, and some talc form at the contact between hornblende gneiss and calcitic bands. In some sections pyroxene is apparently secondary because it contains irregular, unreplaced cores of calcite, plagioclase, and orthoclase.

Type IV hornblende gneiss occurs primarily in the Glenwood syncline and is best developed in the central part. A single thin, discontinuous band occurs within the Franklin band of marble west of McAfee. This type is a dark-green to black gneiss containing closely spaced clusters or augen of medium- to coarse-grained hornblende in a fine-grained biotite-hornblende-plagioclase groundmass. These augen, which range in length from less than a tenth of an inch to a quarter of an inch, give the rock a very distinctive spotted appearance. Where the augen are small the spotted effect is quite subdued. Type IV hornblende gneiss containing large hornblende augen locally grades along strike into rock with smaller hornblende augen and finally into type I hornblende gneiss. Most weathered outcrops of type IV hornblende gneiss are round and are as distinctively spotted as the fresh rock.

Biotite gneiss.—Biotite gneiss is common in the Lake Lenape syncline and in the areas 1 mile north of Sparta, just west of the Franklin mine, three-quarters of a mile west of Franklin, and 1 mile northwest of McAfee. It also forms bands within the hornblende gneiss in many localities. It is a medium-light to dark, fine- to medium-grained gneiss which commonly contains hornblende as a minor constituent and also contains numerous bands of hornblende gneiss. The band of biotite gneiss 3400 feet northwest of Sparta contains abundant hornblende gneiss bands which make up nearly 50 per cent of the rock. The band of biotite gneiss in the core of the fold 6000 feet northwest of Sparta also contains many hornblende gneiss bands. Biotite gneiss apparently locally grades along strike into type I hornblende gneiss by the gradual increase in the abundance of hornblende gneiss bands. Small lenses of microcline gneiss, some of which contain sillimanite, also occur locally within the biotite gneiss.

The biotite content of the rock generally ranges from 15 to 40 per cent. Where the biotite content approaches 40 per cent, the rock becomes schistose. As in type I microcline gneiss, garnets are found locally throughout the biotite gneiss. Banding is uncommon, but a good foliation, formed by the subparallel orientation of biotite flakes, is typically present. The biotite gneiss generally exhibits a rounded, uneven weathered surface.

The biotite gneiss on the west limb of the Lake Lenape syncline is abnormal in its mineral composition. It is a light, fine- to medium-grained gneiss which, unlike normal biotite gneiss, is high in quartz (35–70 per cent) and low in biotite or phlogopite (less than 5 per cent). As a rule, it contains disseminated garnets. This rock would be classified as microcline gneiss if its feldspar were not oligoclase. It exhibits a foliation and weathered surface much like that of the normal biotite gneiss. This particular gneiss has been mapped only in the one area mentioned but may occur locally elsewhere.

Pyroxene gneiss and related rocks.—A light, pyroxene-bearing gneiss occurs in a fairly thin band just west of the Roseville mine and in the Cork Hill gneiss zone in the area 1 mile north of McAfee. It is a light, medium-grained gneiss composed mainly of plagioclase with 5–10 per cent pyroxene, 1–2 per cent sphene, and sparse local hornblende. The weathered surface is very white.

A second variety of pyroxene gneiss is found in a band along the west side of Lake Lenape, in the area 13,500 feet north of Sparta, in several thin bands in the vicinity of Mount Eve, and in numerous other localities as thin discontinuous bands within type III hornblende gneiss. It is a medium dark, fine- to medium-grained gneiss composed mainly of scapolite, or locally plagioclase, and pyroxene. The pyroxene content is usually around 25–30 per cent, and hornblende occurs locally. Sphene is a characteristic acces-

sory mineral of this gneiss and locally becomes very abundant. The gneiss commonly contains thin, discontinuous bands of type I hornblende gneiss. In many places, as hornblende gneiss bands become increasingly abundant, the gneiss grades into type III hornblende gneiss. This medium-dark type of pyroxene gneiss in most places contains, or is associated with, calcitic zones which are represented on the map by marble lenses. The gneiss exhibits a banding formed by thin layers rich in scapolite or feldspar alternating with thin layers rich in pyroxene. The weathered surface is characterized by irregular cavities formed by the leaching of the calcite lenses as in type III hornblende gneiss (Pl. 3, fig. 6).

A structureless, coarse-grained to pegmatitic pyroxene-scapolite rock is commonly associated with the medium-dark type of pyroxene gneiss. In many places sphene is an accessory mineral. This coarse-grained rock forms at the contact of hornblende and pyroxene gneisses with marble and at the contact of calcitic lenses with their enclosing medium-dark pyroxene gneiss. It also rims blocks of gneissic rock within the major bands of marble and occurs as small masses within the marble not associated with gneissic fragments. Many of the rims around hornblende gneiss blocks include coarse-grained hornblende and local apatite. Coarse-grained pyroxene-scapolite rock forms isolated masses 1 mile north of McAfee at the contacts of the light pyroxene gneiss with its enclosing marble bands; dikelike bodies are found within Byram gneiss and Mount Eve granite in the vicinity of Mount Adam. A large mass of pyroxene-scapolite rock is found in the core of a small synclinal structure in intimate association with Mount Eve granite in the area 1 mile S. 20 W. of Amity.

Both the medium-dark pyroxene gneiss and the coarse-grained to pegmatitic pyroxene-scapolite rock are commonly associated with impure calcareous rocks.

The medium-dark pyroxene gneiss at Mount Adam has a granoblastic texture. Grain boundaries are fairly smooth and polyhedral. The grain size of pyroxene and scapolite ranges from 0.1 mm to 2.0 mm. The grain size of sphene ranges from 0.03 to 0.3 mm. A thin section of pyroxene-scapolite rock included in granite on the north side of Mount Adam contained complexly intergrown scapolite and microperthite.

The mineralogical compositions of medium-dark pyroxene gneiss and coarse-grained pyroxene-scapolite rock are given in Table 2. The pyroxenes of both are almost identical and have the following optical properties: β = 1.697 to 1.705; $Z \wedge C$ = 44° to 46°; 2V = 60° to 61°; the color is light green. Scapolite from sample X180 has an index, n_e, of 1.547 ± .002, and scapolite from sample X142 has an index, n_e, of 1.540 ± .002.

A coarse-grained pyroxene-garnet skarn which contains local hornblende is found associated with the ores at the mines north of Andover, the Roseville mine, in numerous magnetite deposits within the gneisses, and in the Franklin and Sterling zinc deposits. At all these localities, calcite is found at least locally, and the ore occurs in association with dark to medium-dark type I hornblende gneiss and/or pyroxene gneiss.

Garnet gneiss.—Garnet gneiss occurs in thin bands in the Lake Lenape syncline, in the folded area 2 miles northwest of Sparta, in the area three-fourths of a mile west of Franklin, and at Mount Eve. It is a medium-dark to dark, medium- to coarse-grained gneiss with abundant large garnet porphyroblasts. A representative sample would contain approximately 30–50 per cent plagioclase, 20–30 per cent quartz, 20–30 per cent garnet, and 10–20 per cent biotite. Garnet gneiss apparently grades into garnet-bearing biotite gneiss both laterally and along strike and is probably just an extremely garnet-rich biotite gneiss. It is classified as a separate variety of gneiss because it forms distinct, thin bands, 5–20 feet wide, which were very useful as traceable horizons for determining structure. The biotite flakes in the garnet gneiss commonly form a rough foliation, and where the rock is fairly rich in biotite it is schistose. Outcrops are rounded but commonly form ridges.

Graphitic gneiss.—Graphitic gneiss occurs 2½ miles north-northwest of Sparta in two places, 2 miles west of Franklin, half a mile west of Hamburg, and in the vicinity of Mounts Adam and Eve where there are several occurrences. In general, the graphitic gneiss is a medium-light, fine- to medium-grained gneiss

composed of plagioclase, quartz, and biotite or chlorite in order of decreasing abundance. It contains less than 5 per cent graphite. In the Mounts Adam and Eve area, and in the area west of Franklin, the gneiss locally contains pyroxene and sphene. This is probably because the graphitic gneiss in these areas is closely associated with pyroxene gneiss. At one locality at Mount Eve the overlying pyroxene gneiss is calcitic. In the areas west of Hamburg and west of Franklin, the graphitic gneiss contains appreciable potash feldspar. In most of the areas just referred to, small graphite-bearing pegmatite veinlets occur locally within the rock. Sparse graphite also occurs in one locality east of McAfee in a band of Byram gneiss which has an unusually high content of dark minerals.

Igneous Gneisses and Rocks

Introductory statement.—Spencer (1908, p. 5) classified all the light igneous gneisses of the area as either Byram gneiss or Losee gneiss. The writers reclassified these gneisses in order to divide them into smaller units for more detailed mapping. The names Byram and Losee are used in this section to describe certain well-defined igneous rocks which fit Spencer's definitions of the dark facies of the Byram gneiss (Spencer, 1908, p. 5) and the typical Losee gneiss (Spencer, 1908, p. 5). Two igneous gneisses, oligoclase gneiss and granodiorite gneiss, have been given separate names because of characteristics which distinguish them from the Byram and Losee gneisses. The Losee gneiss as described in this paper corresponds to the quartz-oligoclase gneiss of the Ringwood area (Hotz, 1953, p. 174–178), and the Byram gneiss to the hornblende granite and related facies (Hotz, 1953, p. 178–182).

Losee gneiss.—Losee gneiss occurs at three localities. It occupies the cores of large anticlinal structures east of Franklin and north of Hamburg and the core of the eastern anticlinal fold in the vicinity of Stag Pond. The contacts of Losee gneiss with other rocks are usually conformable although small-scale discordances are found in some localities (Fig. 5).

The Losee gneiss is a light-colored, medium- to coarse-grained gneiss with a notably small content of dark minerals. Locally the rock contains accessory hornblende or biotite, but in general the only dark mineral is a chlorite that gives the fresh rock a greenish color. Garnet occurs locally as small disseminated red crystals. Local thin bands of medium-dark

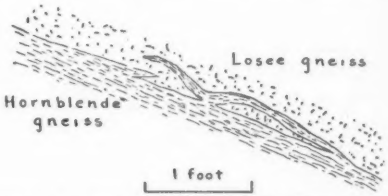

FIGURE 5.—LOCALLY DISCORDANT CONTACT BETWEEN THE LOSEE GNEISS AND INCLUDED HORNBLENDE GNEISS BLOCK
Located west of Wright Pond

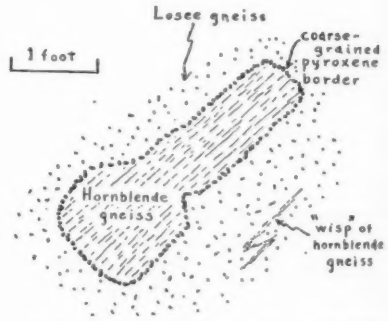

FIGURE 6.—BLOCKY INCLUSION OF HORNBLENDE GNEISS IN THE STAG POND TYPE OF LOSEE GNEISS

hornblende gneiss occur in the Losee gneiss and may be associated with larger bands of dark hornblende gneiss. The medium-dark bands range in thickness from a few inches to several feet and have both gradational and sharp contacts with the adjoining Losee gneiss and dark hornblende gneiss. The dark hornblende gneiss bands are from less than 1 foot to more than 50 feet wide and include both types I and II hornblende gneiss. In places these bands are tightly folded. The hornblende gneiss commonly continues as a band or zone of bands for a considerable distance along strike, but locally, particularly in the Stag Pond area, it forms lenticular or blocky inclusions within the Losee gneiss (Fig. 6). In general, the normal Losee gneiss has a faint folia-

tion formed by a rough parallelism of chlorite or biotite flakes. The foliation is parallel to the banding of the rock. A second type of foliation is formed by disc-shaped quartz grains which lie in planes parallel to the mica foliation.

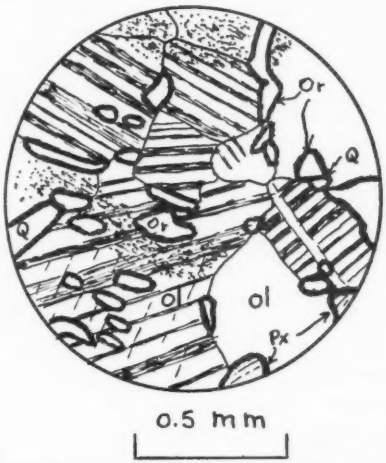

FIGURE 7.—SKETCH OF A PORTION OF A THIN SECTION OF THE LOSEE GNEISS

Most joints in the Losee gneiss have smooth surfaces which become chalky white because of the partial weathering of oligoclase. This smooth, chalky-white weathered surface is characteristic of the Losee gneiss.

The Losee gneiss of the Stag Pond area differs from the normal Losee in the following ways: it is never coarse-grained, hornblende-bearing bands are abundant, and the characteristic chalky-white weathered surface is poorly developed.

The microscopic texture of the Losee gneiss is slightly inequigranular with irregular to interlocking quartz-plagioclase boundaries and irregular to slightly sutured quartz-quartz boundaries. The grain size ranges from about 0.4 mm to 3.2 mm with an average of about 1.4 mm. Small, globular quartz inclusions in plagioclase range from 0.1 to 0.36 mm. The normal Losee gneiss contains interstitial grains of orthoclase and occasionally microcline (Fig. 7), whereas the Stag Pond type does not. Occasional garnet grains are anhedral to subhedral.

The microscopic structures consist of a biotite or chlorite foliation and, in some thin sections, platy arrangement of quartz grains.

The variation in mineralogical composition of the Losee gneiss is shown in Table 3. The plagioclase of normal Losee gneiss ranges from An_{20} to An_{28}, and the plagioclase of the Stag

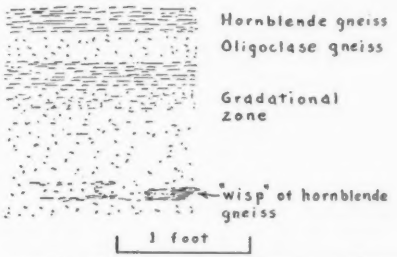

FIGURE 8.—GRADATION OF HORNBLENDE GNEISS INTO OLIGOCLASE GNEISS
On the west side of the Pimple Hills

Pond type ranges from An_8 to An_{12}. Hornblende of the Stag Pond type has a range in 2V of (−) 80°–82° and a range in Z ∧ C of 16°–18°. Its pleochroism is α = pale brownish green, β = colorless, and γ = pale green. Biotite, when present, is pleochroic from straw yellow to reddish brown but is generally almost entirely altered to chlorite.

Oligoclase gneiss.—Oligoclase gneiss is important in the Pimple Hills, where it is the most abundant rock type. It is a light-colored, medium-grained gneiss which is almost identical with Losee gneiss in mineralogical composition. Thin bands of oligoclase gneiss with up to 10 per cent hornblende occur in the same manner as in the Losee gneiss (Fig. 8).

The oligoclase gneiss and the Losee gneiss differ principally in weathering and in mode of emplacement. In general the oligoclase gneiss is granular and has a buff color in outcrop. It forms sill-like masses. Locally it contains pink feldspar. The granularity, the characteristics of its weathered surface, and the local pink color of the oligoclase gneiss are the basis for calling it a separate variety of gneiss. Locally, the weathered surfaces of the oligoclase gneiss are chalky white and not granular, and in such places the rock is indistinguishable from the Losee gneiss. This suggests that the oligoclase gneiss is merely a type of Losee gneiss.

The microscopic texture of the oligoclase

gneiss is the same as the Losee gneiss except that the quartz is not platy as in the Losee gneiss. Interstitial orthoclase is present in the oligoclase gneiss as in the Losee gneiss.

TABLE 3.—MODAL ANALYSES OF LOSEE AND OLIGOCLASE GNEISSES

	Sample no.				
	V 902	V 775	V432-H	V460-C	V847-F
Plagioclase	58.5 (An_{19})	78.3 (An_{28})	68.4 (An_{12})	70.4 (An_{8})	62.2 (An_{10})
Quartz	34.2	15.4	24.7	17.9	33.4
Microcline	4.4	....	0.9	....	tr.
Orthoclase	....	1.9	....	....	1.0
Biotite	1.1	....	0.6	....	3.3
Hornblende	....	3.6	5.2	....	....
Pyroxene	....	0.6	....	....	....
Chlorite	....	tr.	....	5.1*	....
Apatite	....	tr.	tr.	0.4	....
Magnetite	....	tr.	....	2.5	....
Zircon	....	tr.	....	....	tr.†
Garnet	1.9	....	....	....	....
Alteration	....	....	....	3.6	....
Totals	100.1	99.8	99.8	99.9	99.9

* Includes small amount of biotite

† Includes rare epidote

V 902—Losee gneiss, 6100 feet S. 40°E. of the south end of Wright Pond

V 775—Losee gneiss, 8400 feet due south of Sparta

V432-H—Losee gneiss, Stag Pond type, 1800 feet south of the center of Stag Pond

V460-C—Losee gneiss, Stag Pond type (sheared), 5200 feet south of the southwest tip of Stag Pond

V847-F—Oligoclase gneiss 7800 feet S. 85°W. of Ogdensburg

The mineralogical composition of one sample of oligoclase gneiss from the Pimple Hills is given in Table 3. The plagioclase has a composition of An_{10}. Biotite is pleochroic from straw yellow to dark brown.

Granodiorite gneiss.—The granodiorite gneiss occurs in a band 2 miles west of Lake Mohawk and in a large pod-shaped mass 1¾ miles north of Sparta. It is a medium-light to medium-dark, medium-grained gneiss which contains biotite, hornblende, and local pyroxene. The mafic minerals are commonly in concentrations which form discontinuous, very thin, elongated plates, thereby producing a good lineation. This characteristic structure and the relative proportions and quantity of the dark minerals make this gneiss a distinct variety. The plates of dark minerals cause the layers rich in feldspar and quartz to form rod-shaped structures which have lenticular cross sections, with the biotite and hornblende in the interstices. This feature gives a corrugated appearance to the weathered surfaces parallel to the axes of the rods and an augen-gneiss appearance to weathered surfaces perpendicular to the rods. It also produces a semibanding or coarse foliation which is commonly accentuated by a rough, small-scale foliation resulting from the subparallel orientation of individual flakes of mica. The granodiorite gneiss commonly contains small, irregular, lens-shaped inclusions or wisps of dark biotite gneiss and hornblende gneiss whose contacts are gradational with the enclosing gneiss. It also contains more extensive conformable bands of dark biotite gneiss and hornblende gneiss which appear most abundantly near its borders. Several discontinuous, conformable bands of microcline gneiss, some of them sillimanite-bearing, occur in the central part of the granodiorite gneiss band.

The granodiorite gneiss has an inequigranular, granitic texture in thin sections. The grain size ranges from 0.1 to 2.5 mm with an average of about 1.0 mm. Grain boundaries are irregular to interlocking. Hornblende and biotite grains are between quartz and feldspar grains rather than intergrown with them.

A vague banding, in some sections, is formed by the concentration of biotite, hornblende, and local pyroxene.

The mineral compositions of three samples of granodiorite gneiss are given in Table 4. The plagioclase ranges from An_{18} to An_{32}. The optical properties of hornblende from sample V388 are: $\alpha = 1.660 \pm .002$, $\beta = 1.672 \pm .002$, $\gamma = 1.683 \pm .002$; $2V = (-)\ 64° \pm 4°$; $Z \wedge C = 15° \pm 1°$. Its pleochroic formula is α = very light green, β = dark brownish green, γ = dark green. The optical properties of hornblende from sample J295-F are: $\alpha = 1.670 \pm .005$, $\beta = 1.687 \pm .002$, $\gamma = 1.695 \pm .005$; $2V = (-)\ 61°$; $Z \wedge C = 16°$. The pleochroism is α = light yellowish green, $\beta = \gamma$ = dark green. Biotite from J295-F is pleochroic

from straw yellow to dark brown and its index of refraction, β, is 1.652 ± .002. Pyroxene is too altered and too uncommon for optical determination without heavy-media separation.

TABLE 4.—MODAL ANALYSES OF GRANODIORITE GNEISS

	Sample no.			
	V 388	J295-F	V570-F	Average composition
Plagioclase	56.0 (An_{18})	50.0 (An_{22})	55.6 (An_{20})	53.9
Quartz	22.2	28.9	25.2	25.4
Microperthite				
Microcline	10.6	....	....	....
Albite	tr.	....	....	....
Orthoclase		7.0	7.6*	....
Hornblende	0.9	8.8	2.4	4.0
Biotite	9.8	4.1	8.4†	7.4
Magnetite	0.5	1.0	0.7	0.7
Pyroxene	tr.	....	....	tr.
Apatite	....	tr.	tr.	tr.
Zircon	....	....	tr.	tr.
Alteration	....	tr.	....	tr.
Totals	100.0	99.8	99.9	99.8

* Includes a small amount of microcline

† Largely altered to chlorite

V 388—About 6600 feet N. 85° W. of Sparta

J 295-F—About 4000 feet N. 85° W. of Sparta

V 570-F—3000 feet due east of the north end of Lake Lenape

Byram gneiss.—Byram gneiss commonly forms large masses which locally contain bands of other gneisses. The various types of Byram gneiss are closely associated within the large masses and at many places grade into one another. The contact of the Byram with other gneisses is almost everywhere concordant, but locally discordant contacts have been observed (Fig. 9). In one locality south of the map area, Byram gneiss has a gradational contact with type II hornblende gneiss (Fig. 10).

Type I Byram gneiss occurs in the areas south, east, and west of Lake Mohawk, in a large area southeast of McAfee, and on the south end of Mount Adam. It is a medium-light to medium-dark, coarse-grained gneiss characterized in most places by its color and lineation. The microcline-microperthite is generally bronze in color, both on weathered and on fairly fresh surfaces. In extremely fresh rock in road cuts, the feldspar appears to be greenish gray. The hornblende in the rock is con-

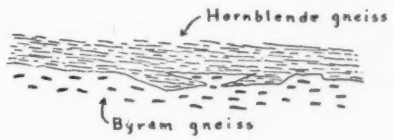

FIGURE 9.—LOCALLY DISCORDANT CONTACT BETWEEN THE BYRAM GNEISS AND TYPE II HORNBLENDE GNEISS

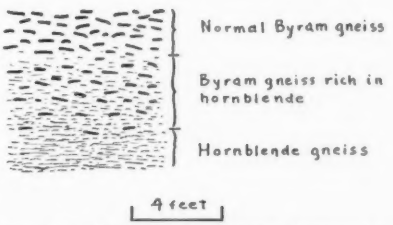

FIGURE 10.—GRADATIONAL CONTACT BETWEEN THE BYRAM GNEISS AND TYPE II HORNBLENDE GNEISS

centrated into small roughly parallel rods up to 1 inch long. This gives the rock a strong lineation which, with the bronze color of the feldspar, makes type I Byram gneiss distinctive. Biotite occurs very locally in the rock, and allanite has been found at one locality. In some places hornblende is absent, and the rock might be classified as alaskite. Banding in type I Byram gneiss is most common near its contacts with other gneisses and consists of layers rich in feldspar and quartz alternating with hornblende-bearing layers. The layers are normally a quarter of an inch–1 inch thick. Toward the center of masses of Byram, banding gives way to a strong hornblende lineation. In the center of some masses of Byram gneiss, particularly the one just west of Stag Pond, the rock becomes a homogeneous hornblende granite.

Type II Byram gneiss may be considered a medium-grained variety of type I Byram gneiss and is listed as a separate type only because in some localities, particularly the area 1½ miles

southeast of Stag Pond, it is a mappable band in contact with type I Byram gneiss. However, in the area just east of this band, in the area southeast of McAfee, and in several other localities, types I and II Byram gneiss occur in such intimate association that they cannot be mapped separately. In many places they grade into each other along strike. The type II Byram gneiss just west of the Roseville mine is further characterized by feldspar augen, about a quarter of an inch long, which occur throughout the rock in that area and to the south. Further work with Byram gneiss of this description might justify its classification as a separate type although it locally grades into type I Byram gneiss.

Type III Byram gneiss is mapped only in the area 1¾ miles east of the Roseville mine. It continues in outcrop northward, however, in the same stratigraphic position just beyond the edge of the map area, into the region 1¾ miles southeast of Sparta. Its northward extent is not well known since little mapping was done in that area, but, since it does not occur in the area east of Franklin, it probably either lenses out or grades into type I or II Byram gneiss. Type III Byram gneiss is a medium-light to medium-dark, medium- to coarse-grained gneiss in which pyroxene and magnetite, rather than hornblende, are the predominant dark minerals. The main feature which distinguishes this type of Byram gneiss from types I and II is the predominance of plagioclase over potash feldspar. This same feature might make it advisable to consider this gneiss a separate variety, since the Byram gneiss normally contains microcline-microperthite as the predominant feldspar. This view is also supported by the fact that in the vicinity of Bear Pond, just east of the eastern boundary of the map area, where the rock was first recognized, it occurs in a distinct, mappable band. However, since the extent of this gneiss in the map area is quite limited, and since the content of potash feldspar seems to increase to the north, it is classified for the purpose of this report as a type of Byram gneiss. The feldspar in type III Byram gneiss becomes pink locally. Banding is fairly common, at least along the western border of the band, and consists of feldspar-quartz bands a quarter to half an inch wide which alternate with thin bands rich in pyroxene, magnetite, and locally hornblende. The rock contains numerous thin bands of hornblende gneiss and pyroxene gneiss and small local concentrations of magnetite along its western boundary. Its western contact with the adjoining gneisses is conformable where observed.

The three types of Byram gneiss are slightly inequigranular in thin section and grain-boundary relationships vary from an irregular

---

PLATE 2.—PHOTOMICROGRAPHS OF FELDSPAR IN THE BYRAM AND MICROCLINE GNEISSES

(all approximately × 50)

FIGURE

1.—Complexly intergrown microcline and albite
Type I Byram gneiss 4000 feet east of Stag Pond. Crossed nicols.

2.—Albite blebs in microcline
Blebs avoid borders and quartz inclusions. Type I Byram gneiss 8000 feet east of Wright Pond Crossed nicols.

3.—Albite blebs in microcline
Locally the blebs criss cross. Type I Byram gneiss 3000 feet northeast of the Roseville mine (10). Crossed nicols.

4.—Sparse albite blebs in microcline
Type I Byram gneiss 9000 feet N. 67° E. of Andover. Crossed nicols.

5.—Microantiperthite
Plagioclase (white) containing microcline (gray). Type I Byram gneiss from northwest side of Losee anticline along New Jersey Highway 23 south of Franklin. Crossed nicols.

6.—Secondary albite (white) on edges of altered plagioclase (gray) in contact with fresh microcline
No secondary albite at plagioclase-plagioclase contacts. Microcline gneiss 2000 feet east of Lake Pochuck. Crossed nicols.

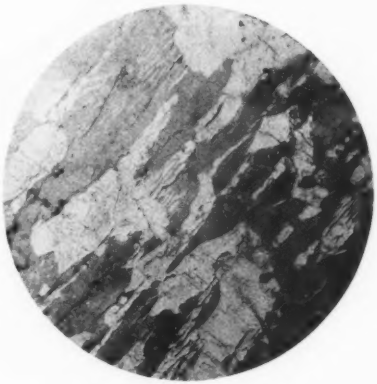

FIGURE 1

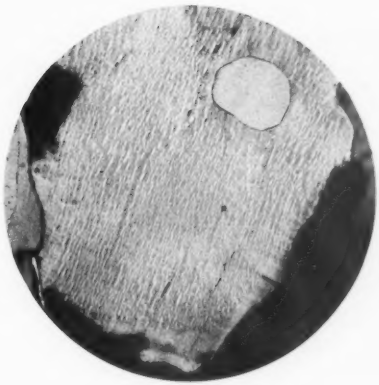

FIGURE 2

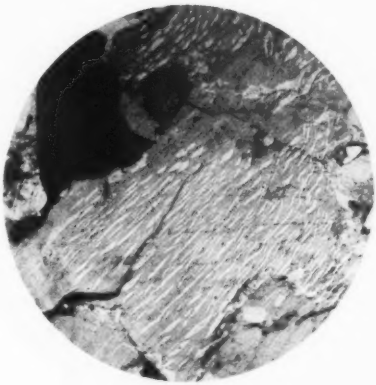

FIGURE 3

FIGURE 4

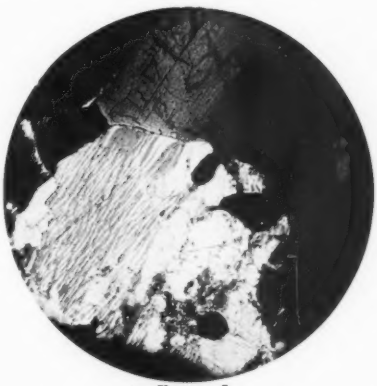

FIGURE 5

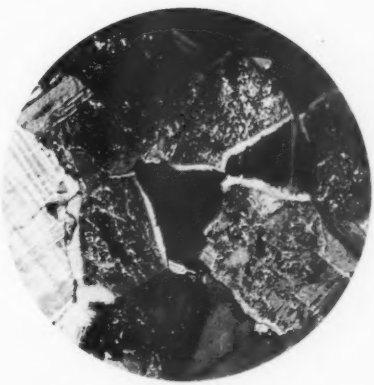

FIGURE 6

PHOTOMICROGRAPHS OF FELDSPAR IN THE BYRAM AND MICROCLINE GNEISSES

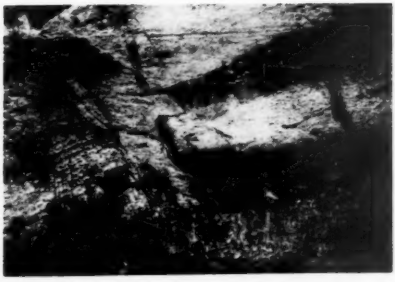

FIGURE 1

FIGURE 2

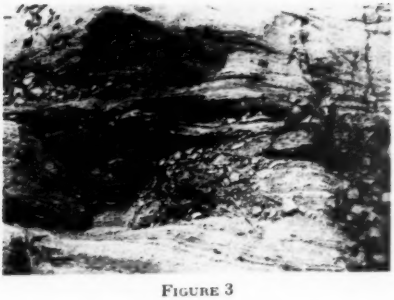

FIGURE 3

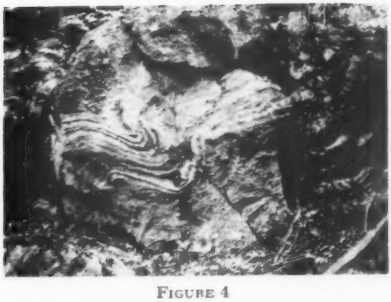

FIGURE 4

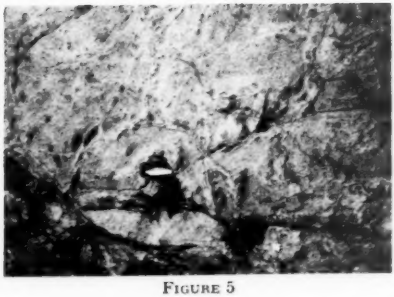

FIGURE 5

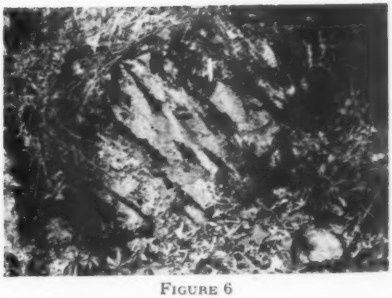

FIGURE 6

STRUCTURES IN THE FRANKLIN MARBLE AND IN THE PYROXENE GNEISSES AND HORNBLENDE GNEISS

intergrowth of quartz, plagioclase, and microcline-microperthite to a complex intergrowth of plagioclase and microcline. The grain size ranges from 0.03 to 2.0 mm in type II Byram and from 0.03 to 3.0 mm in type I Byram. In many places plagioclase grains in contact with microcline-microperthite have lighter myrmekitic borders of secondary albite. Replacement textures are not obvious unless one considers microperthite to have been formed by replacement.

In the Byram gneiss block southeast of Lake Mohawk, between the Zero fault and the Wright Pond fault, plagioclase and microcline are complexly intergrown (Pl. 2, fig. 1), forming microcline-microperthite with a ratio of plagioclase blebs and patches to microcline of approximately 50:50.

South of the Wright Pond fault, microcline-microperthite contains plagioclase blebs and irregular patches which constitute 20–30 per cent of the microperthite grains. In some grains the blebs interconnect near the borders to form partial rims; in other grains the blebs avoid borders as shown in Figure 2 of Plate 2. The blebs also criss-cross in some grains (Pl. 2, fig. 3).

Microcline-microperthite in the Byram gneiss zone west of Lake Mohawk contains a much lower percentage of plagioclase blebs than in the zones just described. The blebs constitute 6 to 20 per cent of the microperthite with an average of only 10 per cent in four thin sections. Furthermore, the blebs are confined mainly to the central portions of the grains (Pl. 2, fig. 4) and do not form partial rims as in the other zones of Byram gneiss.

The Byram gneiss in the nose of the Losee anticline east of Franklin contains microcline-microperthite and/or microcline-microantiperthite with 50 per cent or more of plagioclase blebs (Pl. 2, fig. 5). Samples collected from the east limb of the anticline showed a general, although not systematic, decrease in the plagioclase bleb content from about 30 per cent near the nose to less than 1 per cent in the area southeast of Stag Pond.

Microscopic structures are either not present in the Byram gneiss or are only slightly developed in the form of concentrations of hornblende, pyroxene, and magnetite into vague bands.

The ranges in mineralogical composition of the various types of Byram gneiss and the average composition of the Byram gneiss are given in Table 5. The optical properties of hornblende from sample P80-E are: $\alpha = 1.687 \pm .002, \beta = 1.700 \pm .005, \gamma = 1.715 \pm .005; 2V = (-)\ 50°; Z \wedge C = 14°$. Its pleochroism is α = light green and $\beta = \gamma$ dark green. The optical properties of hornblende from sample P161 are: $\alpha = 1.700 \pm .005$, $\beta = 1.720 \pm .005, \gamma = 1.745 \pm 005$. Its pleochroism is α = light yellowish brown, $\beta = \gamma$ = dark brown. The hornblende from type II Byram gneiss has a pleochroism of α = light green, β = dark brownish green, and γ = dark green. Pyroxene is colorless to light green in thin section, but most of it is so highly altered to limonite that optical properties are difficult to obtain. Pyroxene from Byram gneiss on Mount Adam has an index of refraction, β, of 1.705 ± .005. It is either augite or a member of the diopside-hedenbergite series.

Granites and related rocks.—Two types of granite occur within the map area. Mount Eve granite intrudes the marble and gneisses in the vicinity of the Glenwood syncline and in the Mount Eve area in the form of stocks which have dike- or sill-like apophyses. It occurs as a thick sill-like mass near the nose of the anticline formed by the Losee gneiss west of the Glen-

PLATE 3.—STRUCTURES IN THE FRANKLIN MARBLE, AND IN THE PYROXENE AND HORNBLENDE GNEISSES

FIGURE

1.—Dolomite band or bed (dark) in the Franklin marble. Quarry 6000 feet S. 55° E. of Hamburg

2.—Banding of marble "flowing" around pods of pegmatite. McAfee

3.—Boudins of quartzite in impure marble. McAfee

4.—Interbanded impure marble and pyroxene gneiss, locally tightly folded. Two and one-half miles north of Sparta

5.—"Pilows" in hornblende gneiss, west side of Glenwood syncline

6.—Calcareous hornblende gneiss near Sulphur Hill mine (3), north of Andover

TABLE 5.—MODAL ANALYSES OF BYRAM GNEISS

	Sample no.											Average composition
	P519	V390	P102	B49	V856	V840	P161	P190	J109	P552	X135	
Microcline	....	1.2	37.3	....	....	....	....	....	....	....	....	34.8
Microperthite												
Microcline	31.5	36.2	....	....	36.5	36.6	27.7	14.4	45.9	35.6	53.1	
Albite	6.9	2.5	....	....	12.1	14.9	11.9	0.2	12.4	8.2	1.1	
Antiperthite												9.7
Albite	....	....	....	36.8	....	....	....	....	....	....	....	
Microcline	....	....	....	26.7	....	....	....	....	....	....	....	
Plagioclase	33.1 (An_{15})	38.3 (An_{16})	46.8 (An_{11})	6.2 (An_{19})	18.6 (An_{13})	7.5 (An_{13})	44.2 (An_{16})	67.8 (An_{20})	24.8 (An_{8})	43.3 (An_{15})	5.9 (An_{11})	30.6
Quartz	14.3	7.2	10.4	19.9	25.8	23.7	0.8	6.3	7.1	0.5	18.6	12.2
Hornblende	9.7	7.7	4.1	9.8	3.9	15.6	12.8	....	....	4.2	13.7	7.4
Pyroxene	tr.	3.4	....	....	....	....	tr.	1.8	7.1*	5.4*	4.6	1.9
Biotite	....	....	0.2	....	1.4	....	....	....	....	....	0.5	0.2
Magnetite	2.7	3.4	1.1	0.3	1.0	1.7	0.6	9.4	1.0	2.9	tr.	2.2
Apatite		tr.	....	tr.	0.7	0.1	tr.	tr.	tr.	tr.	0.4	0.1
Sphene	....	....	....	tr.	....	tr.	....	tr.		tr.	2.0	0.3
Zircon	tr.	....	....	tr.	tr.	tr.	tr.		1.6	....	tr.	
Epidote	tr.	....	....	....	....	....	....	tr.		....	....	....
Alteration	1.8	....	....	0.2	....	....	1.9	....	....	....	....	0.4
Totals	100.0	99.9	99.9	99.9	100.0	100.1	99.9	99.9	99.9	100.1	99.9	99.8

* Largely altered to limonite or other material

P519—Type I Byram gneiss, 4500 feet S. 85°W. of the southernmost tip of Lake Mohawk

V390—Type I Byram gneiss, 4800 feet due west of Sparta

P102—Type I Byram gneiss, 3500 feet due south of the southernmost tip of Lake Mohawk

B49—Type I Byram gneiss, 8800 feet S. 23°W. of Sparta

V856—Type I Byram gneiss, 3500 feet N. 75°E. of the northeast corner of Wright Pond

V840—Type II Byram gneiss, 1700 feet northeast of sample V856

P161—Type I Byram gneiss, 3500 feet southeast of sample V856

P190—Type III Byram gneiss, 9200 feet S. 85°E. of the northeast corner of Wright Pond

J109—Type I Byram gneiss, 3000 feet S. 70°E. of the south end of Morris Lake (just east of map area)

P552—Type I Byram gneiss, 13,000 feet S. 48°E. of the south end of the Franklin ore body (just east) of map area)

X135—Type I Byram gneiss from the south end of Mount Adam

wood syncline. A mass of what is apparently the same granite occurs 1½ miles south of Sparta. The Mount Eve granite is a light, coarse-grained rock, mostly structureless, but locally it exhibits a banding which is probably the result of flowage. In the Mount Eve area the granite contains biotite with local hornblende and sparse allanite, but in the area south of Sparta pyroxene and magnetite are the only dark minerals.

At Mount Eve a light, medium-grained granitic gneiss occurs between the Mount Eve granite and the gneisses to the west. It is composed of oligoclase, quartz, microcline, and hornblende in order of decreasing abundance and also contains minor magnetite, apatite, sphene, and epidote. It is strongly banded and contains small masses or bands of hornblende gneiss, oligoclase gneiss, microcline gneiss, and granite. It is considered to be a border facies of the Mount Eve granite, formed by the reaction of the granite with the intruded gneisses. It is represented by the color for granite on the map but is distinguished by a dashed pattern.

A second type of granite is located in the area 1 mile southeast of McAfee. It is considerably thickened in the noses of folds and locally pinches out on the limbs. Its contacts appear

conformable. The rock is a pinkish, equigranular, medium- to coarse-grained granite, composed mainly of pink microcline-microperthite and quartz. It has a rather variable content of dark minerals; sparse magnetite is everywhere present, and biotite and hornblende occur irregularly throughout the rock. Locally the biotite has been altered to chlorite. Biotite or chlorite flakes in roughly parallel orientation give the granite a faint foliation in some places. Quartz grains are in places elongate and flattened and give the rock a faint lineation. Hornblende needles and veinlets or "strung out" blebs of magnetite form a lineation in some localities. The granite exhibits rounded, coarsely granular weathered surfaces.

Pegmatites.—Masses of pegmatite are extremely common in all the Precambrian rocks of the Franklin-Sterling area. They range in width from a few inches for small tabular bodies to over 100 feet for large irregular masses, and they are conformable and disconformable (Figs. 11, 12).

Pegmatites form both large and small masses in the Franklin mine and are found even within the ore. In most cases the pegmatites cut across the banding of the ore at a small angle. Some are known to be later than the ore and others are assumed to be earlier. Many theories have been offered concerning the relationship of the pegmatites to the ore, but no definite connection has been established.

The pegmatites in general are of two types, potassic and sodic. The potassic pegmatites contain microcline, quartz, sparse hornblende, and local allanite. The quartz content is commonly low, and in places the rock consists of microcline only. The rock is light in color, and the feldspar is white, tan, or pink. In the Franklin mine, it is locally green. Dark minerals constitute only 1 or 2 per cent of the rock.

The sodic pegmatites commonly form smaller masses than the potassic pegmatites and consist of plagioclase and abundant quartz with local biotite or chlorite. They are light-colored and become very white on weathered surfaces. They are greenish on fresh surfaces in the Franklin mine.

The potassic pegmatites in the Byram gneiss and the sodic pegmatites in the Losee gneiss are assumed to be genetically related to their host rocks on the basis of color, mineralogy, and spatial relationships. On the other hand, many pegmatites in the field and those which occur in the Franklin mine cannot be related, spatially or otherwise, to the Byram or Losee gneisses. Spectrographic analyses were made of samples of the various pegmatites and the Byram and Losee gneisses to determine whether any of these rocks were similar in trace-element content. Examination of the analyses revealed that there was not enough variation in the relative abundances of trace elements in the samples to establish any such relationships.

FIGURE 11.—PEGMATITE INTRUSIVE INTO THE GRANODIORITE GNEISS
Located approximately 1500 feet east of Andover.

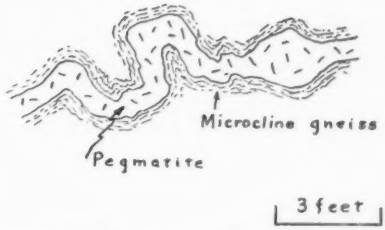

FIGURE 12.—CONCORDANT FOLDED PEGMATITE VEIN IN THE MICROCLINE GNEISS

CAMBRIAN AND LATER ROCKS

The Precambrian rocks in the Franklin-Sterling area are unconformably overlain by the Hardyston formation of Early Cambrian age which is in turn overlain by the Kittatinny

formation of Cambro-Ordovician age. The Hardyston formation is composed in general of conglomerates, sandstones, and sandy or shaly dolomite. Locally, the Hardyston is missing, and the rock just above the Precambrian unconformity is a pure dolomite, which indicates that the Precambrian erosion surface was quite irregular and that the Hardyston was probably formed in depressions on this surface. Hardyston-like conglomerates have been found as fissure and cave fillings in the Franklin band of marble considerable distances below the Precambrian erosion surface.

The Kittatinny formation is mostly dolomite, in part shaly or sandy, with a few beds of limestone near the top. The Hardyston and Kittatinny formations have been described at length by other writers (Kummel, 1940, p. 62–75; Ludlum, 1940), and they will not be dealt with further in this paper. Because a study of the Cambrian and later sediments is not a primary purpose of this paper, the Hardyston and Kittatinny formations are not differentiated on Plate 1.

Basic dikes, which have been identified as camptonite in the vicinity of Franklin, occur in all the rocks of the Franklin-Sterling area. They normally transect the banding in the gneisses and the bedding in the sedimentary rocks at right angles but are locally only very slightly crosscutting. The dikes branch vertically, and, in the open cut of the Franklin mine, they contain ore fragments plucked from the ore body when the dikes were intruded. The dikes commonly do not deform the rocks in which they occur nor do they cause any appreciable alteration near their contacts. They are assumed to have been intruded along minor transverse faults or joints and are generally considered Triassic. The dikes of the Franklin-Sterling area have been described in detail by Milton (1947) so they will not be discussed further in this paper.

The Franklin-Sterling area was extensively glaciated during the Pleistocene period, and much of the bedrock is covered by glacial deposits as well as recent alluvial material. Glacial deposits are not indicated on the map but generally are present where covered contacts are indicated or where blank areas appear. The glacier moved from north to south and, in the areas south of Franklin and Ogdensburg, deposited trains of ore boulders which were plucked from the surface exposures of the ore bodies at the two mines.

Petrogenesis

Introductory Statement

Spencer (1908, p. 2) believed that the Byram and Losee gneisses

> "solidified in part out of silicate solutions or molten magmas, which moved while in a soft or plastic condition from the more or less distant regions in which they had originated into the positions now occupied by the resulting rocks".

He classified the remaining Precambrian rocks of the area into the Franklin limestone (marble) and the Pochuck gneiss, the latter being an undifferentiated type which he believed was a metamorphosed series of dark sedimentary and igneous rocks. In the present study, the Pochuck gneiss is subdivided into a series of light and dark gneisses, most of which are probably of sedimentary origin, but some of which may be of igneous origin.

Origin of the Microcline Gneiss

The structural relationships of the microcline gneiss to the surrounding gneisses and the common occurrence of sillimanite, garnet, and quartz-rich layers within it indicate that it was formed by metamorphism of sediments of appropriate composition. However, the common migmatitic pink and white banding and the replacement textures noted in thin sections indicate a possible replacement origin. In some areas it contains microperthite with the same texture as that in the Byram gneiss. This introduces an added complexity, for, if the microperthite is formed by exsolution as is postulated in the origin of the Byram gneiss, then the microcline gneiss locally appears to be of igneous origin. However, if the microcline gneiss is a migmatite, one might expect the vein material to show igneous features.

The textural and structural features thus indicate a complex origin for the microcline gneiss. It might be a series of rhyolite flows, tuffs, or potash-rich sediments containing numerous thin sandy beds, which was later folded and metamorphosed. The replacement textures

may have resulted from introduced potash-bearing solutions, and the local igneous textures may have resulted from a rise in temperature accompanied by igneous intrusion and metamorphism.

Origin of the Hornblende Gneiss

The hornblende gneiss of the area can be subdivided into metasedimentary, metavolcanic, and meta-igneous types. The calcitic hornblende gneisses (type III) were probably formed as a result of metamorphism of very impure limestone or a sequence of argillaceous and calcareous sediments. This type is closely related mineralogically and structurally to some of the calcareous pyroxene gneisses.

Types I and II hornblende gneiss are similar to type III, and in several places in the area the three types appear to grade into one another. In the Glenwood syncline, however, type I hornblende gneiss contains a zone of "pillow lava" which, if truly a volcanic structure, makes that band of hornblende gneiss of volcanic origin. If all the type I hornblende gneiss is considered to be volcanic, then metavolcanic and metasedimentary hornblende gneisses seem to grade into each other along strike. Either of the following possibilities could explain this: (1) type I hornblende gneiss was formed by metamorphism of two different types of rocks, namely volcanic flows and argillaceous sediments of similar bulk composition, which formed indistinguishable end products; (2) types I and II hornblende gneiss are volcanic in origin and type III was formed by the interfingering of volcanic flows and calcareous sediments.

The type IV hornblende gneiss of the Glenwood syncline is probably meta-igneous because of its texture and its numerous discordant contacts with quartz-rich microcline gneiss.

Origin of the Biotite Gneiss and Related Rocks

The textures, compositions, and structural relationships of the biotite gneiss, garnet gneiss, and graphitic gneiss to the other rocks of the area indicate a sedimentary origin for these rocks.

Origin of the Pyroxene Gneiss and Related Rocks

The sphene-bearing pyroxene-scapolite gneiss and the structureless coarse-grained to pegmatitic rock of the same composition are associated with marble or impure calcareous rocks. The gneiss is assumed to have been formed by the reaction of marble with impurities it contained or by the metamorphism of impure calcareous rocks, and the coarse-grained pyroxene rock is probably the result of recrystallization of such gneiss by near-by igneous intrusions. In the Mount Eve area pyroxene gneiss can be traced into granite containing inclusions of coarse-grained sphene-bearing pyroxene-scapolite rock. The latter rock, which also forms the core of a synclinal structure approximately 1 mile S. 23° W. of Amity, has some granite associated with it, and a granite intrusion lies just north of it. This latter pyroxene rock was probably formed by recrystallization of a flat-lying pyroxene gneiss layer within the marble by the granite intrusions. The coarse-grained pyroxene-scapolite borders around gneissic inclusions in marble may be the result of reaction between the marble and the gneiss during metamorphism.

Origin of the Losee Gneiss

The Losee gneiss is almost as extensive as the Byram gneiss and some of the same problems are involved in finding the origin of both rocks. The Losee gneiss forms the cores of two large anticlines east of Franklin and north of Hamburg. Nowhere along the contacts were large-scale discordant relationships found between the Losee and its host rock. Away from its contacts the Losee gneiss shows no apparent change in its banded structure.

It forms *lit-par-lit* bands within hornblende gneiss in the area west of Franklin where some of the hornblende gneiss seems to grade into Losee gneiss, giving the appearance of replacement by the Losee. The same feature is present in the Stag Pond type of Losee gneiss and in the oligoclase gneiss of the Pimple Hills (Fig. 8.) No definite replacement textures were identified in thin sections of the Losee gneiss.

The Losee gneiss contains numerous continuous and discontinuous layers of dark hornblende gneiss. In the Stag Pond area some of

the smaller layers of hornblende gneiss are actually rectangular blocks (inclusions) which sometimes have coarse pyroxene "reaction" borders (Fig. 6). Remnant folds of hornblende gneiss are present in the Losee gneiss in the area approximately 2 miles S. 80° W. of Stag Pond. Small-scale discordant relationships exist between the Losee gneiss and some of its included hornblende gneiss layers (Fig. 5).

These relationships indicate that the Losee gneiss was formed as a predominantly concordant magmatic intrusion resembling a phacolith.

Origin of the Oligoclase Gneiss

The composition, textures, and structures of the oligoclase gneiss are almost identical with those of the Losee gneiss. Hence the same criteria apply to the origin of both types. Outcrops of oligoclase gneiss appear more linear and hence suggest sills.

Origin of the Granodiorite Gneiss

The granodiorite gneiss appears similar to the Byram gneiss at first glance and was mapped as Byram by earlier workers although Spencer mapped portions of it as Losee gneiss. Both have pronounced lineations and both have a fair to good banding near contacts with their enclosing gneisses. However, significant differences in mineralogy, structure, and weathered appearance distinguish them as separate types. The differences in mineralogy are quite apparent (Tables 4, 5). The Byram gneiss is high in potash feldspar and hornblende, whereas the granodiorite gneiss is high in plagioclase, low in potash feldspar, low in hornblende, and relatively high in biotite. Surface exposures of the Byram gneiss are buff to brown, whereas exposures of granodiorite gneiss are gray. Structurally, the lineation of the Byram gneiss is formed by the orientation of hornblende needles whereas the lineation of the granodiorite gneiss is formed by the concentration of biotite and hornblende in streaks or lenses.

The compositional relationships between the Byram, Losee, and granodiorite gneisses are shown in Figure 13. If the Byram and Losee gneisses are considered as two igneous intrusions, the granodiorite gneiss might be considered an intermediate product of a magmatic sequence which produced the Byram and Losee gneisses as end products. The answer may not be this simple, but the structures and compositions fit this interpretation.

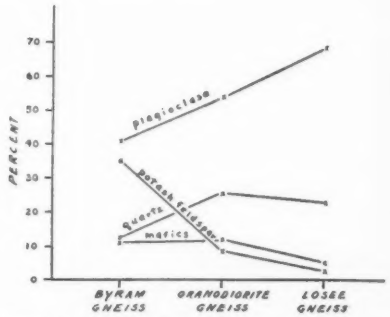

FIGURE 13.—VARIATION DIAGRAM SHOWING THE MINERALOGICAL RELATIONSHIPS AMONG THE BYRAM, GRANODIORITE, AND LOSEE GNEISSES

Even if the granodiorite gneiss is not related to the Byram and Losee gneisses as an intermediate igneous variety, an igneous origin is indicated by its internal structure, its composition, and its structural relationships to the enclosing gneisses.

Origin of the Byram Gneiss

Although large-scale discordant relations do not exist between the Byram gneiss and other rocks of the area, small-scale discordances are present in some areas (Fig. 9). The internal structures of the Byram gneiss are typical of intrusive rocks—*e.g.*, in the Stag Pond area a pronounced banding in the Byram gneiss diminished gradually into a hornblende lineation a short distance away from its contacts. In places the lineation becomes indistinct, and the Byram appears to be a typical coarse-grained hornblende granite.

Microcline-microperthite is always present in the Byram gneiss of the Franklin area and is an additional key to its origin. The variations in the relative abundance of albite blebs within microcline which were noted under the description of the Byram gneiss show a roughly zonal arrangement in which the albite-bleb content is low in the Byram gneiss near its contacts and increases toward interior portions.

The microperthite textures could have three, or possibly more, explanations. They might have been formed by replacement of plagioclase by microcline, by replacement of microcline by plagioclase, by exsolution of a solid-solution mixture of potash and soda feldspar, or perhaps by a combination of replacement and exsolution.

The exsolution hypothesis seems to explain best the microperthite textures seen in thin section. Bowen and Tuttle (1950, p. 500) show that albite and potash feldspar will form a solid solution in any ratio at temperatures above about 700° C, and that upon cooling the mixture will exsolve into albite and potash feldspar. The amount of albite in the microperthite should depend upon the relative amount of potential albite within the rock melt prior to crystallization.

According to the exsolution hypothesis, free plagioclase should be absent in the rock, but it commonly constitutes a rather high percentage (Table 5). This variation from the ideal may be due to a temperature gradient set up in the magma by which the magma would be cooler near its contacts than within the center. If such a temperature gradient once existed and the chemical composition of the Byram gneiss remained constant, the percentage of free plagioclase in the rock should vary inversely as the ratio of albite blebs to potash feldspar varies in microperthite. Although the composition of the Byram is quite variable, this relationship holds true in a general way. Samples of Byram gneiss near contacts commonly contain a high percentage of free plagioclase and a low ratio of albite blebs to potash feldspar in microperthite, whereas samples in central zones contain a low percentage of free plagioclase and a high ratio of albite blebs to potash feldspar. There are exceptions to this general rule, perhaps because of the variability in the composition of the Byram gneiss.

It is unlikely that the microperthitic texture was formed by replacement, because in many thin sections the plagioclase blebs are confined to the central portions of microperthite grains whereas in others the blebs coalesce near the grain boundaries to form partial albite rims. In no case does the albite of one microperthite grain cross into another microperthite grain, and in all cases the albite blebs and patches of a single grain extinguish simultaneously, which indicates optical and crystallographic continuity.

The coalescing of albite blebs at grain boundaries has been used as evidence for replacement by some writers (Faessler and Tremblay, 1946, Figs. 3, 4). Alling (1938, p. 142–165) assigns small elliptical stringlets (blebs) to exsolution phenomena and patches to replacement phenomena. Both blebs and patches are contained in many microperthites of the Byram gneiss, and hence, according to Alling's classification, these grains would have both exsolution and replacement origins.

The roughly zonal arrangement of its microperthite, its relative homogeneity, and its internal structures indicate an igneous origin for the Byram gneiss. The gradational contact between the Byram gneiss and hornblende gneiss in some areas (Fig. 10) could be ascribed either to replacement or igneous action. The lack of large-scale discordant features between the Byram gneiss and other rocks and the inclusion of the large Wildcat marble band in the Byram gneiss west of Lake Mohawk indicate that the Byram was formed either as a phacolithic intrusion or by replacement of a large metasedimentary sequence of rather constant composition.

Most of the field and microscopic evidence points to an igneous origin for the Byram gneiss. However, some of the evidence contradicts the igneous origin, and hence the Byram gneiss may have had a complex history of igneous intrusion coupled with partial replacement.

Structural Geology

Banding and Foliation

Almost all the Precambrian rocks of the area contain either a banding or foliation which is, with few exceptions, parallel to lithologic contacts. The banding is formed by alternating concentrations of dark and light minerals, by variations in grain size, or by concentrations of pink and white feldspars into layers ranging from a few millimeters to several feet in width. The microcline gneiss is commonly distinctive because of its pink and white banding and its quartz-rich layers which stand out as "ribs" on the weathered surface.

The contact of the Franklin band of marble with the overlying gneiss is gradational through a zone of alternating thin layers of marble and gneiss in the area west of Franklin and Ogdensburg. The mineral banding in these zones is parallel to the layering. Likewise, in the area where the Wildcat marble grades laterally into calcareous gneiss, the banding consists of alternating thin marble layers and sphene-bearing pyroxene-scapolite (or plagioclase) gneiss layers. The interlayering and gradation of gneiss and marble suggest that most of the banding of the area parallels original bedding and thus might be termed bedding-plane banding.

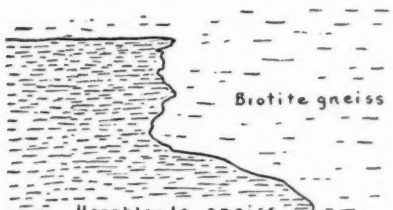

FIGURE 14.—DISCONFORMABLE RELATIONSHIP BETWEEN THE BANDING AND CONTACT OF BIOTITE AND HORNBLENDE GNEISSES

The gneisses of the Glenwood syncline are an exception to this rule, in that banding is often disconformable to lithologic contacts (Figs. 14, 15). However, the banding planes on either side of these disconformable contacts are parallel. The tracing of contacts in the Glenwood syncline where outcrops are plentiful indicated that disconformable banding is common, especially on the east side of the structure. The predominant association of this feature with hornblende augen gneiss points to an intrusive origin for the augen gneiss. Further evidence of probable igneous activity in this area is indicated by the

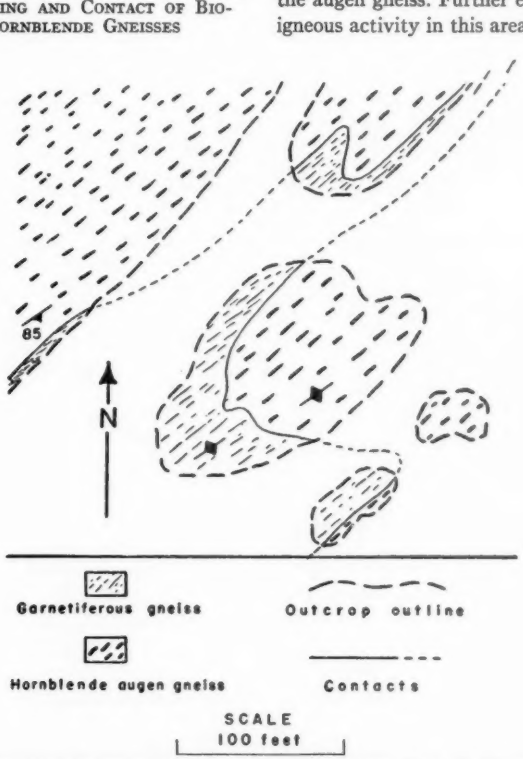

FIGURE 15.—OUTCROP MAP SHOWING RELATIONSHIP OF CONTACTS TO BANDING ON THE EAST SIDE OF THE GLENWOOD SYNCLINE

presence of a pillow-lava (?) zone (Pl. 3, fig. 5) around the lower portion of the syncline.

Banding is pronounced in the Byram gneiss near contacts with other rocks but away from such contacts its place is taken by a hornblende lineation. In some areas, both banding and lineation are missing, and the rock looks like a homogeneous hornblende granite.

The Mount Eve granite contains a banding similar to that of the Byram gneiss, and, except for the discordant contacts which the Mount Eve granite exhibits in many places, the two rocks might be mistaken for one another. The two features which best differentiate them are color of weathering and mineralogy. The Byram gneiss weathers to a bronze color and commonly contains hornblende as the major accessory mineral, whereas the Mount Eve granite weathers to a gray and commonly contains biotite as the major accessory mineral. Banding in the Mount Eve granite is lacking in too many places to be sure of its relationships to contacts except in the area northwest of the Glenwood syncline where the granite forms sills in a series of gneisses. The banding of the granite conforms to the contacts of the sills.

Foliation is less obvious than banding, but it is present in many rocks of the area. It is commonly formed by the subparallel orientation of biotite or other micas but may also be formed by orientation of calcite rhombs and graphite flakes in marble and by the orientation of disc-shaped quartz grains in the Losee gneiss and in some places in the microcline gneiss. Where present in the same rock, banding and foliation are parallel with one another.

Lineation

The metasedimentary and igneous rocks of the area contain a variety of lineations formed during deformation or intrusion. The lineations are generally parallel to *b*, the regional northeasterly trending axis of folding. This relationship between mineral lineations and folding cannot be established directly, but it can be inferred from the parallelism of lineations to the axes of small folds in many parts of the area.

The mineral lineations include: orientation of sillimanite pods in the microcline gneiss; orientation of hornblende in hornblende gneiss, granodiorite gneiss, and Byram gneiss; orientation of elliptical quartz discs in the Losee and microcline gneisses; and the orientation of tremolite in marble.

The hornblende lineation of the Byram gneiss in the area west of Lake Mohawk conforms to the regional northeasterly trend, but immediately east of the Zero fault it changes to a southeasterly trend. The reason for this divergence is not clear, but it may be due to the intrusive nature of the Byram gneiss. The change from a pronounced banding near contacts to a lineation away from contacts may be ascribed to flowage during intrusion and may thus be a primary igneous feature rather than a metamorphic feature. The coincidence of Byram lineation with the regional lineation in some areas may be explained as the result of intrusion during deformation.

The lineations of the hornblende gneiss and hornblende augen gneiss of the south and east sides of the Glenwood syncline conform to the regional trend, but on the northwest side they form a radial pattern. This divergence may be a result of the basinlike folding of the northwest side in contrast to the tight, isoclinal folding of the south and east sides.

Although the lineations of the marble and the metasedimentary and metavolcanic gneisses conform in general to the regional northeasterly trend, changes in bearing and plunge take place throughout the length of the area and form a rolling and sinuous pattern. The regional bearing of lineations in the area from Andover to Sparta is approximately N. 50°E. with plunges ranging from 5° to 30°NE. Northeast of Sparta the regional bearing changes to approximately N. 30°E. with plunges ranging from 15°SW. to 55°NE. Significant divergences from the regional lineation trends occur in a number of localities. East of the Zero fault in the vicinity of Stag Pond, the lineations in the Byram gneiss range in plunge from 25° to 45°S. 55°E. The lineations in the south half of the Lake Lenape syncline plunge approximately 30° N.60°–70°E. whereas in the north half they plunge 10°–30° S.10°–30°W. Just northwest of Sparta the lineations plunge 5°–25° N.80°E., and in the area 2½ miles north of Sparta the lineations plunge 20°–45° N.75°E. to S.50°E. In the Cork Hill gneiss zone west of the Sterling mine the lineations plunge 25°–50° S.80°E. The lineations in the Sterling mine and vicinity

which consist of orientation of tremolite in marble and orientation of willemite in the ore, also plunge 25°–50° S.80°E. The willemite orientation was obtained by making statistical analyses of willemite *c* axes in thin sections mounted on a four-axis universal stage. Just southwest of McAfee the lineations of the Median gneiss zone plunge 20°–40° N.70°E. The divergences of the Glenwood syncline have already been described. In the Mounts Adam and Eve area the lineations radiate, ranging in bearing from N.10°E. to N.55°W. and in plunge from 10°–25°N. to NW.

C. H. Stockwell made a complete study of tremolite lineations in the marble during 1951 and 1952 and found the same pattern there that exists in the gneisses. Most of the lineations of the area obviously are the result of recrystallization during regional deformation and, in the case of the Byram gneiss, perhaps the result of flowage during igneous intrusion. The divergences in the trend of the lineation are generally associated with cross-folding or cross-warping.

Minor Folds

Small-scale, generally isoclinal folds have been observed in many of the gneisses throughout the area. Their amplitude ranges from a few inches to several tens of feet. Because of their comparative incompetence, the calcareous gneisses of the Wildcat marble horizon in the area 2½ miles north of Sparta are deformed into a variety of small parallel to complexly crumpled folds (Pl. 3, fig. 4). The axes of small folds are generally parallel to mineral lineations. Except for cross-folds, small folds are apparently drags formed on the limbs of major folds of the area.

The trace of the banding in places forms a serpentine map pattern, reflecting small-scale undulatory folds whose axes plunge nearly down the dip of the banding. The axes of these folds are oblique to the mineral lineations, and the folds were probably formed after the main period of deformation.

Cross-Folds

Cross-folds are present in the Lake Lenape syncline, in the Pimple Hills syncline, at the north end of Mount Eve, and elsewhere. Analysis of the attitude of folds in the area shows that the average bearing of major fold axes is N.40°E. and the average bearings of the two sets of cross-folds are north-south and N.70°E. If the cross-folds are related to the major folding, the major compressive forces, probably directed from the southeast to the northwest, probably had minor components of force directed so as to produce cross-folds oriented at roughly 30° to the major folds. If the formation of the cross-folds postdated the major folds, the cross-folds may have resulted from compressive forces from the northeast and southwest, roughly at right angles to the major compressive forces, or from horizontal movement along northeast-southwest shears.

Major Folds

Mt. Adam and Mt. Eve area.—The gneisses of Mts. Adam and Eve have been deformed into tight isoclinal folds which were later intruded by the Mt. Eve granite. An accurate analysis of the folding is impossible because of the granite intrusions; the following structural interpretation is based on data obtained by mapping the area on a scale of 1 inch equals 300 feet. Control was obtained by using a 100- by 200-foot staked grid on the north end of Mt. Eve and a 100- by 500-foot staked grid on the north end of Mt. Adam.

Mt. Adam is a tight isoclinal syncline, overturned to the west. On the southeast side of Mt. Adam a small remnant of graphite gneiss is cut off on the west by the Mt. Adam fault and intruded on the north by the Mt. Eve granite. The graphite gneiss horizon can be followed to the southeast on the south side of Mt. Eve until it is intruded by the Mt. Eve granite. Graphite gneiss is again found on the north side of Mt. Eve where it can be traced to the northwest through a series of complex folds until it is overlain by the Cambro-Ordovician sediments. In the central portion of Mt. Eve, now occupied by granite, the graphite gneiss horizon may have previously formed an overturned anticline as shown in Figure 16-A. Secondary folding is indicated by the cross-folds on the north end of Mt. Eve.

The second structural interpretation for the area is similar to the first except that the

graphite gneiss horizon on the south end of Mt. Eve is connected to the graphite gneiss on the north end to form an overturned syncline as shown in Figure 16-B.

The gneisses of Mts. Adam and Eve are granite. This area has not been mapped in detail, but structure symbols and some of the sillimanite-bearing microcline gneiss horizons are placed on the map to show the complexity of the structure.

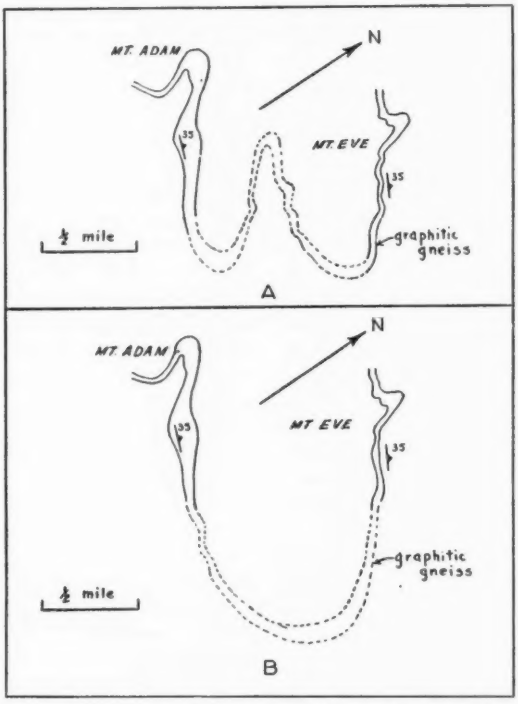

FIGURE 16.—TWO INTERPRETATIONS OF THE PRE-INTRUSION AND PRE-FAULTING STRUCTURE OF THE MOUNTS ADAM AND EVE AREA
Graphite gneiss used as a key horizon

probably correlative with the Cork Hill gneiss zone in other parts of the area.

Glenwood syncline.—The doubly plunging syncline southwest of Glenwood is delineated both structurally and lithologically. A series of hornblende and microcline gneisses forms the central portion of the structure, and the Wildcat marble and microcline gneiss (Cork Hill gneiss zone) form the lower portion of the structure. The west side of the syncline is cut off by a fault (the Pochuck fault?) of unknown displacement.

Northwest of Glenwood the gneisses reappear in a series of anticlines and synclines containing concordant intrusions (sills) of Mt. Eve

Pochuck Mountain syncline.—The gneisses of the Glenwood syncline reappear on Pochuck Mountain as a series of hornblende, microcline, and garnetiferous biotite gneisses which are folded into an elongate, tight syncline, overturned to the west. The structure changes from the basinlike folding near Glenwood to tight, elongate folding presumably because of the influence of the Losee gneiss anticline on the west side of Pochuck Mountain. The Pochuck Mountain syncline becomes more open to form the series of anticlines and synclines northwest of Glenwood.

In the vicinity of Hamburg, the Pochuck Mountain syncline is cut off by the Pochuck

fault but reappears west of Franklin and is finally lost under a cover of glacial drift. Its probable southward extension is outlined on the geologic map by a dotted line.

Pimple Hills syncline.—West of Ogdensburg, in the Pimple Hills, a thick series of oligoclase, microcline, and hornblende gneisses have been folded into a tight isoclinal syncline, overturned to the west. The syncline is bordered on the east and southwest by the Wildcat marble, on the west by the Hamburg fault, and on the south by the Zero fault. Primary drag folds and secondary cross-folds are common in this area. The drag folds are represented by the folding in the western Wildcat marble limb and the tight folding in the trough of the syncline, and the cross-folds are indicated by crumpling of the microcline gneiss bands in the north end of the Pimple Hills.

North Sparta folds.—The area of the north Sparta folds is about 1½ miles northwest of Sparta. The structures consist of two northeasterly plunging overturned synclines separated by an overturned anticline. The axial line of the eastern syncline passes through a hook-nosed fold outlined by sillimanite-bearing microcline gneiss, and the axial line of the western syncline passes through the synclinal trough outlined by a thin garnet gneiss band. The anticline which separates the two synclines is formed by the thickened layer of sillimanite-bearing microcline gneiss.

The Wildcat marble horizon on the southwest side of the Pimple Hills can be traced into the area of the north Sparta folds by following it northward into an area of interlayered marble and gneiss which forms the sharp nose of an anticline, slightly displaced by the Hamburg fault. From there southward, the interlayered marble and gneiss apparently grade into pyroxene-bearing hornblende gneiss. The interpreted gradation cannot be observed because outcrops are very rare in this area. Although the marble band disappears, its horizon can be traced into the hook-nosed fold by following the microcline gneiss band which lies stratigraphically below the marble. This sillimanite-bearing microcline gneiss band was traced around the hook-nosed eastern syncline by walking it out along strike. North of the hook-nosed fold the microcline gneiss widens into the nose of the central anticline.

The folding in the north Sparta area is complicated by the introduction of granodiorite gneiss in the central portion of the eastern syncline and in the large area to the southwest. If the eastern syncline and the central anticline were unfolded, the north Sparta folds would be a single syncline overturned to the west. This syncline would connect directly with the Lake Lenape syncline to the southwest and the Pochuck Mountain syncline to the northeast. The axial line would pass through the Lake Lenape syncline, through the western syncline of the north Sparta area, and through the Pochuck Mountain syncline, as shown on the geologic map.

The north Sparta area was mapped by the pace and compass method using aerial photographs for control. Although lack of outcrops in the central part of the area makes the foregoing explanation interpretive, the gross picture is probably correct. The noninterpretive contacts are drawn as either solid or dashed lines, and the interpretive contacts are drawn as dotted lines on the geologic map.

Lake Lenape syncline.—The Lake Lenape syncline, north of Andover, has been modified by cross-folds of two types, open and tight, in such a way that the north and south halves are very nearly mirror images. This structure has been proven by walking out sillimanite-bearing microcline gneiss bands and garnet gneiss bands.

The western half of the syncline is complicated by repeated folding (Pl. 1, section B–B′).

Stag Pond folds.—In the vicinity of Stag Pond, white marble and adjoining gneiss bands outline a pair of almost isoclinal folds. It cannot be determined which fold is the anticline and which is the syncline because, according to the few lineations obtained in the area, the angle between each fold axis and a horizontal line measured in the axial plane is approximately 90°. The plunge of the folds is about 35°–40°E. The core of the northeast fold is composed of the Stag Pond type of Losee gneiss, and that of the southwest fold is composed of Byram gneiss. The contacts and structures in this area are concordant and conformable.

The relationship between the Stag Pond folds and the other folds of the area is not known because the marble band cannot be related to

the Wildcat marble with assurance, and the structures are at an angle to the regional trend.

Losee gneiss anticlines.—The Losee gneiss forms the core of two anticlinal structures, one east of Franklin and the other north of Hamburg. East of Franklin the greatly thickened nose of the anticline, occupied by Byram gneiss and granite, contains a series of microcline, hornblende, and biotite gneisses (the Hamburgh Mountain gneiss zone).

Post-Ordovician folds.—Folding later than the Precambrian is shown by the structure of the Cambro-Ordovician sediments in the graben between the Zero and East faults (Pl. 1, structure section D–D′) and in the area south of Hamburg (Pl. 1, structure section E–E′). The effect of this folding on the Precambrian rocks cannot be separated from the effect of the complex Precambrian folding. A cross-folding still later than the major post-Ordovician folding may be present in the form of undulations in the trend of the unconformity separating the Precambrian and the Cambrian rocks. Possibly, however, the undulations in this contact may reflect the original irregular nature of the Precambrian erosion surface.

Joints

Two prominent sets of joints in the area strike N. 30°E. and N. 50°E., and a third set strikes N. 60°W. The first two sets roughly parallel the trends of the Zero fault and the cross-fault east of Franklin (Rutherford cross-fault). The third set probably represents tension joints developed perpendicular to the regional northeasterly trending axis of folding, *b*.

Faults

The major faults of the area trend northeasterly, roughly parallel to the regional structure. The most recent direction of movement on most of the major faults apparently was east side down. However, since movement is likely on these faults during Precambrian as well as post-Ordovician time, and since a unique solution concerning net movement cannot be obtained for any of the faults, the history of movement must rely mainly on conjecture. Most fault movements indicated on the geologic map are restricted to relative movements which can be determined from the contacts of Cambrian rocks with Precambrian rocks. The apparent hinge-fault movement on the East fault east of Franklin does not necessarily represent a rotary movement but may only appear to do so because of the greater downward movement of the Kittatinny limestone graben south of Franklin.

Minor cross-faults trending roughly N.10°W. are common in the Stag Pond area, and a major cross-fault trending N.15°W. is present on the west side of the Pimple Hills. The Rutherford cross-fault east of Franklin trends about N.60°E. These minor faults are oriented approximately 30° on either side of the major faults and hence may be shears formed during the major fault movements.

A study was made of minor shearing on the two sides of the Zero fault in the zone between the south end of Lake Mohawk and the north end of Stag Pond to discover whether the horizontal component of movement, if any, could be determined. Two pronounced shear sets were revealed by plotting 122 shears in the lower hemisphere of an equal-area projection. One set trends N.50°E. and dips 55°SE., and the other trends N.22°W. and dips 62°NE. These shears indicate a relative movement of east side up and slightly south, whereas the known displacement of the Zero fault in this vicinity is east side down. The reason for the discrepancy between the shearing and the major fault movement is not known, but other such discrepancies between fault movement and shearing occur in the area between Franklin and Ogdensburg. More than one movement may have taken place on the Zero fault, resulting in shears not necessarily related to the major movement.

Mechanics of Deformation

The structural pattern of the area consists of a major northeasterly trending overturned syncline with superimposed smaller anticlines and synclines in the vicinity of Glenwood. South of the Pimple Hills the major syncline divides into two synclines separated by an anticline which is occupied by Byram gneiss, granodiorite gneiss, and microcline gneiss. Losee gneiss forms the cores of two large anticlinal structures east and west of the major syncline.

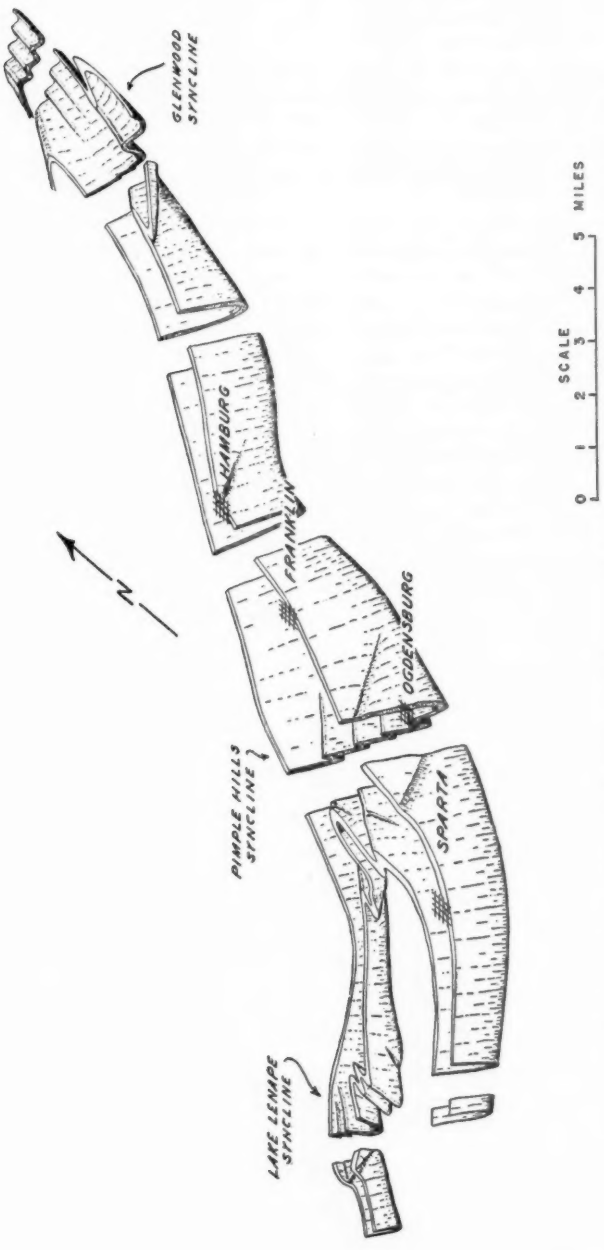

FIGURE 17.—STEREOGRAM ILLUSTRATING PRE-FAULTING STRUCTURAL INTERPRETATION OF THE WILDCAT MARBLE HORIZON

These major structures are illustrated in a stereogram of the Wildcat marble horizon (Fig. 17). The western limb of the Wildcat marble horizon is either missing or does not crop out from the west side of the Pimple Hills northward around the nose of the western Losee gneiss anticline. The eastern limb of the Wildcat horizon is missing from the north end of Lake Lenape to the west side of the Pimple Hills. The structural pattern indicates that the marble and gneisses of the central synclinal area were compressed between the two Losee gneiss anticlines. Compression was apparently greater from the southeast than from the northwest and resulted in the westward overturning of most folds.

The major folds produced drag folds, especially in the region of the Pimple Hills and to the southwest. Cross-folds ranging from slight warps to tight folds were developed in the Pimple Hills, in the Lake Lenape syncline, in the area west of Ogdensburg and Franklin, and on the north end of Mount Eve. These secondary folds were probably produced by late tectonic deformation developed as a result of the major folding. The mechanism by which the cross-folds were formed is not well understood.

Lineation throughout the area trends northeasterly and plunges predominantly to the northeast, but in many places it plunges southwest. The lineations conform to the northeasterly trend of folding in the area and are evidently parallel to *b*, the direction of major folding. The cross-folds have rotated the lineations out of the regional trend in many localities.

Major faults may have formed in Precambrian time and served as loci for the post-Ordovician faults which are visible now.

Precambrian Stratigraphy

Development of the Stratigraphic Approach

In 1946, when the study of the gneisses near Franklin was started, stratigraphic methods were applied hesitantly because of grave doubts concerning the sedimentary origin of many of the stratiform rocks. However, detailed mapping of the area has revealed certain sequences which have been traced for several miles along strike and include layers of marble, a few thin beds of quartzite, pyroxene gneiss, and graphitic gneiss. These four rock types can be called metasediments with confidence, but they are replaced by silicates and are so recrystallized that very few, if any, relict structures remain as useful top-and-bottom data. Some of the other layered gneisses are probably flows, tuffs, or sills whose normal texture and composition have been so altered by metamorphism as to be almost unrecognizable. Still other units in the near-by complex are massive gneisses and granitoid rocks which are probably intrusives or the products of replacement.

Since even the oldest rocks of the area contain remnants of metasedimentary types, and since almost all contacts are conformable within the expected limits of deformation, the belief has grown as the mapping progressed that this part of the Highlands complex contains a highly folded sedimentary and metavolcanic series, invaded by igneous intrusions of several periods.

Method of Construction

To determine the probable stratigraphic sequence it has been necessary to use structure as a guide to stratigraphy, an unusual procedure in mapping sedimentary formations. After certain basic structural elements were determined, marker horizons could be followed for miles and used to relate separate outcrop areas. Sections striking N. 71°W. across the regional strike were constructed at 5000-foot intervals from Andover, New Jersey, to Big Island, New York. A few representative sections were placed on the geologic map (Pl. 1) to show the types of structures in the area. An interpretation of these sections in combination with the surface outcrop map has given a crude picture of the ancient stratigraphy. The sequence is everywhere distorted by the thickening and thinning of bands by close folding, by facies changes, and by possible disconformities.

Proposed Stratigraphic Sequence

Introductory statement.—The Franklin-Sterling area probably consists of interbanded metasediments, metavolcanics, and both concordant

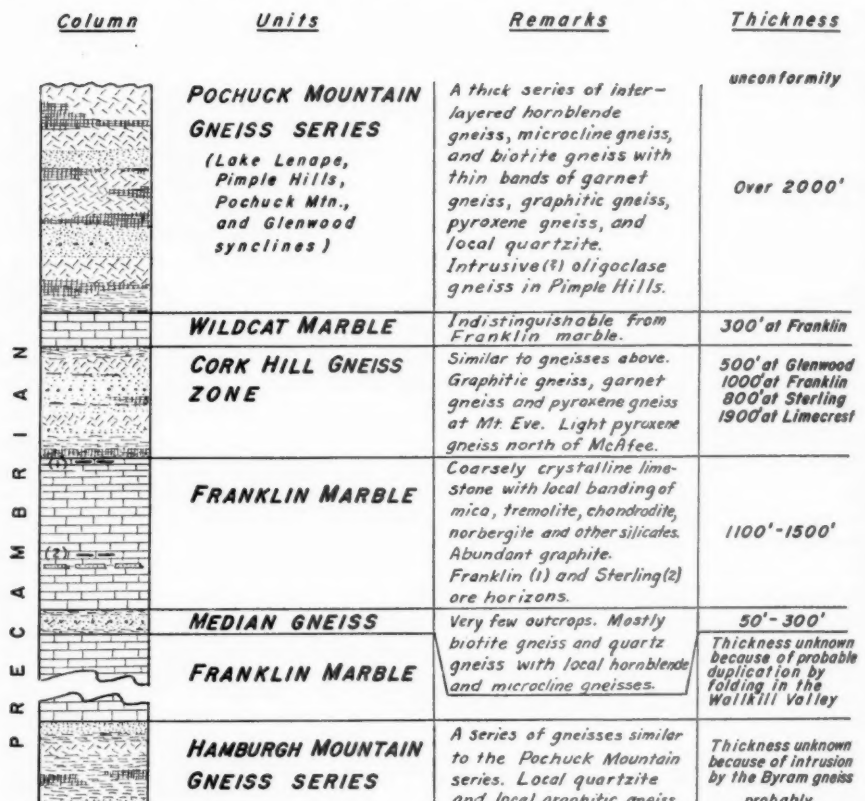
Column
Units
Remarks
Thickness
PRECAMBRIAN
POCHUCK MOUNTAIN GNEISS SERIES
(Lake Lenape, Pimple Hills, Pochuck Mtn., and Glenwood synclines)
A thick series of interlayered hornblende gneiss, microcline gneiss, and biotite gneiss with thin bands of garnet gneiss, graphitic gneiss, pyroxene gneiss, and local quartzite. Intrusive(?) oligoclase gneiss in Pimple Hills.
unconformity
Over 2000'
WILDCAT MARBLE
Indistinguishable from Franklin marble.
300' at Franklin
CORK HILL GNEISS ZONE
Similar to gneisses above. Graphitic gneiss, garnet gneiss and pyroxene gneiss at Mt. Eve. Light pyroxene gneiss north of McAfee.
500' at Glenwood
1000' at Franklin
800' at Sterling
1900' at Limecrest
FRANKLIN MARBLE
Coarsely crystalline limestone with local banding of mica, tremolite, chondrodite, norbergite and other silicates. Abundant graphite. Franklin (1) and Sterling(2) ore horizons.
1100'-1500'
MEDIAN GNEISS
Very few outcrops. Mostly biotite gneiss and quartz gneiss with local hornblende and microcline gneisses.
50'-300'
FRANKLIN MARBLE
Thickness unknown because of probable duplication by folding in the Wallkill Valley
HAMBURGH MOUNTAIN GNEISS SERIES
A series of gneisses similar to the Pochuck Mountain series. Local quartzite and local graphitic gneiss. Byram gneiss intrusive into this series.
Thickness unknown because of intrusion by the Byram gneiss
probably over 2000'

FIGURE 18.—GENERALIZED COLUMNAR SECTION OF THE METASEDIMENTARY AND METAVOLCANIC ROCKS OF THE AREA

and discordant igneous intrusives. Although individual bands of gneiss are not sufficiently persistent for the construction of detailed stratigraphic columns, a generalized column is possible (Fig. 18). The metasedimentary and metavolcanic rocks have been divided, from oldest to youngest, into the Hamburgh Mountain gneiss series, the Franklin marble, the Cork Hill gneiss zone, the Wildcat marble, and the Pochuck Mountain gneiss series. Repetition of rock types is common in all the gneiss zones. The generalized stratigraphic column does not include pegmatites, Byram gneiss, Losee gneiss, granodiorite gneiss, and Mount Eve granite because they are considered igneous, whether generated in place or intruded. The three gneiss zones are similar in that they are all composed of interlayered hornblende gneiss, microcline gneiss, and biotite gneiss, with local bands of garnet gneiss, graphitic gneiss, and pyroxene gneiss. Gneisses rich enough in quartz to be called quartzites are found in some localities.

Hamburgh Mountain gneiss series—The metasedimentary gneisses exposed on Hamburgh Mountain probably represent rocks older than the Franklin marble.

Franklin marble.—The Franklin marble contains numerous discontinuous gneissic horizons separated into large and small boudins. It also

contains a fairly continuous gneiss zone, called the Median gneiss, located 1100–1550 feet stratigraphically below the Cork Hill contact. The Median gneiss varies in composition as noted in the section on the Franklin band of marble. The marble may have been repeated several times by folding, hence it is difficult to estimate its true thickness.

Cork Hill gneiss zone.—This zone, located between the Franklin and Wildcat marble horizons, stratigraphically overlies the Franklin marble. This stratigraphic relationship was deduced from the sequence in the vicinity of Glenwood where the gneisses of the Glenwood syncline overlie the Wildcat marble which in turn overlies the Cork Hill gneiss and Franklin marble. The Franklin marble-Cork Hill gneiss contact is overturned to the west in the vicinity of Franklin and Ogdensburg but at the Limecrest quarry northwest of Sparta it is normal. The Cork Hill gneiss is indistinguishable as a zone from other gneisses except where it occurs between the Franklin and Wildcat marble horizons. The gneisses of the Mts. Adam and Eve area and the microcline gneiss band east of the Wildcat marble in the Lake Lenape area are considered to be in the Cork Hill gneiss zone. This zone is missing on the east side of the Losee gneiss anticline from the area west of Franklin to the nose of the anticline west of Glenwood.

Wildcat marble.—The Wildcat marble closely resembles the Franklin marble. Although it thickens and thins and shows few outcrops, it is remarkably persistent and makes a good marker horizon. In the area 2½ miles north of Sparta the Wildcat marble grades into a zone of interbanded pyroxene gneiss and marble, and finally into hornblende gneiss. The Wildcat marble horizon is missing in the area between the north end of Lake Lenape and the west side of the Pimple Hills. It is also missing on the east side of the Losee gneiss anticline from the area west of Franklin to the nose of the anticline west of Glenwood.

Pochuck Mountain gneiss series.—The Pochuck Mountain gneiss series stratigraphically overlies the Wildcat marble. Its sequence changes from a thick series of oligoclase gneiss containing hornblende and microcline gneiss bands in the Pimple Hills to interlayered hornblende gneiss, microcline gneiss, and biotite gneiss in the Lake Lenape syncline, on Pochuck Mountain, and in the Glenwood syncline. This variation from one area to another seems inconsistent, but the structural position indicates that all were deposited or emplaced above the Wildcat marble. The total thickness of this zone cannot be determined because the Precambrian erosion surface cuts off the series unconformably.

Metamorphism

Most Precambrian rocks of the area have reached the level of the sillimanite zone of metamorphism of Barrow or the amphibolite facies of Eskola. The characteristic minerals are sillimanite and garnet in the microcline gneiss and hornblende and pyroxene in the hornblende gneiss.

Hydrothermal metamorphism is evident in the widespread alteration of plagioclase, the alteration of biotite to chlorite, and the occurrence of numerous epidote veinlets in many of the rocks. The marble shows hydrothermal metamorphism especially well in the alteration of chondrodite to serpentine, the alteration of tremolite to muscovite and/or talc, and the alteration of diopside to serpentine. This hydrothermal metamorphism might be considered a type of retrogressive metamorphism (Turner, 1948, p. 301).

The metamorphism of the Precambrian rocks was apparently caused by high temperatures and pressures which resulted in a high metamorphic grade and widespread development of planar and linear structures. All Precambrian rocks of the area except granites and pegmatites show the effect of metamorphism by the development of these structures. The Byram gneiss may be an exception to this rule because its planar and linear features conform more to the expected pattern of an igneous intrusion.

Economic Geology

Introductory Statement

Mines and quarries described in this section are represented on the geologic map (Pl. 1) by symbols and numbers. The deposit which each number represents is indicated in the following paragraphs. The original surface exposures of the ore bodies at the Franklin and Sterling mines are indicated in solid black.

Zinc Deposits

The best-known and most valuable mineral resources in the area are the zinc deposits mined by the New Jersey Zinc Company at the Franklin mine (1) at Franklin and the Sterling mine (2) at Ogdensburg. Both ore bodies occur within the Franklin band of marble between the Cork Hill and Median gneiss zones and are believed to represent the replacement of certain favorable horizons which had been deformed into large, synclinal folds. This theory of origin was postulated earlier by Spencer (1908, p. 8), Ries and Bowen (1922, p. 566–570), and Pinger (1950, p. 84–87). The scarcity of extreme fracturing within the ore bodies indicates that the ore was introduced in the later stages of Precambrian folding. Local linear orientation of willemite in both ore bodies shows, however, that the forces causing deformation were still active during ore deposition. Later Paleozoic folding is considered not to have been sufficiently intense to produce this lineation.

The folded Sterling ore body plunges 45°NE. and attains a total vertical depth of 2500 feet. The fold axis of the Franklin ore body plunges 25°NE., and the trough reaches a depth of 1150 feet. In both plan and section the two ore bodies have pronounced hook shapes. The shorter east limb of the Franklin ore body dies out at depth because its up-dip termination has a steeper plunge than the trough of the fold. The east limb of the Franklin fold is vertical, but the west limb of the fold dips approximately 55°SE. as do both limbs of the Sterling fold. At the Sterling mine the east limb is the longer and there is a folded "cross-vein" of ore between the limbs of the fold. The composition of Franklin ore is 40 per cent franklinite, 23 per cent willemite, less than 1 per cent zincite, and the remainder is gangue silicates and carbonates. At Sterling the ore is 33 per cent franklinite, 16 per cent willemite, 1 per cent zincite, and the remainder is gangue, principally calcite. At the Sterling mine, a portion of the "cross-vein" is composed of black willemite, which under high magnification appears to be composed of colorless willemite peppered through with minute inclusions of highly magnetic black franklinite which is apparently close to magnetite in composition. The normal Sterling willemite is red or brown, caused by microscopic red high-zinc franklinite inclusions. The willemite at the Franklin mine is commonly green, possibly in large part as a result of "daylight" fluorescence which is activated by both natural and artificial light (R. W. Metsger, 1953, unpublished manuscript).

Although both ore bodies lie within the marble, their positions vary with respect to the near-by Cork Hill-Franklin marble contact. The Cork Hill gneiss is only a few feet west of the Franklin deposit, but at the Sterling mine the contact is 400 feet west of the north end of the ore body and 800 feet west of the south end of the ore body. No conclusive evidence indicates that the two ore bodies replaced portions of a single favorable horizon in the marble or how the ore was emplaced. However, it is presumed that the ore bodies are primary hydrothermal deposits and that their formation is related to that of the abundant magnetite mineralization of the New Jersey Highlands.

Unique at the Sterling mine is the cylindrical mass of gneissic material (referred to in the discussion of the Franklin band of marble) which occupies the core of the Sterling fold between the "cross-vein" and the trough. While pegmatites do not occur within the Sterling ore, they are locally abundant in the Franklin mine where the formation of a great number of mineral species, some of them unique, is ascribed to reaction between the pegmatites and the ore.

As might be expected, the Franklin-Sterling area has been thoroughly prospected. Except for glacial boulders which occur in a fan-shaped area extending southward from the known ore bodies, and a small detrital franklinite deposit in the Hardyston quartzite just northeast of the point where that formation overlies the Franklin ore body, not one grain of franklinite, willemite, or zincite has been found in the area outside the known ore bodies.

A small deposit of sphalerite occurs north of Andover and has been described by Neumann (1952, p. 4) and Sims and Leonard (1952, p. 36–40). The deposit, known as the Sulphur Hill mine (3), consists of a shoot of impure magnetite which trends N. 50°E. and plunges 25°NE. The shoot, where mined, had an irregular diameter averaging 30 feet and was enclosed in a sheath of skarn in which were sporadic masses of sphalerite with lesser galena, iron sulfides,

and sparse chalcopyrite. Diamond drilling failed to prove the existence of economic quantities of any mineral.

Traces of sphalerite and galena have been found at the marble-gneiss contact immediately east of the Limecrest quarry (11). The prospect, known as the Indian mine (4), has received considerable attention but has revealed nothing of value. Similar minor occurrences of sphalerite have been found locally throughout the marble but nowhere in economic amounts.

Iron Deposits

The last iron mining in the Franklin-Sterling area took place around 1893 when Edison's experiments were abandoned at the Edison mine east of Ogdensburg and just off the map area. The numerous large and small mines in the area have been described by Bayley (1910), Sims and Leonard (1952), and others. A group of small magnetite ore bodies on Sparta Mountain appear to represent the mineralization of roof pendants or inclusions within the Byram gneiss. A number of old magnetite mines and prospect pits occur north of Andover. The largest is the Sulphur Hill mine (3) which has already been mentioned in the section on zinc deposits. It had an estimated production of 25,000 tons of high-sulfur iron ore, much of which remains on the dumps. The mineralization occurs in skarn in which a sufficient amount of calcite remains to suggest that the mineralized zone was a calcareous band within the gneiss. At Franklin, a minor band of disseminated magnetite occurs in the marble between the Franklin zinc ore body and the adjacent Cork Hill gneiss zone. The magnetite extends for a mile southward along the contact and gradually crosses it. The pods of recoverable ore are small and apparently have no extension at depth. An appreciable quantity of magnetite was obtained from the Roseville mine (10) south of Sparta where the ore, with associated skarn, occurs in two or more thin bands of marble. Local bands of disseminated magnetite are common in many of the gneisses of the area and several have been found in the marble, but it is believed that the area offers no valuable iron-ore reserves by present standards.

Just north of Andover, some 360,000 tons of mixed hematite and magnetite ore were produced from a trough-shaped ore body known as the Andover mine (9). Diamond drilling failed to locate additional reserves (Sims and Leonard, 1952, p. 31; Neumann, 1952, p. 5–13).

Limonite and hematite were mined as iron ores at certain localities in the area. The Edsall (5) and Pochuck (6) limonite mines near McAfee produced an appreciable amount of ore, but the pits were exhausted prior to 1880. The source of the mineralization is unknown. Also at McAfee, minor showings of hematite have been prospected at the Simpson (7) and Cedar Hill (8) mines. Production was insignificant.

Nonmetallic Deposits

The nonmetallic deposits of the Franklin-Sterling area consist of marble, gneiss, granite, and sand and gravel. The marble is being quarried in two localities, primarily for agricultural limestone, and there are a number of abandoned quarries in the area. South of Franklin, the Farber White Limestone Company operates a small plant and quarry (12). At the Limecrest quarry (11), north of Andover, the Limestone Products Corporation of America has a large output. The reserves of marble for these purposes are large, but topography, the degree of local dolomitization, and the presence of pegmatites and gneissic inclusions are factors which are locally unfavorable.

At Hamburg, Losee gneiss is being quarried for road metal by Sussex Quarries, Inc. (13). Reserves of rock suitable for this purpose are unlimited, but their distance from the major population centers has discouraged establishment of the industry on a wide basis.

There has been no granite production in the area since early in this century. Paving blocks and dimension stone were produced at the Hinchcliff and Carling quarries in New York State west of Amity. The Orange County Granite Company quarried the rock at Mount Adam to a considerable depth. Along with lesser pits in the same vicinity, these ventures were abandoned long before the reserves were exhausted.

Although the largest deposits of sand and gravel in the vicinity of the map area lie to the west in the broad valley underlain by Paleozoic sediments, two pits are operating in the area

and a number of others are worked from time to time. Two miles west of Sparta, F. W. Bennett and Sons produce sized sand and gravel from a stratified glacial deposit. Immediately south of the Limecrest quarry, the Limestone Products Corporation of America is working similar material and produces washed and sized products. Reserves of sand and gravel in the area are large, but at the present time the distance to the metropolitan areas is too great for other than predominantly local usage.

Geologic History and Conclusions

The Precambrian rocks of the Franklin-Sterling area consist of interlayered metasediments, probable metavolcanics, and both concordant and discordant igneous intrusives. The rocks attain a probable maximum thickness of approximately 9000 feet.

The oldest rocks of the area are those metasediments or metavolcanics which occur within the Byram gneiss east of McAfee on Hamburgh Mountain. Their deposition was followed without interruption by the deposition of a thick mass of limestone which is now the Franklin marble. A series of sediments and possible volcanic flows were laid down over the limestone, still without interruption, to form the Cork Hill gneiss, and these were in turn overlain by a mass of limestone which is now the Wildcat marble. Further continuous deposition of sediments and volcanic flows resulted in the formation of the rocks represented by the Pochuck Mountain gneiss series. The gradational contacts of the marble bands with the various gneiss zones suggest continuous deposition.

Following the last-described period of Precambrian deposition, intense folding took place over a long period, and the area was apparently above the level of deposition for the remainder of Precambrian time. During this extended period of folding the large conformable intrusive masses were emplaced, probably in the following order: Losee and oligoclase gneisses; granodiorite gneiss; Byram gneiss. The pink granite which occurs on Hamburgh Mountain and most of the pegmatites were probably intruded during the final stages of deformation. The iron and zinc deposits in the area are assumed to have been formed during the latter part of this period of intrusion and deformation. The Mount Eve granite was intruded after deformation had ceased.

Uplift and erosion during late Precambrian and early Cambrian time formed an irregular surface upon which clastic and, later, biochemical sediments were deposited, forming the Hardyston and Kittatinny formations. Continued deposition formed the other Paleozoic formations which are exposed west of the area.

A period of folding during late Paleozoic time produced the broad open folds exhibited by the Cambro-Ordovician rocks. The folding was followed by extensive faulting which may have followed fault zones established during Precambrian time. After this second period of deformation, basic dikes were intruded, probably during the Triassic period.

Uplift and prolonged erosion during late Mesozoic and Tertiary time carved the land surface into high ridges and deep valleys which were modified into the present topography by extensive Pleistocene glaciation and recent erosion.

The following conclusions resulted from the study of the Franklin-Sterling area: (1) The marble and strongly banded gneisses of the area undoubtedly constitute a metasedimentary sequence containing some interbanded metavolcanics; the masses of Byram gneiss, Losee gneiss, oligoclase gneiss, and granodiorite gneiss apparently represent concordant intrusives emplaced during Precambrian folding; the Mount Eve granite and some of the pegmatites are discordant intrusives emplaced after deformation had ceased; possible pillow or toe structures in the Glenwood syncline indicate that some of the hornblende gneiss may represent basic volcanic flows; in the same area, discordant contacts of the type IV hornblende gneiss give this rock the appearance of having an intrusive origin.

(2) The major structure in the area is an overturned isoclinal syncline which contains some smaller local folds and is flanked on either side by overturned anticlines with cores of intrusive rock; the Franklin marble and Wildcat marble in the vicinity of Franklin and Ogdensburg are overturned.

(3) The generalized stratigraphic sequence in the area was deduced from a study of structures by using the Wildcat marble as a key horizon.

(4) Precambrian folds and post-Ordovician

faults have very similar orientations. The major folds and major faults of the area trend in a northeasterly direction. Cross-folds trend north-south and N.70°E., and cross-faults trend N.10°W. and N.60°E. Although these relationships could be coincidental, it is more likely that the faults were controlled by shears developed in the Precambrian rocks as a result of Precambrian folding.

(5) Metamorphism has reached the level of the sillimanite zone throughout the area, but there is evidence of subsequent hydrothermal metamorphism. Dolomite bands and zones in the marble have been formed as a result of replacement by hydrothermal solutions.

(6) The occurrence of detrital franklinite in the lower part of the Hardyston formation near the Franklin mine indicates conclusively that the Franklin and Sterling ore bodies were deposited during Precambrian time.

References Cited

Alling, H. L., 1938, Plutonic perthites: Jour. Geology, v. 46, p. 142–165

Bayley, W. S., 1910, Iron mines and mining in New Jersey: N. J. Geol. Survey, Final Rept. ser., v. 7, 512 p.

——, 1941, Pre-Cambrian geology and mineral resources of the Delaware Water Gap and Easton quadrangle, New Jersey and Pennsylvania: U. S. Geol. Survey, Bull. 920, 98 p.

Bayley, W. S., Salisbury, R. D., and Kümmel, H. B., 1914, Raritan folio: U. S. Geol. Survey, Geol. Atlas, no. 191, 32 p.

Bowen, N. L., and Tuttle, O. F., 1950, The system $NaAlSi_3O_8$-$KAlSi_3O_8$-H_2O: Jour. Geology, v. 58, p. 489–511

Faessler, C., and Tremblay, L. P., 1946, Perthite as an age indicator: Canadian Min. Met. Bull. 405, p. 58–70

Hotz, P. E., 1953, Magnetite deposits of the Sterling Lake, N. Y.-Ringwood, N. J. area: U. S. Geol. Survey Bull. 982-F, p. 153–244

Kemp, J. F., 1893, On the granite on Mounts Adam and Eve, Warwick, Orange County, New York, and its contact phenomena: N. Y. Acad. Sci. Annals, v. 7, p. 638–654

Kummel, H. B., 1940, The geology of New Jersey: N. J. Geol. Survey, Bull. 50, 203 p.

Ludlum, J. C., 1940, Continuity of the Hardyston formation in the vicinity of Phillipsburg, New Jersey: N. J. Geol. Survey Bull. 47, 21 p.

Milton, C., 1947, Diabase dikes of the Franklin Furnace, N. J. quadrangle: Jour. Geology, v. 55, p. 522–526

Nason, F. L., 1889, Geological studies of the Archaean rocks: N. J. Geol. Survey, Ann. Rept. of State Geologist for 1889, p. 12–65

Neumann, G. L., 1952, Diamond drilling for zinc ore at Andover-Sulphur Hill iron mines, Sussex County, N. J.: U. S. Bur. Mines Rept. Inv. 4911, 13 p.

Palache, C., 1935, The minerals of Franklin and Sterling Hill, Sussex County, New Jersey: U. S. Geol. Survey Prof. Paper 180, 135 p.

Pinger, A. W., 1950, Geology of the Franklin-Sterling area, Sussex County, New Jersey: Internat. Geol. Cong. Rept. of 18th Sess. (1948), pt. VII, p. 77–87

Ries, H., 1897, Geology of Orange County, N. Y.: State Geologist Ann. Rept. 15, p. 18–19, 393–475.

Ries, H., and Bowen, W. C., 1922, Origin of the zinc ores of Sussex County, New Jersey: Econ. Geology, v. XVII, no. 7, p. 517–571

Sims, P. K., 1953, Geology of the Dover magnetite district, Morris County, New Jersey: U. S. Geol. Survey Bull. 982-G, p. 245–304

Sims, P. K., and Leonard, B. F., 1952, Geology of the Andover mining district, Sussex County, New Jersey: N. J. Geol. Survey, Bull. 62, 46 p.

Spencer, A. C., Kümmel, H. B., Wolff, J. E., Salisbury, R. D. and Palache, Charles, 1908, Franklin Furnace folio: U. S. Geol. Survey Geol. Atlas, no. 161, 27 p.

Turner, F. J., 1948, Mineralogical and structural evolution of the metamorphic rocks: Geol. Soc. America, Mem. 30, 342 p.

Wolff, J. E., and Brooks, A. H., 1898, The age of the Franklin white limestone of Sussex County, N. J.: U. S. Geol. Survey, 18th Ann. Rept., pt. II, p. 425–458

Box 217, Platteville, Wisconsin; 399 Rutherford Ave., Franklin, New Jersey; 700 Long St., Lexington, N. C.; 666 E. 5th N. Street, Provo, Utah

Manuscript Received by the Secretary of the Society February 28, 1955

BULLETIN OF THE GEOLOGICAL SOCIETY OF AMERICA
VOL. 67, PP. 475-510, 3 PLS. APRIL 1956

SEISMIC-REFRACTION MEASUREMENTS IN THE ATLANTIC OCEAN PART VII: ATLANTIC OCEAN BASIN, WEST OF BERMUDA

By Samuel Katz and Maurice Ewing

Abstract

Results of 25 seismic-refraction stations in the Atlantic Ocean west of Bermuda are incorporated with other available data into four seismic cross sections through the oceanic crust and continental margins along tracts from Bermuda to the continent. These provide additional evidence for the marked contrast between oceanic and continental crustal structure. Under the northeast American continent the velocity of near-surface rocks is close to 6.0 km/sec and may increase with depth to near 7.0 km/sec at about 35 km, with the mantle (velocity exceeding 7.7 km/sec) below. The upper continental crust (6.0–6.3 km/sec) thins seaward, disappearing near the foot of the continental slope. For the deep stations of this paper (mean depth 4.9 km) the mean thickness of sediments is 1.3 km. Mean thickness of crustal rocks underlying this thin sedimentary layer is 5.1 km, with velocities up to 7.1 km/sec, but significantly less near Bermuda. Arrivals from the mantle were observed on five of the longer stations, giving velocities of 7.7–8.5 km/sec at 9.4 to 13.4 km below sea level. Exclusive of the water column, this oceanic crust is less than one-fifth as thick as the continental crust. Toward Bermuda, the mean crustal velocity decreases; observed values range from 5.6 to 6.5 km/sec. In several areas near Bermuda velocities near 4.5 km/sec (volcanics and other consolidated sediments) are observed.

A conspicuous, constant-frequency arrival, appearing at a range of 40–50 seconds (59–74 km) and at the travel time of the first reflection, is interpreted as refracted along the ocean floor, possibly within a layer of low-velocity sediment from 0 to about 150 feet thick. On the basis of reflection at the critical angle sound velocity in sediments near the ocean floor is calculated from the maximum number of bottom reflections recorded under favorable conditions. Recorded sub-bottom reflections are described, and two methods of interpretation presented. Resulting sediment thicknesses and velocities compare with those from refraction and vertical reflection data.

CONTENTS

TEXT

	Page
Introduction	476
Acknowledgments	476
Method of measurement	476
Corrections	480
Refraction data	480
Interpretation and discussion	489
R_{1b} arrival	493
Reflections	499
Reflections from ocean floor	499
Sub-bottom reflections	502
Conclusions	505
Appendix—calculated shot distances	507
References cited	508

ILLUSTRATIONS

Figure	Page
1. Seismic-refraction stations, western Atlantic Ocean	477
2. Seismic-refraction stations described in this paper	479
3. Refraction station A164-9	482
4. Refraction station A164-11	482
5. Refraction station A164-12	483
6. Refraction station A164-13 and 14	483
7. Refraction station A164-15	484
8. Refraction station A164-16	484
9. Refraction station A164-23	485
10. Refraction station A164-24	485
11. Refraction station A164-25	486
12. Refraction station A164-26	486
13. Refraction station A164-27	486
14. Refraction station A179-5	487
15. Refraction station A179-6	488
16. Refraction station A179-7	489
17. Refraction station A179-8	490
18. Refraction station A179-9	491
19. Refraction station A179-10	492
20. Refraction station A179-11	493
21. Refraction station A179-12	494
22. Refraction station A179-13	495
23. Refraction station A179-14	496
24. Refraction station A179-15	497

Figure Page
25. Frequency diagram of seismic velocities, Atlantic Ocean (depths exceeding 100 fms).. 498
26. Velocity structure for low velocity bottom 499
27. Ray path, normal-mode propagation, low velocity bottom..... 501
28. Angle of incidence for ocean with velocity gradient..... 501
29. Travel times of R_{1a} and R_{1b}..... 502
30. Reflection coefficient versus incident angle for various velocity and density contrasts... 502
31. Universal curves for bottom and sub-bottom reflection arrivals for two constant velocity layers..... 504
32. Universal curves for bottom reflection and sub-bottom refraction arrivals, linear velocity gradient in the sediments..... 505
33. Sub-bottom reflection data..... 506

Plate Facing page
1. Seismic sections, western Atlantic Ocean... 475
2. Examples of R_{1b} and R_{2b} arrivals..... 494
3. High-order and sub-bottom reflections..... 495

TABLES

Table Page
1. Seismic-refraction stations, Cruises A164 and A179..... 478
2. Summary of calculations, stations from cruise A164..... 481
3. Summary of calculations, stations from cruise A179..... 481
4. Wave velocities..... 498
5. Summary of data on R_{1b} arrival..... 500
6. Comparison of ratio of surface to bottom sound velocity from two different methods.. 502
7. Sediment velocity from critical angle reflections..... 503
8. Sediment velocity and thickness from sub-bottom reflections..... 504
9. Comparison of approximate and exact distance calculations..... 507
10. Comparison of observed mean vertical sound velocity with British Admiralty tables..... 507

Introduction

Seismic-refraction measurements have been used to investigate elastic wave velocities and thicknesses of rock layers beneath the ocean since 1937 (Ewing *et al.*, 1937). Locations of all available measurements in the area discussed in this paper in water depths greater than 1000 fathoms are shown in Figure 1, including the stations of Gaskell and Swallow (1951), Tolstoy *et al.* (1953), and Hersey *et al.* (1952).

This study describes the 23 seismic-refraction stations shown in Table 1 and Figure 2 and summarizes currently available seismic-refraction data in this area. These stations, occupied in the summer of 1950 by Atlantis (Cruise 164) and Caryn (Cruise 17) and in the spring of 1952 by Atlantis (Cruise 179) and Albatross (Cruise 43), are located between Bermuda and the North American continent. Twenty-two of the stations are in water exceeding 1000 fathoms.

Acknowledgments

Research described in this paper was supported by the Bureau of Ships, U. S. Navy under Contract NObsr-43355, and by the Office of Naval Research under Contract N6-onr-271, T.O. 13 and 24. The Bureau of Ordnance furnished the explosives. The Woods Hole Oceanographic Institution made available the research vessels Atlantis (Cruise 164) and Caryn (Cruise 17) during the summer of 1950, and Atlantis (Cruise 179) and Albatross (Cruise 43) during the spring of 1952. Among members of the 1950 expedition without whose help no data would have been obtained are C. R. Bentley, M. G. Cheney, Jr., L. Davis, R. C. DuBois, G. Duys, R. S. Edwards, B. C. Heezen, J. Hazelworth, T. Madden, J. Northrop, C. B. Officer, Jr., H. J. Pincus, G. Shaeffer, E. G. Smith, G. H. Sutton, and P. C. Wuenschel. On the 1952 expedition the following were of invaluable assistance: B. C. Heezen, R. Heningham, J. Hennion, and D. Warren. To all these the authors express their grateful appreciation. The critical reading of the manuscript and the valuable suggestions of Professors J. Nafe, F. Press, and J. L. Worzel are gratefully acknowledged. The wide dynamic-range amplifiers designed and built by G. H. Sutton made it possible to record the fine structure of reflected water waves.

Method of Measurement

The experimental techniques are similar to those described in Part IV of this series by Officer *et al.* (1952). Two ships, each equipped to shoot and record, participate in a reversed refraction station. On the forward half of the station one ship heaves to and records sound waves generated by depth charges dropped by the second ship as it steams away. Shot times are transmitted by radio. The sound waves

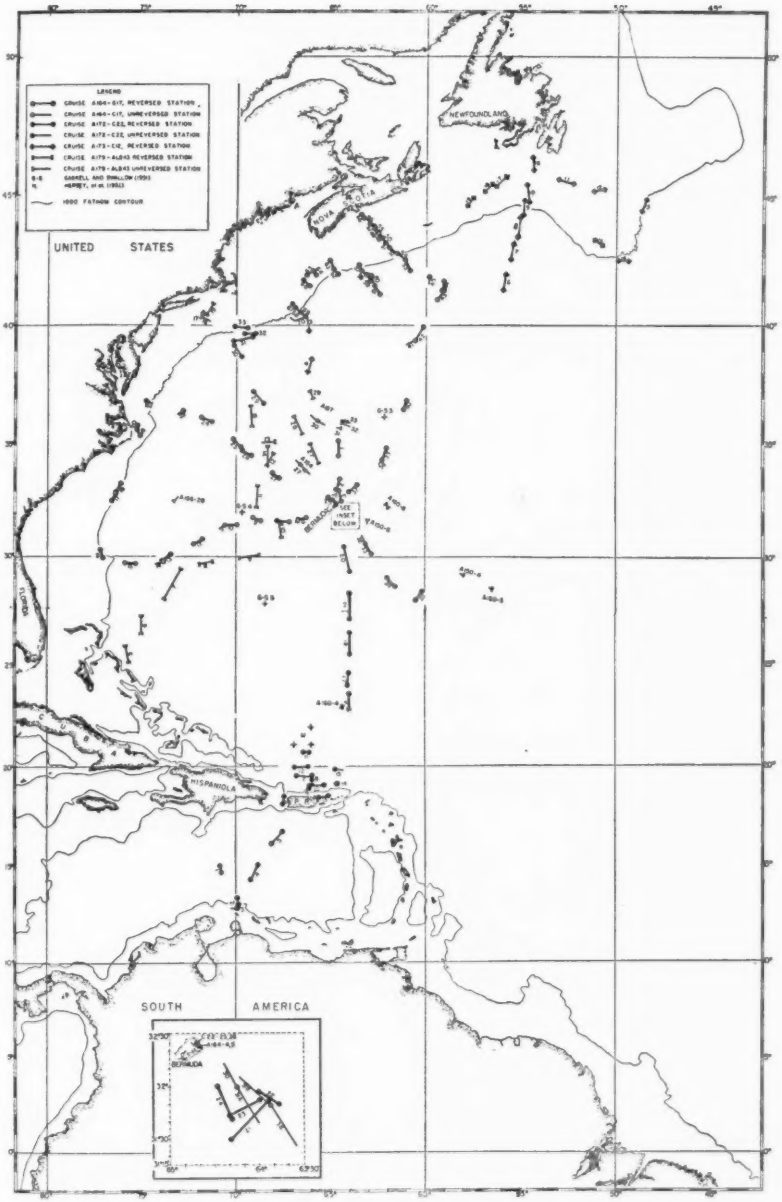

FIGURE 1.—SEISMIC-REFRACTION STATIONS, WESTERN ATLANTIC OCEAN

include direct and multiply-reflected waves in the water, and waves refracted in the sediments and rocks. The shooting ship proceeds usually 45 to 90 km, shooting at intervals of 5 to 10 km, and then heaves to, ready to listen. On the reverse half the first ship steams to rejoin the second ship, shooting at similar intervals, thus completing the reversed stations. With suitable

TABLE 1.—SEISMIC-REFRACTION STATIONS, CRUISES A164 AND A179

Station no.	Receiving position	
	Latitude (N)	Longitude (W)
	° ′	° ′
A164-9A	31–40.5	68–41
A164-9B	31–48	69–05.5
A164-11	31–30.2	70–26
A164-12A	30–51	71–45
A164-12B	30–37	72–13
A164-13A	30–09	73–26
A164-13B	29–51	73–53
A164-14	29–48.6	73–51
A164-15A	29–44	75–18
A164-15B	29–45	75–52
A164-16A	29–59	77–01
A164-16B	30–22	77–09
A164-23	36–29	72–47
A164-24A	36–23	71–50
A164-24B	36–01	71–16
A164-25A	35–15.5	70–07
A164-25B	34–56	69–44
A164-26A	36–46	69–39
A164-26B	34–34	69–20
A164-27A	33–48	68–03
A164-27B	33–33	67–43
A179-5A	25–02	75–19
A179-5B	25–54	75–46
A179-6A	26–24.5	75–02.5
A179-6B	27–17	75–01.5
A179-7A	28–03	73–44
A179-7B	29–25.5	72–53
A179-8A	29–38.5	71–57
A179-8B	29–44.5	71–17
A179-9A	29–56.5	69–52
A179-9B	30–06.5	68–47
A179-10A	30–51	67–33.5
A179-10B	31–41	67–43
A179-11A	32–13.5	68–51.5
A179-11B	33–13.5	68–49
A179-12A	34–03.5	68–19
A179-12B	34–37	68–01
A179-13	35–03.5	67–58
A179-14	34–55	68–15.5
A179-15A	35–53.5	69–06
A179-15B	36–40.5	69–12

corrections, resulting data are used to calculate sediment and rock velocities and thicknesses.

On cruises after the fall of 1951 amplifiers designed and described by Sutton (1952) were used. To discriminate against spurious noise signals each listening ship recorded the output of two independent Brush AX-58 hydrophones. These hydrophones were connected to amplifiers by cables floated to provide slightly negative buoyancy, resulting in considerable improvement in overall sensitivity by discriminating against noise from surface-water waves and mechanical vibration.

In the seismic-refraction method two quantities must be determined: distance between source and receiver, and time required for sound or elastic waves to travel this distance by all possible paths.

On land surveying or careful use of maps enables one to obtain the distance accurately. At sea the measurement of travel time of sound in sea water from source to receiver, either by a direct path or by one or more bottom reflections, provides a simple and usually sufficiently accurate method. When one or more near-surface sound channels exist, and source and receiver are both located within one of these sound channels, direct sound may be detected out to 50 miles or more. With adequate bathythermograph data, one can compute mean horizontal velocity and, knowing the elapsed time, obtain distance to an accuracy of within 0.5 per cent.

In the absence of a surface sound channel the direct sound can be heard only at short ranges. If the direct sound is not received, the once-reflected sound can be used to determine the distance. Ewing *et al.* (1950) showed that if R_n is the travel time of the nth reflection and D the travel time of the direct water wave, the relationship between R_n^2 and D^2 is linear for $n = 1$, 2, and 3. By graphical extrapolation Officer *et al.* (1952) used the linear relationship between R_1^2 and D^2 observed at short ranges to find D at long ranges. An alternative, analytical method is to find the ratio of mean horizontal to mean vertical sound velocity for each shot. Let H_w = depth of water, c_o = mean horizontal near-surface sound velocity obtained from temperature and salinity data, c_z = sound velocity at depth z measured from sea level, and

$$c_v = \frac{H_w}{\int_0^z \frac{dz'}{c_z}},$$

the mean vertical sound velocity. Assuming an ocean with constant vertical sound velocity

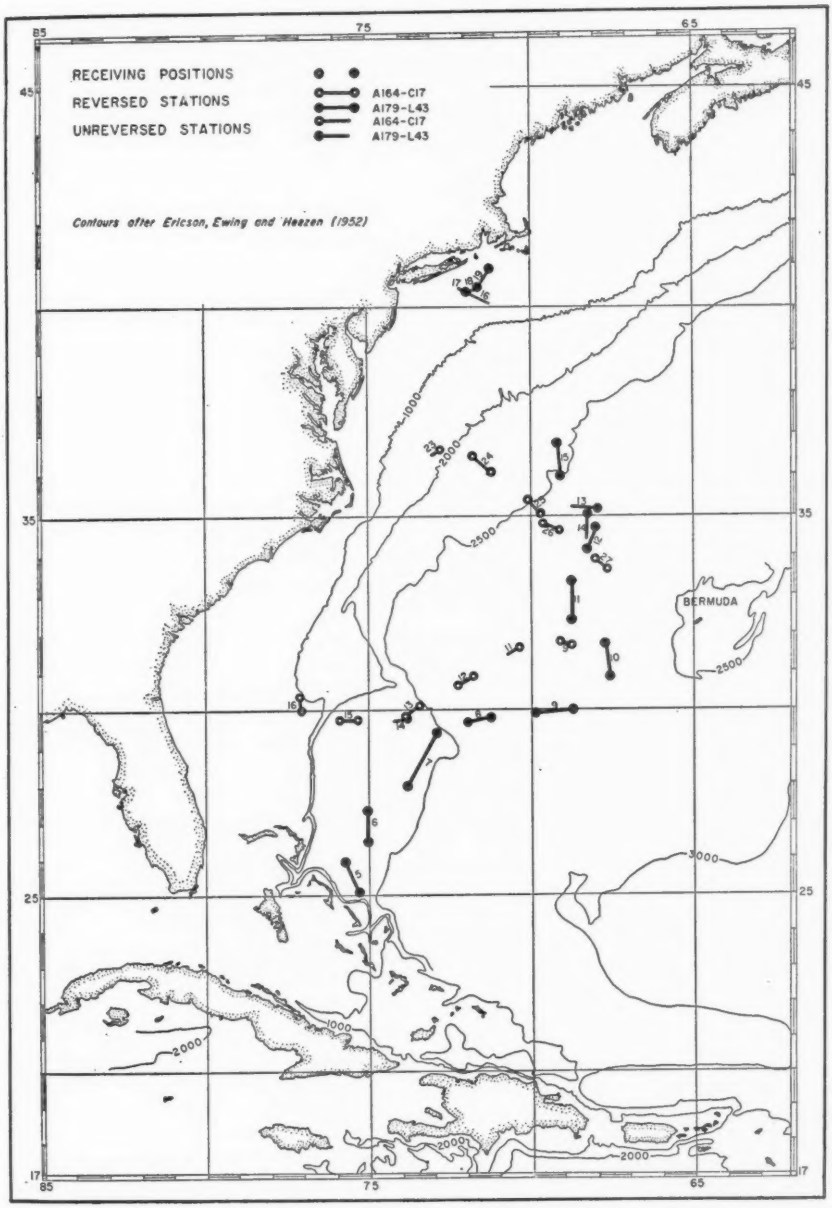

FIGURE 2.—SEISMIC-REFRACTION STATIONS DESCRIBED IN THIS PAPER

c_v and a surface sound channel with velocity c_0, it is easy to show that

$$\frac{c_0}{c_v} = \frac{1}{D}\sqrt{R_n^2 - \left(\frac{2nH_w}{c_v}\right)^2} \qquad (1)$$

Each quantity on the right side of Equation (1) can be measured directly. Quantities D and R_n are obtained from short-range shots and $2H_w/c_v$ is twice the depth of water in

seconds obtained directly from records of the shooting ship. With the value of c_o/c_v for close shots D is computed from R_n for distant shots, where no D is observed. By averaging $2H_w/c_v$ for successive shots beginning with the closest no topographic correction is required for regions of small relief. The effect on Equation (1) of ray curvature from actual sound-velocity gradients is discussed in the Appendix.

This method is open to several objections. Generally mean horizontal sound velocity varies less than 0.5 per cent over the station. Shot and receiver depths may vary considerably, however, depending on charge size and firing method, making it difficult to assign one depth for finding mean horizontal sound velocity. Since on stations described here the temperature change from 75 to 400 feet is small, this problem arises in only a few shots. For refraction stations in water depths exceeding about 2500 fms, once-reflected sound (R_1) can be detected as such only to about 41 seconds, and twice-reflected sound to about 82 seconds. Beyond this distance Equation (1) is no longer applicable, and as shown below the apparent velocity is that in the near-surface sound channel.

Knowing all values of D on a station, either by direct observation or by computation by the above method, travel times of all other arrivals may be plotted as function of D and all velocity and thickness computations carried out with c_o as parameter. The value of c_o at the average receiver-shot depth for the station is used to compute final values.

Corrections

Corrections made by Officer *et al.* (1952) were also made in this study. These include a shot-instant correction, involving the time required for sound to reach the detector aboard the shooting ship from the depth charge; a correction reducing all travel times to sea level; and a correction for irregular topography, which was required on only one station and was very small. Hill (1952) corrects both distance and travel time of each sound arrival—refracted, reflected, and direct—as though both receiver and shot were at sea level, on the assumption that the sound continues along its path. As a result refracted and reflected arrivals from a given shot appear to travel different horizontal distances. For large distances and angles of incidence the distance and time corrections become quite large. In this paper all arrivals have been corrected to sea level keeping the shot distance equal to the observed value. By this method the largest correction is about 0.15 second for distant and deeper shots.

Refraction Data

Seismic-refraction data presented in the travel-time curves of Figs. 3–24 are discussed below and are summarized in Tables 2 and 3 and Pl. 1.

The method of interpretation described by Ewing *et al.* (1939) and used in this paper assumes that the crust beneath the ocean is layered and that each layer is characterized by constant elastic-wave velocities, with refraction according to Snell's Law. On a reversed station the travel time of all sound—reflected, refracted, and direct—must be equal for the two halves of the station at the reverse distance. In the absence of rapid drift the reverse distance is the separation between the listening positions of the two ships. This requirement serves as a convenient and stringent check on reading and plotting data, as well as on navigation. It is equivalent to a reciprocity condition on shot and receiver position.

Since on many stations observed ground-wave lines are not tangent to the R_1 curve, there must be a considerable thickness of material beneath the ocean floor for which no refraction arrivals are observed. Under Reflections from Ocean Floor a method for calculating the velocity contrast at the ocean floor is described. This has been used on stations A179-6, 7, 9, 10, 11, 12, 13, and 15. For other stations which did not record all high-order reflections a mean velocity (1.89 km/sec) obtained from all available measurements was assumed.

On some long stations no refraction arrivals from the mantle are observed (A179-8, 9, and 15). There is some evidence (A179-7) that near the break in the travel-time curves the high-velocity arrival has abnormally small amplitude and would therefore be picked late near

TABLE 2.—SUMMARY OF CALCULATIONS, STATIONS A164

Station	h_{1a}	h_{1b}	h_{2a}	h_{2b}	h_{3a}	h_{3b}	h_{4a}	h_{4b}	v_1	v_2	v_3	v_4	v_5
9	5.02	5.09	0.73	1.34	....	....	....	....	1.511	(1.89)	6.55	....	....
11	5.29	....	1.88	....	5.09	....	....	....	1.534	(1.89)	6.46	....	....
12	5.40	5.40	1.97	2.19	....	....	....	....	1.526	(1.89)	6.87	....	....
13	4.07	4.22	1.46	1.45	1.91	1.66	....	....	1.507	(1.89)	2.53	6.24	....
14	4.23	....	1.54	....	1.49	....	....	....	1.511	(1.89)	2.49	6.25	....
15	4.85	....	2.13	....	....	....	....	....	1.515	1.95	6.82	....	....
16A	....	1.02	....	0.35	....	....	....	....	1.505	(1.89)	4.47	....	....
16B	1.02	1.55	.39	.70	1.89	....	....	....	1.503	(1.89)	3.95	6.23	....
16B (alt.)	1.02	1.55	.39	.70	1.07	2.94	....	....	1.503	(1.89)	3.95	6.82	....
23	3.56	....	3.48	....	....	....	....	....	1.504	(1.89)	6.35	....	....
24	4.05	4.16	1.01	1.03	1.82	1.28	6.65	4.21	1.507	(1.89)	2.25	5.50	7.97
25	4.87	5.10	1.68	1.59	....	....	....	....	1.512	(1.89)	7.06	....	....
26	5.24	5.24	1.36	1.54	....	....	....	....	1.514	(1.89)	6.82	....	....
27	5.25	5.10	1.03	1.09	....	....	....	....	1.512	(1.89)	6.94	....	....

h_n, nth layer thickness in km; v_n, compressional wave velocity in km/sec.

TABLE 3.—SUMMARY OF CALCULATIONS, STATIONS A179

Station	h_{1a}	h_{1b}	h_{2a}	h_{2b}	h_{3a}	h_{3b}	h_{4a}	h_{4b}	v_1	v_2	v_3	v_4	v_5
5	4.84	4.70	0.99	1.24	4.23	3.64	....	....	1.508	(1.76)	5.02	7.12	....
6	4.58	4.64	0.82	0.68	1.17	1.32	5.81	5.93	1.508	1.76	2.26	6.73	7.87
7	4.62	4.32	1.56	1.51	0.57	1.32	7.21	5.76	1.516	1.79	2.38	6.75	8.50
8	5.41	5.44	1.69	1.61	....	....	....	....	1.519	1.89	6.88	....	....
9	5.37	5.20	1.10	1.03	....	....	....	....	1.512	(1.81)	6.57	....	....
10	(5.14)	5.14	(0.68)	0.68	4.71	5.65	....	....	1.516	1.98	5.62	8.05	....
11	5.23	5.25	1.00	0.95	4.65	3.48	....	....	1.512	2.08	6.32	7.68	....
12	5.31	5.25	0.97	0.98	2.74	3.84	....	....	1.514	2.12	6.36	7.83	....
13	5.18	....	0.44	....	2.93	....	....	....	1.507	1.99	4.47	6.82	....
14	5.22	....	0.70	....	2.04	....	....	....	1.504	(1.91)	4.60	6.73	....
15	4.65	4.50	1.72	1.92	....	....	....	....	1.506	1.82	6.65	....	....

Shear-Wave Data

Station No.	v_p km/sec	v_s km/sec	σ	H_p km	H_s km
A179-6	6.73	4.0	0.25	6.6	8.6
A179-9	6.50	3.93	0.22	5.8	7.2
	6.64	3.98	0.22	....	....
A179-11	6.31	3.88	0.21	6.2	6.8
	6.32	3.82	0.22	....	....

the break and for some distance beyond, and might not be observed.

Arrivals without sharp beginning, comparable in amplitude with ambient noise, or with poor shot or distance data are called *weak*. Unless otherwise stated the direct water wave was observed on all shots. All depths are given with respect to sea level.

Some data obtained on Cruise A164 leave much to be desired. They are presented because of lack of better data in the area and because of their general agreement with the results of later data in other parts of the Atlantic Ocean.

REFRACTION STATION A164-9 (Fig. 3): Because of inoperative listening gear, CARYN was able only to shoot. CARYN first shot away from ATLANTIS, com-

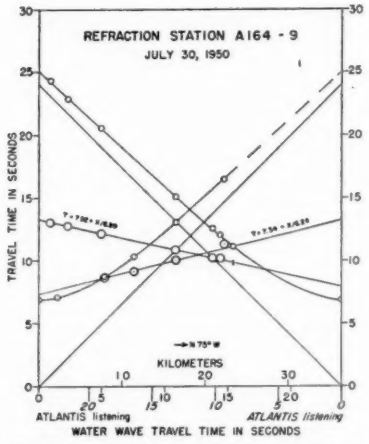

FIGURE 3.—REFRACTION STATION A164-9

pleting half the station. On the reverse CARYN fired all shots at the same position, while ATLANTIS steamed toward her, stopping long enough to receive each shot. The last point on the forward half and the first point on the reverse are weak. Since this station is removed from the line of Section C of Plate 1, the velocities and depths are projected onto the section.

REFRACTION STATION A164-11 (Fig. 4): This is an unreversed station. The farthest two points are weak. The three closest points determine a 6.46 km/sec velocity. Because of insufficient data this interpretation is ambiguous. An alternative is to consider the closest point as a refraction from a shallower layer and to draw a 6.92 km/sec line through four points. The most distant point is low marking the beginning of refraction from the upper mantle. From the fathograms, the ocean floor is horizontal. Velocities and depths have been calculated on the assumption that the basement is also horizontal.

REFRACTION STATION A164-12 (Fig. 5): On the forward half, since the closest point is at 15.9 seconds, there is no information on structure near the ocean floor. Third and fourth points are weak. Since the farthest two points fall low, it is reasonable to regard these as refractions from the mantle. On the reverse there are adequate data at close but none at long range. Simplicity of the structure made a satisfactory interpretation possible from the reverse distances.

REFRACTION STATION A164-13 AND 14 (Fig. 6): On A164-13 the farthest two points on the forward half and the farthest point on the reverse are weak. On A164-14 the point at 14.2 seconds is weak. On each leg of these two stations late ground arrivals determined lines which reversed and gave velocities and depths close to those observed to the south on Stations A179-6 and 7 (Pl. 1, C, D). This may represent a sedimentary layer associated with the outer ridge of the Blake-Bahama Basin, which rises approximately 300 fathoms above the surrounding ocean floor in this area. The direct water wave appears out to 13 and 19 seconds on the two halves. Depths and velocities on unreversed Station A164-14 were obtained by using the corresponding determination on A164-13.

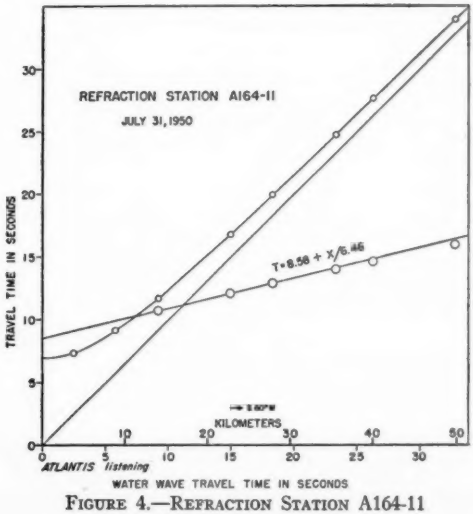

FIGURE 4.—REFRACTION STATION A164-11

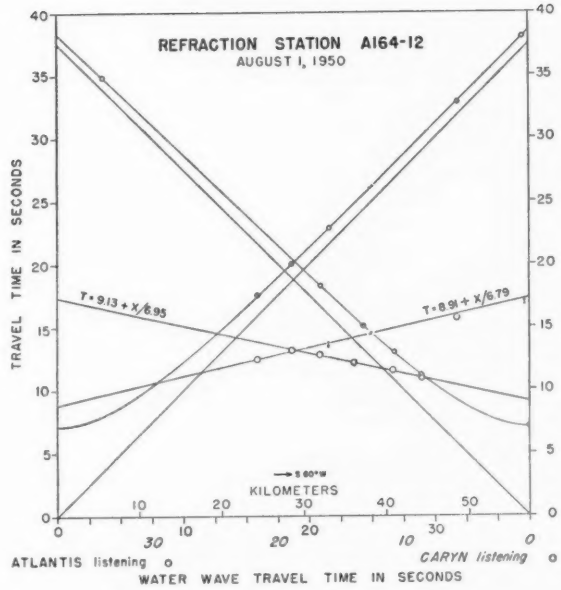

FIGURE 5.—REFRACTION STATION A164-12

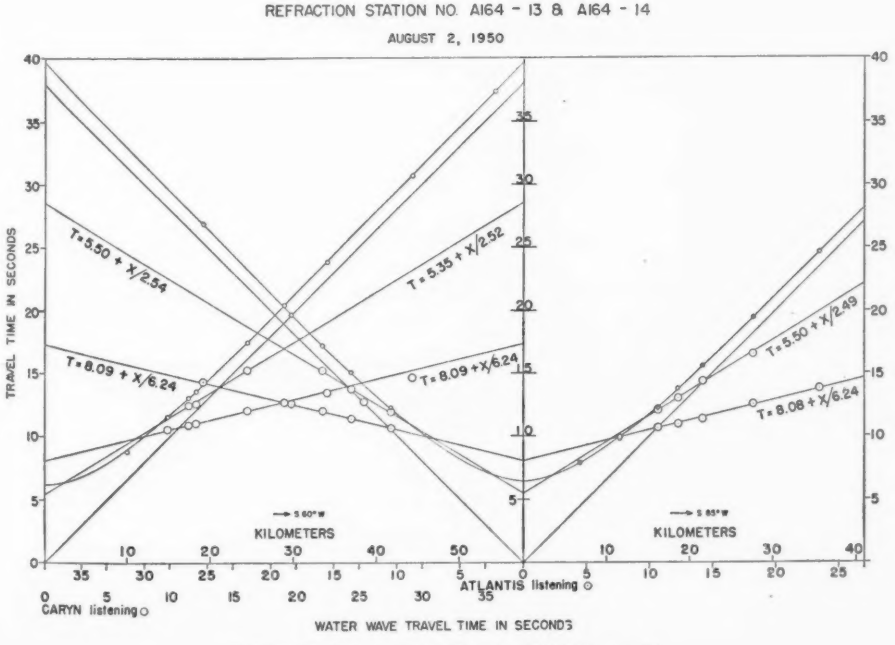
REFRACTION STATION NO. A164 - 13 & A164 - 14
AUGUST 2, 1950
TRAVEL TIME IN SECONDS
T = 5.50 + X/2.54
T = 8.09 + X/6.24
T = 5.35 + X/2.52
T = 8.09 + X/6.24
T = 5.50 + X/2.49
T = 8.08 + X/6.24
KILOMETERS
KILOMETERS
CARYN listening
ATLANTIS listening
WATER WAVE TRAVEL TIME IN SECONDS

FIGURE 6.—REFRACTION STATION A164-13 AND 14

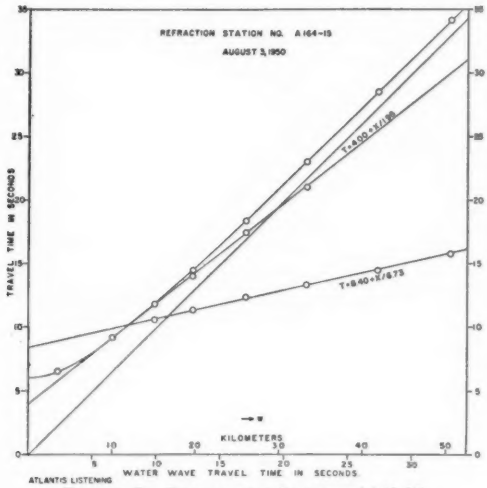

FIGURE 7.—REFRACTION STATION A164-15

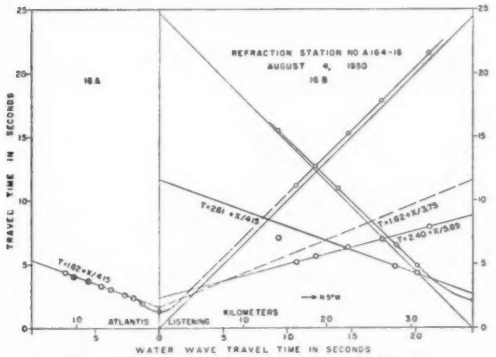

FIGURE 8.—REFRACTION STATION A164-16

REFRACTION STATION A164-15 (Fig. 7): On the forward half the farthest two points are weak. Three late ground arrivals determine a line closely tangent to the first reflection curve, giving the velocity of unconsolidated sediments near the ocean floor (1.95 km/sec). Since the reverse is very poor, it has been omitted.

REFRACTION STATION A164-16 (Fig. 8): Listening gear aboard CARYN was inoperative, making it necessary for ATLANTIS to listen on both halves, as described under Station A164-9. On the forward half of 16B the first shot has not been included on the travel-time curve because of poor shot information. On the reverse the last point is weak.

Continuation of the 4.15 km/sec line of 16A was not found on the forward half of 16B for lack of close points, although it appears on the reverse of 16B. The sea floor has a slope of 48.4′, resulting in larger velocity contrasts than observed on other stations.

Using the reverse point determined by the 5.89 km/sec line and the one strong distant point on the reverse of 16B at 15.2 seconds, a velocity of 6.82 km/sec at a mean depth of 3.8 km with a slope of 3.9° is obtained. An alternative is to ignore this point and assume that the deepest horizon is horizontal. On this assumption velocity and depth are 6.23 km/sec and 3.7 km, respectively.

REFRACTION STATION A164-23 (Fig. 9): CARYN shot away from and back in to ATLANTIS, which was hove to and remained east of CARYN. Data are plotted on one travel-time curve. All but the closest and two farthest points are weak. Obviously velocities and slopes cannot both be calculated. Even

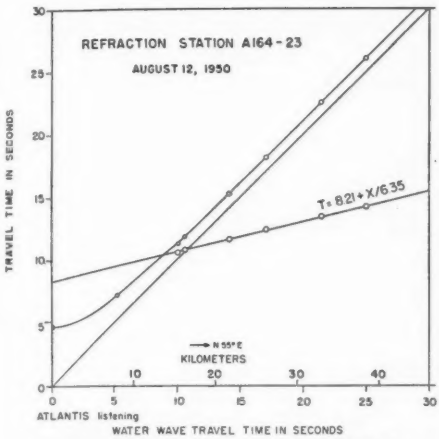

FIGURE 9.—REFRACTION STATION A164-23

mantle does not correlate with neighboring stations A164-23 and 25 (Pl. 1, B).

REFRACTION STATION A164-25 (Fig. 11): On the forward half distance was obtained from the direct water wave out to 16 seconds and calculated beyond.

REFRACTION STATION A164-26 (Fig. 12): On the reverse the three distant points are weak.

REFRACTION STATION A164-27 (Fig. 13): The fourth and fifth points on the forward half and the farthest point on the reverse are weak. Distance was obtained from the direct water wave out to 12 and 17 seconds on the two halves and calculated beyond.

REFRACTION STATION A179-5 (Fig. 14): On the forward half the low-velocity line can be followed for 6 seconds beyond the break to the high-velocity line. This station provides a good measurement of velocities and thicknesses of the two observed crustal layers. Distance was measured from the

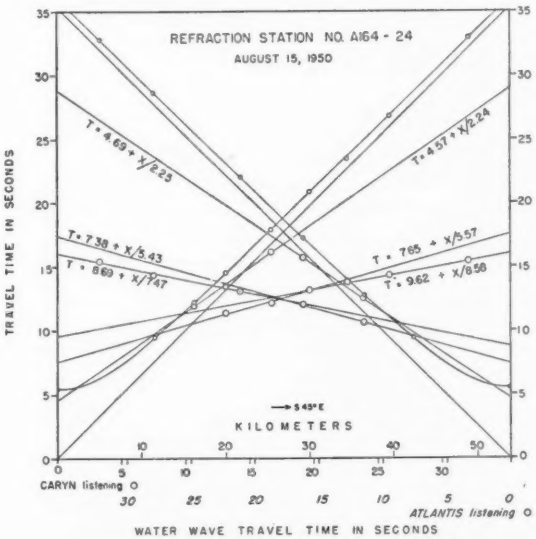
REFRACTION STATION NO. A164 - 24
AUGUST 15, 1950
T = 4.69 + X/2.23
T = 7.38 + X/5.43
T = 8.69 + X/7.47
T = 4.57 + X/2.24
T = 7.65 + X/5.57
T = 9.62 + X/8.50
S 45° E
KILOMETERS
TRAVEL TIME IN SECONDS
CARYN listening
ATLANTIS listening
WATER WAVE TRAVEL TIME IN SECONDS

FIGURE 10.—REFRACTION STATION A164-24

assuming one of these no unique interpretation is possible. A single line through all points gives a velocity of 6.35 km/sec. Fathograms indicate a horizontal sea floor. In the calculations the basement was assumed horizontal.

REFRACTION STATION A164-24 (Fig. 10): The fourth and fifth points on the forward half and the two closest points on the reverse are weak. On both halves late ground arrivals gave a velocity of 2.24 km/sec. The receiving data are poor, and the results presented only for lack of better data in the area. The velocity of 5.50 km/sec directly above the direct water-wave arrivals to 12 and 30 seconds on the two halves and calculated beyond.

REFRACTION STATION A179-6 (Fig. 15): The two distant points on the forward half and the seventh and farthest points on the reverse are weak. Late ground arrivals appear on both halves of this station with velocities of 2.28 and 2.24 km/sec, corresponding to comparable velocities on A164-13 and 14 and A179-7. Arrivals of moderate amplitude appear on the forward half of three successive records from 25 to 35 seconds, with a velocity of 4.0 km/sec. If these are transformed shear waves from the 6.73

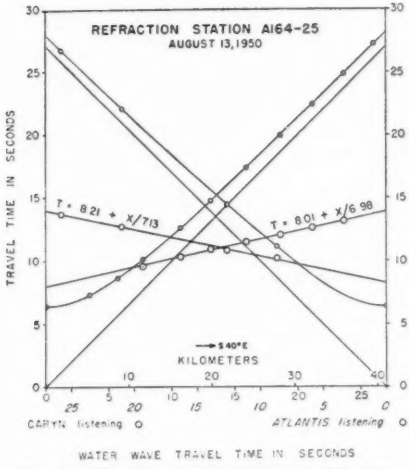

FIGURE 11.—REFRACTION STATION A164-25

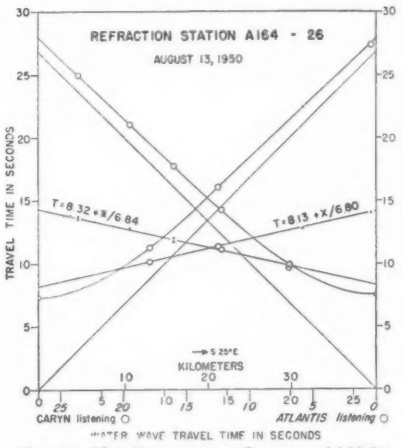

FIGURE 12.—REFRACTION STATION A164-26

km/sec layer, Poisson's ratio is 0.23. They were not observed on the reverse.

Using the method described in Reflections from Ocean Floor a velocity of 1.75 km/sec was found for the unconsolidated sediments and used in the calculations. Distance was measured from the direct water wave to 19 and 29 seconds on the two halves and calculated beyond.

REFRACTION STATION A179-7 (Fig. 16): On the forward half refraction arrivals are observed to a distance of 86 seconds. From 30 to about 45 seconds refraction-arrival amplitude is abnormally small in spite of normal charges (46½ and 94 pounds). The break in the curve is at about 32.5 seconds. Although a similar effect seems to occur on the reverse between 30 and 40 seconds, it is less clear because smaller charges were used. On the reverse refraction arrivals are observed out to 99 seconds. Late ground arrivals appear on both halves and determine a velocity of 2.38 km/sec, compared with 2.26 km/sec on Station A179-6 (Fig. 15) and 2.53 and 2.49 km/sec on A164-13 and 14 (Fig. 6). Unconsolidated-sediment velocity was measured as 1.78 km/sec. Mantle velocity, 8.50 km/sec, is high, but similar values have been found on other deep stations, both in the Atlantic and Pacific oceans. The direct water wave was observed to 27 and 13 seconds on the forward and reverse halves. Beyond this, calculated distance should vary less than 0.3 per cent from true distance (Appendix; Table 9). High-order reflections were observed on all shots.

REFRACTION STATION A179-8 (Fig. 17): The sixth and seventh points on the forward half and the two farthest points on the reverse are weak. Late ground arrivals on both halves give a good determination

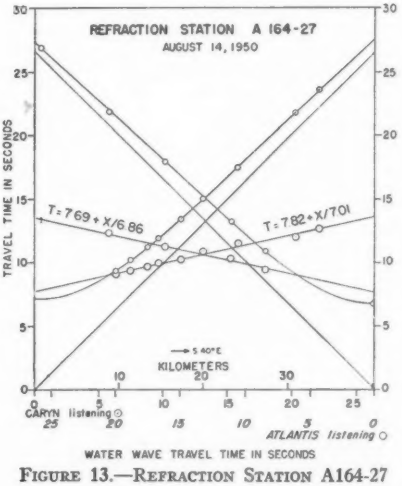

FIGURE 13.—REFRACTION STATION A164-27

of unconsolidated-sediment velocity (1.89 km/sec). Basement velocity and slope are well determined. Distance was measured directly to 13 and 29 seconds on the two halves and calculated beyond.

REFRACTION STATION A179-9 (Fig. 18): The three farthest points on the forward half and the farthest point on the reverse are weak. On the forward half numerous late arrivals were observed, one set of which could be followed on successive records and determined a line with a velocity of 3.98 km/sec. The intercept, 8.80 seconds, results in a negative thickness for an assumed layer. If this arrival is a transformed shear wave through the basement rocks,

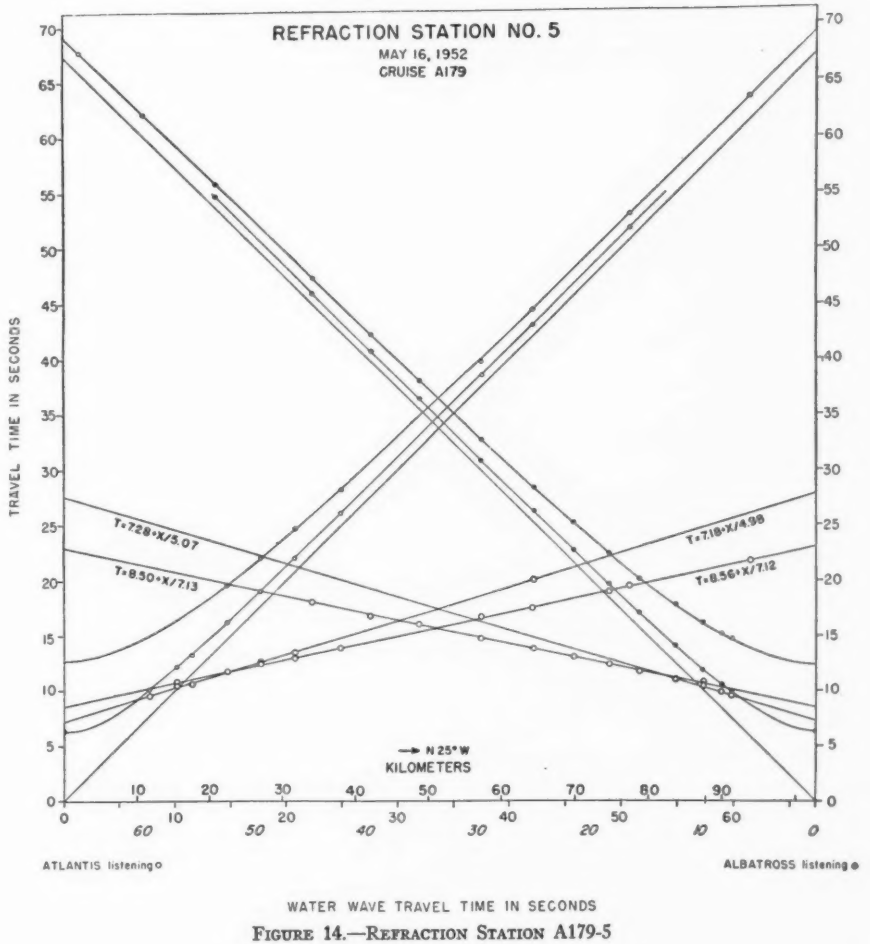

FIGURE 14.—REFRACTION STATION A179-5

the ratio of its velocity to that of the observed compressional waves results in reasonable values of Poisson's ratio and of thicknesses of overlying layers (Table 3).

The average of the unconsolidated sediments on the three preceding stations (1.81 km/sec) was used in the calculations. Distance was obtained from the direct water arrival which appeared sporadically depending on charge depth to 35 and 27 seconds on the two halves and was calculated beyond.

REFRACTION STATION A179-10 (Fig. 19): The three farthest points on the reverse are weak. The low velocity (5.62 km/sec) indicated on the reverse can also be interpreted as two lines, with velocities of 4.7 and 6.0 km/sec. Since it is unreversed, this is an apparent velocity and is bracketed in Plate 1, D. Lack of data at short range on both halves makes impossible a detailed determination of structure near the ocean floor. Since the ocean floor is horizontal, velocities and thicknesses have been calculated on the assumption of a uniformly horizontal basement. Unconsolidated-sediment velocity was measured as 1.97 km/sec.

REFRACTION STATION A179-11 (Fig. 20): The three farthest points on the forward half and the ninth point on the reverse are weak. Late ground arrivals determine velocities of 3.88 and 3.82 km/sec with intercepts 7.76 and 7.72 sec. If interpreted, as in Station A179-9, as shear waves through the low-velocity (6.31, 6.32 km/sec) rock, the velocity ratio is 1.63 and 1.66 with $\sigma = 0.21$ and 0.22. Thickness of overlying rocks calculated from shear velocities

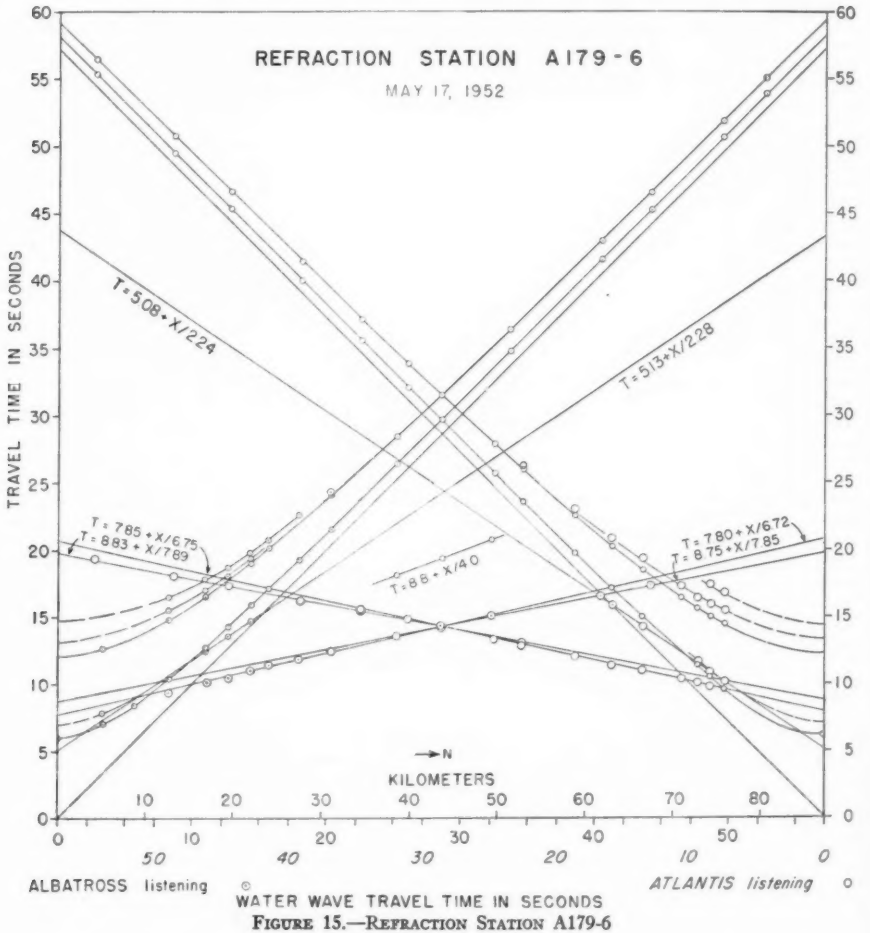

FIGURE 15.—REFRACTION STATION A179-6

is compared with that from compressional-wave velocities in Table 3. Unconsolidated sediment velocity was measured as 2.08 km/sec.

REFRACTION STATION A179-12 (Fig. 21): All points on the forward half except the second, fourth, and sixth are weak. No late ground arrivals can be followed on successive records. It is difficult to understand why the data obtained on the two halves have such different quality. The three low points on the forward half could not be reconciled with the good velocity determination on the reverse on any basis other than that shown. If a buried geologic structure such as a horst had resulted in the early arrivals, some evidence for this should appear on the reverse, unless the listening ship drifted laterally during the course of the station and did not cross the same local structure in shooting the reverse. The navigational data is not adequate to discard this possibility. Unconsolidated sediment velocity was measured as 2.12 km/sec.

REFRACTION STATION A179-13 (Fig. 22): Strong winds and currents, and engine and mast difficulties made it impossible for ATLANTIS to steam; therefore stations 13 and 14 were obtained with ALBATROSS firing all charges and ATLANTIS hove to. An effort to shoot an end-to-end station resulted in two unreversed legs, more or less at right angles. The most distant point is weak. Two lines with a low velocity of 4.47 km/sec breaking into 6.83 km/sec are clearly indicated. There may be a break to a higher velocity beyond 33.2 seconds, since the last arrival is weak. While late ground arrivals appeared, they could not be followed on successive records. Unconsolidated-sediment velocity was measured as 1.99 km/sec.

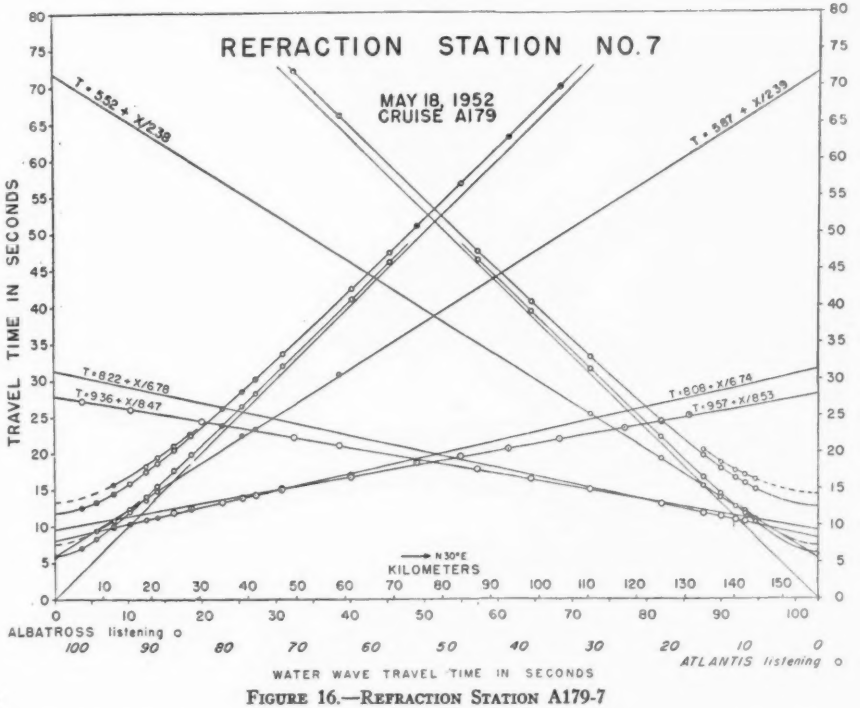

FIGURE 16.—REFRACTION STATION A179-7

REFRACTION STATION A179-14 (Fig. 23): The farthest point is weak. The high velocity found on this station agrees well with the high-velocity line found on A179-13, and the two lines reverse, but on this station no low-velocity material was found. If a line reversing with the low-velocity line (4.47 km/sec) of A179-13 is drawn through the closest point of A179-14, a maximum thickness of this material, compatible with the data, of 2.04 km is obtained, compared with 2.86 km on A179-13. No late ground arrivals could be followed on successive records. The average of the values found for unconsolidated-sediment velocity on the two closest stations, A179-13 and 15, was used, 1.91 km/sec.

REFRACTION STATION A179-15 (Fig. 24): The closest and the two farthest points on the forward half are weak. No late ground arrivals could be followed on successive records. Unconsolidated-sediment velocity was measured as 1.82 km/sec.

INTERPRETATION AND DISCUSSION

Seismic velocities obtained in refraction surveys of the Atlantic Ocean range from slightly higher than the velocity of sound in water for unconsolidated sediments to 8.5 km/sec for compressional waves in the upper mantle. All available velocities reported in the Atlantic Ocean in water depths exceeding 1000 fathoms, including those of Gaskell and Swallow (1951), Hill (1952), and Hersey *et al.* (1952) are plotted in the frequency diagram of Figure 25. Unconsolidated-sediment velocities for which few reliable refraction measurements are available and velocities based on meager data have been omitted. This frequency diagram shows the number of velocity measurements falling within an interval of 0.1 km/sec.

Although the velocities have a wide range, well-defined groups center about 2.4, 4.4, 5.5, 6.3, 6.8, and 8.1 km/sec. The range of velocities within each group may result from real variation in compressional wave velocity of the rock under the ocean floor or from scatter in velocity measurement of rocks which are fairly constant in lithology and elastic properties, or from both. One important source of scatter is that, where a break in a travel-time curve is not well defined, a line representing an average of two velocities is likely to be drawn.

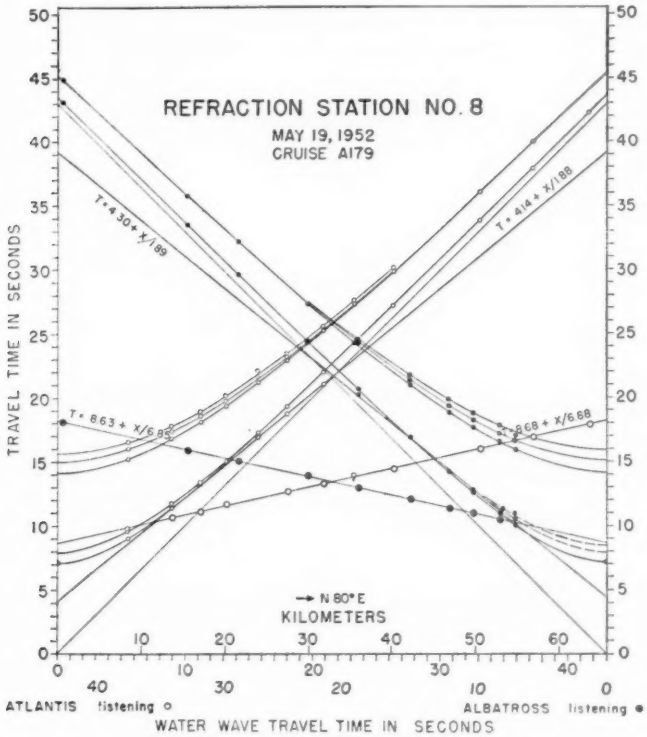

FIGURE 17.—REFRACTION STATION A179-8

In most recent investigations of continental crustal (all rocks above the mantle, with velocities appreciably less than 8.0 km/sec.) structure *e.g.*, Gutenberg (1951), Hodgson (1953), Katz (1955), Tatel *et al.* (1953), Willmore *et al.* (1952)—velocities from 6.0 to 6.3 km/sec have been measured for upper continental crustal rocks. In some of these investigations velocities near 7.0 km/sec are measured for rocks near the base of the crust, and in several others these velocities are compatible with the data, although not uniquely indicated. Accordingly velocities up to 7.3 km/sec have been called "crustal" in Figure 25. Six measurements in the range 6.3 ± 0.1 km/sec are less than 400 km from Bermuda and may be associated with the activity and structure of the Bermuda volcanoes.

Adams (1951) calculated the theoretical wave velocities at three pressures for rock types ranging from syenite through dunite (Table 4). Some experimental values measured by Hughes *et al.* (1950; 1951) appear in Table 4 and are generally in agreement with Adams' results. These values have been used to identify the seismic velocities of Figure 25, taking into account the appropriate ocean depths.

It is clear from Figure 25 that in the Atlantic the preponderance of rocks underlying the deep-ocean sediments have velocities in the range 6.8 ± 0.3 km/sec, corresponding to a basaltic composition.

Seismic thickness and velocity results appear in Plate 1. Sections A through D are based largely on data presented in this paper, with the addition of several stations near the line of the sections. (In Section A, preliminary results for stations A172-30, 31, 32, and 33 were generously made avilable by G. H. Sutton; Station A172-29 is from Ewing *et al.* (1954); New England and Eastern New York data are from Leet (1941) and Katz (1955), re-

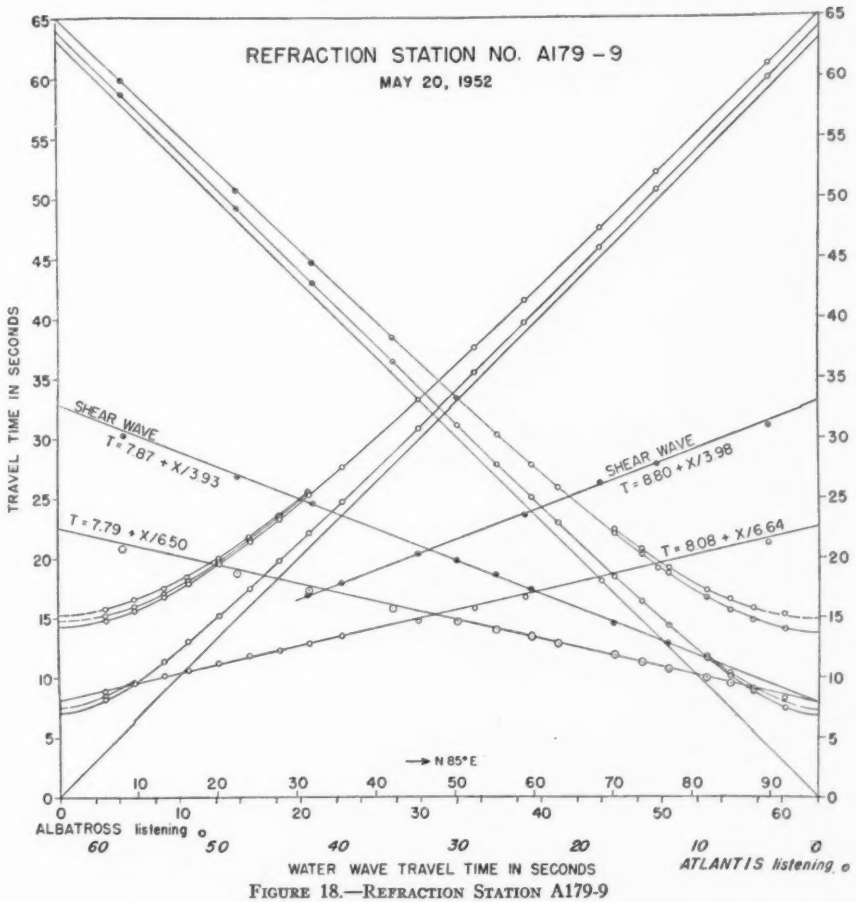

FIGURE 18.—REFRACTION STATION A179-9

spectively. In Section B Washington, D. C. and off-shore data are from Tatel *et al.* (1953) and Ewing *et al.* (1950). In Section C Station M-27 is from Worzel and Ewing (1948), Station A154-27 from Ewing *et al.* (1950), and Station A172-27 from Officer *et al.* (1952). In Section D A172-24 is from Officer *et al.* (1952). Section E, entirely from Officer *et al.* (1952), is presented for comparison.) Assumed or uncertain velocities are in parentheses with calculated thickness of the overlying layer correspondingly uncertain. The layers observed on neighboring stations are correlated according to measured depths and velocity. Where no correlation can be made, a horizontal variation in lithology is shown in the sections by solid jagged lines. Scarcity of data made inclusion of some stations desirable in spite of poor quality; for these no correlation was attempted.

Southwest of A179-11 in 2920 fms, Gaskell and Swallow (1951) found a structure consisting of three layers beneath the ocean floor, 0.46 km with a velocity of 1.85 km/sec, and 1.68 km of 4.63 km/sec, underlain by 6.34 km/sec. Although the velocity measured at A179-11 (Fig. 20), 6.32 km/sec, agrees well, no 4.63 km/sec layer was observed. Therefore depth to this velocity is only 0.98 km beneath the ocean floor on A179-11 as compared with 2.14 km on their station.

The contrast between continental and Atlantic oceanic crustal structure is brought out

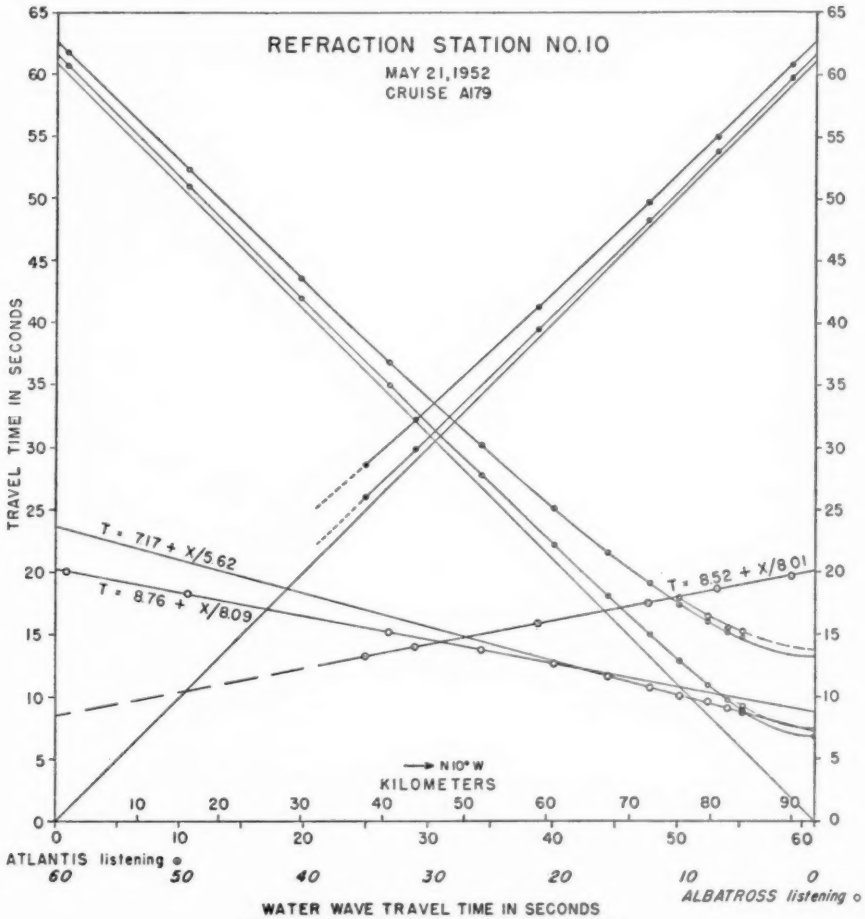

FIGURE 19.—REFRACTION STATION A179-10

in the sections of Plate 1. The upper continental crust (6.0–6.3 km/sec) thins seaward, disappearing near the foot of the continental slope. Under the deep ocean the depth to the mantle ranges from 10 to less than 14 km, in contrast with 33 to 44 km under the continent. For stations of this paper (mean water depth 4.92 km) the mean thickness of sediments and underlying crustal rocks is 1.29 km and 5.05 km. Thus the oceanic crust exclusive of the water column is less than one-fifth of the continental crust in thickness. Velocities up to 7.1 km/sec are measured beneath the thin sedimentary cover at depths from 6.8 km below sea level, while on land such velocities are reported in some experiments near the base of the continental crust (20–30 km).

Toward Bermuda crustal velocities decrease to 5.6–6.5 km/sec. In several areas near Bermuda velocities of 4.4–4.6 km/sec are observed, probably corresponding to volcanics and consolidated sediments.

The outer ridge of the Blake-Bahama Basin was crossed on three stations (A164-13, -14, A179-6, A179-7). On these a layer under the usual thin sedimentary cover was observed with velocities 2.51, 2.26, and 2.38 km/sec, and thicknesses 1.5, 0.75, and 1.54 km.

On many deep-water stations in the Pacific Raitt (1954) found a layer of 5 km/sec mate-

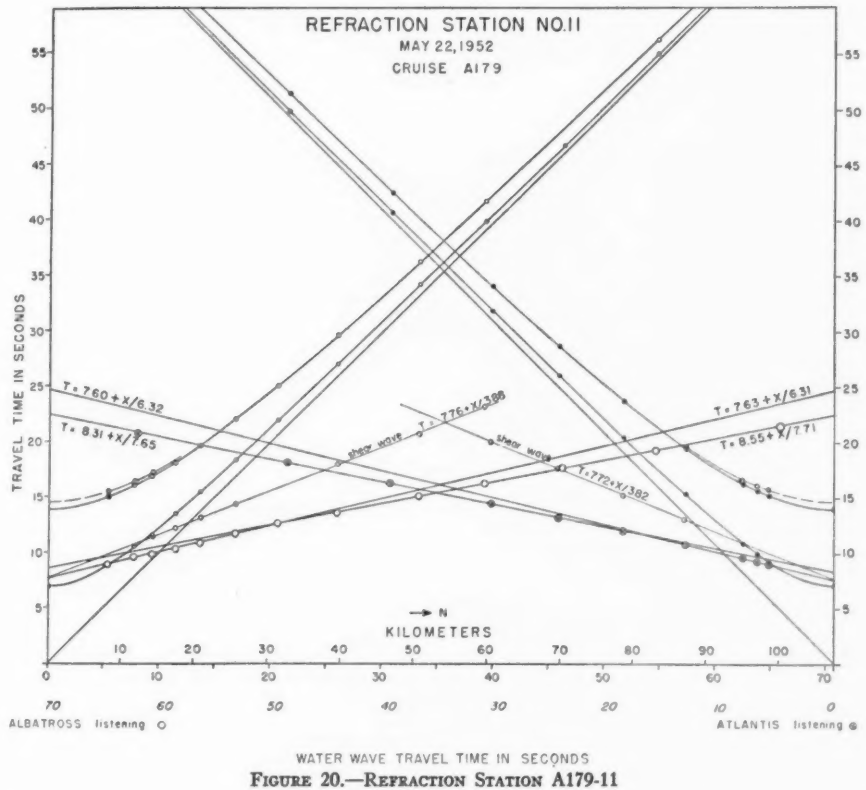

FIGURE 20.—REFRACTION STATION A179-11

rial from 0 to 4 km beneath the ocean floor underlain by several kilometers of 6.8 km/sec material, with the mantle 5 to 10 km beneath the ocean floor. Velocities of 4 to 5 km/sec appear on several stations (*e.g.*, A172-19, 20, 24, and A179-13 and 14) but are absent under most of the western Atlantic.

Velocity distribution and structure northwest of Bermuda are complicated. Unpublished gravity data indicate variations in lithology or crustal thickness in this area (J. L. Worzel, private communication).

R_{1b} ARRIVAL

Hersey *et al.* (1952) reported a large arrival, preceding the RSR ray, lasting for about 1 second, and appearing beyond 35 to 40 miles at a constant frequency of 63 cycles per second. (RSR (Ewing and Worzel, 1948) refers to a ray which originates in a sound channel—the surface sound channel in this instance—with an inclination close to horizontal, and which is successively reflected at the surface and refracted within the sound channel.) They interpreted this arrival as a refraction along the ocean floor, following the RSR path in the water, with a coupling mechanism responsible for the constant frequency.

During the spring of 1952 the authors also discovered this arrival and obtained 34 records, some of which are shown in Plate 2 at various locations and distances. The arrival usually consists of two groups, corresponding to the direct and first bubble pulses, and lasts less than 0.5 second. Besides the prominent, constant-frequency character, several other features of this arrival are apparent from Table 5. On a given station its frequency is relatively constant and therefore must be independent of charge and hydrophone depth and of charge

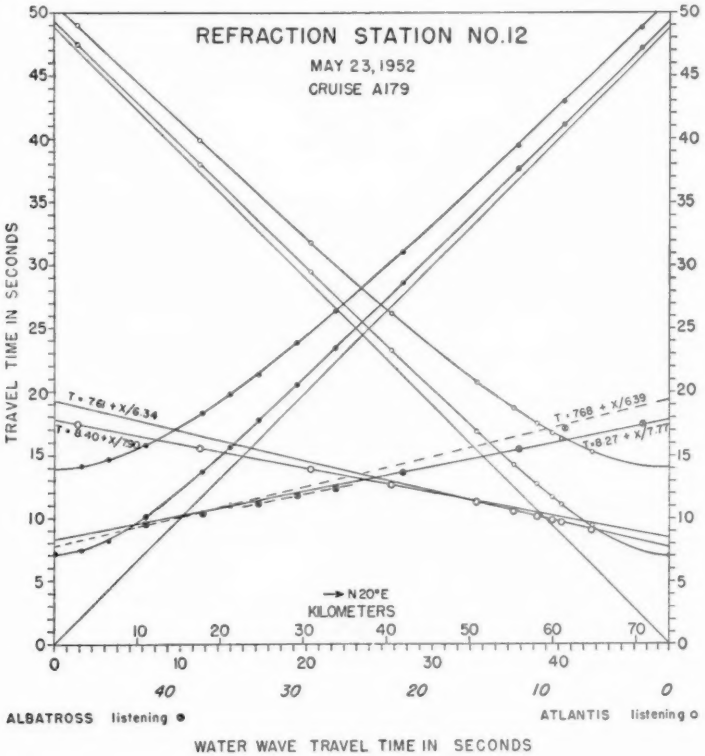

FIGURE 21.—REFRACTION STATION A179-12

size, since these varied over a wide range. The arrival is not always observed over the whole distance covered by one refraction station; on A179-5 the arrival is observed at 51.8 and 54.6 seconds and not at longer ranges; on A179-10 it is prominent at 53.8 seconds and not at 59.8 seconds. On stations differing 20 per cent in water depth the mean R_{1b} frequency may be nearly the same (*e.g.* A172-18A and 19B vs. A179-7), while on other stations in almost the same depth the R_{1b} frequency may differ by a factor of 2 (*e.g.*, A179-7 vs. 15). Therefore, water depth does not determine frequency. Since R_{1b} appears clearly on several stations (*e.g.*, A179-7) with poorly developed surface sound channels, this also cannot be the frequency-controlling factor. As shown by Hersey *et al.* (1952) and further below, the velocity of this arrival and other considerations indicate that a portion of its path must be near the ocean floor, in the water or in the sediments.

Ray calculations in the Appendix may be used to find angles of incidence at the bottom and range and depth of penetration for various rays. Figure 28 shows the results for rays from a source in a surface sound channel, for the velocity structure given by Ewing and Worzel (1948) with a slightly modified surface layer, an ocean 2600 fms deep, and shot and hydrophone depths of 260 feet. Let θ_1 be the angle of departure with respect to the horizontal, and θ_b the angle of incidence on the ocean floor. For decreasing values of θ_1, θ_b decreases, until for $\theta_1 = 7.93°$, the ray grazes the bottom horizontally and returns to the hydrophone at a range of almost 59 km (41 sec). Rays which start out at 6°, become horizontal at a depth of 2380 fms, and never touch the ocean floor.

In the presence of a surface sound channel

SHOT No. AL-157 D=49.02 sec. H_W=2530 Fm. R_{1b}=30 cps.

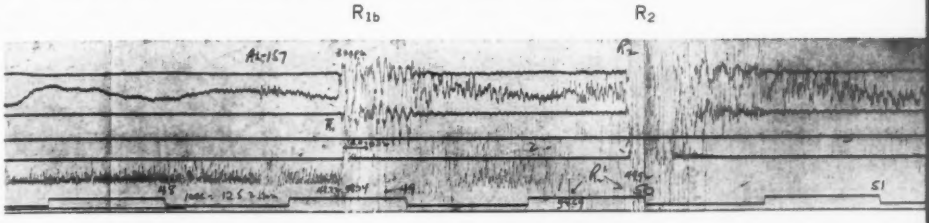

SHOT No. AL-160 D=68.18 sec. H=2490 Fm. R=39 cps.

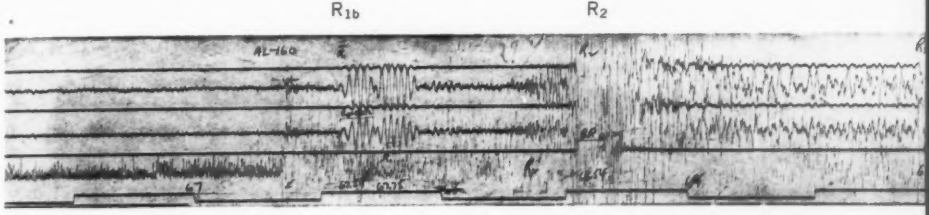

SHOT No. AL-162 D=85.64 sec. H_W=2355 Fm. R_{1b}=36 cps.

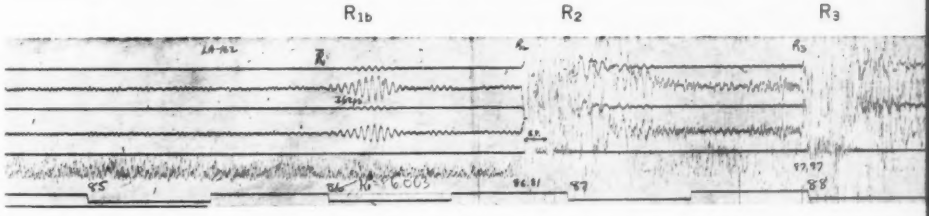

SHOT No. AL-268 D=54.45 sec. H_W=2910 Fm. R_{1b}=67 cps.

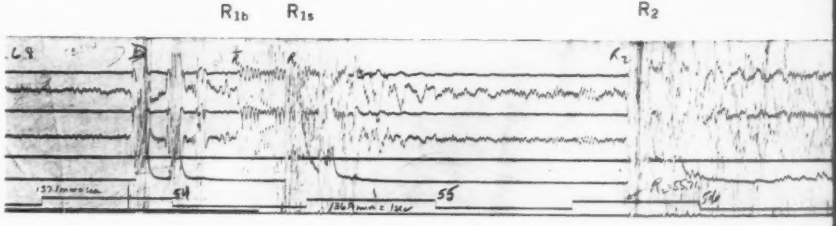

SHOT No. AL-269 D=65.89 sec. H_W=2900 Fm. R_{1b}=75 cps.

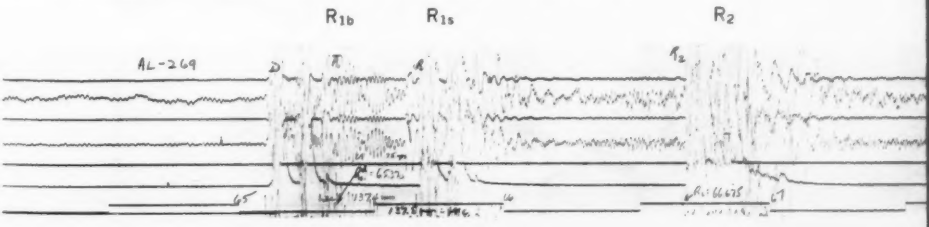

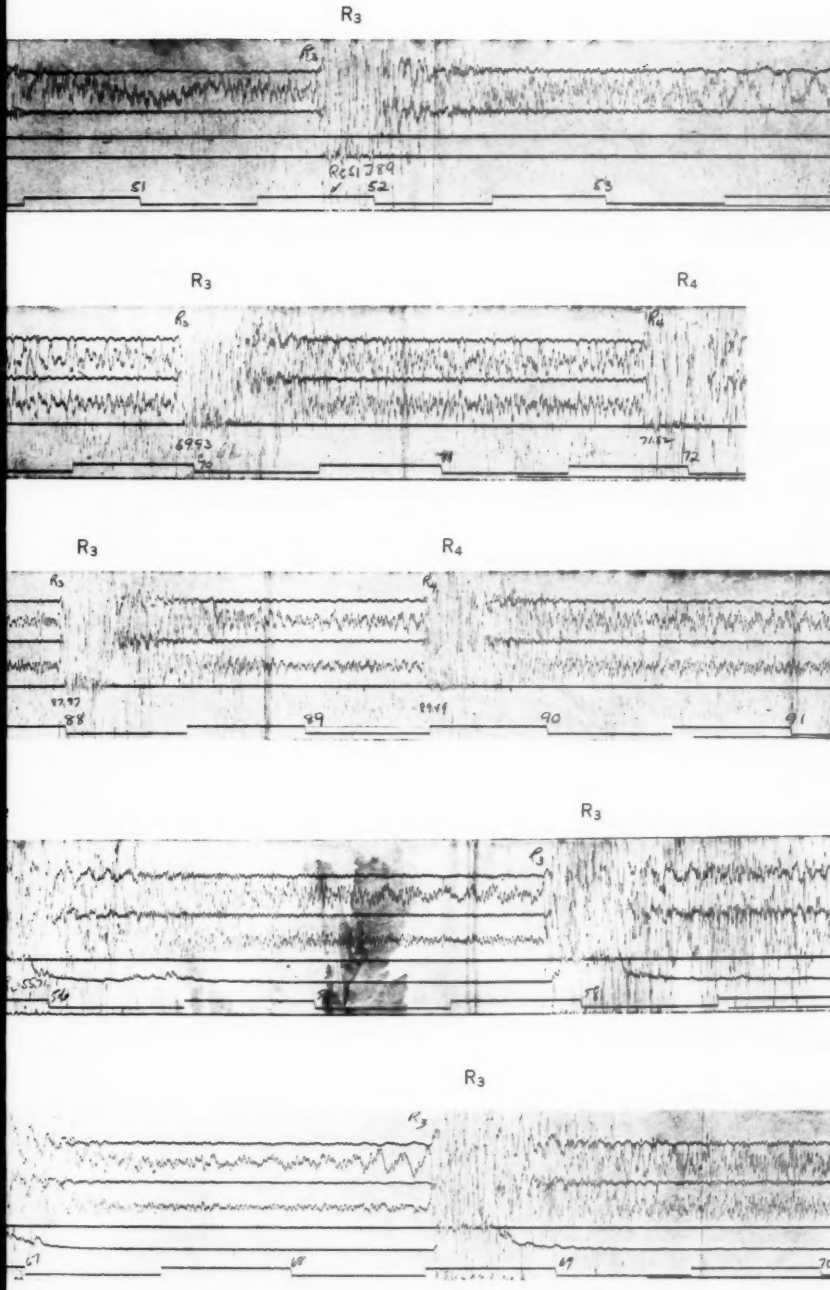

ES OF R_{1b} AND R_{2b} ARRIVALS

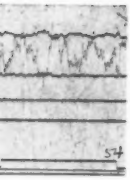
54

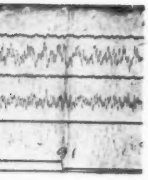
61

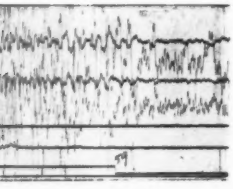
59

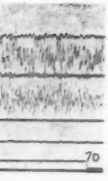
70

SHOT No. LA 182 D=13.22 sec. H_W=3005 Fm.

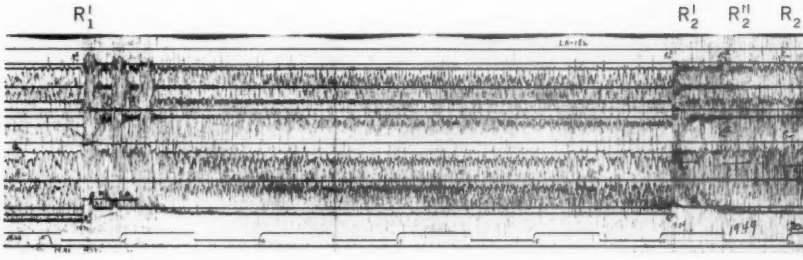

SHOT No. LA 183 D=15.75 sec. H_W=3010 Fm.

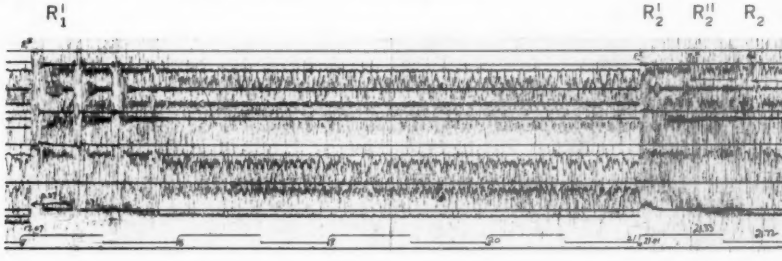

SHOT No. LA 226 D=12.46 sec. H_W=2920 Fm.

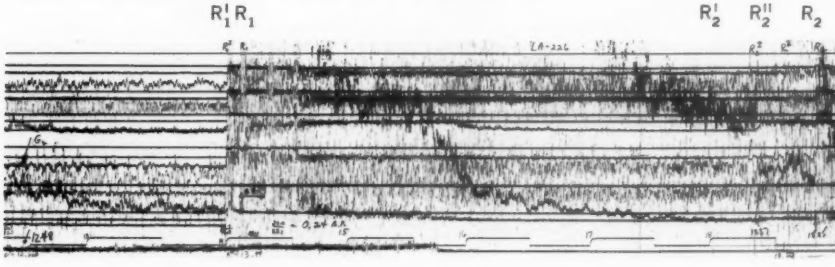

SHOT No. LA 325 D=5.96 H_W=2910 Fm.

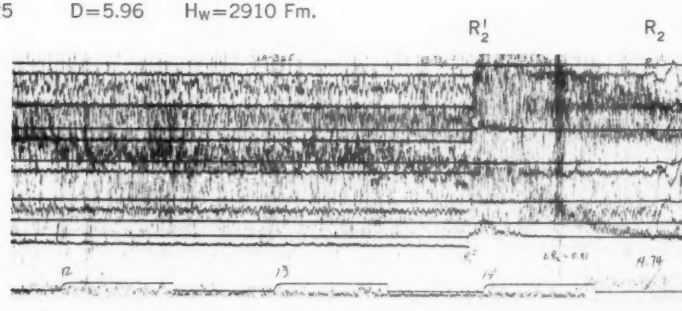

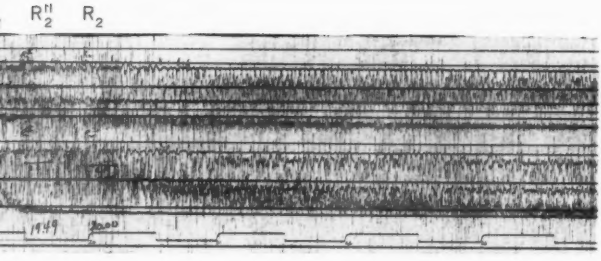

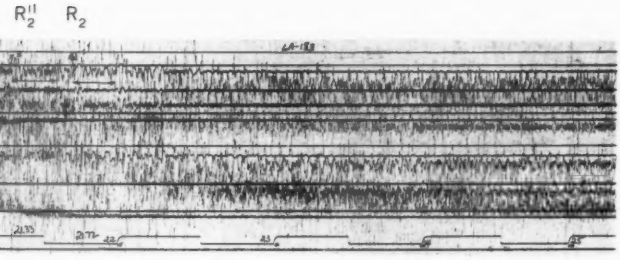

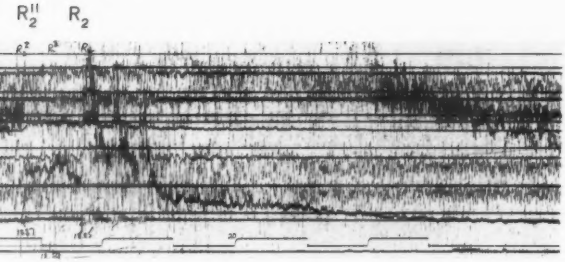

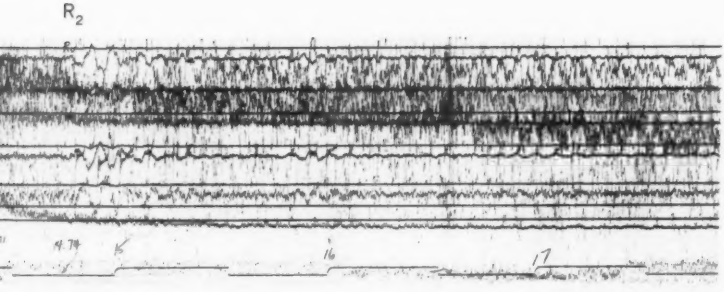

SHOT No. A

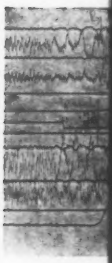

SHOT No. A

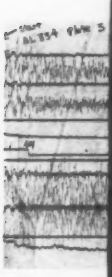

SHOT No. A

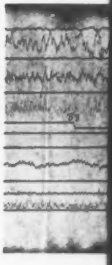

SHOT No. AL-333 D=35.04 sec.

R_3

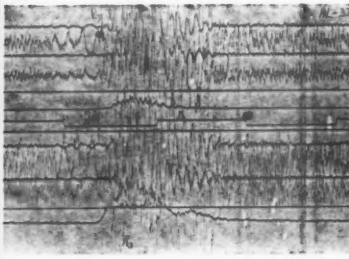

SHOT No. AL-334 D=39.85 sec.

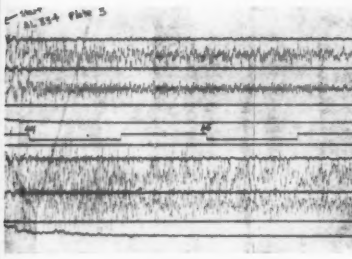

SHOT No. AL-161 D=76.98 sec.

R_7

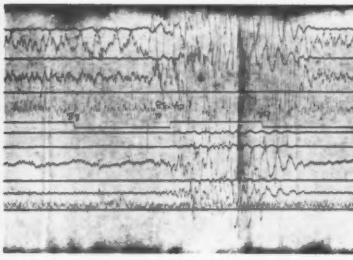

R AND SUB-BOTTOM REFLECTIONS

35.04 sec. H_W=2505 Fm.

R_4

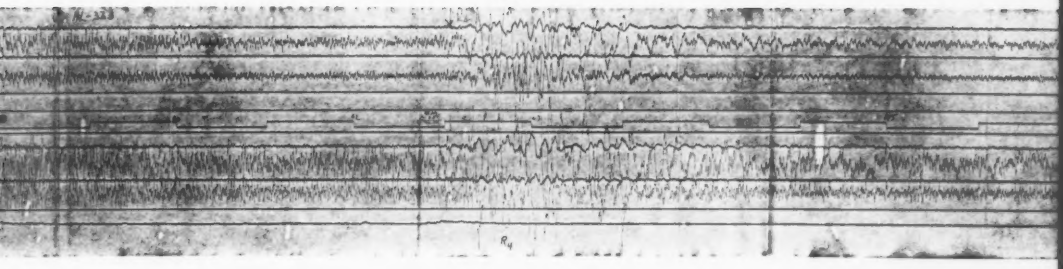

39.85 sec. H_W=2475 Fm.

R_4 R_5

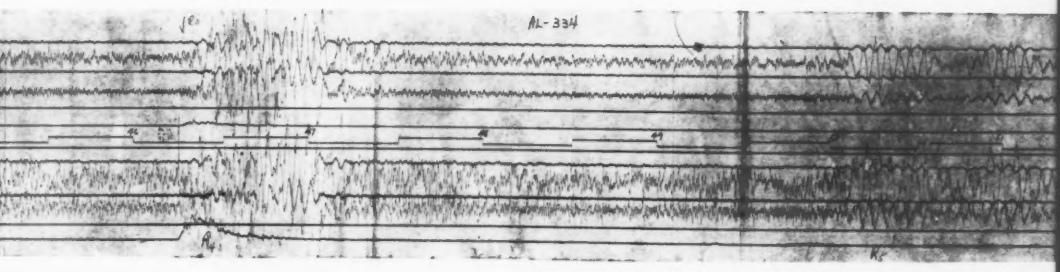

46.98 sec. H=2430 Fm.

R_8

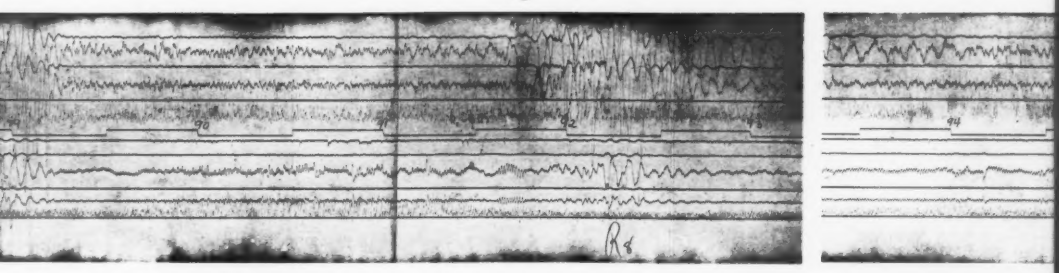

ECTIONS

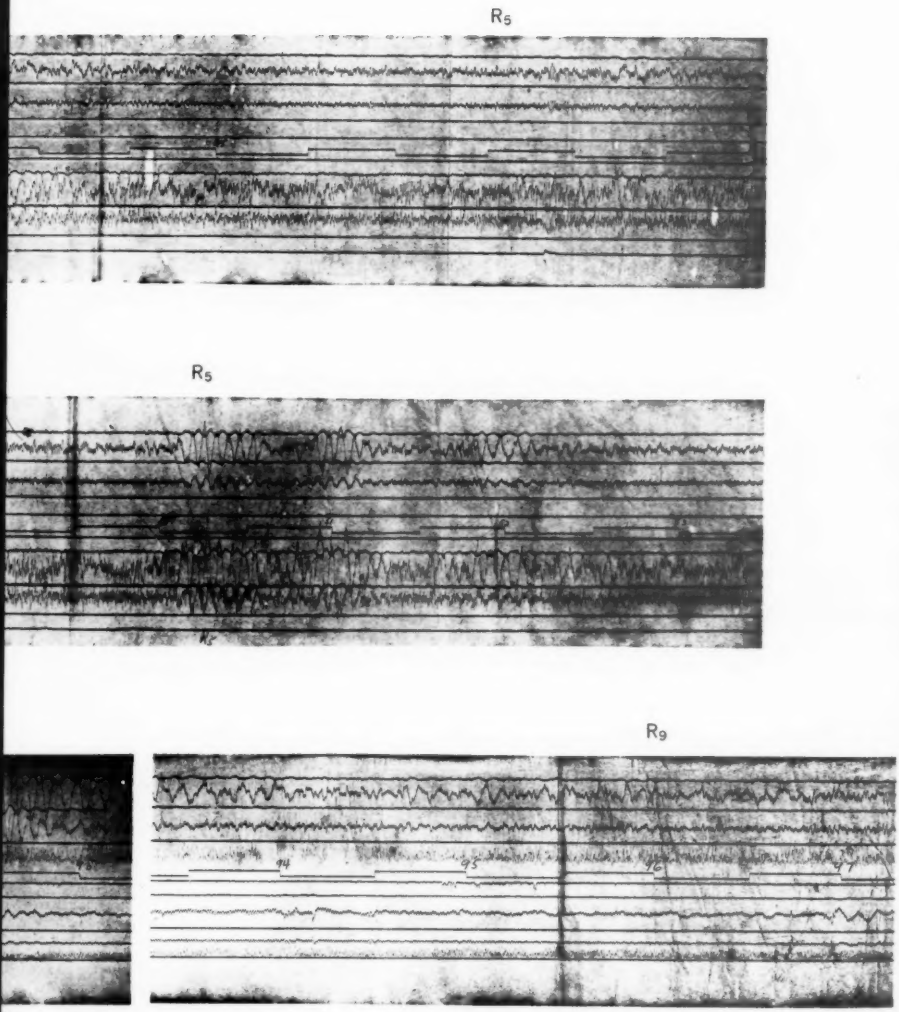

TRAVEL TIME IN SECONDS

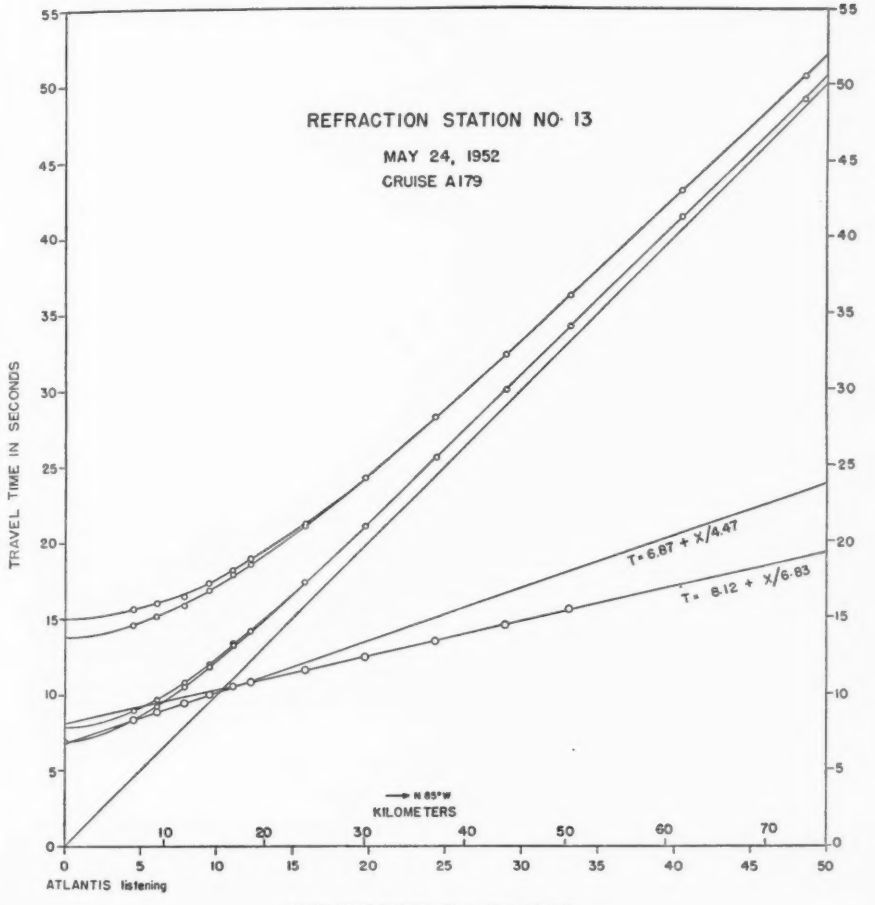

FIGURE 22.—REFRACTION STATION A179-13

some energy is trapped by successive refraction and reflection with rays becoming horizontal within the sound channel at the lowest point of their trajectory. This is the direct wave. Remaining energy is refracted downward, returning to the surface as the once-reflected ray out to a distance of about 59 km in a depth of 2600 fms. Entirely water borne the spectrum of the once-reflected arrival is relatively rich in high-frequency components (greater than 200 cps). Beyond this distance a high-frequency arrival corresponding to the once-reflected ray and similar to it appears with a velocity equal to that in the surface sound channel and is called R_{1s}. The constant-frequency arrival described above appearing at these greater distances with a velocity close to that at the ocean bottom (Matthews, 1939) is called R_{1b} (Fig. 29). The same effect is observed in R_2 at approximately twice the distance.

Data for this arrival appear in Table 5. Following Hersey $R_{1s} - R_{1b}$ is plotted as a function of R_{1s} in Figure 29. Because of the shallow-surface sound channel on A179-7B no R_{1s} is observed beyond 64 seconds. Let the travel time of the longest R_1 predicted by ray theory be R_{1m}, c_o the mean surface-channel sound velocity, and c_b the average velocity

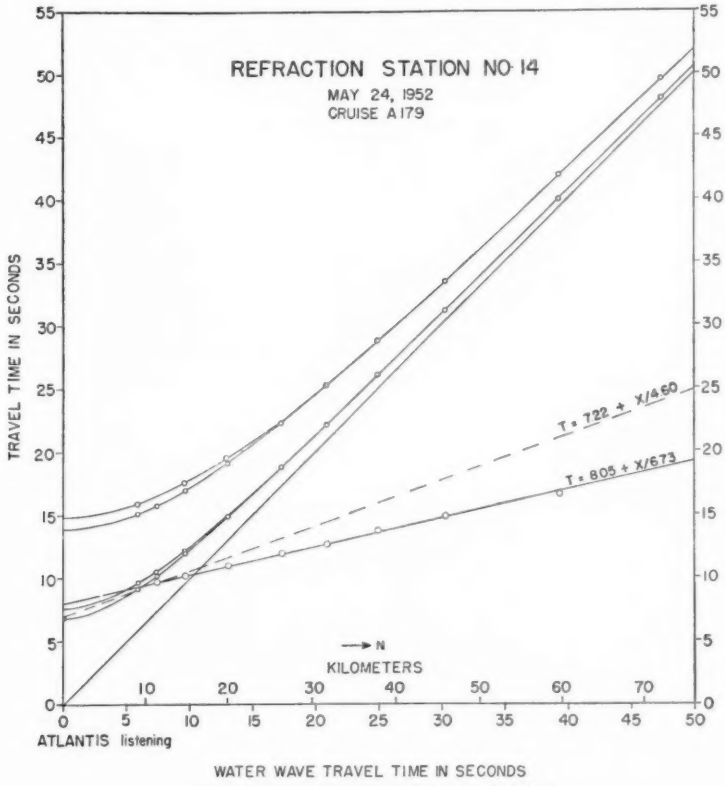

FIGURE 23.—REFRACTION STATION A179-14

near the ocean floor. R_{1m} depends on the velocity structure in the ocean, as well as shot and hydrophone depths. Since total horizontal distances for the two paths are equal,

$$(R_{1s} - R_{1m})c_o = (R_{1b} - R_{1m})c_b ,$$

or

$$R_{1s} - R_{1b} = R_{1s}(1 - c_o/c_b) + R_{1m}(c_o/c_b - 1). \quad (2)$$

Thus slopes in Figure 29 are given by $1 - c_o/c_b$, while intercepts on the abscissa, obtained by setting $R_{1s} = R_{1b}$, are R_{1m}. There are two groups of points; one group includes data from stations A179-5, 6, and 7, and is lower than the second group, which contains data from stations A179-9, 11, 13, and 15. From Table 5 it is evident that each station in the first group is in water with a higher surface sound velocity and a smaller depth than those in the second group (except A179-15). Table 6 shows mean surface sound velocities from bathythermograph data, bottom sound velocities obtained from the British Admiralty Tables for measured depths, and their ratio. The mean of Stations 5, 6, and 7 is 0.993, while that of Stations 9, 11, and 13 is 0.983; this compares well with values obtained from the curves of Figure 29, 0.993 and 0.985. The good agreement between bottom sound velocity determined from measured depth and the British Admiralty Tables and from the above analysis is evidence that the portion of the path of R_{1b} which determines its apparent velocity must lie near the ocean floor. The depth at Station A179-15 is too shallow to include it in the second group, and the surface sound velocity is too low to include it in the first group.

For the first group R_{1m} is 45.8 seconds; for the second group R_{1m} is 42.6 seconds, which compares well with the travel time of the

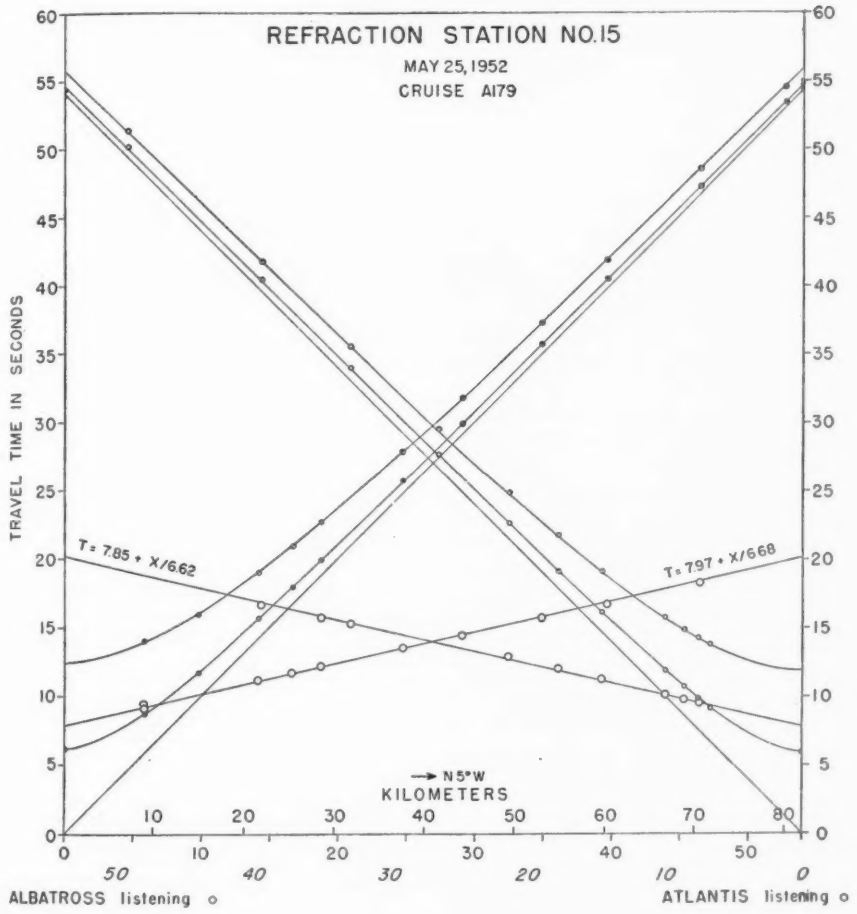

FIGURE 24.—REFRACTION STATION A179-15

limiting R_1 ray, 41 seconds. This agreement is additional evidence for the interpretation of R_{1b} given above and first presented by Hersey *et al.* (1952).

The constant-frequency character of R_{1b} suggests a resonant seismic structure near the ocean floor. Several velocity structures may generate such a constant frequency signal. The sound-velocity gradient may reverse in the water near the ocean floor; however there is no evidence available for this. The mean sound velocity for a depth of about 50 feet in the bottom sediments may be slightly lower than in the directly overlying water. There is some evidence for such a low-velocity bottom in shallow water. Ide *et al.* (1943) found a low sound velocity in sediments in summer. Ousterhoudt (1946) reports a velocity of 3800 feet per second for 1500 feet of sediments in the Gulf of Mexico. Laboratory measurements (G. H. Sutton, private communication) in cores of ocean bottom sediments give many values less than sound velocity in sea water, with a few values as low as 1.45 km/sec.

One velocity structure in accord with this evidence and with the required frequency-

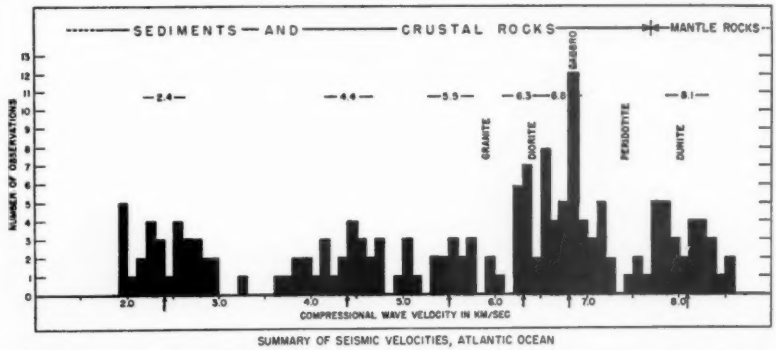

FIGURE 25.—FREQUENCY DIAGRAM OF SEISMIC VELOCITIES, ATLANTIC OCEAN. DEPTHS EXCEEDING 1000 FMS

selective property consists of a three-layer structure with water underlain by two types of sediments (Fig. 26).

The general dispersion equation for a three-layered liquid half space was first given by Pekeris (1948) and later by Press and Ewing (1948) for a low-velocity bottom. The dispersion equation for this simple model may be obtained either from Pekeris' or from Press and Ewing's result by letting the thickness of the top layer increase indefinitely. For the normal modes of this system the phase velocity must be less than c_b; otherwise energy would leak from the c_b–c_2 interface. Let

d_b, c_b = water density and sound velocity at the bottom
d_2, c_2 = desnity, mean sound velocity in low-velocity sediments
d_3, c_3 = density, sound velocity in underlying layer
$s_b = (1 - (c/c_b)^2)^{1/2}$
$s_2 = ((c/c_2)^2 - 1)^{1/2}$
$s_3 = (1 - (c/c_3)^2)^{1/2}$
h = thickness of low-velocity sediments
c = phase velocity
f = frequency
$k = 2\pi f/c$

The dispersion equation for $c_b > c_2$ becomes

$$\tan khs_2 = \frac{d_b s_2 s_3/d_3 + s_b s_2}{d_b s_2^2/d_2 - d_2 s_b s_3/d_3} \qquad (3)$$

For the R_{1b} arrival, $c \to c_b$, for which Equation (3) reduces to

$$\tan khs_2 = d_2 s_3/d_3 s_2 \text{, with } c = c_b \text{,} \qquad (4)$$

giving the thickness of the low-velocity layer as an implicit function of the observed frequency and the various velocities. Physically Equation (4) expresses the condition for constructive interference between the ray totally reflected by the c_3–c_3 boundary and incident at the critical angle on the c_b–c_2 boundary, and the RSR ray tangent to the ocean bottom (Fig. 27). Equation (4) may also be obtained directly from the condition of constructive interference and the phase shifts at the two

TABLE 4.—WAVE VELOCITIES

Rock type	σ	In idealized rock types*					
		5 km		15 km		35 km	
		V_p	V_s	V_p	V_s	V_p	V_s
Syenite	0.26	5.9	3.4	6.1	3.5	6.4	3.6
Granite H	0.22	5.8	3.5	5.9	3.6	6.2	3.7
Quartz diorite	0.25	6.0	3.5	6.1	3.6	6.4	3.7
Diorite	0.26	6.4	3.6	6.5	3.7	6.8	3.9
Gabbro	0.27	6.8	3.8	6.9	3.9	7.2	4.0
Peridotite	0.27	7.4	4.2	7.5	4.2	7.7	4.3
Dunite	0.27	7.9	4.5	8.1	4.5	8.2	4.6

Measured compressional wave velocities†
(Hughes et al, 1950 and 1951)

Rock	Temp °C	Depth km	Vel km/sec
Granite	25	.33	5.88
	300	6.1	6.23
Norite	32	.13	6.18
	152	4.0	6.83
Dunite	24.5	.33	8.60
	300	9.4	8.70

* Adams (1951, p. *74*)
† Hughes *et al.* (1950, p. *849;* 1951, p. *592*)

boundaries. The dispersion curve for the system shows that the group velocity is smaller than and approaches the phase velocity as $c \to c_b$.

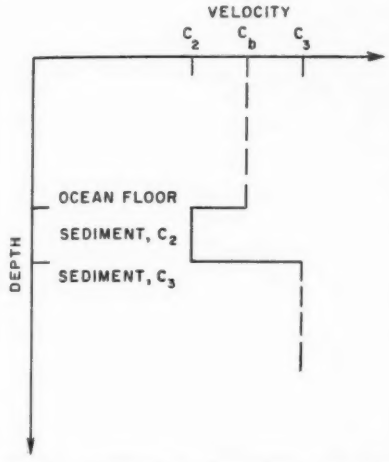

FIGURE 26.—VELOCITY STRUCTURE FOR LOW VELOCITY BOTTOM

c_1/c_2	c_2/c_b	d_2/d_1	h, meters	
			100 cps	30 cps
1.05	1.05	1.05	5.5	18.4
1.05	1.10	1.10	5.1	16.9
1.02	1.25	1.05	15.1	50.3

Layer thickness from R_{1b}

The table shows values of h for several velocity ratios and for 30 and 100 cps, between which all but one observed frequency fell. The range of h is from 5 to 50 meters. In the absence of other data on sediment velocity the thickness of this low-velocity layer cannot be further determined.

REFLECTIONS

Reflections from Ocean Floor

Reflections up to fourth order have been reported by Ewing *et al.* (1950) and Officer *et al.* (1952), and up to fifth order by Dyk and Swainson (1953). If R_n is the travel time of the nth reflection and D the travel time of the direct water wave,

$$R_n^2 = aD^2 + b \tag{5}$$

where a and b are constants. This linear relationship verified the identification of the direct and bottom-reflected sound arrivals.

In the eastern Atlantic approximately 400 km southwest of Ireland (47°40′ N., 13°40′ W., 2540 fms) Hill (1952) observed arrivals following the direct sound which did not fall along reflection curves predicted for $c_s = c_o$; the reflections arrived later than predicted the higher their order. Hill interpreted these arrivals as refractions from within a sea floor with a velocity gradient extending over several thousand feet. On all stations in the western Atlantic Ocean described in this paper, on which both direct and reflected sound were recorded, Equation (5) holds, indicating an appreciable velocity increase at or slightly beneath the ocean floor. A thin low-velocity layer would not affect this conclusion provided there were a reflector below.

Hill found that the number of refractions was limited and depended upon shot distance; he explained this observation by a velocity gradient in the ocean bottom. Rays entering the sea floor at an angle less than a minimum determined by the velocity gradient cannot return to the ocean surface. Higher-order rays enter the ocean floor at an angle less than this minimum. The velocity contrast established by Equation (5) however, suggests the number of reflections is limited by the dependence of reflected-sound amplitude on the angle of incidence. Dyk and Swainson (1953), found higher-order reflections absent at short distances and attributed this to reflection at an angle smaller than the critical angle. In one shot they observed four reflections at 37.5 km and found a velocity of 1.580 km/sec.

Rayleigh (1896) showed that for nonrigid, compressible media the reflection coefficient for plane waves incident at angle θ_n upon a boundary between two media with densities and sound velocities d_1, c_1 and d_2, c_2 is

$$K_n = \frac{d_2c_2/d_1c_1 - (1 + \tan^2\theta_n(1 - c_2^2/c_1^2))^{\frac{1}{2}}}{d_2c_2/d_1c_1 + (1 + \tan^2\theta_n(1 - c_2^2/c_1^2))^{\frac{1}{2}}} \tag{6}$$

TABLE 5.—SUMMARY OF DATA ON R_{1b}

Station	Water depth km	Shot no.	Charge size pounds	Distance seconds	Travel time seconds		Frequency cps	Mean frequency cps
					R_{1b}	R_{1a}-R_{1b}		
A179-5	4.77	LA-93	92	50.77	51.75	0.05	83	75.5
		AL-97	100	53.59	54.55	0.08	68	
-6	4.61	AL-126	100	52.73	53.83	0.02	37	37
-7	4.49	AL-157	100	49.02	49.70	0.015	30	34.4
		AL-158	100	54.89	55.54	0.04	35	
		AL-159	100	61.24	61.91	0.13	31	
		AL-160	100	68.18	68.89	0.16	39	
		AL-161	100	76.98	77.67	0.19	33	
		AL-162	50	85.64	86.42	R_{1a} not obs.	36	
		LA-168	46½	64.50	65.04	R_{1a} not obs.	33	
		LA-167	46½	70.59	71.10	R_{1a} not obs.	33	
		LA-166	92	83.01	83.46	R_{1a} not obs.	36	
		LA-165	92	92.58	93.10	R_{1a} not obs.	36	
		LA-164	92	99.13	99.63	R_{1a} not obs.	36	
-9	5.27	AL-214	100	49.84	50.48	0.14	51	54.0
		AL-215	100	58.91	59.66	0.25	57	
		LA-216	94	57.68	58.38	0.25	60	
		LA-217	94	48.55	49.08	0.09	48	
-11	5.24	AL-268	100	54.45	54.86	0.19	67	67.2
[illegible]		AL-269	100	65.88	66.16	0.33	69	
[illegible]		LA-270	94	62.67	62.97	0.33	60	
[illegible]		LA-271	94	49.22	49.72	0.11	73	
-13	5.18	LA-315	94	48.26	49.07	0.045	166	166
-15	4.56	AL-335	50	46.68	47.26	0.05	87	86.6
		AL-336	100	52.91	53.42	0.07	94	
		LA-337	94	49.55	50.22	0.045	79	
A172-4B	4.57	AC-47	50	47.8	49	.....	75	75
-5A	4.75	AC-64	100	43.5	44.7	.....	87	87
-18A	5.71	AC-256	300	55.72	56.89	.....	29	29
-19B	5.32	AC-280	300	60.57	61.15	.....	37	38.2
	5.36	AC-281	100	47.51	48.40	.....	37.5	
	5.30	AC-282	50	43.92	44.11	.....	40	
-20B	4.85	AC-304	300	57.29	57.79	.....	42	46
	4.84	AC-303	300	67.81	68.71	.....	50	

Equation (6) plotted for several values of d_2/d_1 and c_2/c_1 is shown in Figure 30. The reflection coefficient decreases rapidly from unity for angles less than critical. This decrease becomes abrupt for n reflections, the reflection coefficient being K^n.

Assuming the number of reflections on a given record is determined by the critical angle of reflection and that ray curvature is negligible, a simple analysis makes it possible to find the approximate value of sound velocity beneath the reflector. Let H_w be the water depth, n the number of observed reflections, c_v the mean vertical sound velocity, c_m the sound velocity beneath the reflector, and D the travel time of direct sound in seconds for a record on which no more than n reflections appear. Assuming the nth reflection incident at the critical angle and the straight ray approximation,

$$c_m = c_v \sqrt{1 + \left(\frac{2H_w}{c_v} \cdot \frac{c_v}{c_o} \cdot \frac{n}{D}\right)^2} \qquad (7)$$

Each quantity in parentheses can be obtained directly from shot and receiving data. Determination of distance (c_oD) at which the angle of reflection equals the critical angle is limited only by shot spacing. Neglecting curva-

ture of reflected rays is justified for the angles of incidence involved here. No velocity information can be obtained in areas of rough topography, since even the first order is complicated.

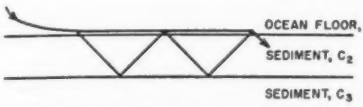

FIGURE 27.—RAY PATH, NORMAL-MODE PROPAGATION, LOW VELOCITY BOTTOM

crete frequencies in the reflected arrivals. A layer of thickness H, sound velocity c_2, and density d_2 underlying sediments with c_1, d_1, and overlying sediments or rocks with c_3, d_3, would re-enforce normally incident, plane sound waves at a frequency $f = nc_2/2H$, $n = 1, 2, 3..$, provided $c_3d_3 > c_2d_2 > c_1d_1$. If $c_1d_1 > c_2d_2$ or $c_3d_3 > c_2d_2$, constructive interference would take place for $f = c_2/4H\ (2n - 1)$, $n = 1, 2, 3...$ For $H = 50$ feet and $c_2 = 6000$ fps, a 60 cps signal would be reflected in the first

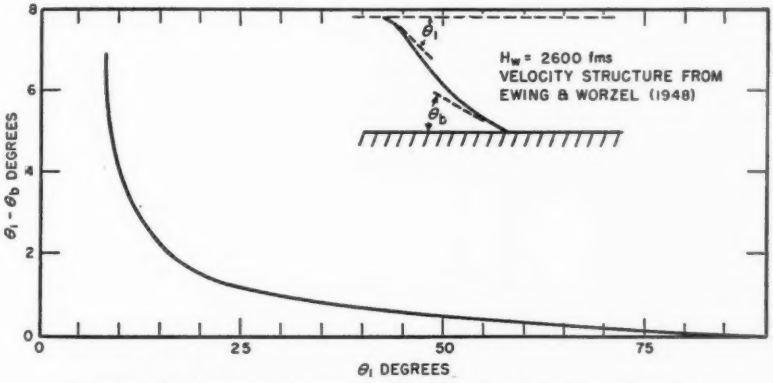

FIGURE 28.—ANGLE OF INCIDENCE FOR OCEAN WITH VELOCITY GRADIENT

While in usual refraction operations recording is stopped after one or two reflections, in the present work particular attention was given to recording all higher-order reflections. On many stations the decrease in amplitude of successive reflections can be understood in terms of Figure 30, often exceeding 40 db beyond the highest-order recorded reflection, as shown by shots AL-333, AL-334, and AL-161 (Pl. 3).

At other stations low-frequency components (less than 40 cps) persist for one more reflection than high-frequency components (greater than 200 cps), and the last clear reflection has a constant frequency in the range of 8 to 40 cps. At these stations the velocity deduced from high-frequency components falls within the range observed at neighboring stations. Persistence of low frequencies is attributed to the presence of an additional reflector at such a depth that it influences only longer waves and produces constructive interference of dis-

case and a 30 cps signal in the second case, as well as higher harmonics. Such layering may be expected from lava flows and from sediments deposited by turbidity currents.

Other possible frequency-selective mechanisms include a rough sea surface, which would discriminate against high-frequency components, and partial penetration of sound on reflection, which would absorb high-frequency components selectively. These two mechanisms do not explain the sinusoidal single-frequency character of high-order reflections. Furthermore when reflections studied in this paper were observed the sea roughness was 0 or 1, so for frequencies less than about 500 cps the sea surface should be an efficient reflector.

In Table 7 are listed the shots, charge sizes, number of reflections, and sound velocity beneath the ocean floor calculated by Equation (7). The number of reflections is relatively independent of charge size; a 10-fold increase

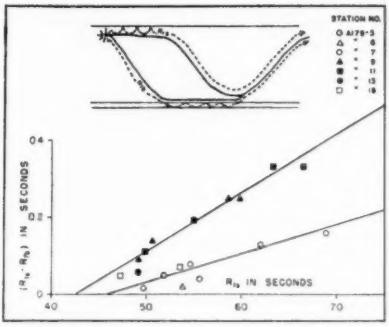

FIGURE 29.—TRAVEL TIMES OF R_{1a} AND R_{1b}

diminishing in amplitude, following the high-frequency beginning of the second reflection. Although these are among the best records, photographically, many records displayed the same features. Whenever such distinct arrivals were observed and could be distinguished from bubble-pulse arrivals, they were plotted on the travel-time curves of Figs. 14–24 and appear directly above the first and second reflection curves.

Similar arrivals were observed by Officer *et al.* (1952) who identified them as wide-angle reflections which had penetrated the bottom. Prior to the present work the limited dynamic range of the seismic equipment and the large charges chosen to obtain refraction data resulted in poor reflection data.

TABLE 6.—COMPARISON OF RATIO OF SURFACE TO BOTTOM SOUND VELOCITY FROM TWO DIFFERENT METHODS

Station	Water depth km	Mean near-surface sound vel. c_b* km/sec	Bottom sound vel. c_0† km/sec	c_0/c_b	c_0/c_b, av.	c_0/c_b**
A179-5	4.77	1.527	1.540	.9916		
A179-6	4.61	1.527	1.537	.9935	0.993	0.993
A179-7	4.49	1.526	1.535	.9941		
A179-9	5.27	1.523	1.549	.9832		
A179-11	5.24	1.520	1.549	.9813	0.983	0.985
A179-13	5.18	1.522	1.547	.9838		
A179-15	4.56	1.519	1.536	.9889	....	....

* Bathythermograph Data
† British Admiralty Tables (Matthews, 1939)
** Figure 29 and Equation 2

produces no increase in number of reflections. Sound velocities obtained from the highest-order reflection are remarkably constant for a given station.

Sub-bottom Reflections

On many refraction stations clear arrivals follow the high-frequency beginning of the first and second reflections (Pl. 3). Records from shots LA-182 and LA-183 show the second reflection from the ocean floor (R_2^I) followed by two distinct, low-frequency arrivals (R_2^{II} and R_2), each accompanied by the first bubble pulse. The record from shot LA-226 shows both a high-frequency arrival following the first reflection (R_1^I), and low-frequency arrivals (R_2^{II} and R_2) following the second reflection (R_2^I). The record from shot LA-325, at closer range, shows a series of low-frequency arrivals approximately equally spaced and

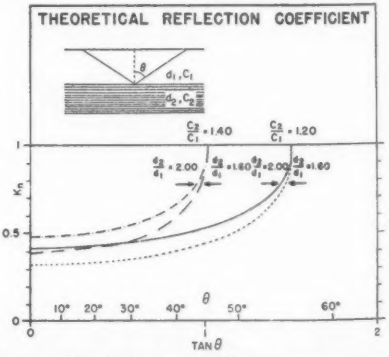

FIGURE 30.—REFLECTION COEFFICIENT VERSUS INCIDENT ANGLE FOR VARIOUS VELOCITY AND DENSITY CONTRASTS

TABLE 7.—SEDIMENT VELOCITY FROM CRITICAL ANGLE REFLECTIONS

Station	Charge size lbs.	Distance seconds	Number of reflections n	Velocity km/sec	Mean velocity km/sec
6	22½	40.49	4	1.78	
	22½	44.18	4	1.74	1.75
	96	44.39	4	1.74	
7	100	40.21	4	1.78	
	6½	45.28	4	1.73	
	100	54.89	6	1.83	
	94	49.02	5	1.79	
	100	76.98	8	1.80	
	100	68.18	7	1.80	
	24½	30.68	3	1.74	1.78
	24½	38.61	4	1.77	
	24½	45.74	5	1.80	
	48½	70.59	7	1.76	
	100	83.01	8	1.75	
9	22½	35.33	5	2.12	
	94	48.23	7	2.15	2.21
	100	49.70	6	2.05	
	12½	23.51	4	2.38	
	6½	18.32	3	2.33	
10	94	53.16	6	1.92	1.97
	100	38.81	5	2.02	
11	100	65.89	8	2.00	
	50	33.31	5	2.20	
	100	54.56	7	2.04	2.08
	100	62.67	8	2.04	
	94	49.22	7	2.14	
12	94	46.96	5	1.90	
	22½	22.32	4	2.44	2.12
	94	40.45	5	2.01	
13	94	40.49	5	1.99	1.99
15	22½	35.04	4	1.86	
	50	46.68	5	1.82	1.84

For interpreting these reflections, consider the ocean of depth H_1 and mean vertical sound velocity c_v, underlain by horizontal sediments with mean sound velocity c_m and thickness H_2. Let R_n and R_{nr} be the travel times of the high-frequency, impulsive beginning of the nth order reflection, and of the following lower-frequency sub-bottom reflections, respectively, observed at shot distance D. Let θ be the angle of incidence on the ocean floor, and θ_m the angle of refraction into the sediments. From Figure 31 it is not difficult to derive the following nondimensional relationships:

$$\frac{c_v}{2nH_1}(R_{nr} - R_n) = \sec\theta + \frac{H_2}{H_1}\cdot\frac{c_v}{c_m}\sec\theta_m - \left[1 + \left(\frac{D}{2nH_1}\right)^2\right]^{\frac{1}{2}} \tag{8}$$

$$\frac{D}{2nH_1} = \tan\theta + \frac{H_2}{H_1}\tan\theta_m \tag{9}$$

$$\sin\theta_m = \frac{c_m}{c_v}\sin\theta \tag{10}$$

In these derivations straight rays are assumed, both in the ocean and in the sediments (Fig. 28). The curves of Fig. 31, prepared from Equations (8)–(10), give the relationship between $R_{nr}-R_n$ and D, in nondimensional form for various values of H_1/H_2 and c_m/c_v. As they are independent of water depth and mean vertical sound velocity, they are universal curves which may be fitted to data of any station. For data presented here one unit along the ordinate corresponds to about $0.13n$ seconds, and one unit along the abscissa to a horizontal distance of about 7.5 km.

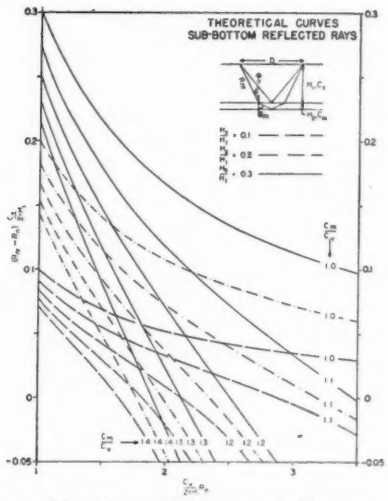

FIGURE 31.—UNIVERSAL CURVES FOR BOTTOM AND SUB-BOTTOM REFLECTION ARRIVALS FOR TWO CONSTANT VELOCITY LAYERS

Figure 31 providing the best fit appear in Figure 33. Table 8 lists water depths; mean vertical sound velocity (c_v); estimated range of H_2/H_1 and c_m/c_v from Figures 31 and 33; and sediment velocity and thickness calculated from (1) sub-bottom reflection hypothesis, (2) refraction data and reflections and (3) data of Hersey and Ewing (1949), using their nearest stations and a mean sediment velocity of 1.9 km/sec. Velocities from sub-bottom reflections used in the refraction calculations fall within the range predicted by sub-bottom reflections in five of the stations, but are low by 10 per cent on A179-7 and high by 20 per cent on A179-11. Thickness range from sub-botton reflections agrees with Hersey and Ewing's results on three stations (A179-8, 9, 11). It is less than refraction results on all but two stations (A179-13, 14). This is in agreement with unpublished data on many vertical reflection measurements in the North Atlantic

TABLE 8.—SEDIMENT VELOCITY AND THICKNESS FROM SUB-BOTTOM REFLECTIONS

Station No.	Water depth km	c_v km/sec	H_2/H_1*	Sediment thickness* km	Sediment thickness† km	c_m/c_v*	Sediment velocity* km/sec	Sediment velocity† km/sec	Sediment thickness** km
A179-6	4.61	1.51	.25–.35	1.2–1.6	0.75 0.97 } 1.72††	1.35–1.45	2.0–2.2	1.76 2.26 } 2.01††	0.3
A179-7	4.49	1.52	.4–.5	1.8–2.2	1.54 .83 } 2.36††	1.35–1.45	2.1–2.2	1.79 2.38 } 1.96††	0.3
A179-8	5.43	1.52	.1–.12	.5– .7	1.65	1.1–1.3	1.7–2.0	1.88	0.5
A179-9	5.27	1.51	.08–.12	.4– .6	1.00	1.2–1.5	1.8–2.3	1.81	0.4
A179-11	5.24	1.51	.02–.05	.1– .3	0.98	1.0–1.1	1.5–1.7	2.08	0.2
A179-13	5.18	1.51	.08–.12	.4– .6	0.44	1.2–1.5	1.8–2.3	1.99	
A179-14	5.22	1.50	.08–.12	.4– .6	0.70	1.1–1.4	1.7–2.1	1.91	

* Two layer sub-bottom reflection analysis
† Refraction and critical-angle reflection data
** Hersey and Ewing (1949), with mean sediment velocity 1.9 km/sec
†† Two sedimentary layers observed on refraction station

On some shots (*e.g.*, LA-226, Pl. 3) second-order reflections consist of three approximately equally spaced arrivals. In this interpretation the first arrival is reflected at the bottom twice, the second arrival is reflected once and penetrates the bottom once, while the third arrival penetrates the bottom twice. The first of these sub-bottom reflections is plotted by doubling the time interval between its arrival and the bottom reflection.

Data for these arrivals and the curves from which usually show one or more reflections, all within the sedimentary layer.

On Stations A179-6, 7, and possibly 9, points beyond 1.8 units of the abscissa (about 19 km) are not explained by the model consisting of two layers each with a constant velocity. Figure 32 has been prepared for a two-layer model, with a velocity gradient and with and without a velocity contrast in the lower layer, using formulas analogous to Equations (8)–(10). Each curve has two branches, corre-

sponding to two rays emerging from the source at different angles and requiring different travel times for the same horizontal distance. On several stations the upper curves can be

velocities of 7.68 to 8.50 km/sec at 9.4 to 13.4 km below sea level. Under the northeast American continent the velocity of near-surface rocks is close to 6.0 km/sec and may increase

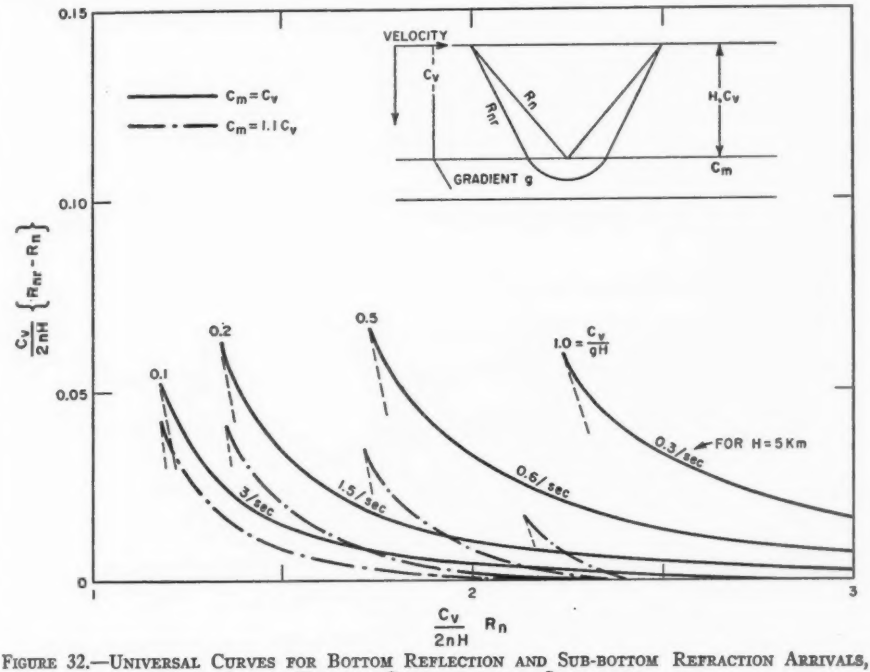

FIGURE 32.—UNIVERSAL CURVES FOR BOTTOM REFLECTION AND SUB-BOTTOM REFRACTION ARRIVALS, LINEAR VELOCITY GRADIENT IN THE SEDIMENTS

made to fit the points beyond 1.8 units for velocity contrasts of 0 to 10 per cent and velocity contrasts of about 0.6/sec, implying an increase from about 1.6 to 2.2 km/sec, at the base of 1 km of sediments.

CONCLUSIONS

The data provide a fairly closely spaced network of refraction and reflection measurements. Salient features of these measurements are:

(1) On the 21 deep-water stations of this paper (mean depth 4.9 km), mean sediment thickness is 1.3 km. Crustal rocks underlying this thin sedimentary layer have a mean thickness of 5.1 km and velocities as high as 7.1 km/sec. Arrivals from the mantle were observed on only five of the longer stations with

with depth to near 7.0 km/sec at about 35 km, with the mantle (velocity exceeding 7.7 km/sec) below. The upper continental crust (6.0–6.3 km/sec) thins seaward and disappears near the foot of the continental slope. Exclusive of the water column, this oceanic crust is less than one-fifth as thick as the continental crust.

(2) Toward Bermuda the mean crustal velocity decreases; observed values range from 5.6 to 6.5 km/sec. This decrease may be associated with the structure of the Bermuda volcanoes. In several areas near Bermuda velocities near 4.5 km/sec (volcanics and other consolidated sediments) are observed.

(3) The outer ridge of the Blake-Bahama Basin was crossed in three areas in each of which a layer with a mean thickness of 1.3 km and mean velocity of 2.4 km/sec was observed under the sediments.

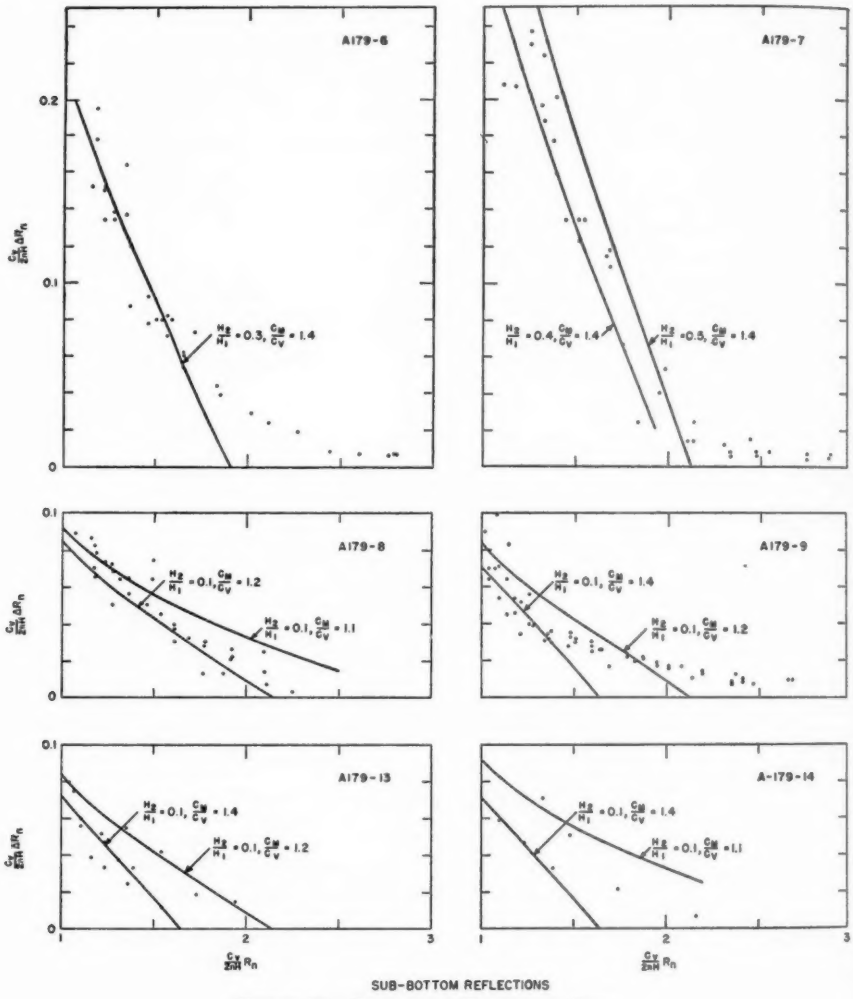

FIGURE 33.—SUB-BOTTOM REFLECTION DATA

(4) Data for a conspicuous, constant-frequency arrival, appearing at a range of 40–50 seconds (59–74 km) at the travel time of the first reflection, are presented. This arrival is interpreted as refracted along the ocean floor. A simple theory explains the constant-frequency character as normal-mode propagation within a sedimentary layer of slightly lower velocity than the overlying water and from 0 to about 150 feet thick.

(5) On many stations the amplitude of recorded reflections diminishes sharply beyond a certain order. On the basis of reflection at the critical angle sound velocity in the sediments near the ocean floor is calculated from the maximum number of recorded bottom reflections. Resulting sound velocities are remarkably constant for a given station and agree with the few available refraction measurements.

(6) Two models for interpreting sub-bottom reflections recorded on several stations are presented: two layers (ocean and sediments) each with a constant velocity of sound, and two layers with a velocity gradient in the lower layer. Resulting velocities compare with those obtained from refraction and critical-angle re-

TABLE 9.—COMPARISON OF APPROXIMATE AND EXACT DISTANCE CALCULATIONS

θ	R_1 seconds	True distance km	Estimated distance km	% error
2°	44.96	67.648	67.528	−0.18
3°	43.82	65.809	65.783	−0.04
6°	42.54	64.454	63.792	−0.08
8°	40.70	60.943	60.972	+0.05
9°	34.20	50.975	50.984	+0.02
12°	26.34	38.812	38.812	0
15°	21.84	31.730	31.755	+0.08
20°	17.12	24.137	24.207	+0.29
30°	12.06	15.675	15.710	+0.23
50°	8.00	7.728	7.729	+0.01

make it possible to calculate shot distance. When no surface sound channel exists and the direct wave is recorded only to a short distance, reflected arrivals must be used in calculating the distance. Using symbols defined above the shot distance is

$$c_0 D = \sqrt{(c_v R_1)^2 - (2H_w)^2} \qquad (11)$$

where

$$c_v = \frac{H_w}{\int_0^{H_w} \frac{dz}{c}}$$

In the derivation it is assumed that the ocean floor is an efficient reflector and that direct and reflected sound paths are straight. Because of the known velocity structure and resulting ray curvature, the latter assumption requires justification. Also values of c_0/c_v obtained by this method on each station should agree with values given for the area and depth in the British Admiralty Tables (Matthews, 1939).

Following Ewing and Worzel (1948, p. 17),

TABLE 10.—COMPARISON OF OBSERVED MEAN VERTICAL SOUND VELOCITY WITH BRITISH ADMIRALTY TABLES

Station	c_v/c_0, obs.	c_0* km/sec	c_v, km/sec	c_v, av. km/sec	Water depth km	c_v† km/sec	Error in c_v %
A179-5A	.9876	1.528	1.509	1.509	4.77	1.513	−.3
5B	.9876	1.528	1.509				
6A	.9857	1.530	1.508	1.507	4.61	1.512	−.3
6B	.9891	1.528	1.506				
7A	.9940	1.526	1.517	1.517	4.49	1.512	+.3
7B	.9940	1.525	1.516				
8A	.9945	1.526	1.518	1.520	5.43	1.517	+.2
8B	.9964	1.526	1.521				
9A	.9942	1.525	1.516	1.512	5.27	1.516	−.3
9B	.9908	1.522	1.508				
10A	.9972	1.520	1.516	1.517	5.14	1.515	+.1
10B	.9979	1.520	1.517				
11A	.9953	1.519	1.512	1.512	5.24	1.517	−.3
11B	.9940	1.520	1.511				
12A	.9989	1.519	1.517	1.516	5.27	1.515	+.1
12B	.9973	1.519	1.515				
13	.9904	1.522	1.507	1.507	5.18	1.515	−.5
14	.9913	1.518	1.505	1.505	5.22	1.515	−.6
15A	.9945	1.519	1.511	1.507	4.56	1.511	−.3
15B	.9879	1.520	1.502				

* Bathythermograph Data
† British Admiralty Tables (Matthews, 1939)

flection data. Thicknesses are usually less than those obtained from refraction data, indicating that the reflecting surface is within the sediments.

APPENDIX—CALCULATED SHOT DISTANCES

Travel time of the direct water wave through a surface sound channel and bathythermograph data obtained aboard the shooting ship

the velocity structure in the ocean may be approximated by a series of layers (thickness h_n) each with a constant sound-velocity gradient (g_n). Sound leaving a given point in a layer at an angle with the horizontal, θ_n, and incident on the lower boundary at θ_{n+1}, has traversed a vertical distance $h_{n,n+1}$, the nth layer thickness, and a horizontal distance

$$x_{n,n+1} = h_{n,n+1} \cot \frac{\theta_n + \theta_{n+1}}{2}$$

in a time

$$t_{n,n+1} = \frac{1}{g_n} (\sin h^{-1} \tan \theta_{n+1} - \sin h^{-1} \tan \theta_n),$$

where $$\theta_{n+1} = \cos^{-1} \frac{v_{n+1}}{v_n} \cos \theta_n$$

Total horizontal distance traversed by a bottom-reflected ray is

$$X = 2 \sum_{n=1}^{7} x_{n,n+1} \qquad (12)$$

in time

$$T = 2 \sum_{n=1}^{7} t_{n,n+1} \qquad (13)$$

For a given value of θ_1, X and T are obtained from Equations (12) and (13). Inserting T for R_1 in Equation (11), c_oD, the straight-ray approximation for X from Equation (12), is obtained. Results and comparison of c_oD with X are shown in Table 9. Table 10 summarizes values of c_v/c_o, c_o, and c_v computed from these data, as well as c_v given by the British Admiralty Tables. It is evident from these tables that the straight ray assumption is adequate in ocean depths near 2600 fathoms out to a distance of about 41 seconds, beyond which the effect described under R_{1b} Arrival becomes important.

References Cited

Adams, L. H., 1951, Internal constitution of the earth: Chap. IV, N. Y., Dover Pub., 2d ed., p. 50–80

Dyk, Karl, and Swainson, O. W., 1953, The velocity and ray paths of sound waves in deep sea water: Geophysics, v. 18, p. 75–103

Ewing, Maurice, Crary, A. P., and Rutherford, H. M., 1937, Geophysical investigations in the emerged and submerged Atlantic coastal plain, Pt. I, methods and results: Geol. Soc. America Bull., v. 48, p. 753–802

Ewing, Maurice, Wollard, G. P., and Vine, A. C., 1939, Geophysical investigations in the emerged and submerged Atlantic coastal plain, Pt. III, Barnegat Bay, New Jersey section: Geol. Soc. America Bull. v. 50, p. 257–296

Ewing, Maurice, and Worzel, J. L., 1948, Long-range sound transmission; *in* Worzel, J. L., Ewing, Maurice, and Pekeris, C. L.: Propagation of sound in the ocean: Geol. Soc. America Mem. 27, 205 p.

Ewing, Maurice, Worzel, J. L., Hersey, J. B., Press, Frank, and Hamilton, G. R., 1950, Seismic refraction measurements in the Atlantic Ocean basin, Pt. I: Seismol. Soc. America Bull., v. 4, p. 233–242

Ewing, Maurice, Worzel, J. L., Steenland, N. C., and Press, Frank, 1950a, Geophysical investigation in the emerged and submerged Atlantic coastal plain, Pt. V, Woods Hole, New York, and Cape May sections: Geol. Soc. America Bull., v. 61, p. 877–892

Ewing, Maurice, Sutton, G. H., and Officer, C. B., Jr., 1954, Seismic refraction measurements in the Atlantic Ocean, Pt. VI, typical deep stations, North American basin: Seismol. Soc. America Bull., v. 44, p. 21–38

Gaskell, T. F., and Swallow, J. C., 1951, Seismic refraction experiments in the North Atlantic: Nature, v. 167, p. 723

Gutenberg, Beno, 1951, Crustal layers of the continents and oceans: Geol. Soc. America Bull., v. 62, p. 427–440

Hersey, J. B., and Ewing, Maurice, 1949, Seismic reflections from beneath the ocean floor: Am. Geophys. Union Trans., v. 30, p. 5–14

Hersey, J. B., Officer, C. B., Johnson, H. R., and Bergstrom. S., 1952, Seismic refraction observations north of the Brownson Deep: Seismol. Soc. America Bull. v. 42, p. 291–306

Hill, M. N., 1952, Seismic refraction shooting in an area of the eastern Atlantic: Royal Soc. London Philos. Trans., ser. A, no. 890, v. 244, p. 561–596

Hodgson, J. H., 1953, A seismic survey in the Canadian Shield, Pt. I, Refraction studies based on rockbursts at Kirkland Lake, Ontario: Pub. Dominion Observatory, Ottawa, v. 16, p. 113–163

Hughes, D. S., and Cross, J. H., 1951, Elastic wave-velocities at high pressures and temperatures: Geophysics, v. 16, p. 577–593

Hughes, D. S., and Jones, H. J., 1950, Variation of elastic moduli of igneous rocks with pressure and temperature: Geol. Soc. America Bull., v. 61, p. 843–856

Ide, J. M., Post, R. F., and Fry, W. S., 1943, The propagation of underwater sound at low frequencies as a function of the acoustic properties of the bottom: Naval Research Lab. Rept. S-2113

Katz, Samuel, 1955, Seismic study of crustal structure in Pennsylvania and New York: Seismol. Soc. America Bull., v. 45, p. 303–326

Leet, L. D., 1941, Trial travel times for northeastern America: Seismol. Soc. America Bull., v. 31, p. 325–334

Lord Rayleigh, 1896, Theory of sound, v. II: Reprinted 1945, N. Y., Dover Pub., 504 p

Matthews, D. J., 1939, Tables of the velocity of sound in pure water and sea water for use in

echo-sounding and sound-ranging: Admiralty Hydrographic Dept., London

Officer, C. B., Ewing, Maurice, and Wuenschel, P. C., 1952, Seismic refraction measurements in the Atlantic Ocean, Pt. IV, Bermuda, Bermuda Rise, and Nares Basin: Geol. Soc. America Bull., v. 63, p. 777–808

Ousterhoudt, W. J., 1946, The seismograph discovery of an ancient Mississippi River channel: Geophysics, v. 11, p. 417

Pekeris, C. L., 1948, Theory of propagation of explosive sound in shallow water, *in* Worzel, J. L., Ewing, Maurice, and Pekeris, C. L.: Propagation of sound in the ocean: Geol. Soc. America Mem. 27, 205 p

Press, Frank, and Ewing, Maurice, 1948, Low speed layer in water-covered areas: Geophysics, v. 13, p. 404–420

Raitt, R. W., 1954, Some results of seismic studies on Capricorn Expedition (Abstract): Geol. Soc. America Bull., v. 65, p. 1348

Sutton, G. H., 1952, Three channel amplifier for use in refraction and sound measurements at sea: Lamont Geol. Observatory, Tech. Rept. 2

Tatel, H. E., Adams, L. H., and Tuve, M. A., 1953, Studies of the earth's crust from explosions: Am. Philos. Soc. Proc., v. 97, p. 658–669

Tolstoy, I., Edwards, R. S., and Ewing, M., 1953, Seismic refraction measurements in the Atlantic Ocean, Pt. 3: Seismol. Soc. America Bull., v. 43, p. 35–48

Willmore, P. L., Hales, A. L., and Gane, P. G., 1952, A seismic investigation of crustal structure in the western Transvaal: Seismol. Soc. America Bull., v. 42, p. 53–80

Worzel, J. L., and Ewing, Maurice, 1948, Explosion sounds in shallow waters, *in* Worzel, J. L., Ewing, Maurice, and Pekeris, C. L.: Propagation of sound in the ocean: Geol. Soc. America Mem. 27, 205 p

Stanford Research Institute, Menlo Park, Calif.; Lamont Geological Observatory, Columbia University, Palisades, N. Y.

Manuscript Received by the Secretary of the Society April 28, 1955

Lamont Geological Observatory Contribution No. 184.

BULLETIN OF THE GEOLOGICAL SOCIETY OF AMERICA
VOL. 67, PP. 511-534, 4 FIGS., 1 PL. APRIL 1956

GRAVITY RECONNAISSANCE SURVEY OF PUERTO RICO

BY G. LYNN SHURBET AND MAURICE EWING

ABSTRACT

Three hundred and ninety-six new gravity observations form a reconnaissance survey of Puerto Rico with an average station spacing of about 2 miles in lines approximating nine north-south profiles and four east-west profiles.

A contour map of modified Bouguer anomalies shows positive values of about 90 milligals along the northern and southern coasts, increasing to about 165 milligals in the central part of the island. Utilizing this gravity information, with gravity and seismic information at sea in the area, a north-south structure section through San Juan is deduced.

The gravity anomalies are correlated briefly with surface geologic formations. The writers compare observed gravity anomalies across one section of the north Tertiary sedimentary basin with computed anomalies using reasonable density assumptions and sedimentary thicknesses deduced from geologic evidence.

CONTENTS

TEXT

	Page
Introduction	511
Acknowledgments	512
Instrumentation	512
Calibration of Frost gravimeter	512
Method of Survey	513
Position control	513
Elevation control	513
Observed gravity	514
Comparison with previous measurements	514
Modified Bouguer anomalies	515
North-south structure section through San Juan	519
Brief correlation of gravity anomalies with surface geologic formations	524
Tertiary sedimentary basins	527
Deflection of the vertical	533
Conclusions	534
References cited	534

ILLUSTRATIONS

Figure	Page
1. Frost gravimeter calibration curve	513
2. North-south profiles of modified Bouguer anomalies	531
3. North-south structure and gravity sections through San Juan	532
4. Structure and gravity sections across northern Tertiary basin	533

Plate	Facing page
1. Contoured modified Bouguer anomalies and surface geologic formations in Puerto Rico	534

TABLES

Table	Page
1. Comparison of observed gravity values	514
2. Comparison of observed gravity values from the S-21 cruise with other values	515
3. Modified Bouguer corrections in gals	515
4. Summary of gravimeter observations in Puerto Rico	516
5. Isostatic anomalies in the Puerto Rico area	533

INTRODUCTION

The following gravity survey was undertaken in connection with a program of measuring gravity at sea initiated in 1947 (Worzel and Ewing, 1950). One purpose of this program is the investigation of the gravitational field associated with island arcs. This reconnaissance gravity survey of Puerto Rico was designed primarily to connect two profiles of gravity stations at sea extending from about 200 miles north of San Juan, Puerto Rico, to about 150 miles south of the southern coast of Puerto Rico (Worzel and Ewing, 1954).

This survey was conducted during February and March 1953. In April 1953, 30 of the 396 new stations were reoccupied to determine the scale constant of the gravimeter for the lower portion of the scale.

Before this survey, 5 gravity stations had

been established in Puerto Rico. Four pendulum gravity stations were established by the U. S. Coast and Geodetic Survey (Principal facts for gravity stations in the Bahamas and the West Indies, G-50, Part I) in San Juan, Aibonito, Ponce, and Mayaguez. One gravity station was established in San Juan Harbor by Vening Meinesz and Wright (1930, p. 56). The pendulum stations at San Juan and Mayaguez have been reoccupied by Woollard *et al.* (Unpublished manuscript).

Acknowledgments

The authors are indebted to Dr. Raoul C. Mitchell, Visiting Professor of Geology, 1952–1953, College of Agricultural and Mechanical Arts, University of Puerto Rico, and to Don Luis Stefani, Vice-Chancellor, College of Agricultural and Mechanical Arts, for making funds available from the University of Puerto Rico to cover the expense of the observer during the field work.

Dr. R. Fernandez Garcia, Director, Industrial Research Department, Economic Development Administration, Commonwealth of Puerto Rico, generously provided transportation for the observer during the field work. This transportation constituted a large portion of the expense of the survey, and the co-operation of Doctor Garcia contributed greatly to the success of this work.

Dr. Raymond J. Smith, U. S. Geological Survey, made available the detailed topographic maps of Puerto Rico and provided valuable local information. Dr. J. Lamar Worzel gave valuable advice on reducing the data and in discussion and criticism of the manuscript. Miss Annette Trefzer did the drafting.

This work was partially supported by Contract N6-onr-271 Task Order 8 with the Office of Naval Research, Department of the Navy.

Instrumentation

A gravimeter built in 1947 by the Frost Gravimeter Corporation was used in this survey. The instrument, especially designed and built for geodetic work, has a range of about 4000 mgal for a single setting of the latitude adjustment; its sensitivity is about 2.7 mgal per scale division, and its drift is less than the reading error for periods up to several days. The instrument reading is accurate to within about ±0.1 scale division.

Calibration of the Frost Gravimeter

Before this survey, the instrument was calibrated twice. Worzel first calibrated it by occupying 31 U. S. Coast and Geodetic Survey pendulum stations over a range of 500 mgal. His determination of the scale constant was 2.667 mgal per scale division. Later Ewing recalibrated the instrument by occupying 48 U. S. Coast and Geodetic Survey pendulum stations over a range of 936 mgal. The least-square solution gave the scale constant again as 2.667 mgal per scale division.

The present survey was made with the instrument set to read at the lower end of the scale where subsequent information showed the reading spring to be nonlinear, and it was necessary to reoccupy several stations to determine the corrections to be applied to the original readings for nonlinearity. On April 10, 1953, the instrument was reset at Lamont Geological Observatory from a scale reading of 750.9 to a reading of 1223.3. The instrument was flown to Puerto Rico on April 13 and 14, and on April 15 and 16, 30 of the original stations covering the entire range of scale divisions used in the original survey were reoccupied. The instrument showed zero drift from the time it was reset on April 10 until it was taken from the laboratory and from arrival in Puerto Rico until completion of the reoccupations. Drift during the transit time (about 2 days) is assumed to be zero. The portion of the reading spring used in these reoccupations is linear with a scale constant of 2.667 mgal per scale division. In Figure 1 the difference between the reading (corrected for drift) using the nonlinear portion and using the linear portion is plotted against the nonlinear reading for each of the 30 stations. The mean line drawn through these points gives the corrections to be added to the original scale readings for nonlinearity. The largest discrepancy of the points from the mean line is one value of 0.25 scale division (0.7 mgal). All other points are within 0.15 scale division (0.4 mgal) of the mean line. Point P is the

number of scale divisions the instrument was reset on April 10 plotted against 250 scale divisions, the point below which investigations show that the reading spring is nonlinear. Thus the correction has the constant value 472.4 for readings greater than 250, and the values in Figure 1 for lesser readings. The maximum error introduced by nonlinearity of the reading spring is probably less than 0.7 mgal.

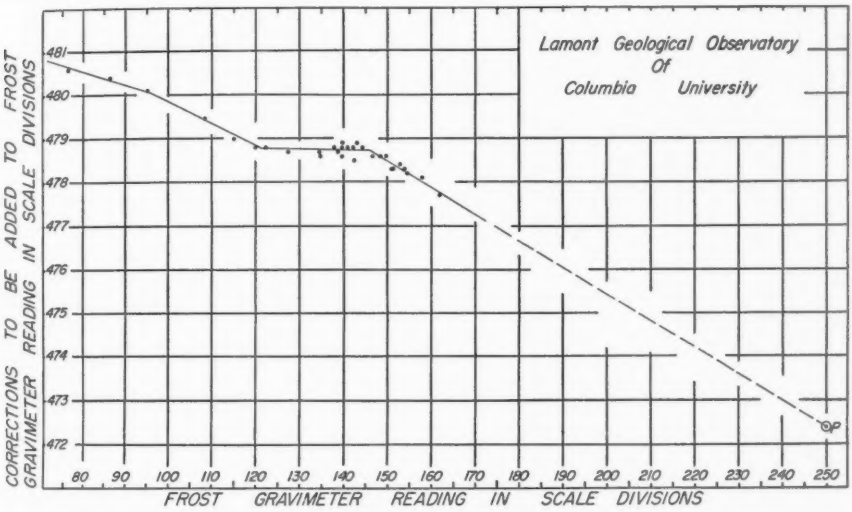

FIGURE 1.—FROST GRAVIMETER CALIBRATION CURVE

Abscissa represents nonlinear gravimeter readings. Ordinate represents linear minus nonlinear readings for 30 stations reoccupied.

METHOD OF THE SURVEY

Since the drift of the gravimeter is less than the reading error for periods up to several days, reoccupation of the base stations once a day is adequate for drift control. During the first day of field work, base stations were established in San Juan and Mayaguez. The instrument was read at one or the other of these bases every morning and at the end of each day. Reoccupations of other stations were made at convenient opportunities (about 35 occupations). The instrument showed a drift of 0.3 scale division from the time it was taken from Lamont Geological Observatory on February 15, 1953, until it was returned to the laboratory on March 30, 1953. This drift was proportioned over the entire time, and the maximum error which may be attributed to instrument drift is probably 0.3 mgal.

Most stations were located at bench marks or at road junctions, bridges, schools, etc., where accurate positions and elevations could be read from topographic maps. In most instances no attempt was made by the observer to choose station locations for which the topographic corrections would be small.

POSITION CONTROL

All stations were located on U. S. Geological Survey quadrangle sheets, scale 1:30,000, from which the positions can be read to $\pm 0.05'$. An error of $0.05'$ in latitude would introduce a negligible error of approximately 0.05 mgal in the gravity anomalies.

ELEVATION CONTROL

Elevations of all except 20 stations were taken from U. S. Coast and Geodetic Survey and U. S. Geological Survey bench marks or from elevations of road junctions, schools, etc., indicated on the quadrangle sheets. Of the 20 stations made at positions where elevations were not given, 4 were made on the road near positions of known elevation. In these cases

the difference in elevation of the station from the known elevation was estimated. The maximum error introduced into the modified Bouguer anomalies by this procedure is probably 0.5 mgal. The elevations of the remaining 16 stations were estimated from U. S. Geological Survey quadrangle sheets, scale 1:10,000, with a contour interval of 5 meters or, in a few instances, a contour interval of 1 meter. The maximum error introduced into the modified Bouguer anomalies by this procedure is probably 2 mgal.

TABLE 1.—COMPARISON OF OBSERVED GRAVITY VALUES

Station	USC & GS pendulum 1929	Vening Meinesz pendulum 1928	Woollard gravimeter 1951	LGO gravimeter 1953	Woollard-USC & GS	LGO-USC & GS
San Juan	978.674	...	978.6766	978.6790	.003	.005
Aibonito	.566	...	....	.563	..	−.003
Ponce	.626	...	....	.6314	..	.005
Mayaguez	.667	...	.6645	.6675	−.002	.001
San Juan Harbor		978.695	....	.6816	..	

OBSERVED GRAVITY

Corrections for nonlinearity of the reading spring (taken from Figure 1) and for drift were applied to all the original instrument readings. These corrected readings were used in the normal manner to compute the values of observed gravity given in Table 4, using a scale constant of 2.667 mgal per scale division and a base value of 980.1180 gals for the U. S. Coast and Geodetic Survey base in the Department of Commerce Building, Washington, D. C. Lamont Geological Observeratory Base No. 1 (980.2584 gals) served as an intermediate base. With random errors of 0.3 mgal for drift, 0.3 mgal for reading error, and 0.7 mgal for nonlinearity of the reading spring, the values of observed gravity are accurate to within 1 mgal.

COMPARISON WITH PREVIOUS MEASUREMENTS

A comparison of the values of observed gravity obtained in this survey with previous measurements is made in Table 1. A free-air correction of 4 mgal has been applied to the value given in Table 4 for the Aibonito station (169) because the reading was made 12 meters below and approximately 50 meters east of the original station.

The U. S. Coast and Geodetic Survey pendulum values, the Woollard *et al.* (Unpublished manuscript) gravimeter values, and the Vening Meinesz pendulum value have been corrected by −2, −1, and +6 mgal, respectively, to base them on the Department of Commerce Building, Washington, D. C., at the value 980.1180 gals (Duerksen, 1949, p. 3). The discrepancy of about 15 mgal between the Vening Meinesz value and the other values for San Juan is discussed.

Vening Meinesz and Wright established base stations on the S-21 cruise in the following order: Washington (D. C.), Hampton Roads (Virginia), Key West, Galveston, Key West, Morro Castle (Santiago, Cuba), Guantanamo Bay, San Juan (P. R.), St. Thomas (V. I.), Guantanamo Bay, Washington (D. C.). No information is given in the publication about reoccupations, if any, in Key West, Guantanamo Bay, or Washington. Table 2 lists all available data on the stations. The Vening Meinesz, USS BARRACUDA, U. S. Coast and Geodetic Survey, Woollard, and Collins (1933, p. 17) values have been corrected by +6, 0, −2, −1, and +5 mgal, respectively, to base them on the Department of Commerce Building, Washington, D. C. The USS TUSK value, the USS CHOPPER and the USS MEDREGAL values, and the USS DIABLO and the Frost gravimeter values are based on the Department of Commerce Building base with Woods Hole, Massachusetts (980.3250 gals), Columbia University (980.2680 gals), and Lamont Geological Observatory Base No. 1 (980.2584 gals), respectively, serving as intermediate bases.

In Table 2, values by Vening Meinesz check with all other values for Hampton Roads, Key West, Galveston, and Guantanamo Bay. The Vening Meinesz values only are available for the Morro Castle station. For the next available stations, San Juan and St. Thomas, the values by Vening Meinesz are 10–20 mgal higher than all other values. Either damage was done to the pendulums on the S-21 cruise

between Guantanamo Bay and San Juan or there is a computational error in the San Juan and St. Thomas stations. It is more likely that

Elevation corrections were applied using 0.3086 mgal per meter as the vertical gradient of gravity. If the more accurate formula given

TABLE 2.—COMPARISON OF OBSERVED GRAVITY VALUES FROM THE S-21 CRUISE WITH OTHER VALUES

Station	Observation by	Date	Observed gravity gals	North lat.	West long.
Hampton Roads	Vening Meinesz	October 1928	979.880	36–56.7	76–19.9
	USS TUSK	July 1947	.887	–57.2	–19.7
	Frost Gravimeter	July 1947	.886	–57.0	–19.7
Key West	Vening Meinesz	October 1928	978.970	No position given	
	USC & GS	1896	.973	24–33.6	81–48.4
	USS MEDREGAL	May 1948	.969	–33.2	–48.5
	USS CHOPPER	April 1949	.975	–33.2	–48.5
Galveston	Vening Meinesz	October 1928	979.280	29–18.6	94–47.4
	USC & GS	1895	.275	–18.2	–47.5
	USC & GS	1936	.277	–18.2	–47.5
Guantanamo Bay	Vening Meinesz	Nov. 1928	978.748	19–54.5	75–08.9
	Collins	Feb. 1932	.745	No position given	
	Woollard	1951	.750	19–54.5	75–08.9
San Juan, P. R.	Vening Meinesz	Nov. 1928	978.695	18–27.8	66–06.8
	USS DIABLO	March 1953	.681	–27.9	–06.7
	Frost Gravimeter	March 1953	.682	–27.9	–06.7
	USS DIABLO	March 1953	.686	–27.7	–05.5
	USC & GS	1929	.674	–28.1	–06.4
	Woollard	1951	.677	–28.1	–06.4
	Frost Gravimeter	March 1953	.679	–28.1	–06.4
St. Thomas, V. I.	Vening Meinesz	Nov. 1928	978.693	18–20.0	64–56.0
	USS BARRACUDA	January 1937	.686	–20.2	–55.2
	USS DIABLO	March 1953	.682	–20.1	–57.3
	Frost Gravimeter	Feb. 1953	.684	–20.1	–57.3

the pendulums were damaged, and most of the values for the stations after Guantanamo Bay are thus about 15 mgal too high as given by Vening Meinesz. This cannot be determined definitely until information about the Washington measurements and the Guantanamo Bay reoccupation becomes available.

MODIFIED BOUGUER ANOMALIES

Latitude corrections were applied in the usual manner using the International Gravity Formula of 1930. The correction at the latitude of Puerto Rico is approximately 0.9 mgal per minute of latitude.

by Swick (1942, p. 65) were used, the additional correction would be zero for about 75 per cent of the stations and 0.1 mgal for the others.

The Bullard modification of the Hayford-

TABLE 3.—MODIFIED BOUGUER CORRECTIONS IN GALS

Station	USC & GS	Vening Meinesz	Lamont Geol. Obs.
San Juan	–.0043	...	–.0062
Aibonito	+.0628	...	+.0620
Ponce	–.0035	...	–.0046
Mayaguez	–.0023	...	–.0040
San Juan Harbor		–.0052	–.0069

STATION NUMBER	DATE 1953	LATITUDE NORTH	LONGITUDE WEST	ELEVATION METERS	OBSERVED GRAVITY GALS	INTERNATION FORMULA GRAVITY	FREE AIR ANOMALY IN MGALS	MOD. BOUGUER ANOM. MGALS
1	25 Feb.				978.7017			
"	27 Feb.				.7019			
"	28 Feb.				.7022			
"	10 Mar.				.7017			
"	15 Apr.				.7017			
1*		18-23.58	66-04.90	14.7	978.7018	978.5619	145	149
2	25 Feb.	-24.5	-06.54	15.2	.6985	.5623	141	146
3	"				.6753			
"	4 Mar.				.6753			
"	15 Apr.				.6750			
3*		18-24.43	66-12.01	47.6	978.6752	978.5627	127	128
4	25 Feb.				.6833			
"	12 Mar.				.6833			
"	13 Mar.				.6830			
4*		-24.79	-15.18	8.7	.6832	.5630	123	129
5	25 Feb.	18-26.79	66-22.28	10.4	978.6830	978.5648	122	128
6	"				.6739			
"	15 Apr.				.6737			
6*		-26.32	-27.94	50.3	.6738	.5644	125	126
7	25 Feb.	-25.86	-31.66	8.7	.6745	.5640	113	120
8	25 Feb.				978.6526			
"	15 Apr.				.6518			
8*		18-25.97	66-33.95	79.6	.6522	978.5641	113	111
9	25 Feb.	-26.14	-36.87	96.4	.6433	.5642	109	105
10	"				.6518			
"	15 Apr.				978.6518			
10*		18-26.59	66-37.92	41.7	.6518	978.5646	100	103
11	25 Feb.	-28.23	-42.59	3.4	.6481	.5661	83	90
12**	26 Feb.	-12.22	67-08.72	12***	.6675	.5518	119	123
13	"				.6718			
"	27 Feb.				978.6718			
13*		18-10.41	67-09.08	2.2	.6718	978.5502	123	127
14	26 Feb.				.6678			
"	27 Feb.				.6675			
"	13 Mar.				.6673			

*** Adopted Value**

**** Reoccupation USC & GS West Indies No. 4**

***** Estimated from USGS Topographic Maps Scale 1:10,000**

TABLE 4.—SUMMARY—GRAVITY OBSERVATIONS IN PUERTO RICO

Based on Washington, D. C. at 980.1180 gals

Observer—G. Lynn Shurbet, Lamont Geological Observatory of Columbia University

Bowie method of computing the effect of topography as a whole from the station to the outer limit of zone O as described by Swick (1942, p. 68) was used in computing the modified Bouguer anomalies listed in Table 4. A density of 2.67 was assumed, and U. S. Geological Survey topographic maps, scales 1:10,000, 1:30,000, and 1:120,000, were used in determining the corrections for the land compartments. The topographic map, scale 1:120,000, was reduced photographically to a convenient scale (approximately 1:312,000) for use in computing the effects of the outer zones. U. S. Coast and Geodetic Survey

TABLE 4.—*Continued*

STATION NUMBER	DATE 1953	LATITUDE NORTH	LONGITUDE WEST	ELEVATION METERS	OBSERVED GRAVITY GALS	INTERNATION FORMULA GRAVITY	FREE AIR ANOMALY IN MGALS	MOD. BOUGUER ANOM. MGALS
14	16 Mar.				978.6673			
"	"				.6670			
"	17 Mar.				.6673			
"	"				.6673			
"	18 Mar.				.6673			
"	18 Mar.				978.6667			
"	19 Mar.				.6675			
"	"				.6673			
"	20 Mar.				.6678			
"	"				.6675			
"	21 Mar.				978.6675			
"	"				.6673			
"	23 Mar.				.6675			
"	"				.6675			
"	24 Mar.				.6675			
14*		18-12.68	67-08.57	25**	978.6674	978.5521	123	126
15	27 Feb.	-07.89	-08.19	8.2	.6641	.5479	119	123
16	"	-05.88	-04.70	23.8	.6646	.5461	126	129
17	"	-04.82	-00.21	67.8	.6531	.5452	129	127
18	"				.6483			
"	16 Apr.				978.6483			
18*		18-02.94	66-57.03	72.5	.6483	978.5436	127	125
19	27 Feb.				.6398			
"	23 Mar.				.6401			
19*		-01.27	-52.27	41.6	.6400	.5420	111	112
20	27 Feb.	18-02.01	66-47.95	21.2	978.6473	978.5427	111	116
21	"	-00.42	-43.76	6.2	.6419	.5413	103	108
22	"	17-59.09	-39.66	8.4	.6347	.5401	97	102
23	"	18-00.67	-34.54	6.3	.6297	.5415	90	95
24	"				.6307			
"	16 Mar.				978.6305			
24*		17-59.68	66-28.22	1.5	.6306	978.5406	91	96
25	27 Feb.	-57.98	-23.69	9.2	.6329	.5392	97	102
26	"	18-00.34	-15.83	35.8	.6635	.5412	134	135
27	"	-05.79	-12.44	615.5	.5673	.5460	211	153

* Adopted Value

** Estimated from USGS Topographic Maps Scale 1:10,000

charts numbers 901, 902, 903, and 904, and U. S. Hydrographic Office chart number 2318 were used in determining the corrections for sea compartments.

Elevations for zones A to L were read from the maps for all stations. Elevations for zones M, N, and O were determined for 135 stations from the maps. A contour map of the correction for zones M + N + O was constructed for 113 of these stations, and values of the correction were read from these contours for the 22 additional stations. The largest difference between corrections determined directly and those obtained by interpolation was 0.3 mgal, and the probable error of an interpolated value was estimated by least squares to be 0.1 to 0.2 mgal. The interpolation map was modified to include the 22 additional stations, and corrections for zones M + N + O for the remaining stations were estimated from this contour map.

Modified Bouguer corrections for the four

TABLE 4.—*Continued*

STATION NUMBER	DATE 1953	LATITUDE NORTH	LONGITUDE WEST	ELEVATION METERS	OBSERVED GRAVITY GALS	INTERNATION FORMULA GRAVITY	FREE AIR ANOMALY IN MGALS	MOD. BOUGUER ANOM. MGALS
28	28 Feb.				978.6833			
"	"				.6835			
"	2 Mar				.6835			
"	"				.6835			
"	10 Mar				.6830			
"	24 Mar				978.6833			
"	28 Mar				.6833			
"	15 Apr				.6833			
28*		18-27.97	66-05.26	3**	.6833	978.5659	118	125
29	28 Feb	-23.95	-01.51	35.2	.6971	.5623	146	148
30	28 Feb	18-23.59	65-58.88	27.4	978.6995	978.5619	146	149
31	"	-22.67	-56.07	13.0	.7033	.5611	146	151
32	"	-22.96	-53.82	8.5	.7035	.5614	145	150
33	"				.7049			
"	12 Mar				.7046			
33*		18-22.77	65-51.74	9.8	978.7048	978.5612	147	152
34	28 Feb	-22.68	-49.66	8.3	.7067	.5611	148	153
35	"	-22.74	-47.56	17.2	.7033	.5612	148	152
36	"				.7035			
"	3 Mar				.7033			
36*		18-22.34	65-46.20	10.2	978.7034	978.5608	146	151
37	28 Feb				.7041			
"	3 Mar				.7038			
37*		-23.04	-44.03	2.0	.7040	.5614	143	149
38	28 Feb	-22.22	-42.91	4.9	.7035	.5607	145	150
39	28 Feb	18-21.25	65-41.90	7.4	978.7014	978.5598	144	149
40	"	-20.57	-39.67	13.6	.6961	.5592	141	145
41	" "	-18.97	-39.07	7.4	.6899	.5578	135	139
42	" "	-17.15	-38.36	4.4	.6843	.5561	130	134
43	" "	-15.46	-39.13	29.7	.6686	.5546	123	125
44	28 Feb	18-13.78	65-40.31	10.7	978.6729	978.5531	123	127
45	" "	-12.91	-42.32	8.4	.6702	.5523	121	125
46	" "	-12.82	-45.63	7.5	.6739	.5523	124	129
47	" "				.6755			
"	3 Mar				.6755			

* Adopted Value

** Estimated from USGS Topographic Maps Scale 1:10,000

U. S. Coast and Geodetic Survey pendulum stations and the Vening Meinesz pendulum station were recomputed for this survey. A comparison of the new values with the original values is made in Table 3. The difference of about 1.5 mgal in the original and new corrections is probably due to the use of different nautical charts, since most of the difference occurs in zones M, N, and O.

With random errors of about 1 mgal for observed gravity, 0.5 mgal for elevation (2 mgal for the 16 stations for which elevations were estimated from topographic maps), and 1.5 mgal for the modified Bouguer correction, the modified Bouguer anomalies given in Table 4 are accurate to within about 2 mgal (3 mgal for the 16 stations). In Plate 1, a contour map of the anomalies is shown. The U. S. Coast and Geodetic Survey and Vening Meinesz stations are shown by circled points and the new gravimeter stations by points on the map. The anomalies are contoured with a 5 mgal interval.

TABLE 4.—*Continued*

STATION NUMBER	DATE 1953	LATITUDE NORTH	LONGITUDE WEST	ELEVATION METERS	OBSERVED GRAVITY GALS	INTERNATION FORMULA GRAVITY	FREE AIR ANOMALY IN MGALS	MOD. BOUGUER ANOM. MGALS
47*		18-13.14	65-46.95	15.0	978.6755	978.5525	128	132
48	28 Feb	-13.27	-49.96	95.0	.6683	.5526	145	141
49	"	-13.81	-51.51	87.1	.6726	.5531	147	143
50	"	-14.41	-53.21	83.0	.6753	.5537	147	145
51	"				.6785			
"	2 Mar				978.6785			
51*		18-13.69	65-55.07	68.9	.6785	978.5530	147	145
52	28 Feb	-14.96	-56.76	56.9	.6897	.5542	153	153
53	"	-15.18	-58.83	63.8	.6942	.5544	160	158
54	"	-14.59	66-00.58	56.5	.6854	.5538	149	148
55	28 Feb	18-16.21	66-02.40	82.8	978.6894	978.5553	160	157
56	"	-17.63	-03.03	65.4	.6886	.5566	152	151
57	"	-18.93	-05.38	113.8	.6785	.5577	156	150
58	"	-20.56	-06.32	85.8	.6838	.5592	151	148
59	"	-21.98	-06.72	34.5	.6942	.5605	145	147
60	2 Mar	18-13.61	66-02.33	81.2	978.6699	978.5530	142	138
61	"	-12.14	-03.24	106.3	.6670	.5517	148	143
62	"	-11.33	-04.25	225.9	.6451	.5510	164	147
63	"	-10.64	-05.40	453.5	.6001	.5504	190	147
64	"	-08.37	-07.31	390.4	.6214	.5483	194	157
65	2 Mar	18-08.20	66-08.29	373.2	978.6238	978.5482	191	156
66	"				.6185			
"	11 Mar				.6182			
66*		-07.06	-09.74	390.7	.6184	.5472	192	155
67	2 Mar	-06.52	-09.49	434.2	.6062	.5467	194	154
68	2 Mar	18-05.98	66-09.35	592.2	978.5715	978.5462	208	153
69	"	-05.52	-09.26	681.5	.5526	.5458	221	156
70	"	-05.12	-09.50	726**	.5422	.5454	221	153
71	"	-04.28	-08.59	719.7	.5398	.5447	217	152
72	"	-03.87	-08.30	714.1	.5401	.5444	216	152
73	2 Mar	18-02.87	66-08.08	647.8	978.5537	978.5435	210	150
74	"	-02.03	-07.21	511.7	.5750	.5427	190	149
75	"	-02.15	-07.48	451.0	.5894	.5428	186	148
76	"	-01.62	-07.85	333.1	.6137	.5424	174	148
77	"	-01.13	-07.47	225.2	.6310	.5419	159	145

***Adopted Value**

**** Observation made on road below BM. Elevation difference estimated by observer**

NORTH-SOUTH STRUCTURE SECTION THROUGH SAN JUAN

During the period in which this survey was conducted, a profile of gravity values at sea was determined, using a Vening Meinesz pendulum apparatus aboard USS DIABLO (SS 479). The profile of sea stations extends from about 200 miles north of San Juan, Puerto Rico, to San Juan, and from the southern coast of Puerto Rico at about the same longitude to 150 miles south of the island. Gravity observations were made at 44 new stations. The main purpose of this land gravity survey is to provide a firm connection across the island for the sea profile.

To establish a typical profile across the island, a mean of five north-south profiles was used. The five profiles at longitudes indicated in Plate 1 by A–A′, B–B′, C–C′, D–D′, and E–E′ are shown in Figure 2 with the mean profile. A point on a profile indicates the

TABLE 4.—*Continued*

STATION NUMBER	DATE 1953	LATITUDE NORTH	LONGITUDE WEST	ELEVATION METERS	OBSERVED GRAVITY GALS	INTERNATION FORMULA GRAVITY	FREE AIR ANOMALY IN MGALS	MOD. BOUGUER ANOM. MGALS
78	2 Mar	18-00.34	66-07.02	108.9	978.6585	978.5412	151	148
79	"	17-58.90	-06.65	42.8	.6702	.5399	144	145
80	"	-58.58	-03.54	15.8	.6742	.5397	140	144
81	"	18-00.24	-01.45	18.0	.6758	.5411	140	146
82	"	17-58.67	65-57.91	3.5	.6702	.5397	132	138
83	2 Mar				978.6649			
"	9 Mar				.6646			
83*		18-00.53	65-54.02	11.7	.6648	978.5414	127	132
84	2 Mar	-04.62	-52.24	10.4	.6619	.5450	120	124
85	"	-07.45	-49.26	33.7	.6614	.5475	125	126
86	2 Mar				978.6539			
"	9 Mar				.6539			
86*		18-10.86	65-51.82	126**	.6539	978.5506	142	133
87	3 Mar				.6833			
"	"				.6833			
"	4 Mar				978.6833			
"	"				.6833			
"	5 Mar				.6830			
"	"				.6827			
"	6 Mar				.6830			
"	6 Mar				978.6827			
"	9 Mar				.6833			
"	"				.6830			
"	10 Mar				.6833			
"	"				.6830			
"	11 Mar				978.6833			
"	"				.6833			
"	12 Mar				.6833			
"	"				.6830			
87*		18-27.43	66-05.00	13***	.6831	978.5654	122	127
88	3 Mar	18-20.53	65-45.61	164.0	978.6694	978.5592	161	151
89	"	-19.24	-46.31	444.6	.6051	.5580	185	152
90	"	-18.18	-47.14	639.7	.5667	.5571	207	149
91	"	-16.66	-47.28	651.3	.5579	.5557	203	143
92	"	-16.03	-48.08	480.6	.5897	.5551	183	143

***Adopted Value**

**** Observation made on road below BM. Elevation diff. est. by observer**

***** Estimated from USGS Topographic Maps Scale 1:10,000**

intersection of a gravity contour with the profile line.

Utilizing the mean gravity profile and gravity and seismic information at sea, Worzel and Ewing (1954, p. 198) have deduced a north-south structure section through San Juan. The large negative anomaly over the Puerto Rico Trench has been explained by a small downward deflection (about 7 km) of the crust with a large accumulation (about 6 km) of sediments in the trench (Ewing and Worzel, 1954, p. 171). The small negative "gravity trench" discovered by the measurements in USS DIABLO south of Puerto Rico is explained by a small downward deflection of the crust with an accumulation of sediments.

Worzel and Ewing assumed densities of 1.03 for sea water, 2.30 for sediments, 2.67 for the crustal rocks and 3.27 for the mantle. Recent correlations of seismic measurements of crustal

TABLE 4.—*Continued*

STATION NUMBER	DATE 1953	LATITUDE NORTH	LONGITUDE WEST	ELEVATION METERS	OBSERVED GRAVITY GALS	INTERNATION FORMULA GRAVITY	FREE AIR ANOMALY IN MGALS	MOD. BOUGUER ANOM. MGALS
93	3 Mar	18-14.84	65-47.99	145.0	978.6561	978.5541	147	142
94	"	-14.44	-47.11	25.3	.6758	.5537	130	136
95	"	-12.85	-47.87	31.3	.6739	.5523	131	135
96	4 Mar	-25.49	66-05.89	1.0	.6961	.5636	133	139
97	"	-23.84	-08.60	10.9	.6867	.5622	128	133
98	4 Mar	18-24.47	66-18.03	78.4	978.6809	978.5627	143	140
99	"				.6915			
"	15 Apr				.6918			
99*		-25.58	-20.58	13.3	.6917	.5637	132	138
100	4 Mar	-26.01	-25.02	85.4	.6737	.5641	134	131
101	4 Mar	18-25.81	66-27.01	82.7	978.6710	978.5639	133	130
102	"	-25.57	-29.15	59.9	.6718	.5637	127	127
103	"	-23.92	-29.70	35.3	.6803	.5622	129	133
104	"	-21.92	-28.58	98.4	.6795	.5604	150	146
105	"	-21.06	-28.37	47.1	.6945	.5597	150	152
106	4 Mar	18-19.60	66-28.52	210.9	978.6622	978.5583	169	154
107	"	-18.48	-28.69	361.7	.6318	.5573	186	154
108	"	-17.74	-30.05	393.1	.6219	.5567	194	159
109	"	-16.57	-30.93	378.6	.6257	.5556	188	155
110	"	-15.50	-30.93	543.0	.5929	.5547	206	157
111	4 Mar				978.5833			
"	19 Mar				.5838			
111*		18-14.27	66-31.34	580.7	.5836	978.5535	210	155
112	5 Mar	-24.30	-15.61	10.1	.6867	.5626	127	133
113	"	-23.13	-15.00	10.2	.6977	.5615	140	146
114	5 Mar	18-21.82	66-15.95	115.2	978.6841	978.5603	160	149
115	"	-20.82	-16.64	177.2	.6745	.5594	170	157
116	"				.6921			
"	12 Mar				.6921			
116*		-20.58	-19.05	94.5	.6921	.5592	162	159
117	5 Mar	18-17.36	66-12.58	71.7	978.6862	978.5563	152	154
118	"	-15.75	-12.42	199.8	.6654	.5549	172	160
119	"	-14.44	-12.73	198.0	.6683	.5537	176	163
120	"	-13.19	-13.61	201.0	.6643	.5526	174	160
121	"	-12.43	-14.94	299.8	.6438	.5519	185	161

***Adopted Value**

thicknesses, on continents and under oceans, with elevations and gravity anomalies in the areas of seismic measurements indicate an average density of 2.84 for crustal rocks (Worzel and Shurbet, 1955, p. 91). Since all rocks other than granites normally found in the crustal column are generally of greater density than 2.67, this average crustal density of 2.84 seems very reasonable and is in close agreement with values used by many other authors.

The section through San Juan has been recomputed using the density of 2.84 for crustal rocks (Fig. 3). Figure 3A shows the seismic and topographic evidence. Figure 3B shows the assumed structure and densities which give the computed gravity curve shown by the solid line in Figure 3C. The open circles are free-air anomalies observed in USS DIABLO, the black circles are free-air anomalies observed by Vening Meinesz (1948, p. 156, 230; Heiskanen, 1939, p. 98), and the triangles are modified

TABLE 4.—*Continued*

STATION NUMBER	DATE 1953	LATITUDE NORTH	LONGITUDE WEST	ELEVATION METERS	OBSERVED GRAVITY GALS	INTERNATION FORMULA GRAVITY	FREE AIR ANOMALY IN MGALS	MOD. BOUGUER ANOM. MGALS
122	5 Mar	18-12.09	66-15.84	517.3	978.5993	978.5517	207	161
123	"	-11.20	-16.63	660.1	.5715	.5509	225	163
124	"	-11.01	-18.77	682.9	.5715	.5507	232	166
125	"	-09.70	-18.58	563.5	.5859	.5495	211	157
126	"	-08.31	-17.50	627.8	.5678	.5483	213	152
127	5 Mar	18-07.91	66-17.17	642.9	978.5635	978.5479	214	151
128	"				.5763			
"	11 Mar				.5763			
128*		-08.48	-16.14	597.5	.5763	.5484	213	154
129	5 Mar	-08.94	-14.85	563.0	.5851	.5489	210	156
130	5 Mar	18-09.07	66-14.15	392.8	978.6195	978.5490	192	159
131	"	-08.52	-12.18	320.4	.6339	.5485	185	157
132	"	-07.88	-11.20	347.5	.6270	.5479	187	157
133**	6 Mar				.6787			
"	10 Mar				.6790			
"	15 Apr				978.6793			
133**		18-28.14	66-06.42	8***	.6790	978.5660	116	122
134	6 Mar				.6814			
"	10 Mar				.6817			
"	15 Apr				.6817			
134*		18-27.94	66-06.74	2***	978.6816	978.5659	116	123
135	9 Mar	-13.55	-01.64	62.4	.6739	.5529	140	139
136	"	-13.29	-00.67	61.1	.6774	.5527	144	142
137	"				.6814			
"	"				.6809			
137*		18-12.33	65-59.40	72.6	978.6812	978.5519	152	150
138	9 Mar	-11.28	-57.82	107.0	.6638	.5510	146	139
139	"	-10.39	-58.64	94.8	.6654	.5502	145	140
140	"	-09.03	-58.93	158.0	.6510	.5489	151	140
141	"	-07.89	-59.08	179.5	.6435	.5479	151	137
142	9 Mar	18-06.63	65-59.56	228.1	978.6350	978.5468	159	140
143	"	-04.79	-59.45	332.9	.6177	.5451	176	146
144	"	-03.15	-59.24	403.2	.6011	.5437	182	147
145	"	-02.21	66-00.48	99.6	.6638	.5429	152	151
146	"	17-58.88	65-59.92	8.9	.6718	.5399	135	140

***Adopted Value**
**** Reoccupation USC & GS West Indies No. 1**
***** Estimated from USGS Topographic Maps Scale 1:10,000**

Bouguer anomalies observed by the U. S. Coast and Geodetic Survey. The dashed line is the mean profile of modified Bouguer anomalies determined by the present survey. The agreement of the computed curve with observed points is considered adequate.

The structure in Figure 3B is essentially unchanged from the section deduced by Worzel and Ewing (1954, p. 171), except that the crustal rock layers are thickened slightly (about 1.5 km). The only appreciable thickening occurs under Puerto Rico where the crustal rocks have their maximum thickness. This new calculation indicates that the mantle is about 29 km below sea level under Puerto Rico. Slightly different rectangular blocks have

TABLE 4.—*Continued*

STATION NUMBER	DATE 1953	LATITUDE NORTH	LONGITUDE WEST	ELEVATION METERS	OBSERVED GRAVITY GALS	INTERNATION FORMULA GRAVITY	FREE AIR ANOMALY IN MGALS	MOD. BOUGUER ANOM. MGALS
147	9 Mar	17-58.74	65-55.82	3.8	978.6611	978.5398	123	130
148	"	-59.18	-54.49	13.1	.6614	.5402	125	131
149	"	18-02.05	-54.40	232.0	.6193	.5427	148	131
150	"	-02.55	-52.76	47.1	.6545	.5432	126	128
151	"	-05.85	-50.38	62.2	.6470	.5461	120	119
152	9 Mar	18-09.03	65-47.08	3.8	978.6742	978.5489	127	131
153	"	-10.60	-44.37	2.6	.6651	.5503	116	120
154	"	-11.43	-43.52	2.2	.6667	.5511	117	121
155	"	-09.22	-49.88	24.8	.6718	.5491	131	133
156	"	-10.61	-53.12	108.9	.6579	.5504	141	135
157	9 Mar	18-10.61	65-55.21	135.3	978.6531	978.5504	145	135
158	11 Mar	-14.69	66-03.90	85.3	.6806	.5539	153	150
159	"	-15.11	-05.41	170.8	.6691	.5543	168	156
160	"	-15.54	-06.21	259.5	.6507	.5547	176	154
161	"	-14.71	-07.78	286.4	.6478	.5539	183	158
162	11 Mar	18-14.38	66-09.44	319.1	978.6401	978.5536	185	158
163	"	-14.17	-11.17	356.7	.6347	.5535	192	160
164	"	-12.93	-12.08	249.1	.6539	.5523	179	161
165	"	-11.72	-11.73	326.6	.6331	.5514	183	155
166	"	-10.68	-09.69	425.5	.6110	.5504	192	151
167	11 Mar	18-09.37	66-09.82	425**	978.6134	978.5492	195	156
168	"	-08.20	-10.03	347**	.6297	.5482	189	157
169*	"	-08.07	-15.77	636.0	.5670	.5481	215	153
170	"	-07.98	-15.75	650**	.5643	.5480	217	153
171	"	-06.57	-17.65	470.0	.5902	.5467	189	146
172	11 Mar	18-05.32	66-19.06	154.4	978.6470	978.5456	149	139
173	"	-05.16	-21.05	123.6	.6505	.5454	143	137
174	"	-05.42	-22.28	226.4	.6291	.5457	154	136
175	"	-06.77	-22.78	375.6	.6001	.5469	169	139
176	"	-08.11	-23.45	583.7	.5638	.5481	196	141
177	11 Mar	18-09.33	66-23.66	637.8	978.5563	978.5492	204	146
178	"	-10.26	-24.40	772.9	.5347	.5500	223	149
179	"	-11.27	-24.09	809.4	.5363	.5509	235	156
180	"	-12.39	-23.80	695.1	.5670	.5519	230	163
181	"	-13.38	-23.66	551.0	.5977	.5527	215	164

*** Near USC & GS West Indies No. 2**

**** Estimated from USGS Topographic Maps Scale 1:10,000**

been used to approximate better the sea-water section immediately north and south of the island and over the trench itself. At the northern side of the trench, the sediment-basement and basement-mantle interfaces have been raised slightly from the depth previously indicated so that the computed curve agrees better with the observed curve. These changes do not affect the conclusions of Ewing and Worzel (1954). Since the density of 2.67 was used in computing the modified Bouguer anomalies for the land survey, a discrepancy occurs in the computations, but it is not greater than 6 mgal and may be neglected for present purposes.

Isostatic anomalies have not been computed

TABLE 4.—*Continued*

STATION NUMBER	DATE 1953	LATITUDE NORTH	LONGITUDE WEST	ELEVATION METERS	OBSERVED GRAVITY GALS	INTERNATION FORMULA GRAVITY	FREE AIR ANOMALY IN MGALS	MOD. BOUGUER ANOM. MGALS
182	11 Mar	18-14.25	66-22.59	470.4	978.6123	978.5535	204	161
183	"	-15.87	-22.16	613.3	.5907	.5550	225	166
184	"	-16.02	-21.37	412.9	.6318	.5551	204	170
185	"	-16.87	-20.12	368.8	.6406	.5559	199	167
186	"	-17.53	-21.23	477.5	.6185	.5565	210	164
187	11 Mar	18-18.49	66-20.74	305.2	978.6523	978.5573	189	164
188	"	-19.55	-20.59	205.0	.6678	.5583	173	158
189	12 Mar	-27.13	-03.16	2.1	.6854	.5651	121	128
190	"	-26.63	-00.88	2.4	.6873	.5647	124	130
191	"	-24.81	65-54.07	2.8	.7038	.5630	142	148
192	12 Mar	18-26.08	65-52.37	1.8	978.6990	978.5642	136	142
193	"	-25.58	-50.60	2.5	.7014	.5637	139	145
194	"	-25.06	-49.66	1.2	.7022	.5633	140	146
195	"	-21.01	-53.86	34.4	.6993	.5596	151	153
196	"	-19.10	-53.52	86.0	.6889	.5579	158	155
197	12 Mar	18-17.44	65-53.71	295.2	978.6446	978.5564	180	154
198	"	-24.82	66-22.11	70.7	.6859	.5630	145	144
199	"	-23.46	-22.82	119.0	.6790	.5618	154	148
200	"	-21.69	-22.93	163.6	.6710	.5602	162	150
201	"	-20.46	-22.60	148.2	.6769	.5591	164	155
202	12 Mar	18-19.42	66-17.83	229*	978.6641	978.5582	177	158
203	"	-18.59	-15.81	163*	.6737	.5574	167	156
204	"	-18.18	-14.77	105*	.6822	.5571	158	154
205	"	-19.06	-12.30	51.9	.6931	.5579	151	154
206	"	-20.47	-12.04	107.0	.6862	.5591	160	154
207	12 Mar	18-21.68	66-11.42	95.9	978.6862	978.5602	156	152
208	"	-23.15	-10.30	40.0	.6814	.5615	132	134
209	13 Mar	-26.77	-15.26	5.5	.6782	.5648	115	121
210	"	-24.53	-34.73	146.8	.6419	.5628	125	115
211	"	-23.38	-34.15	180.1	.6433	.5617	137	124
212	13 Mar	18-22.39	66-33.91	187.2	978.6478	978.5609	145	131
213	"	-20.45	-35.42	248.5	.6382	.5591	156	137
214	"	-19.49	-35.14	145.5	.6630	.5582	150	143
215	"	-29.22	-59.25	66.8	.6582	.5670	112	112
216	"	-29.92	67-00.91	60.5	.6614	.5676	113	114

*** Estimated from USGS Topographic Maps Scale 1:10,000**

for these new land measurements or for the observations at sea in USS DIABLO. The isostatic anomalies for the Vening Meinesz stations at sea and the U. S. Coast and Geodetic Survey stations on land were computed by Vening Meinesz and Heiskanen (*in* Ewing and Worzel, 1954, p. 170) and are shown in Table 5. The Hayford and the available Airy isostatic anomalies show that this area is strongly out of isostatic equilibrium. Forces arising from this isostatic unbalance are tending to uplift the areas of large negative anomaly and depress the area of positive anomaly.

BRIEF CORRELATION OF GRAVITY ANOMALIES WITH SURFACE GEOLOGIC FORMATIONS

In Plate 1, the contours of modified Bouguer anomaly may be compared with surface geologic formations adapted from the geologic map of Puerto Rico published by Meyerhoff

TABLE 4.—*Continued*

STATION NUMBER	DATE 1953	LATITUDE NORTH	LONGITUDE WEST	ELEVATION METERS	OBSERVED GRAVITY GALS	INTERNATION FORMULA GRAVITY	FREE AIR ANOMALY IN MGALS	MOD. BOUGUER ANOM. MGALS
217	13 Mar	18-16.94	67-08.18	7.5	978.6726	978.5560	119	124
218	"	-16.71	-07.00	15.2	.6769	.5557	126	130
219	"	-16.81	-05.46	15**	.6737	.5558	122	127
220	"	-17.07	-04.41	65**	.6614	.5561	125	126
221	"	-15.05	-09.66	2.4	.6747	.5542	121	126
222	16 Mar	18-00.17	66-32.30	9.4	978.6289	978.5411	91	95
223	"	17-59.89	-30.27	4.7	.6342	.5408	95	100
224	"	-59.70	-27.65	1.8	.6302	.5406	90	96
225	"	-59.35	-26.28	6.4	.6278	.5403	90	95
226	"	-58.52	-25.02	10.2	.6286	.5396	92	97
227	16 Mar	17-58.21	66-22.12	4.5	978.6358	978.5394	98	103
228	"	-58.77	-20.48	3.8	.6438	.5398	105	111
229	"	-58.68	-18.26	6.7	.6489	.5397	112	116
230	"	-58.35	-16.38	12.7	.6534	.5395	118	122
231	"	-58.45	-14.12	11.5	.6649	.5396	129	133
232	16 Mar	17-58.29	66-12.54	3.2	978.6707	978.5394	133	138
233	"	-58.07	-10.86	14.3	.6694	.5393	135	139
234	"	-57.74	-08.18	19.7	.6694	.5390	137	141
235	"	-58.97	-04.94	26.9	.6734	.5400	142	145
236	"	-59.02	-01.90	5.6	.6761	.5400	138	144
237	16 Mar	17-58.74	66-24.25	17.0	978.6302	978.5398	96	100
238	"	18-00.71	-23.39	39.5	.6513	.5415	122	124
239	"	-01.47	-22.22	72.3	.6441	.5422	124	122
240	"	-02.96	-21.84	103.7	.6446	.5436	133	127
241	"	-04.07	-22.03	91.8	.6513	.5446	135	131
242	16Mar	18-03.32	66-23.97	134.6	978.6363	978.5439	134	125
243	"	-02.57	-26.18	108.7	.6350	.5432	126	120
244	"	-02.91	-28.31	100.8	.6382	.5435	126	121
245	"	-03.28	-31.15	50.1	.6457	.5439	117	118
246	"	-01.15	-36.48	20.5	.6331	.5419	98	101
247	17 Mar				978.6710			
"	16 Apr				.6713			
247*		18-12.68	67-07.38	21.5	.6712	978.5521	126	130
248	17 Mar				.6454			
"	16 Apr				.6457			

* Adopted Value

** Estimated from USGS Topographic Maps Scale 1:10,000

(1933). The large area of strong positive gravity anomaly trending northwest with its center near 18° 15′ N., 66° 20′ W., shows no correlation with outcrops indicated on the map. Concerning the Cretaceous sediments in this area, Meyerhoff, in a personal communication, says, "The incompetent sediments in the basin are highly deformed and compressed—also hydrothermally altered and silicified." This positive anomaly may result in part from increased densities of the surface and near-surface rocks, and in part from concealed intrusive rocks which have produced the alterations observed at the surface.

Gravity features which may be correlated with outcrops are the gravity minima (1) at 18° 14′ N., 66° 40′ W., (2) at the southeast corner of the island, (3) at 18° 14′ N., 66° 01′ W., near Caguas, and (4) associated with the

TABLE 4.—*Continued*

STATION NUMBER	DATE 1953	LATITUDE NORTH	LONGITUDE WEST	ELEVATION METERS	OBSERVED GRAVITY GALS	INTERNATION FORMULA GRAVITY	FREE AIR ANOMALY IN MGALS	MOD. BOUGUER ANOM. MGALS
248*		18-12.77	67-06.04	150.0	978.6456	978.5522	140	130
249	17 Mar				.6318			
"	16 Apr				.6313			
249*		-12.83	-04.61	234.0	.6316	.5523	152	133
250	17 Mar				.6123			
"	16 Apr				978.6121			
250*		18-12.68	67-03.60	328.8	.6122	978.5521	162	133
251	17 Mar				.5987			
"	16 Apr				.5987			
251*		-12.65	-01.96	393.1	.5987	.5521	168	132
252	17 Mar	18-12.70	66-59.97	557.2	978.5643	978.5522	184	134
253	"				.5635			
"	16 Apr				.5635			
253*		-11.98	-59.29	564.8	.5635	.5516	186	134
254	17 Mar				.5929			
"	16 Apr				978.5926			
"	"				.5923			
254 *		18-11.13	66-58.91	418.3	.5926	978.5508	171	132
255	17 Mar	-10.90	-57.92	381.1	.5987	.5506	166	133
256	"				.5803			
"	16 Apr				978.5801			
256*		18-11.51	66-57.02	476.0	.5802	978.5512	176	132
257	17 Mar	-10.99	-55.90	696.6	.5323	.5507	197	131
258	"				.5075			
"	16 Apr				.5075			
258*		18-10.08	66-54.33	805.5	978.5075	978.5499	206	131
259	17 Mar				.4814			
"	18 Mar				.4816			
"	16 Apr				.4811			
259*		-09.21	-53.11	925.2	.4814	.5491	218	131
260	17 Mar	18-10.12	66-52.26	700.4	978.5323	.5499	199	132
261	"	-11.55	-50.93	598.2	.5529	.5512	187	130
262	"	-13.01	-51.28	488.7	.5734	.5524	172	128
263	"	-14.34	-51.52	339.5	.6059	.5536	157	129
264	"	-15.93	-51.38	519.5	.5721	.5550	178	129

*** Adopted Value**

Tertiary sedimentary basins on the north and south coasts of the island.

The gravity minima (1) to (3) are associated with outcrops called granitoid intrusives and intrusive porphyries, chiefly andesitic, by Meyerhoff, or diorites, quartz diorites, and quartz monzonites, and shallow intrusives by Mitchell (Manuscript). Mitchell states that outcrop (1) is more diabasic than the others. This correlation of gravity minima with granitic rocks is characteristic of continental gravity studies. Meyerhoff (Personal communication) points out that minima (1) and (3) "coincide with Cretaceous volcanic centers to which the somewhat younger granitoid intrusives may be genetically related".

TABLE 4.—*Continued*

STATION NUMBER	DATE 1953	LATITUDE NORTH	LONGITUDE WEST	ELEVATION METERS	OBSERVED GRAVITY GALS	INTERNATION FORMULA GRAVITY	FREE AIR ANOMALY IN MGALS	MOD. BOUGUER ANOM. MGALS
265	17 Mar	18-16.62	66-52.45	445.3	978.5862	978.5557	168	127
266	"	-18.18	-54.01	387.1	.5963	.5571	159	124
267	"	-18.87	-55.58	365.5	.5974	.5577	153	121
268	"	-20.08	-56.99	254.5	.6198	.5588	140	120
269	"				.6593			
"	20 Mar				978.6593			
269*		18-20.08	66-59.26	71.0	.6593	978.5588	123	121
270	17 Mar	-20.98	67-00.82	49.8	.6617	.5596	118	118
271	"	-21.98	-02.43	48.7	.6603	.5605	115	116
272	"	-22.72	-03.76	66.0	.6561	.5612	116	115
273	17 Mar	18-22.92	67-05.35	81.3	978.6542	978.5613	118	116
274	"	-23.82	-06.84	42**	.6657	.5621	117	119
275	"	-24.22	-08.75	19.0	.6686	.5625	112	117
276	18 Mar	-03.82	66-51.74	81.0	.6385	.5443	119	119
277	"	-05.86	-52.10	146.8	.6299	.5461	129	122
278	18 Mar	18-07.00	66-51.99	380.3	978.5851	978.5471	156	125
279	"				.5299			
"	16 Apr				.5299			
279*		-08.25	-52.57	664.0	.5299	.5482	187	129
280	18 Mar	-11.04	-50.14	463.1	.5801	.5507	173	130
281	18 Mar	18-10.83	66-48.78	650.2	978.5425	978.5506	193	129
282	"	-12.07	-47.83	484.5	.5745	.5517	173	127
283	"	-11.25	-45.92	553.0	.5598	.5509	180	126
284	"	-10.24	-43.89	463.2	.5779	.5500	171	128
285	"	-09.35	-41.99	625.2	.5417	.5492	186	127
286	18 Mar	18-09.22	66-40.58	855.7	978.4910	978.5491	206	123
287	"	-09.71	-39.00	792.9	.5094	.5495	205	129
288	"	-11.00	-38.37	589.1	.5531	.5507	184	128
289	"				.5931			
"	19 Mar				.5934			
289*		18-12.17	66-37.41	391.5	978.5933	978.5517	163	128
290	18 Mar	-13.32	-38.17	408.7	.5889	.5527	163	126
291	"	-14.29	-39.79	349.8	.6001	.5536	155	124
292	"	-15.14	-40.57	199.1	.6313	.5543	139	125
293	"	-16.11	-42.52	134.9	.6457	.5552	132	125

*** Adopted Value**

**** Observation made on road below BM. Elevation difference estimated by observer**

The Puerto Rico platform narrows considerably eastward from the southeast corner of the island (Pl. 1). Outcrops of granitoid rocks at this corner and at the western end of Vieques Island are probably two separate intrusive bodies since the anomaly contours at the southeast corner trend toward deep water. The narrowing of the platform also probably accounts for the general northeast trend of the gravity contours at the eastern end of Puerto Rico.

THE TERTIARY SEDIMENTARY BASINS

Plate 1 shows the effects of the Tertiary sediments on the gravity anomalies. On the

TABLE 4.—*Continued*

STATION NUMBER	DATE 1953	LATITUDE NORTH	LONGITUDE WEST	ELEVATION METERS	OBSERVED GRAVITY GALS	INTERNATION FORMULA GRAVITY	FREE AIR ANOMALY IN MGALS	MOD. BOUGUER ANOM. MGALS
294	18 Mar	18-16.77	66-44.24	436.9	978.5851	978.5558	164	125
295	"	-17.48	-45.82	419.6	.5918	.5564	165	125
296	"	-18.02	-46.97	294.6	.6182	.5569	152	127
297	"	-17.95	-49.38	293.1	.6206	.5569	154	129
298	"	-17.59	-51.47	395.0	.6027	.5565	168	132
299	19 Mar	18-02.21	66-35.33	35.2	978.6430	978.5429	111	113
300	"	-02.89	-33.77	71.4	.6387	.5435	117	115
301	"	-03.28	-32.36	59.1	.6419	.5439	116	116
302	"	-04.72	-30.05	75.0	.6497	.5451	128	126
303	"	-06.25	-30.44	109.7	.6483	.5464	136	132
304	19 Mar	18-07.67	66-29.66	146.5	978.6465	978.5477	144	138
305	"	-09.09	-30.70	679.6	.5430	.5490	204	142
306	"	-10.64	-30.66	654.1	.5566	.5504	208	148
307	"	-12.62	-30.93	463.2	.5990	.5521	190	154
308	"	-13.89	-33.44	753.6	.5462	.5532	226	151
309	19 Mar	18-13.24	66-35.50	435.9	978.5955	978.5526	178	138
310	"	-08.08	-40.66	648.4	.5358	.5481	188	127
311	"	-06.78	-39.76	505.6	.5643	.5469	174	127
312	"	-04.30	-39.06	127.2	.6350	.5447	130	123
313	"	-02.57	-38.68	52.9	.6449	.5432	118	119
314	19 Mar	18-01.10	66-38.28	20.2	978.6358	978.5419	100	104
315	"	-03.08	-43.27	39.9	.6550	.5437	124	127
316	"	-03.08	-46.88	106.9	.6406	.5437	130	125
317	20 Mar	-13.82	67-00.93	360.5	.6083	.5531	167	134
318	"	-15.18	-00.04	236.8	.6353	.5544	154	135
319	20 Mar	18-16.18	66-59.35	211.8	978.6398	978.5553	150	134
320	"	-17.58	-59.92	199.0	.6337	.5565	139	123
321	"	-18.66	-58.86	157.3	.6417	.5575	133	122
322	"	-19.41	-49.58	304.4	.6147	.5582	151	125
323	"	-20.95	-49.17	301.7	.6166	.5596	150	124
324	20 Mar	18-22.12	66-47.91	287.3	978.6227	978.5606	151	126
325	"	-23.42	-46.66	239.7	.6209	.5618	133	115
326	"	-24.87	-47.35	158.8	.6294	.5631	116	105
327	"	-25.73	-47.69	135.9	.6289	.5639	107	99
328	"	-27.06	-48.16	68.6	.6374	.5651	94	93

south coast, the gravity gradient increases eastward from Long. 67° 00′ W., which marks approximately the western margin of the basin. This high gradient is maintained eastward along the length of the basin although the contours are influenced at the eastern end by the large gravity maximum.

The high gravity gradient is evident also along the northern basin although the eastern end is again influenced by the large gravity maximum. The gradient is especially noticeable at Long. 66° 45′ W., where the sediments on this coast have a maximum thickness of about 1.1 km at the shore line (Zapp *et al.*, 1948). Gravity contours at the northwest corner of the island do not show the marked gradient characteristic of other parts of the basin. Since the sediment thickness here is more than 0.5 km at the shore line (Zapp *et al.*, 1948), some

TABLE 4.—*Continued*

STATION NUMBER	DATE 1953	LATITUDE NORTH	LONGITUDE WEST	ELEVATION METERS	OBSERVED GRAVITY GALS	INTERNATION FORMULA GRAVITY	FREE AIR ANOMALY IN MGALS	MOD. BOUGUER ANOM. MGALS
329	20 Mar	18-28.48	66-48.92	29.6	978.6419	978.5663	85	90
330	"				.6427			
"	21 Mar				.6425			
"	15 Apr				.6425			
330 *		-29.36	-49.51	10.6	.6426	.5671	79	86
331	20 Mar	18-28.74	66-51.22	62.0	978.6345	978.5666	87	88
332	"	-28.48	-52.42	72.7	.6363	.5663	93	92
333	"	-26.82	-55.79	156.6	.6334	.5648	117	107
334	"	-25.46	-54.98	204.5	.6235	.5636	123	108
335	"	-24.23	-55.27	233.2	.6195	.5625	129	111
336	20 Mar	18-22.85	66-55.75	244.8	978.6198	978.5613	134	115
337	"	-21.99	-55.28	229.5	.6259	.5605	136	118
338	"	-21.30	-56.77	287.7	.6115	.5599	141	115
339	"	-20.94	-58.57	262.7	.6155	.5596	137	115
340	21 Mar				.6681			
"	16 Apr				978.6681			
340*		18-12.52	67-09.12	2.1	.6681	978.5520	117	122
341	21 Mar	-16.68	-09.63	5.2	.6670	.5557	113	118
342	"				.6638			
"	15 Apr				.6635			
342*		18-17.88	67-11.96	4.4	978.6637	978.5568	108	114
343	21 Mar	-18.95	-13.48	15.7	.6611	.5578	108	113
344	"				.6574			
"	15 Apr				.6574			
344*		-20.02	-15.02	3.5	.6574	.5587	100	106
345	21 Mar	18-22.02	67-14.08	9.1	978.6619	978.5605	104	110
346	"	-22.82	-11.52	7.4	.6657	.5612	107	112
347	"	-23.71	-09.47	4.5	.6673	.5620	107	113
348	"				.6542			
"	15 Apr				.6545			
348*		18-26.77	67-08.59	142.5	978.6544	978.5648	134	126
349	21 Mar	-26.87	-06.82	147.7	.6499	.5649	131	122
350	"				.6451			
"	15 Apr				.6451			
350*		-27.53	-04.40	140.7	.6451	.5655	123	115

*** Adopted Value**

other factor must mask the effect of the sediments in this area.

In Figure 4B, a section (Pl. 1, F–F′) by Zapp *et al.* (1948) has been reproduced (generalized). Extrapolation seaward of the basement surface (dashed line) indicates that it approaches the ocean bottom near the edge of the Puerto Rico Trench at about 1500 fm. Bottom cores from submarine canyon walls in this area might show evidence of this surface. The sediment structure has been approximated by the rectangular blocks at the bottom of the diagram. The attraction of these blocks has been computed (assuming the east-west dimension to be infinite) for density contrasts of −.37 and −.54 (Fig. 4A). In the first case a density of 2.30 is assumed for the sediments and 2.67 for basement rocks. Since the density

TABLE 4.—*Continued*

STATION NUMBER	DATE 1953	LATITUDE NORTH	LONGITUDE WEST	ELEVATION METERS	OBSERVED GRAVITY GALS	INTERNATION FORMULA GRAVITY	FREE AIR ANOMALY IN MGALS	MOD. BOUGUER ANOM. MGALS
351	21 Mar	18-28.19	67-01.97	124.2	978.6459	978.5661	118	112
352	"	-28.45	-00.45	108.9	.6497	.5663	117	113
353	"	-28.87	66-58.45	86.6	.6515	.5667	112	110
354	"				.6403			
"	15 Apr				.6403			
354*		18-28.86	66-56.46	121.6	978.6403	978.5667	111	106
355	21 Mar	-27.91	-53.53	112.3	.6350	.5658	104	99
356	"				.6451			
"	15 Apr				.6446			
356*		-28.44	-44.11	9.8	.6449	.5663	82	88
357	21 Mar	18-26.98	66-43.03	5.6	978.6531	978.5650	90	97
358	"	-25.79	-42.66	9.1	.6585	.5639	98	104
359	"	-23.67	-41.40	23.8	.6638	.5620	109	116
360	"	-21.56	-41.04	73.1	.6611	.5601	124	125
361	"	-20.50	-40.30	131.0	.6521	.5592	134	129
362	21 Mar	18-18.62	66-41.40	99**	978.6563	978.5575	129	129
363	"	-17.60	-42.39	124.7	.6521	.5565	134	130
364	"	-14.32	-43.34	183.4	.6313	.5536	135	124
365	"	-12.83	-43.45	266.1	.6147	.5523	145	125
366	"	-11.88	-43.82	443.9	.5793	.5515	165	125
367	23 Mar	18-09.37	67-09.04	5.2	978.6686	978.5492	121	126
368	"	-06.40	-07.79	10.8	.6622	.5466	119	123
369	"	-05.10	-09.06	22.9	.6651	.5454	127	130
370	"	-04.10	-09.19	38.2	.6627	.5446	130	131
371	"	-01.78	-08.41	26.6	.6635	.5425	129	132
372	23 Mar	18-00.26	67-09.09	3.4	978.6651	978.5411	125	130
373	"	-01.86	-07.17	20.4	.6675	.5426	131	134
374	"	-01.91	-05.66	22.9	.6673	.5426	132	135
375	"	-02.35	-03.13	26.9	.6665	.5430	132	134
376	"	17-59.04	-02.44	32.8	.6590	.5400	129	131
377	23 Mar	18-00.05	67-02.46	19.2	978.6630	978.5409	128	132
378	"	17-59.71	66-59.72	26.4	.6563	.5406	124	127
379	"	-59.11	-57.35	23.0	.6534	.5401	121	124
380	"	-58.56	-54.87	2.9	.6505	.5397	112	117
381	"	-59.98	-53.62	15.0	.6467	.5409	111	115

*Adopted Value

** Observation made on road above BM. Elevation difference estimated by observer

of 2.67 was used in computing the modified Bouguer corrections, the curve computed for the density contrast of −.37 is strictly comparable with the observed modified Bouguer anomaly curve. The lack of agreement between the computed and observed curves is seen. In the second case the same sediment density is assumed and the density of 2.84 is used for basement rocks since it is considered a better average crustal rock density (Worzel and Shurbet, 1955). Since this density was not used in computing the modified Bouguer corrections, the curve computed for the density contrast of −.54 is not strictly comparable with the observed modified Bouguer anomaly curve, but the discrepancy is negligible. The computed

TABLE 4.—*Continued*

STATION NUMBER	DATE 1953	LATITUDE NORTH	LONGITUDE WEST	ELEVATION METERS	OBSERVED GRAVITY GALS	INTERNATION FORMULA GRAVITY	FREE AIR ANOMALY IN MGALS	MOD. BOUGUER ANOM. MGALS
382	23 Mar	18-01.92	66-53.61	80.0	978.6377	978.5426	120	117
383	"	-02.22	-55.53	53.1	.6491	.5429	123	123
384	"	-02.20	-58.47	17.6	.6579	.5429	121	124
385	"	-02.47	67-00.89	25.5	.6625	.5431	128	130
386	"	-03.94	-03.20	105.7	.6502	.5445	139	132
387	23 Mar	18-07.04	67-06.66	13.9	978.6633	978.5471	121	124
388	24 Mar	-05.02	-02.79	74.5	.6537	.5453	132	129
389	"	-05.00	66-57.50	108***	.6411	.5453	129	123
390	"	-02.12	-50.87	31.7	.6459	.5428	113	116
391	"	-02.24	-49.01	61.7	.6406	.5429	117	117
392	24 Mar	18-00.77	66-46.32	2.7	978.6435	978.5416	103	108
393	"	17-58.69	-41.76	3.0	.6329	.5398	94	100
394	"	-59.81	-38.11	7.2	.6342	.5407	96	101
395**	"				.6315			
"	16 Apr				.6313			
395**		18-00.54	66-37.23	10***	978.6314	978.5414	93	98
396	24 Mar	17-59.29	-17.35	15.0	.6563	.5403	121	125
397	"	18-02.13	-14.61	72.2	.6633	.5428	143	142
398	"	-04.03	-14.58	162.3	.6505	.5445	156	147
399	"	-05.27	-13.95	448.0	.5947	.5455	188	150
400	24 Mar	18-06.33	66-11.12	475.1	978.5977	978.5465	198	154

*Adopted Value

** Reoccupation USC & GS West Indies No. 3

*** Estimated from USGS Topographic Maps Scale 1:10,000

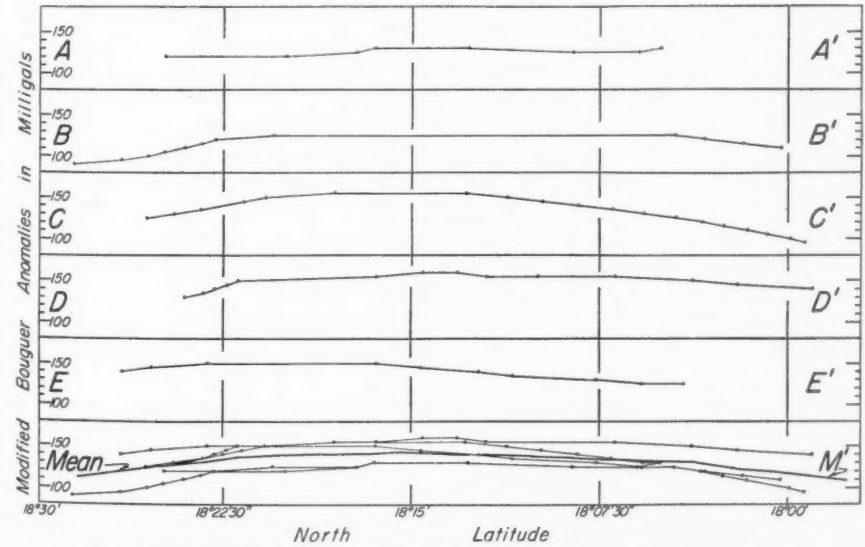

FIGURE 2.—NORTH-SOUTH PROFILES OF MODIFIED BOUGUER ANOMALIES

Profile locations shown in Plate 1. Points indicate intersections of gravity contours with profile lines.

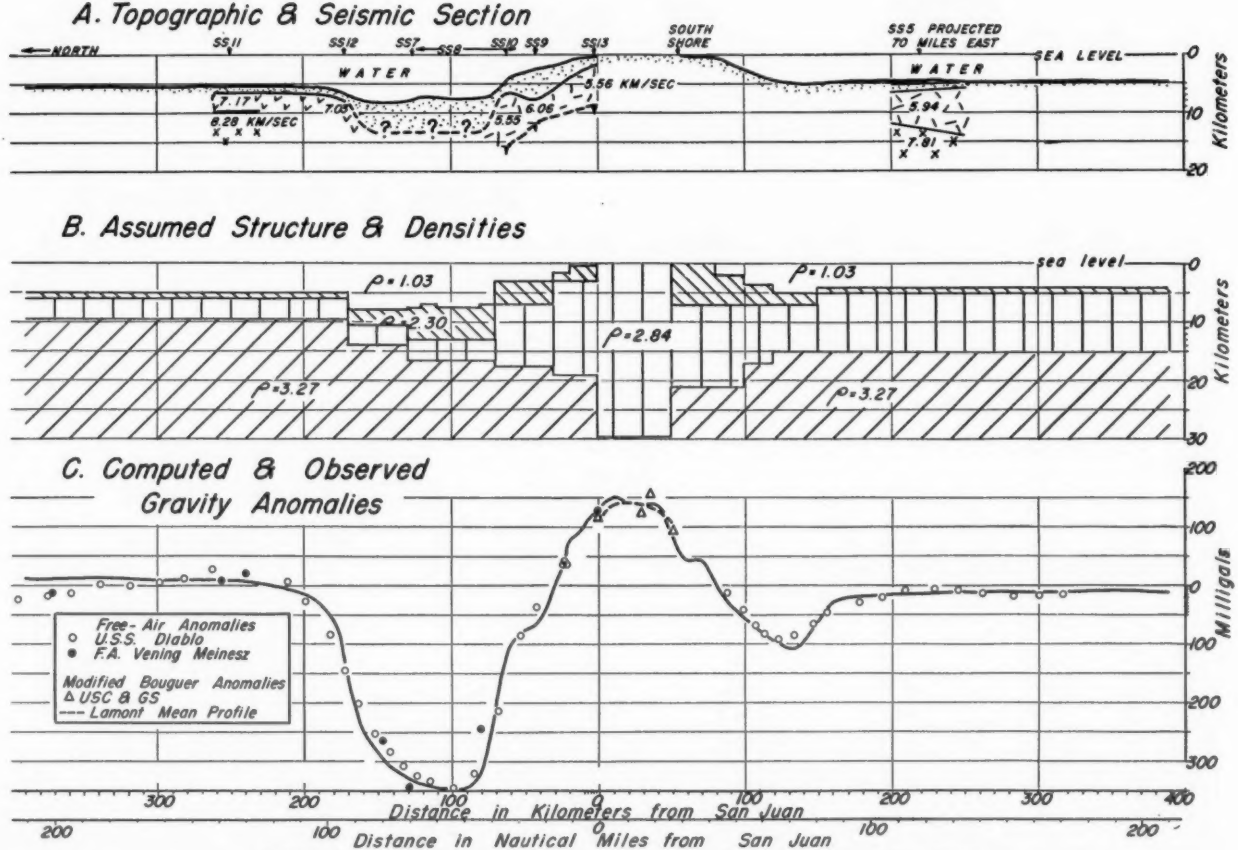

FIGURE 3.—NORTH-SOUTH STRUCTURE AND GRAVITY SECTIONS THROUGH SAN JUAN

Gravity anomaly curve in Section C computed from Section B by comparison with standard crustal sections of Worzel and Shurbet (1955, p. 91)

TABLE 5.—ISOSTATIC ANOMALIES IN THE PUERTO RICO AREA

Station		Water depth (Meters)	Free-air anomaly (Mgals)	Hayford isostatic anomaly (Mgals)	Airy local isostatic anomaly (T = 30 km)
S-21	34	5569	−18	−1	.....
	35	5340	+21	+31	.....
	36	7699	−264	−125	.....
	37	9	+129	−19	.....
Vening Meinesz	67	5510	+9	+7	+7
	68	8040	−341	−193	−292
	824	7370	−244	−226	−222
Elevations					
USC & GS	1	+8	+112	−43	on land
	2	+648	+220	+23	
	3	+14	+91	−48	
	4	+16	+122	−20	

curve using the density contrast of −.54 is in reasonable agreement with the observed curve except near the shore line. Here, a sedimentary section slightly thicker than shown by Zapp *et al.* (1948) is necessary to fit the observed data, and the dotted line in Figure 4B is probably a better approximation of the basement surface. If a density higher than 2.30 is assumed for the sediments, a thicker sedimentary section is necessary to account for the observed gravity anomaly.

DEFLECTION OF THE VERTICAL

The new gravity information available from this survey will be useful in computing the deflections of the vertical in Puerto Rico discussed by Hayford (1902, Unpublished report of the U. S. Coast and Geodetic Survey). Since more gravity information in this area will become available in the near future, this problem will be discussed in a later publication.

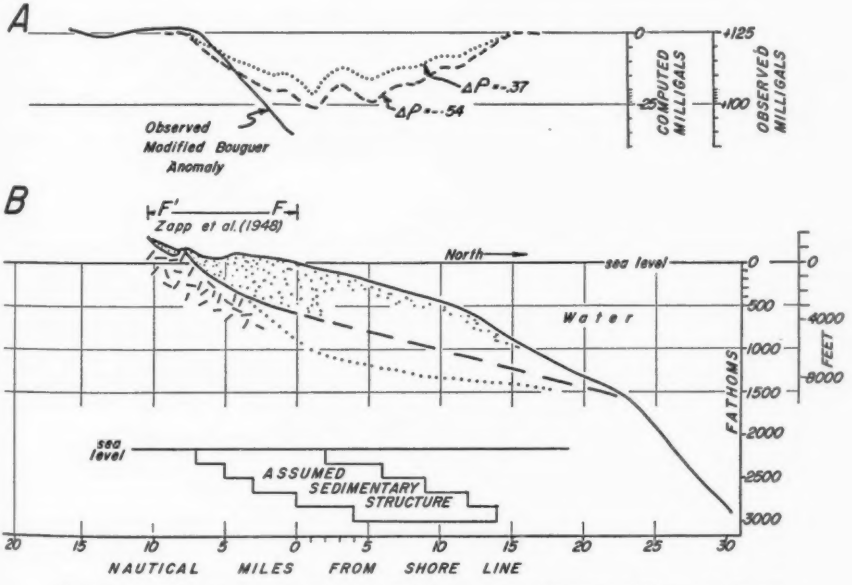

FIGURE 4.—STRUCTURE AND GRAVITY SECTIONS ACROSS NORTHERN TERTIARY BASIN

Location of section F-F' (Zapp *et al.*, 1948) shown in Plate 1. Diagram A shows observed anomaly curve and computed curves assuming two density differentials between sedimentary and basement rocks. Sedimentary structure approximated in bottom diagram.

FIGURE 3.—NORTH-SOUTH STRUCTURE AND GRAVITY SECTIONS THROUGH SAN JUAN

Gravity anomaly curve in Section C computed from Section B by comparison with standard crustal sections of Worzel and Shurbet (1955, p. 91)

Conclusions

Modified Bouguer anomalies in Puerto Rico show large positive values of about 90 mgal along the northern and southern coasts, increasing to about 165 mgal in the central part of the island. The Tertiary sedimentary basins and the large outcrops of the Antillean granitoid intrusives and intrusive porphyries, chiefly andesitic, are characterized by gravity minima. According to Meyerhoff, two of these gravity minima correlate with the two main volcanic centers in Puerto Rico. The largest gravity maximum in Puerto Rico cannot be correlated with surface geologic formations.

The mantle is determined by gravity calculations to lie about 29 km below sea level under Puerto Rico.

There is a discrepancy of about 15 mgal in the values published by Vening Meinesz and Wright for the gravity stations established after the Guantanamo Bay occupation on the S-21 cruise.

References Cited

Collins, E. B., 1933, Computations of sea observations for determining the value of gravity, *in* The Navy-Princeton gravity expedition to the West Indies in 1932: U. S. Hydrographic Office, Washington, D. C., 54 p.

Duerksen, J. A., 1949, Pendulum gravity data in the United States: U. S. Coast and Geod. Survey Special Pub. 244, 218 p.

Ewing, M., and Worzel, J. L., 1954, Gravity anomalies and structure of the West Indies, Part I: Geol. Soc. America Bull., v. 65, p. 165–173.

Heiskanen, W., 1939, Catalogue of the isostatically reduced gravity stations: Isos. Inst. Inter. Assoc. Geod. Pub., no. 5, 139 p.

Meyerhoff, H. A., 1933, Geology of Puerto Rico: Puerto Rico Univ. Mon., ser. B., no. 1, 306 p.

Swick, C. H., 1942, Pendulum gravity measurements and isostatic reductions: U. S. Coast and Geod. Survey Spec. Pub. 232, 82 p.

Vening Meinesz, F. A., 1948, Gravity expeditions at sea, 1923–1938: Delftsche Uitgevers Maatschappij—Delft, v. 4, 233 p.

Vening Meinesz, F. A., and Wright, F. E., 1930, The gravity measuring cruise of the U. S. Submarine S-21: Pub. U. S. Naval Observatory, 2d ser., v. 13, app. 1, 94 p.

Worzel, J. L., and Ewing, M., 1950, Gravity measurements at sea, 1947: Am. Geophys. Union Trans., v. 31, p. 917–923.

——1954, Gravity anomalies and structure of the West Indies, Part II: Geol. Soc. America Bull., v. 65, p. 195–199.

Worzel, J. L., and Shurbet, G. L., 1955, Gravity interpretations from standard oceanic and continental crustal sections; *in* Poldervaart, Arie, Editor, Crust of the earth: Geol. Soc. America Special Paper 62, p. 87–100.

Zapp, A. D., Bergquist, H. R., and Thomas, C. R., 1948, Tertiary geology of the coastal plains of Puerto Rico: U. S. Geol. Survey Oil and Gas Inv.

Lamont Geological Observatory, Columbia University, Palisades, N. Y.

Manuscript Received by the Secretary of the Society, May 23, 1955.

Lamont Geological Observatory Contribution No. 178.

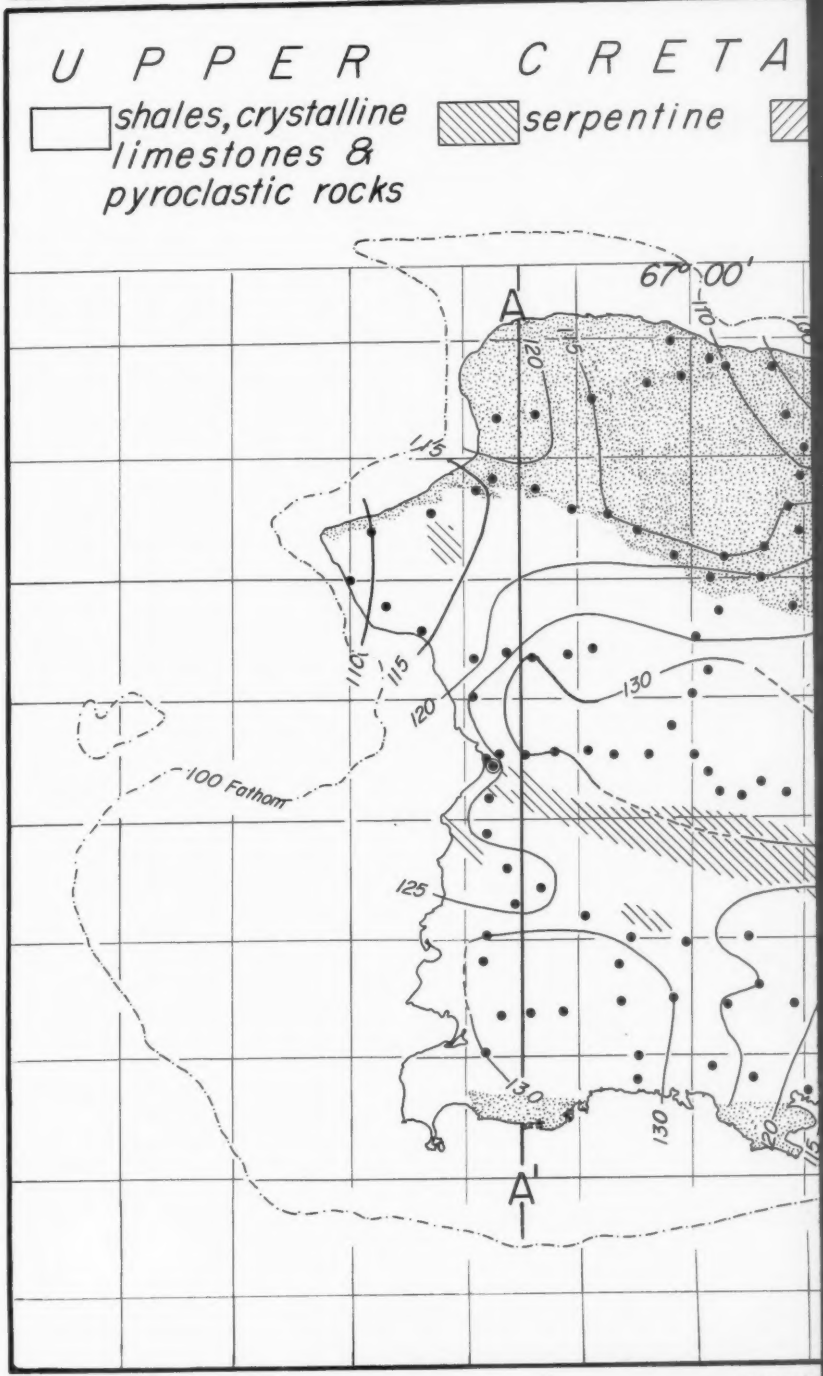
U P P E R
C R E T A
shales, crystalline limestones & pyroclastic rocks
serpentine
67° 00'
A
A'
100 Fathom
110
115
120
125
130

CONT

TACEOUS

surface flows & intrusive porphyries

ANT

granit

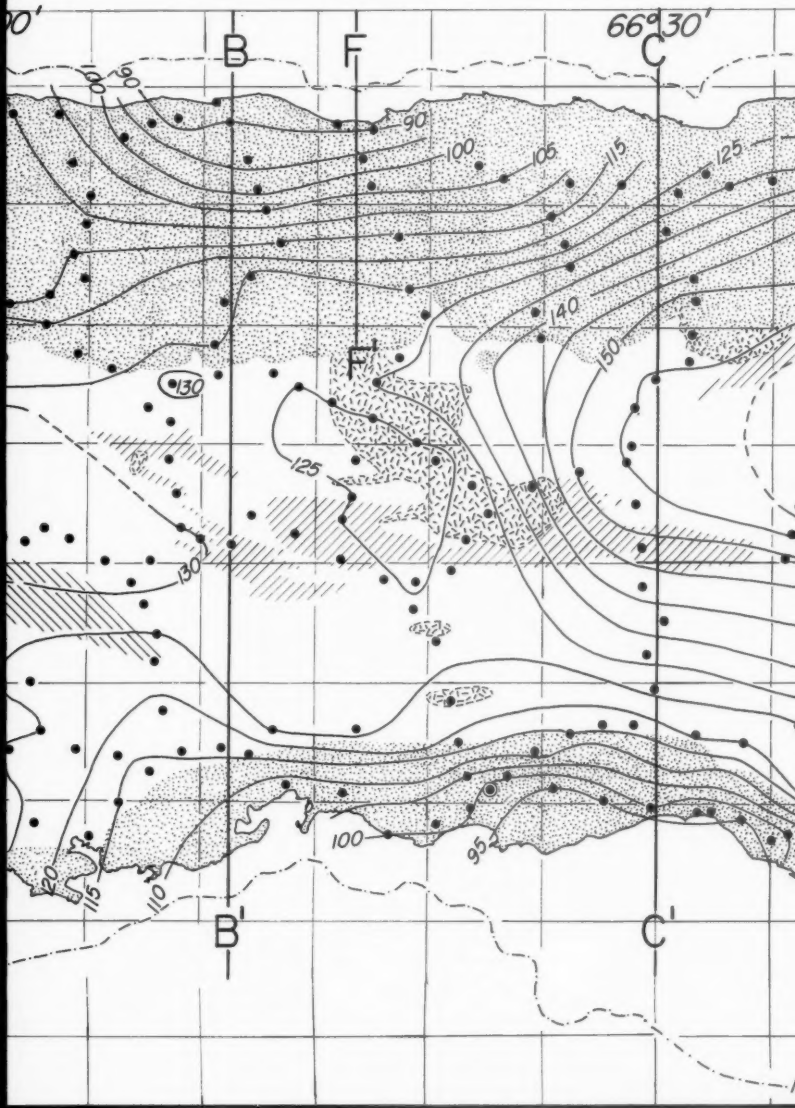

CONTOURED MODIFIED BOUGUER ANOMALIES

Geology adapted from

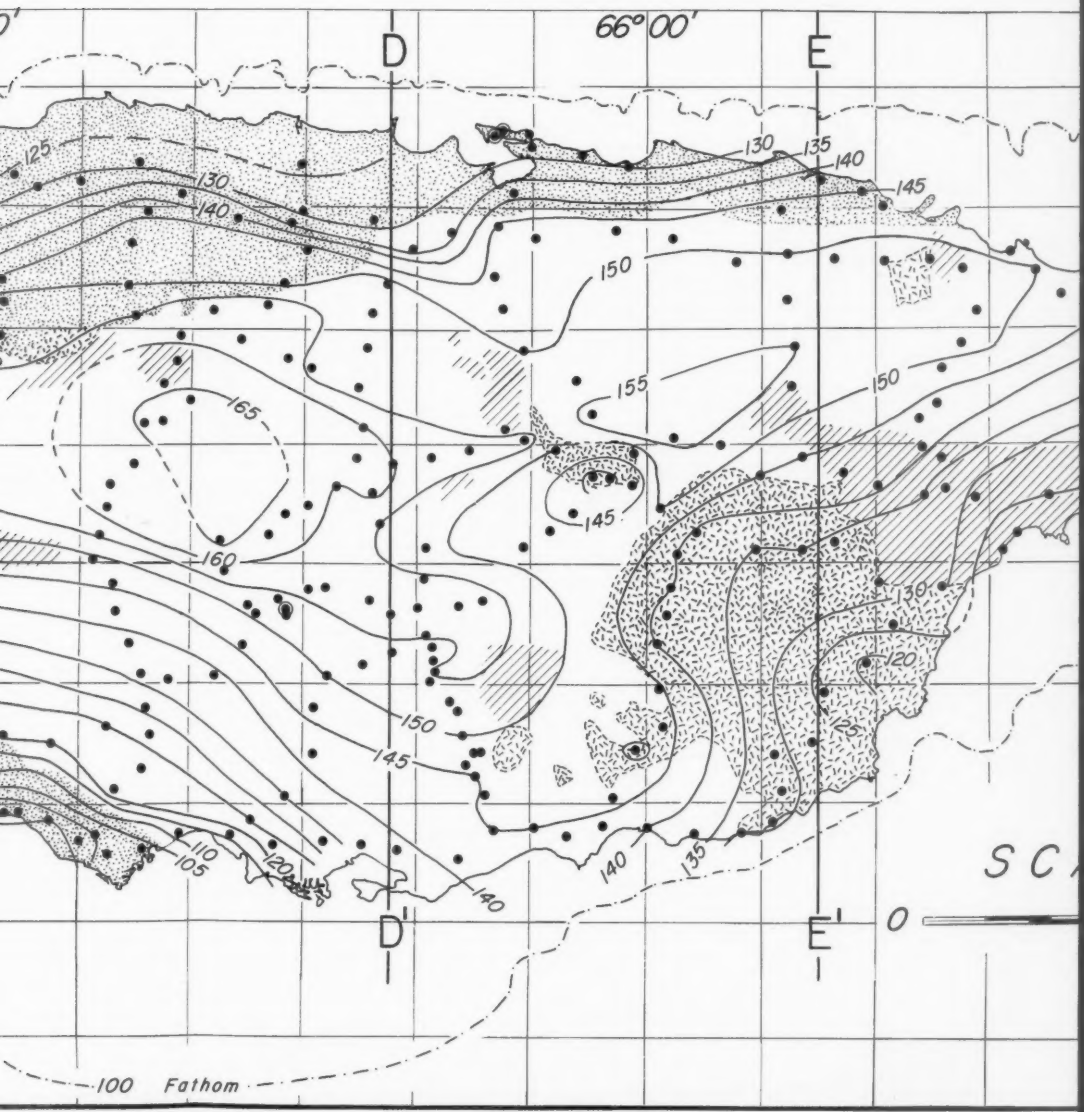

ALIES AND SURFACE GEOLOGIC FORMATIONS IN PUERTO RICO

oted from Meyerhoff (1933), Quaternary omitted

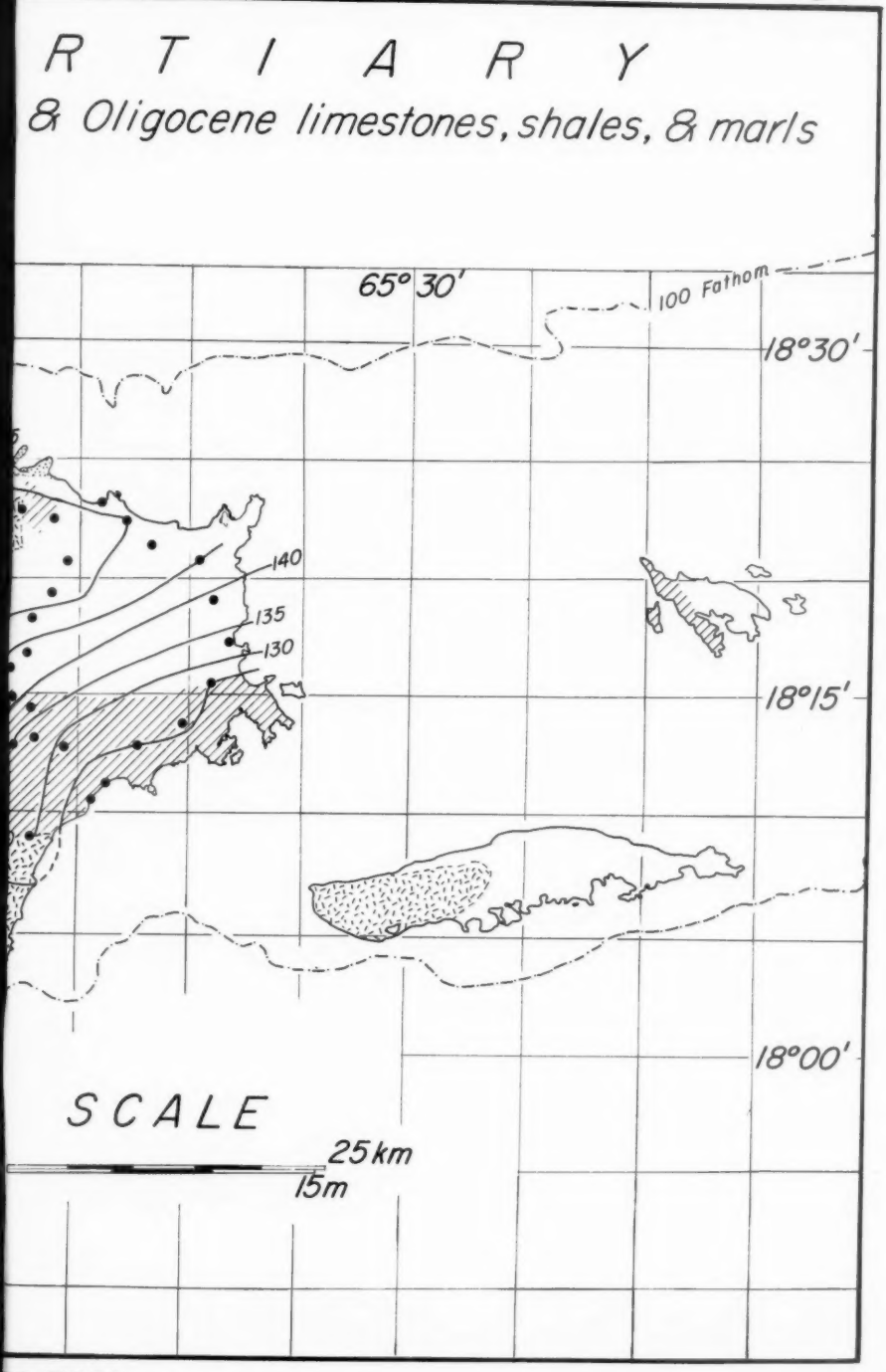
R T I A R Y
& Oligocene limestones, shales, & marls
65° 30'
100 Fathom
18°30'
140
135
130
18°15'
18°00'
SCALE
25 km
15 m

TO RICO

Short Note

BULLETIN OF THE GEOLOGICAL SOCIETY OF AMERICA
VOL. 67, P. 535 APRIL 1956

SIZE AND ROUNDNESS IN SEDIMENTS: A DISCUSSION

By William F. Tanner

Curray and Griffiths (1955) report no significant difference, from one grain size to another, in sphericity of certain quartz sand grains. Their data, representing more than 2000 grains, were obtained from ½, ¼, ⅛, and ⅛ mm sizes. This note does not purport to be, in any way, a criticism of their work.

Einstein (1950) indicated an important "break" in the size scale at about $\frac{1}{17}$ mm. Research carried out by the present writer, over a period of nearly 20 years on many different sand samples from various environments, suggests another important "break" at about $\frac{1}{10}$ mm. The former probably concerns buoyancy as it affects transportation; the latter, as it affects abrasion. Specifically, grains finer than about $\frac{1}{10}$ mm do not, in general, exhibit the rounded shapes so common among coarser sand grains.

The problem involves both sphericity and roundness, as is well known. Curray and Griffiths did not present figures on relationships between roundness and grain sizes. It is hoped that future work will include roundness measures and include grains at least finer than $\frac{1}{10}$ mm, and perhaps also finer than $\frac{1}{17}$ mm.

References Cited

Curray, J. R., and Griffiths, J. C., 1955, Sphericity and roundness of quartz grains in sediments: Geol. Soc. America Bull., v. 66, p. 1075–1096

Einstein, H. A., 1950, The bed-load function for sediment transportation in open channel flows: U. S. Dept. Agric., Soil Conserv. Service, Tech. Bull. 1026

Department of Geology, Florida State University, Tallahassee, Fla.